

**UC Davis**

**UC Davis Electronic Theses and Dissertations**

**Title**

Geometrization of Scattering Amplitudes in Supersymmetric Yang-Mills Theory

**Permalink**

<https://escholarship.org/uc/item/88z7582s>

**Author**

Zheng, Minshan

**Publication Date**

2022

Peer reviewed|Thesis/dissertation

Geometrization of Scattering Amplitudes  
in Supersymmetric Yang-Mills Theory

By

MINSHAN ZHENG  
DISSERTATION

Submitted in partial satisfaction of the requirements for the degree of

DOCTOR OF PHILOSOPHY

in

Physics

in the

OFFICE OF GRADUATE STUDIES

of the

UNIVERSITY OF CALIFORNIA  
DAVIS

Approved:

---

Jaroslav Trnka, Chair

---

Veronika Hubeny

---

Andrew Waldron

Committee in Charge

2022

Dedicated to my parents

# CONTENTS

Abstract	vi
Acknowledgments	viii
<b>1 Introduction</b>	<b>1</b>
<b>2 Positive geometry, Local Triangulations, and the Dual of the Amplituhedron</b>	<b>9</b>
2.1 Introduction	9
2.2 Amplituhedron geometry	11
2.2.1 Topological sign-flip definition of the Amplituhedron	14
2.2.2 One-loop MHV and $\overline{\text{MHV}}$ spaces	17
2.2.3 Boundaries of MHV amplitudes	18
2.2.4 Positivity and the dual Amplituhedron	28
2.3 Geometry of $d \log$ forms	32
2.3.1 $d \log$ forms for pentagon integrands	33
2.3.2 From $d \log$ 's to geometry	37
2.3.3 No-go theorem for external triangulation	47
2.4 Sign-flip regions	48
2.5 Local geometries and the Amplituhedron-Prime	60
2.5.1 Chiral regions for boxes and pentagons	61
2.5.2 Two-dimensional projections	65
2.5.3 Gluing regions	71
2.5.4 Amplituhedron-Prime	79
2.6 Triangulation of the dual Amplituhedron	87
2.6.1 Dualizing polygons	88
2.6.2 Dual spaces of chiral pentagons	91
2.6.3 Two-dimensional triangulations	95
2.7 Conclusion	103

<b>3</b>	<b>Integrands of Less-Supersymmetric Yang-Mills at One Loop</b>	<b>104</b>
3.1	Introduction and Overview	104
3.2	A Prescriptive, Bubble Power-Counting Basis at One Loop	108
3.2.1	Brief Review of Prescriptive Integrand Bases for Amplitudes	109
3.2.2	Defining a Bubble Power-Counting Basis $\mathfrak{B}_2^{(4)}$	110
3.2.2.1	A Spanning Set of Maximal-Dimension Contours	113
3.2.2.2	Illustrations of the Resulting Numerators in the Basis	118
3.2.2.3	Stratification of UV/IR Structure and Transcendental Weight	124
3.3	Leading Singularities in $\mathcal{N} \leq 4$ Super Yang-Mills Theory	125
3.3.1	Decorated On-Shell Diagrams: Singlet vs. Non-Singlet	127
3.3.2	Generalized Unitarity for Massless Bubble Coefficients	129
3.4	Amplitude Integrands for $\mathcal{N} \leq 4$ Super Yang-Mills Theory	132
3.4.1	General Structure of Amplitude Integrands	133
3.4.2	<i>Exempli Gratia</i> : MHV Amplitude Integrands	134
3.4.3	<i>Exempli Gratia</i> : a Six-Point NMHV Amplitude Integrand	137
3.4.4	Finite Observables at One Loop	139
3.5	Conclusion	143
<b>4</b>	<b>Non-planar BCFW Grassmannian Geometries</b>	<b>145</b>
4.1	Introduction	145
4.2	Background: From BCFW to Positive Geometry	148
4.2.1	From BCFW to On-shell Diagrams	149
4.2.2	From On-Shell Diagrams to Grassmannian Geometry	153
4.2.3	Canonical dlog forms	159
4.2.4	Dual formulation	160
4.2.5	Cells for NMHV Tree-level Amplitudes	163
4.3	Holomorphic expressions for BCFW terms	170
4.4	Non-adjacent BCFW recursion and non-planar positive geometry	177
4.4.1	MHV amplitudes	180
4.4.2	NMHV amplitudes	183

4.5	Non-planar tree-level $R$ -invariants	196
4.5.1	Non-planar $\mathcal{R}$ -invariant	198
4.5.2	Planar expansion	203
4.6	Kinematical dlog forms	207
4.6.1	Super-functions as kinematical differential forms	207
4.6.2	Holomorphic dlog forms	212
4.6.3	Non-planar generalization	215
4.7	$N^2$ MHV and Beyond	216
4.7.1	$N^2$ MHV geometries	217
4.7.2	Holomorphic on-shell functions	222
4.8	Conclusion	228
<b>5</b>	<b>Summary</b>	<b>230</b>
<b>A</b>	<b>Configuration of lines in momentum twistor space</b>	<b>233</b>
A.1	External triangulations	237
A.2	Fixed signs in sign-flip-zero, two and four spaces	251
A.3	Gluing local geometries from two-dimensional projections	257
<b>B</b>	<b>Complete Bubble Power-Counting Integrand Basis <math>\mathfrak{B}_2^{(4)}</math></b>	<b>269</b>
B.1	Spanning-Set of Integration Contours Defining the Basis	270
B.2	Explicit Numerators for Basis Integrands in $\mathfrak{B}_2^{(4)}$	271
B.3	Integrals of Basis Integrands in Dimensional Regularization	272
	<b>Bibliography</b>	<b>273</b>

## ABSTRACT

### Geometrization of Scattering Amplitudes in Supersymmetric Yang-Mills Theory

A geometric formulation of scattering amplitudes in perturbative quantum field theory has surfaced in recent years where, in place of the summations of all off-shell Feynman diagrams for an amplitude, a single geometric object in the kinematic space of on-shell scattering data completely dictates the final answer. By far the most sophisticated example of this new formulation is the *amplituhedron* geometry for the planar  $\mathcal{N} = 4$  super Yang-Mills theory, whose boundary structure encodes all singularities of any amplitude at any loop-order.

While an amplituhedron describes an amplitude (prior to loop integration) as a differential form with logarithmic singularities on its boundary, a *dual amplituhedron* whose *bulk volume* directly reproduces the same amplitude is much desired. In chapter two of this thesis, we provide nontrivial evidence for the dual amplituhedron from the perspective of *local triangulation*. We classify all the elementary geometric spaces relevant for one-loop Feynman integrands which allow for further identification of geometrical spaces associated with the chiral pentagon-integrands in the local expansion of one-loop MHV amplitudes. Using projective duality maps on certain two-dimensional boundaries where the geometry reduce to polygons, we show that the real purpose of life of chiral pentagons is to triangulate the putative dual amplituhedron.

The discovery of amplituhedron originated from a reformulation of amplitudes at the level of the *integrand* –the unintegrated sum of Feynman diagrams, in terms of *positive Grassmannians* and *on-shell diagrams*. Extending the geometric formulation to more general theories after the example of  $\mathcal{N} = 4$  sYM requires both a wealth of theoretical data from explicit computations of loop integrands and further understanding of the connection between on-shell diagrams and Grassmannian geometry without planarity.

In chapter three, we discuss one-loop *integrand* construction for planar Yang-Mills amplitudes with  $1 \leq \mathcal{N} < 4$  supersymmetry based on a *generalized unitarity* method. We trace the source of ambiguity in defining “the loop integrand” for non-maximally supersymmetric amplitudes to the ill-defined non-singlet massless “bubble-cuts”, and pinpoint two prescriptions for *defining* the loop integrand, paving the way for future exploration of amplituhedron-like geometric objects for less supersymmetric Yang-Mills theories.

In chapter four, we go beyond the planar sector of  $\mathcal{N} = 4$  sYM, exploring the geometry of non-planar on-shell diagrams — essential building blocks of any non-planar amplitudes — that arise in the context of BCFW recursion relations of tree-amplitudes using non-adjacent shifts of momenta. We show that individual terms in the non-adjacent BCFW expansions are associated with a particular class of non-planar positive geometries which generalize the positroid cells of the positive Grassmannian into the Grassmannian.



## ACKNOWLEDGMENTS

First and foremost, I would like to thank my advisor, Jaroslav Trnka, who has been both a constant source of intellectual inspiration and a great source of support and encouragement throughout the five years I spent in Davis. From Jaroslav, I have learned a tremendous amount about physics, academics, and life in general, the influence of which will undoubtedly continue beyond graduate school.

In addition to the mentorship I received from Jaroslav, I have benefited heavily from interacting with my collaborators Jacob Bourjaily, Enrico Herrmann, Cameron Langer, Kokkimidis Patatoukos, and Shruti Paranjape. Without them, much of this thesis research would not have been possible.

Thanks to everyone in the Fields, Strings and Gravity group. I have learned much from each of them during journal club and seminar discussions. Thanks also to all the members of the Center for Quantum Mathematics and Physics for creating an interactive and supportive academic environment. Special thanks to Veronika Hubeny and Andrew Waldron for serving on my thesis committee.

Thanks to my fellow students and friends in the Physics Department, in particular, Taro Brown, Umut Oktem, Sean Colin-Ellerin, Andrew Ballin, Miranda Chen, and Guga Mikaberidze, who have made my time at Davis an overwhelmingly enjoyable experience.

I am deeply thankful to the people who have encouraged and guided me on my road to learning theoretical physics while I was an undergraduate nuclear engineering student. Thanks to Hong-Jian He, my undergraduate academic advisor, for giving me the chance to work on particle phenomenology. Thanks to Wei Song, who exposed me to conformal field theory and holographic duality during the year I spent in the String Theory Group at YMSC. Thanks to Song He, who took me as a visiting student during my gap year and shared with me his passion and insight about scattering amplitudes. I cannot imagine where I would be if it were not for their help.

I would like to thank my friends from home who have always been a great source of comfort, especially during the COVID pandemic.

Finally and most importantly, words cannot express my gratitude to my parents. It is their unwavering, unconditional support at all times that carry me this far.

# Chapter 1

## Introduction

Scattering amplitudes are fundamental observables in quantum field theory. Traditionally they are calculated perturbatively using Feynman diagrams, invoking a spacetime image of summing over all ways the collisions between particles could take place. Calculations of Feynman diagrams are notoriously complicated beyond the simplest process, yet the final results are often strikingly simple. The first glimpse of hidden simplicity in scattering amplitudes is the Parke-Taylor formula [1] discovered in 1986 for the tree level, color-ordered, maximally-helicity-violating (MHV) gluon amplitude, where among  $n$  massless external gauge bosons,  $n - 2$  gauge bosons have a particular helicity and the other two (denoted by  $i$  and  $j$  below) have the opposite helicity

$$A_{\text{MHV}}^{\text{tree}}(1^+ 2^+ \cdots, i^-, \cdots, j^-, \cdots n^+) = \frac{\langle ij \rangle^4}{\langle 12 \rangle \langle 23 \rangle \langle 34 \rangle \cdots \langle n1 \rangle}.$$

This single line formula for the amplitude using the modern helicity-spinor notation is equal to pages of algebraic expressions in terms of momenta and polarization vectors coming out of direct calculations of Feynman diagrams. Initially obtained for a  $2 \rightarrow 4$  process involving thousands of Feynman diagrams, this formula proves to hold for all-multiplicity processes. It was natural to wonder if a deeper theory for scattering amplitudes exists behind all the apparently complicated computations.

The years since Parke and Taylor's pioneering discovery have seen many computational and conceptual advances in the study of scattering amplitudes such as generalized

unitarity methods [2, 3], on-shell recursion relations[4, 5], color-kinematics duality[6–8], twistor string theory[9], scattering equations[10–13], and various bootstrap methods [14–19]. Discoveries of new structures and symmetries have led to and been further fueled by the development of alternative theoretical frameworks for scattering amplitudes in various quantum field theories using different organizing principles than the Feynman diagrammatic expansion. These various new formulations make different hidden aspects of scattering amplitudes manifest and, besides facilitating calculations, often connect physics to new areas of mathematics. In the recent decade, amid all of these developments, surfaced for the first time a purely *combinatoric-geometric* origin of scattering amplitudes, which does not refer to any spacetime processes, in the study of the maximally supersymmetric gauge theory ( $\mathcal{N} = 4$  super-Yang-Mills theory) [20, 21] in the planar limit of a large number of colors. (For reviews of modern amplitude methods see [22–24])

Planar  $\mathcal{N} = 4$  sYM, arguably the simplest quantum field theory, is an ideal laboratory for exploring new ideas about scattering amplitudes. Intensive study in the past three decades has revealed many remarkable analytic properties of the planar  $\mathcal{N} = 4$  sYM amplitudes, including the dual conformal symmetry [25–27] and Yangian symmetry [28], the connection to cluster algebra [29–35], the amplitude/Wilson-loop duality[36–40], and the all-loop extension of BCFW recursion relations [41]. The new geometric picture arose from the dual formulation of scattering amplitudes in terms of *Grassmannians* [42–46] and *on-shell diagrams* [47] and, precluded by the use of momentum twistor methods [48–55], culminated in the construction of the *Amplituhedron*[56–59].

An amplituhedron is a particular example of “*positive geometries*” [60] which generalize the notion of *convex* polytopes to geometric objects with non-linear boundaries as specified by a set of inequalities, generally referred to as positivity conditions. While the original definition of the Amplituhedron [56] involved an auxiliary Grassmannian space, a more recent reformulation of the Amplituhedron defines the geometry di-

rectly in the *kinematic space* of external scattering data (represented by momentum twistors [48]  $Z_i$  for particles  $i = 1, \dots, n$ ), using certain topological sign-flip conditions [58] on sequences of twistor invariants. Encapsulated in the boundary structure of an amplituhedron is any tree-amplitude or the integrand of any loop-amplitude in planar  $\mathcal{N} = 4$  sYM. Rather than functions of external kinematic (and loop) variables, the (color-stripped) super-amplitudes have the interpretation of canonical differential forms with *logarithmic singularities* (“dlog forms”) on the boundaries of the amplituhedron. Concrete expressions of scattering amplitudes can be obtained by *triangulating* the space, with various natural triangulations reproducing the well-known BCFW and CSW representations [56, 61]. All physical properties of scattering amplitudes, such as unitarity and locality, are consequences of the amplituhedron geometry [57, 62].

While there is no direct derivation of this geometric construction from first principles of quantum field theory, by now we have ample evidence for the relation between the Amplituhedron geometry and scattering amplitudes. In particular, one can explicitly compute the differential forms by triangulating the amplituhedron and comparing them to existing tree-level amplitudes and loop integrands available in the literature [58, 63–65]. The geometric picture has also been used to obtain a large amount of explicit all-loop data [57, 66–69] currently inaccessible from any diagrammatic approach. In parallel, there has been significant progress trying to understand more formal aspects of the amplituhedron, including its boundary and combinatorial structure, the connection to symbol alphabets, properties of final amplitudes (rather than integrands), and many others (see e.g., [70–91]). Despite this progress, there remain many open questions. Among which, notably, is the search for a *dual amplituhedron* [50, 54], of which a scattering amplitude would literally be the *volume*.

The amplituhedron arises as a generalization of the positive Grassmannian which appears in the context of on-shell diagrams and all-loop recursion relations in planar  $\mathcal{N} = 4$  sYM. Despite their origin in maximally supersymmetric Yang-Mills theory, on-shell diagrams and the associated construction in the Grassmannian can be defined

in various other theories [47, 92–98]. This naturally leads to the question whether or not Amplituhedron-like structures also exist more generally. Even within  $\mathcal{N} = 4$  sYM theory, the striking similarity of the analytic structure of planar and non-planar integrands, and the natural non-planar extension of on-shell diagrams [99–104] suggests that an Amplituhedron-like object should exist for  $\mathcal{N} = 4$  sYM amplitudes beyond the planar limit. A crucial first step in this direction has been achieved at tree-level by formulating the geometry of the Amplituhedron directly in momentum space [90, 105]. The momentum space formulation seems crucial beyond the planar limit, since one no longer has access to momentum-twistor variables which are at the heart of the kinematic space underlying the original Amplituhedron. At loop-level, the main obstruction is the non-uniqueness of the non-planar loop momentum, although recent works [106, 107] suggest possible paths to remedy this situation.

Ongoing efforts also attempt to extend the positive geometry framework to amplitudes in other field and string theories. Another example of a positive geometry is the associahedron, which is relevant for bi-adjoint  $\varphi^3$  amplitudes and is also connected to cluster polytopes and string amplitudes [108–111]. For attempts to include other interactions and matter, c.f. [112–116]. Recent advances have also uncovered positive geometries in conformal field theory correlation functions, the Wilson coefficients of effective field theories and the cosmological wavefunctions [117–122].

The exploration of the geometric picture of scattering amplitudes and the consequences of this connection is still in its infancy. The ideas outlined above form the foundations for the work presented in this thesis, consisting of three chapters after this general introduction.

In the second chapter of this thesis, based on the following papers

- E. Herrmann, C. Langer, J. Trnka and M. Zheng, *Positive geometries for one-Loop chiral octagons*, [2007.12191]
- E. Herrmann, C. Langer, J. Trnka and M. Zheng, *Positive geometry, local trian-*

we initiate a systematic study of “local” positive geometries associated with one-loop Feynman integrals (integrand) in the context of  $\mathcal{N} = 4$  sYM, motivated by the amplituhedron construction. We classify the elementary geometric spaces by certain topological “sign-flip” conditions, the simplest of which correspond to the well-known chiral octagon integrands. These sign-flip spaces form a basis for constructing positive geometries associated with any one-loop local integrands that are free of spurious poles.

The geometric origin of an arbitrary local integrand in the amplituhedron picture is non-obvious: any internal triangulation of amplituhedra would result in subspaces with spurious boundaries and hence summands with non-local poles. Indeed, the association of an integrand (as a canonical dlog form) to some geometry is often non-unique. Of particular interest is the geometrical interpretation of *chiral pentagon* integrands, which constitute highly compact representations of one-loop MHV amplitudes, manifesting an intriguing property the full amplitude — being positive when evaluated inside the amplituhedron region — term by term. This positivity property is reminiscent of the property of a signed volume, and closely related to the search for putative *dual amplituhedra*, of which triangulations should yield manifestly local expansions.

By studying the local triangulations by chiral pentagon spaces, we reveal a direct evidence for the yet-to-be discovered dual amplituhedron. Insisting on a faithful correspondence between poles of differential forms and geometric boundaries in gluing chiral pentagon spaces into a larger positive geometry of the amplitude, we conclude that the chiral pentagon expansion triangulates externally, not the original amplituhedron but its twin, an “amplituhedron-prime” space with identical boundaries but a completely non-overlapping bulk. We then show that all the various positive geometries computing the the same canonical form map to the same region in the dual space with some reasonable dualization prescription; while the precise duality mapping for the full geometry awaits definition, we demonstrate, on two-dimensional boundaries where the

MHV one-loop amplituhedron reduces to a polygon, the chiral pentagon expansion corresponds to an internal triangulation the dual polygon.

Moving beyond planar  $\mathcal{N} = 4$  sYM, an immediate direction to extend the geometrical framework is the planar but less-supersymmetric Yang-Mills theories. Crucial for exploring various geometric structures is a plenitude of explicit theoretical data. Notably, at the loop level, the prerequisite knowledge is the amplitude integrand—the gauge-invariant, unintegrated sum of Feynman diagrams. In chapter three based on

- J. L. Bourjaily, E. Herrmann, C. Langer, K. Patatoukos, J. Trnka and M. Zheng, *Integrands of less-supersymmetric Yang-Mills at one loop*, JHEP 03 (2022) 126 [2112.06901]

we use the method of generalized unitarity to construct amplitude integrands in less-supersymmetric Yang-Mills theory with  $\mathcal{N} = 1, 2$  at one loop. In contrast to the maximally supersymmetric theory, where integrands are protected by the dual conformal symmetry, important subtleties arise due to the presence of poles at infinity  $\ell \rightarrow \infty$ .

The amplitude-integrands, being rational differential forms of external kinematic and loop variables, can be expanded on any sufficiently large basis of rational integrands, with loop-independent coefficients fixed by unitarity in terms of on-shell, tree-level scattering processes. The basis suitable for representing  $1 \leq \mathcal{N} < 4$  sYM amplitude integrands requires ‘bubble’ power-counting in four dimensions, and standard analysis of generalized unitarity “cuts”, i.e. discontinuities of loop amplitudes across branch-cuts, determine the integrand only up to the contributions of “massless bubble” integrands. These outliers, despite integrating to zero in dimensional regularization, are important for disentangling the UV and IR structure and indispensable for a complete on-shell definition of amplitude integrands. Their coefficients, however, are intrinsically ambiguous for the lack of meaningful non-singlet bubble cuts of the field-theoretic amplitudes. In the text we show there are two natural definitions of the



non-singlet bubble cuts which lead to different integrands, leaving for future work the pursuit of geometrization along either path.

On a technical note, we offer a “prescriptive” basis in which every coefficient is exactly a “leading singularity” of the amplitude, and with the additional benefit of being divided into to separately UV- and IR-finite sectors of fixed transcendental weight. For concreteness, we construct the all-multiplicity integrands for MHV amplitudes, and the split-helicity integrand for six-particle NMHV amplitude.

Leaving the planar sector, in chapter four based on the following paper

- S. Paranjape, J. Trnka and M. Zheng, *Non-planar BCFW Grassmannian Geometries* [2208.02262],

we begin an investigation into the basic on-shell building blocks of scattering amplitudes for any theory regardless of planarity: *on-shell diagrams*, also known to mathematicians by the name *plabic graphs*. Physically, on-shell diagrams represent certain singularities of amplitudes which can be obtained by unitarity from merging simpler tree amplitudes. In the planar theory, BCFW expansions based on deforming two *adjacent* momenta at all orders of recursion have a diagrammatic realization in terms of *planar* on-shell diagrams. Notably, every on-shell diagram in the planar expansions individually enjoy the hidden dual conformal (hence also Yangian symmetry) of the full amplitude, and has a well-understood correspondence to a positroid cell in the *positive Grassmannian* [47]. It was this correspondence together with the diagrammatic realization of BCFW recursion that gave rise to the discovery of the amplituhedron originally.

The general connection between on-shell diagrams and Grassmannian holds even without planarity, but much less is understood about the geometry and combinatorics of non-planar diagrams (generic Grassmannian cells). We focus on a special class of non-planar on-shell diagrams which arise from BCFW recursion (still of planar amplitudes) with *non-adjacent* shifts, anticipating non-trivial but especially simple generalization of the the positroid geometry. In particular, we identify the  $(2n - 4)$ -dimensional non-

planar geometries associated with BCFW cells for NMHV tree-amplitudes, laying down the stepping stone in the further quest for non-planar geometries of higher-dimensional cells. While its full potential is yet to be grasped, the geometric picture has enabled a direct extraction of the analytic expressions of on-shell diagrams, either as a superfunction or a kinematical dlog form. Associated with these non-planar geometries are a new type of on-shell functions that generalize the familiar planar R-invariants; indeed, using the Kleiss-Kuijf relations, we show that they correspond to a linear combination of the planar R-invariants. Investigation of the residual dual conformal (and Yangian) symmetry in the non-planar sector starting with these objects is an open question for the future.

# Chapter 2

## Positive geometry, Local Triangulations, and the Dual of the Amplituhedron

### 2.1 Introduction

In this chapter, we revisit one major open question central to Amplituhedron research. In particular, we investigate the role of “local triangulations” of the Amplituhedron and their relation to a putative dual Amplituhedron space. The original idea of interpreting scattering amplitudes as volumes appeared in the work of Hodges [48] where the original momentum twistor space formulation for planar  $\mathcal{N} = 4$  sYM amplitudes was defined. In [48], the six-point NMHV tree-level amplitude is given by the volume of a certain polyhedron in *dual* momentum-twistor space and the BCFW expansion of the amplitude [4, 5] was interpreted as a particular triangulation of this volume. This picture was later extended to all NMHV tree-level amplitudes [50]. In contrast, higher  $k$  tree-level amplitudes and loop integrands have *not* as of yet been directly identified as volumes. Instead, the Amplituhedron is defined in momentum twistor space, where tree-level amplitudes and all-loop integrands are differential forms rather than volumes. The existence of a *dual Amplituhedron* where amplitudes are

interpreted as literal volumes is a very natural and important open problem. Non-trivial evidence for the existence of such a dual picture was given in [54, 60, 86]. In particular, it was shown for many examples that both tree-level amplitudes and loop integrands are *positive* when evaluated inside the Amplituhedron, which is reminiscent of the volume positivity. Interestingly, this property also seems to hold for some IR safe quantities post integration [83]. Here, we make a further major step in this direction. In particular, we show that the local expansion of the one-loop MHV amplitudes in terms of chiral pentagon integrals [123] can be naturally interpreted as the internal triangulation of the putative dual Amplituhedron. We make this statement precise on two-dimensional boundaries of the full geometry, where the space reduces to polygons and the dualization procedure is well-defined. Our main tool is the reformulation of the Amplituhedron using sign flips [58]. In the process of interpreting the chiral pentagons geometrically, we introduce more general positive spaces defined by sign-flip conditions. Surprisingly, the logarithmic forms of the maximal sign-flip spaces are chiral octagons, originally introduced in [123] as local building blocks for one-loop integrands.

This chapter is organized as follows: In section 2.2, we introduce the Amplituhedron geometry and then focus on the MHV one-loop case, where we discuss the projective geometry of lines in  $\mathbb{P}^3$  and the positions of physical and unphysical singularities. We also pose the question of the role of the chiral pentagon expansion in the context of the dual Amplituhedron. In section 2.4, we discuss how to associate a geometric space to a  $d$  log form and classify all such one-loop geometries. We show that the set of these one-loop spaces is bounded by the number of sign flips in the propagator space, and we determine the logarithmic forms for all of these spaces. In section 2.5, we discuss the geometry of chiral pentagons in detail and show that they naturally triangulate a different positive space which we call the Amplituhedron-Prime. This space has an identical boundary structure as the original Amplituhedron and therefore corresponds to the same logarithmic form. In section 2.6, we show that on all two-dimensional

boundaries both spaces map under dualization to the same geometry, and the chiral pentagons internally triangulate this dual Amplituhedron space. We finally conclude with some future directions in section 2.7. Various technical details are covered in four appendices.

## 2.2 Amplituhedron geometry

### Momentum twistors and the Amplituhedron's kinematic space

Scattering amplitudes in planar  $\mathcal{N} = 4$  sYM are naturally described in momentum twistor space [48]. Since the same kinematic space also plays a major role in the definition of the Amplituhedron geometry [56], we briefly review some of the salient features of projective geometry and momentum twistor space that are relevant to our discussions. These concepts are of course well known (see e.g. [48, 57, 123]), but for convenience we recall them telegraphically.

A key feature of the twistor correspondence [124] is the relation between points  $x$  in Minkowski spacetime and lines  $\mathcal{L}$  in twistor space. For planar scattering amplitudes, the relevant "spacetime" is dual momentum space where region momenta  $x_a$  are related to cyclically ordered external momenta  $p_a$  via  $p_a = x_a - x_{a-1}$ . Dual momentum space trivializes momentum conservation by the identification  $x_{n+1} = x_1$ .

The kinematic data for  $n$ -point massless planar scattering amplitudes can be efficiently encoded in  $n$  momentum twistors [48], denoted  $Z_a^I$ , where  $a = 1, \dots, n$  labels the particles and  $I = 1, \dots, 4$  is an  $SL(4)$  index on which dual conformal symmetry acts linearly. The natural  $SL(4)$  invariant is the antisymmetric contraction of four momentum twistors with the Levi-Civita tensor, which we denote as

$$\langle abcd \rangle := \epsilon_{IJKL} Z_a^I Z_b^J Z_c^K Z_d^L. \quad (2.2.1)$$

Scattering amplitudes in planar  $\mathcal{N} = 4$  sYM are invariant under both  $SL(4)$  transformations and the action of the little group i.e., the rescaling  $Z_a \mapsto t_a Z_a$ . This rescaling invariance implies that the external data lives in the projective space  $\mathbb{P}^3$ . Moreover,

in terms of the  $Z_a$  the amplitudes are invariant under a (twisted) cyclic symmetry: for the  $N^k$ MHV helicity sector the amplitude is invariant under the transformation  $Z_1 \mapsto Z_2, Z_2 \mapsto Z_3, \dots, Z_n \mapsto \widehat{Z}_1 := (-1)^{k-1} Z_1$  of the external data.

Incorporating (dual) loop momenta  $y$  into the picture is achieved by associating a line  $\mathcal{L}$  to  $y$ . We will often make use of the following notation: since lines in twistor space are characterized by the linear span of two representative points, we denote the line associated to  $x_a \leftrightarrow \mathcal{L}_a := (Z_a, Z_{a+1}) := (a\ a+1)$  and  $y \leftrightarrow \mathcal{L}_y := (AB)$ . For each loop, we can represent the corresponding line by two arbitrary momentum twistors  $Z_A$  and  $Z_B$ , defined modulo  $GL(2)$  transformations that leave the line invariant. We can furthermore expand  $Z_A$  and  $Z_B$  in an arbitrary basis of four linearly independent twistors  $Z_i, Z_j, Z_k$ , and  $Z_\ell$  and fix the  $GL(2)$  redundancy,<sup>1</sup>

$$Z_A = Z_i + \alpha_1 Z_k + \alpha_2 Z_\ell, \quad Z_B = Z_j + \alpha_3 Z_k + \alpha_4 Z_\ell. \quad (2.2.2)$$

In this chapter, we make regular use of such expansions, and depending on the purpose, we chose convenient expansion twistors. Quite nicely, the four unconstrained parameters  $\alpha_i$  in the twistor expansion of eq. (2.2.2) match the four degrees of freedom of an off-shell Feynman loop momentum.

If we consider the analog of a generic Lorentz-invariant in dual momentum space  $x_{ab}^2 = (p_a + p_{a+1} + \dots + p_{b-1})^2$  in momentum twistor space, we realize that this quantity breaks conformal invariance,

$$x_{ab}^2 = \frac{\langle aa+1b+1 \rangle}{\langle aa+1 \rangle \langle bb+1 \rangle}, \quad (2.2.3)$$

as signaled by the appearance of the two-brackets in the denominator. In dual conformally invariant quantities, all two-brackets drop out and we therefore do not discuss them any further. Crucially, such non-light-like Lorentz invariants are important to characterize loop-propagators, where any local pole of the integrand is given by

$$\text{local pole} \leftrightarrow \langle ABii+1 \rangle. \quad (2.2.4)$$

---

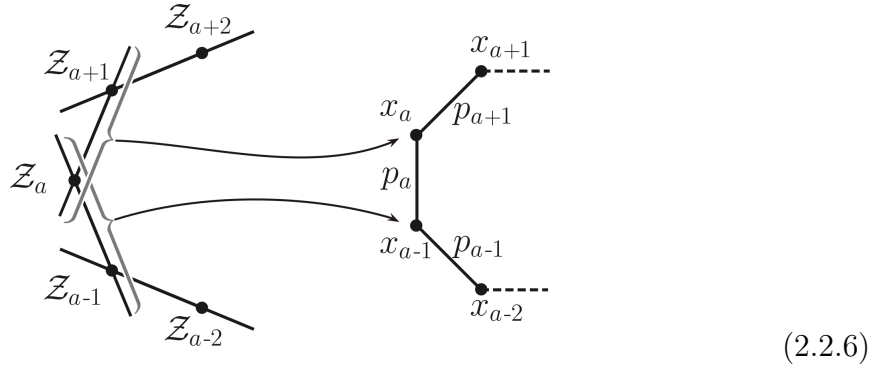
<sup>1</sup>Note that this choice of coordinates fixes the bracket  $\langle ABk\ell \rangle = \langle ijkl \rangle$  to be a loop-momentum independent function of the external kinematics.

In the following it will be important that any other four-bracket involving the loop-line  $(AB)$  together with an arbitrary “external” line  $X$  constitutes a *spurious pole* if it appears in the denominator of some integrand

$$\text{spurious pole} \leftrightarrow \langle ABX \rangle, \quad \text{if } X \neq (ii+1). \quad (2.2.5)$$

Below, we will see many examples of spurious poles that occur in various expansions of a scattering amplitude.

One additional feature of the twistor correspondence is the following fact: whenever two spacetime points  $x_a$  and  $x_b$  are null separated, the associated lines in twistor space  $\mathcal{L}_a$  and  $\mathcal{L}_b$  intersect. This leads to special configurations of lines which can be concisely summarized in the following image [123]



For a more detailed introduction to the twistor correspondence, we refer directly to the above references [48, 57, 123].

Finally, let us elaborate on the connection between twistor geometry and the analytic structure of scattering amplitudes that will play an important role in this chapter. There is an intimate relation between configurations of (loop) lines in momentum twistor space and certain restricted kinematic configurations of loop momenta on unitarity cuts of loop integrands or local integrals. At one loop, we can depict the off-shell configuration of lines in twistor space corresponding to a generic loop integrand (either of the amplitude or of an integral) by a set of lines corresponding to external dual momenta, together with a line  $(AB)$  in a generic configuration (parameterized via

eq. (2.2.2)),

$$(2.2.7)$$

In this setup, the loop-line  $(AB)$  does not intersect any of the lines associated to external kinematic points. In the next step, one could go to codimension one configurations by imposing one condition, e.g.  $\langle ABii+1 \rangle = 0$ , which geometrically means that the lines  $(AB)$  and  $(ii+1)$  intersect.

$$(2.2.8)$$

At the level of cuts, this corresponds to setting a single propagator  $\langle ABii+1 \rangle = 0$  to zero. This codimension-one configuration for the line  $(AB)$  can be parameterized by three degrees of freedom. The intersection implies that one of the defining points of the  $(AB)$ -loop lies on the line  $(ii+1)$ . Taking into account the projectivity of the external data, one possible parametrization is

$$Z_A = Z_i + \alpha_1 Z_{i+1}, \quad Z_B = Z_j + \alpha_2 Z_k + \alpha_3 Z_\ell. \quad (2.2.9)$$

In subsequent steps, one can impose additional constraints to end up on codimension-two, three, or four configurations of the line  $(AB)$ . For completeness, we have included a list of higher codimension boundaries and their associated cut configurations in appendix A.

### 2.2.1 Topological sign-flip definition of the Amplituhedron

The Amplituhedron is defined by three types of positivity conditions [58]. First, we have inequalities which carve out the positive part of the external kinematic space; these



conditions depend only on the helicity configuration of interest and are loop-momentum independent. For  $N^k$ MHV amplitudes the conditions read

$$\begin{aligned} N^k\text{MHV ext. positivity: } \langle ii+1jj+1 \rangle &> 0, \\ \text{sequence } \{\langle abb+1i \rangle\}_{i \neq a, b, b+1} &\text{ has } k \text{ sign flips,} \end{aligned} \tag{2.2.10}$$

where the twisted cyclic symmetry implies that  $(-1)^{k-1} \langle n1ii+1 \rangle > 0$ . For the simplest case of MHV ( $k = 0$ ) amplitudes the positivity of the external data as defined in eq. (2.2.10) is equivalent to all ordered brackets being positive,

$$\text{MHV ext. positivity: } \langle ijkl \rangle > 0, \quad \text{for } i < j < k < l. \tag{2.2.11}$$

Second, there are inequalities between the loop variables  $(AB)$  and the external data, again naturally expressed in terms of sign flips,<sup>2</sup>

$$\begin{aligned} N^k\text{MHV loop positivity: } \langle ABii+1 \rangle &> 0, \\ \text{sequence } \{\langle ABij \rangle\}_{j \neq i} &\text{ has } k+2 \text{ sign flips.} \end{aligned} \tag{2.2.12}$$

Finally, for multi-loop calculations, the third type of positivity conditions demand that all loops are mutually positive,

$$\text{multi-loop positivity: } \langle (AB)_i (AB)_j \rangle > 0, \quad \text{for } i \neq j = 1, \dots, L. \tag{2.2.13}$$

The set of conditions in eqs. (2.2.10), (2.2.12), and (2.2.13) define the general loop-level Amplituhedron  $\mathcal{A}^{(n,k,L)}$  relevant for  $n$ -particle  $N^k$ MHV  $L$ -loop integrands in the space of  $L$  lines  $(AB)_1, \dots, (AB)_L$  and  $n$  momentum twistors  $Z_1, \dots, Z_n$ . As such, the space defined by eqs. (2.2.10), (2.2.12), and (2.2.13) constitutes a highly nontrivial example of a *positive geometry* [60]. In this setup, the  $n$ -point  $N^k$ MHV  $L$ -loop integrand is conjectured to be the unique degree  $4(k+L)$  differential form on this space defined by having logarithmic singularities on all its boundaries. We denote this form (that is, the

---

<sup>2</sup>As we will see in subsection 2.2.2, for MHV and  $\overline{\text{MHV}}$  amplitudes, there is an equivalent formulation of the loop-positivity given in eqs. (2.2.31) and (2.2.32), respectively.

integrand) by  $\Omega^{(n,k,L)}$ ,<sup>3</sup>

$$\Omega^{(n,k,L)} = \prod_{i=1}^L \langle (AB)_i d^2 A_i \rangle \langle (AB)_i d^2 B_i \rangle \times \omega^{(n,k,L)}, \quad (2.2.14)$$

where  $\omega^{(n,k,L)}$  is a  $4k$ -form in external momentum twistors  $Z_a$ , but is simply a rational function in the loop variables  $(AB)_1, \dots, (AB)_L$ . The loop integrand can be obtained by replacing the differentials  $dZ_a$  with the fermionic Grassmann variables  $\eta_a$  to work directly in on-shell superspace. For MHV amplitudes,  $\omega^{(n,0,L)}$  is just a rational function of  $Z_a$  and  $(AB)_i$  and directly constitutes the loop integrand.

### Rudiments of positive geometry

In the course of exploring the geometric properties of the local representation of loop integrands, we shall naturally encounter a variety of “spaces.” Loosely speaking, we define a *geometric space* in this chapter to be a collection of inequalities imposed on four-brackets involving the loop line  $(AB)$ . By parametrizing  $(AB)$  as above in terms of four (real) degrees of freedom  $x_1, \dots, x_4$ , any four-bracket between  $(AB)$  and a bitwistor  $X_i$  becomes a polynomial  $\mathbf{p}_i(x_1, \dots, x_4) := \langle ABX_i \rangle$ . A more precise definition of a geometric space  $S$  is then a semialgebraic set defined by some number say,  $d$ , of inequalities

$$S = \{(x_1, \dots, x_4) | \mathbf{p}_1 > 0, \dots, \mathbf{p}_d > 0\}. \quad (2.2.15)$$

Note that this definition does not require the existence of a canonical form, and thus may or may not be a positive geometry satisfying the recursive definition of [60]. It may happen that no line in  $\mathbb{P}^3$  satisfies the conditions we impose, which means eq. (2.2.15) would be equivalent to the empty set; we shall refer to such spaces as *empty*.

The existence of a canonical form with logarithmic singularities on all boundaries puts further constraints on the general geometric space  $S$ . In particular, since any logarithmic form in the one-loop space is of degree four and can be written as the  $d \log$

---

<sup>3</sup>We commonly use the notation that all capital forms  $\Omega$  include the loop measure, whereas for lower-case forms  $\omega$  the measure has been stripped off.

of four (projectively invariant) ratios,<sup>4</sup> any one-loop *positive geometry* must be defined by at least five inequalities. Any space defined by four or fewer inequalities must have only the trivial form  $\Omega = 0$ ; throughout this chapter we refer to such geometries as *zero form spaces*.

### 2.2.2 One-loop MHV and $\overline{\text{MHV}}$ spaces

Following the general Amplituhedron definitions above, let us now specialize to the geometry relevant to MHV one-loop amplitudes. As stated previously, for MHV integrands (i.e.,  $k = 0$ ) the positivity conditions on the external data eq. (2.2.10) simplify significantly to eq. (2.2.11). Besides the MHV integrand, there is another one-loop integrand which naturally lives in the same kinematic space: namely, its parity conjugate. In twistor space, spacetime parity is implemented by the duality under the exchange of points and planes,  $Z_a \leftrightarrow W_a := (a-1aa+1)$  (often, we will use the alternative notation  $\bar{a} := (a-1aa+1)$ ). Thus, we will refer to this “dual” space, as well as its corresponding canonical form, with the moniker “ $\overline{\text{MHV}}$ ,” despite the fact that the actual  $\overline{\text{MHV}}$  Amplituhedron corresponds to setting  $k = n-2$ , which yields a slightly different set of positivity constraints on the external data (see eq. (2.2.10)). Despite the fact that these two spaces are not equivalent (because the definition of each involves different positivity conditions on the external data!), their canonical forms are trivially related by stripping the overall tree-level amplitude prefactor.

Both the MHV and  $\overline{\text{MHV}}$  integrands have only *local* poles; equivalently, the only codimension-one boundaries of both geometries are the loci where  $\langle ABii+1 \rangle = 0$ . We can think of the MHV and  $\overline{\text{MHV}}$  spaces as being cut out from a “larger” space defined only by  $\langle ijkl \rangle > 0$ , for  $i < j < k < l$ , and  $\langle ABii+1 \rangle > 0$ , *without any additional constraints*. For reasons which will become more clear below, we call this space an “achiral” one-loop space. By construction, its codimension-one boundaries are the same

---

<sup>4</sup>Since we can always rescale the entry of any  $d$  log form by a four-bracket involving only the external data, it is always trivial to make any entry projective in all  $Z_i$ , without modifying the canonical form (or, in the case of MHV data, affecting the overall sign of the entry). In this chapter we shall often neglect to write such factors, meaning our  $d$  log entries will be manifestly projective only in  $(AB)$ .

as those of the MHV and  $\overline{\text{MHV}}$  subspaces. From this perspective, it is quite nontrivial that there even exist two distinct ways of slicing the achiral space without introducing additional codimension-one (spurious) boundaries. Since the notion of chiralization plays a pivotal role in our analysis of local triangulations throughout this chapter, in the following subsection we review some salient features of the MHV and  $\overline{\text{MHV}}$  one-loop geometries.

### 2.2.3 Boundaries of MHV amplitudes

In this subsection, we briefly discuss the geometric boundaries of the “Kermit” expansion of one-loop MHV amplitudes [125]. In particular, we will show how to detect whether or not certain boundaries are present in the geometry and if the corresponding poles appear in the logarithmic form. This discussion allows us to introduce the necessary notation and concepts used in our later analysis of chiral pentagons.

The inequalities defining the one-loop MHV Amplituhedron are a special case of eq. (2.2.12), and involve the usual positivity of adjacent brackets as well as a sign-flip condition:

$$\begin{aligned} \text{MHV loop positivity: } \quad \langle ABi+1 \rangle &> 0, \\ \{\langle AB12 \rangle, \dots, \langle AB1n \rangle\} &\text{ has two sign flips,} \end{aligned} \tag{2.2.16}$$

where we have chosen the sequence  $\{\langle AB1i \rangle\}_{i=2, \dots, n}$  only for specificity and to easily handle the twisted cyclic symmetry in the last bracket of the sequence. There are a number of sign choices for the brackets appearing in eq. (2.2.16) consistent with two sign flips, which can be labelled by two indices  $i, j$  indicating the brackets  $\langle AB1i \rangle$  and  $\langle AB1j \rangle$  where the sign flip occurs. The geometry of these individual sign-flip patterns is completely well understood: the pattern where the sign flips occur at indices  $i$  and  $j$  is directly associated to a “Kermit” which corresponds to a particular cell in the positive Grassmannian. In the following, we make repeated use of these sign-flip patterns and

often denote brackets by their respective sign, e.g., for the  $(i, j)$  flip term,

$$\begin{aligned} & \{\langle AB12 \rangle, \dots, \langle AB1i \rangle, \langle AB1i+1 \rangle, \dots, \langle AB1j \rangle, \langle AB1j+1 \rangle, \dots, \langle AB1n \rangle\} \\ & \mapsto \{+, \dots, +, -, \dots, -, +, \dots, +\}. \end{aligned} \quad (2.2.17)$$

For the  $(i, j)$  sign-flip region, the line  $(AB)$  can be conveniently parametrized as

$$A = Z_1 + \alpha_i Z_i + \alpha_{i+1} Z_{i+1}, \quad B = -Z_1 + \alpha_j Z_j + \alpha_{j+1} Z_{j+1}. \quad (2.2.18)$$

In this coordinate chart, the inequalities in eq. (2.2.17) are equivalent to  $\alpha_i, \alpha_{i+1}, \alpha_j, \alpha_{j+1} > 0$  and therefore the canonical form is simply the  $d \log$  form in all variables.<sup>5</sup> Written projectively, this yields the expression for the canonical form (stripping off the measure  $\langle ABd^2A \rangle \langle ABd^2B \rangle$ )

$$\omega^{(n,0,1)} = \sum_{i < j} \omega_n^{(i,j)} \equiv \sum_{i < j} \frac{\langle AB(1ii+1) \cap (1jj+1) \rangle^2}{\langle AB1i \rangle \langle AB1i+1 \rangle \langle ABii+1 \rangle \langle AB1j \rangle \langle AB1j+1 \rangle \langle ABjj+1 \rangle}, \quad (2.2.19)$$

where  $(1ii+1) \cap (1jj+1)$  is the line in which the planes  $(1ii+1)$  and  $(1jj+1)$  intersect.<sup>6</sup> By construction, each term in this expansion is associated with a non-overlapping piece of the amplitude; in other words, this collection of cells provides an honest triangulation by introducing term-wise spurious poles of the form  $\langle AB1i \rangle$  in the denominator. The fact that these individual sign-flip spaces are non-overlapping follows directly from the observation that different Kermit cells differ by the signs of at least one of the inequalities defining their regions.

Let us provide a simple concrete five-point example where there are three different sign patterns with two sign-flips. Since the  $\langle AB12 \rangle$  and  $\langle AB15 \rangle$  brackets are forced to be positive by the loop conditions in eq. (2.2.16), the three sign patterns are labelled

---

<sup>5</sup>For detailed discussions and numerous examples of going from inequalities to forms, see e.g. [58, 64].

<sup>6</sup>A review of the projective geometry relevant to this work is given in section 2.2 and appendix A.

by the signs of  $\langle AB13 \rangle$  and  $\langle AB14 \rangle$ , i.e.,

$(i, j)$	$\langle AB12 \rangle$	$\langle AB13 \rangle$	$\langle AB14 \rangle$	$\langle AB15 \rangle$
(3,4)	+	+	-	+
(2,3)	+	-	+	+
(2,4)	+	-	-	+

(2.2.20)

In the first column we indicate the locations  $(i, j)$  at which the sign flips occur, which directly match the labels in eq. (2.2.19). Note that although all spaces are naïvely defined by the same number of inequalities, in this table, the spaces where  $j = i+1$  are geometrically simpler than the generic case. To illustrate this point and make our notion of “geometric boundaries” clear, we now consider the (3, 4) cell in more detail. The analysis of the properties of this space is particularly amenable to the following parametrization:

$$A = Z_2 + wZ_1 + xZ_5, \quad B = Z_3 + yZ_1 + zZ_5. \quad (2.2.21)$$

This choice of coordinates gauge-fixes  $\langle AB15 \rangle = \langle 1235 \rangle > 0$ . Imposing  $\langle ABi+1 \rangle > 0$ ,  $\langle AB13 \rangle > 0$  and  $\langle AB14 \rangle < 0$  defines the (3, 4) Kermit space:

$$\begin{aligned}
\langle AB12 \rangle &= -x\langle 1235 \rangle > 0, \\
\langle AB23 \rangle &= (wz - xy)\langle 1235 \rangle > 0, \\
\langle AB34 \rangle &= -y\langle 1234 \rangle + (wz - xy)\langle 1345 \rangle + z\langle 2345 \rangle > 0, \\
\langle AB45 \rangle &= -y\langle 1245 \rangle + w\langle 1345 \rangle + \langle 2345 \rangle > 0, \\
\langle AB15 \rangle &= \langle 1235 \rangle > 0, \\
\langle AB13 \rangle &= -z\langle 1235 \rangle > 0, \\
\langle AB14 \rangle &= \langle 1234 \rangle - z\langle 1245 \rangle + x\langle 1345 \rangle < 0.
\end{aligned} \quad (2.2.22)$$

The codimension-one boundaries of this space correspond to localizing one (and only one) of the variables  $w, x, y, z$  by setting one of the brackets in eq. (2.2.22) to zero. However, not all of the inequalities in eq. (2.2.22) are boundaries. In particular, we will

now demonstrate that setting either  $\langle AB12 \rangle \rightarrow 0$ ,  $\langle AB23 \rangle \rightarrow 0$ , or  $\langle AB14 \rangle \rightarrow 0$  leads to an inconsistent set of inequalities in the three remaining variables, thus proving that none of these brackets are geometric boundaries of the (3, 4) Kermit. First, consider  $\langle AB12 \rangle \rightarrow 0$  which, in our parametrization, corresponds to sending  $x \rightarrow 0$ . From eq. (2.2.22), we have

$$\langle AB14 \rangle \xrightarrow{x \rightarrow 0} \langle 1234 \rangle - z \langle 1245 \rangle < 0, \quad (2.2.23)$$

which implies that  $z > \langle 1234 \rangle / \langle 1245 \rangle > 0$ . This is inconsistent with  $\langle AB13 \rangle = -z \langle 1235 \rangle > 0$ , which demands that  $z < 0$ . Thus,  $\langle AB12 \rangle \rightarrow 0$  is not a codimension-one boundary of the space. Next, consider  $\langle AB23 \rangle \rightarrow 0$ , which can be parametrized as  $w \rightarrow xy/z$ . In this case, the space defined by eq. (2.2.22) is equivalent to  $x, z < 0$  and, after some algebraic manipulation,

$$\begin{aligned} \langle AB34 \rangle &\xrightarrow{w \rightarrow xy/z} -y \langle 1234 \rangle + z \langle 2345 \rangle > 0, \\ \langle AB45 \rangle &\xrightarrow{w \rightarrow xy/z} y(x \langle 1345 \rangle - z \langle 1245 \rangle) + z \langle 2345 \rangle < 0, \\ \langle AB14 \rangle &\xrightarrow{w \rightarrow xy/z} \langle 1234 \rangle - z \langle 1245 \rangle + x \langle 1345 \rangle < 0. \end{aligned} \quad (2.2.24)$$

The first inequality in eq. (2.2.24) together with  $z < 0$  implies that  $y < 0$ . Multiplying the third inequality in eq. (2.2.24) by  $y$  and adding  $z \langle 2345 \rangle$  to both sides, we find

$$y(x \langle 1345 \rangle - z \langle 1245 \rangle) + z \langle 2345 \rangle > -y \langle 1234 \rangle + z \langle 2345 \rangle > 0, \quad (2.2.25)$$

which is incompatible with the second inequality of eq. (2.2.24). Finally, consider setting  $\langle AB14 \rangle \rightarrow 0$ , which corresponds to  $x \rightarrow (z \langle 1245 \rangle - \langle 1234 \rangle) / \langle 1345 \rangle$ . In this case, eq. (2.2.22) yields

$$\begin{aligned} \langle AB34 \rangle &\rightarrow z(-y \langle 1245 \rangle + w \langle 1345 \rangle + \langle 2345 \rangle) > 0, \\ \langle AB45 \rangle &\rightarrow -y \langle 1245 \rangle + w \langle 1345 \rangle + \langle 2345 \rangle > 0, \end{aligned} \quad (2.2.26)$$

which, together with  $z < 0$ , are incompatible.

In contrast to the three examples just considered, it is straightforward to verify that no such inconsistency is found upon setting either  $\langle AB34 \rangle \rightarrow 0$ ,  $\langle AB45 \rangle \rightarrow 0$  or

$\langle AB13 \rangle \rightarrow 0$ . Thus, these three brackets are geometric boundaries of the space defined in eq. (2.2.22). In fact,  $\langle AB15 \rangle \rightarrow 0$  is also a geometric boundary of the full projective space; while this fact is obscured in our choice of gauge-fixing, it can be proven with a similar argument as above by working in an alternative parametrization (which fixes the sign of some other four-bracket).

Thus, the (3, 4) cell has four codimension-one boundaries  $\langle AB34 \rangle$ ,  $\langle AB45 \rangle$ ,  $\langle AB15 \rangle$  and  $\langle AB13 \rangle$  which also correspond to the allowed poles in the associated canonical form. An analogous argument holds for the (2, 3) cell, while the (2, 4) cell is a generic Kermit with six accessible codimension-one boundaries. A straightforward computation yields the following expressions for the canonical forms:

$$\begin{aligned} \omega_5^{(3,4)} &= \frac{\langle 1345 \rangle^2}{\langle AB13 \rangle \langle AB34 \rangle \langle AB45 \rangle \langle AB15 \rangle}, & \omega_5^{(2,3)} &= \frac{\langle 1234 \rangle^2}{\langle AB12 \rangle \langle AB23 \rangle \langle AB34 \rangle \langle AB14 \rangle}, \\ \omega_5^{(2,4)} &= \frac{\langle AB(123) \cap (145) \rangle^2}{\langle AB12 \rangle \langle AB23 \rangle \langle AB13 \rangle \langle AB14 \rangle \langle AB15 \rangle \langle AB45 \rangle}. \end{aligned} \quad (2.2.27)$$

The spurious boundary  $\langle AB13 \rangle = 0$  cancels geometrically between the first and third sign-flip terms in eq. (2.2.20). This can be seen in the parametrization of eq. (2.2.21) by sending  $z \rightarrow 0$  in both spaces, and observing that the contributions completely overlap and therefore cancel. A similar analysis shows that the spurious boundary  $\langle AB14 \rangle = 0$  cancels between the second and third space in eq. (2.2.20). Algebraically, the cancellation of spurious poles can be observed between the corresponding forms in eq. (2.2.27). We will see later that the algebraic cancellation of a spurious pole in the form is not, in general, sufficient to imply a geometric cancellation of the corresponding spurious boundary.

As indicated earlier, the one-loop MHV Amplituhedron space is a slice of a larger “achiral” positive space given only by the  $\langle AB_{i+1} \rangle > 0$  conditions. In the five-point example, the achiral space allows for arbitrary signs of the “spurious-pole” brackets  $\langle AB13 \rangle$ ,  $\langle AB14 \rangle$ . This means that in addition to the three sign-flip patterns of eq. (2.2.20), we have one additional sign-flip-zero space where both  $\langle AB13 \rangle$  and  $\langle AB14 \rangle$



are positive,

$\langle AB12 \rangle$	$\langle AB13 \rangle$	$\langle AB14 \rangle$	$\langle AB15 \rangle$
+	+	+	+

(2.2.28)

Having zero sign flips in the sequence  $\{\langle AB1i \rangle\}$  actually implies that all  $\langle ABij \rangle > 0$  are positive for any  $i < j$ . The corresponding logarithmic form reproduces the five-point  $\overline{\text{MHV}}$  amplitude, and the  $\{++\}$  sign pattern is an example of the  $\overline{\text{MHV}}$  space discussed above and is directly related to the MHV space by parity conjugation. This has a direct generalization to higher points: the MHV space has two sign flips in the  $\{\langle AB1i \rangle\}$  sequence, while the  $\overline{\text{MHV}}$  parity conjugate has zero sign flips. At higher points, naïvely, there are additional subregions of the larger achiral space with more than two sign-flips. For example, at six points we can have

$\langle AB12 \rangle$	$\langle AB13 \rangle$	$\langle AB14 \rangle$	$\langle AB15 \rangle$	$\langle AB16 \rangle$
+	-	+	-	+

(2.2.29)

However, this combination of inequalities is an example of an *empty space* discussed in subsection 2.2.1. In fact, it is known [58] that, for MHV external data, the same is true for all spaces with more than two sign flips! Thus, remarkably the achiral space can be cut into two (and only two) chiral subspaces, MHV and  $\overline{\text{MHV}}$ , which have only local boundaries of the form  $\langle ABii+1 \rangle = 0$ .

Note that the sign-flip-zero ( $\overline{\text{MHV}}$ ) space in the five-point example of eq. (2.2.28) was not triangulated further into simpler subspaces (with spurious poles). Therefore, the generalization of this space at  $n$ -points has  $n$  boundaries, while any individual sign-flip-two region only has (up to) six codimension-one boundaries, as can be seen from the Kermit canonical form in eq. (2.2.19). It is therefore natural to ask whether or not we can analogously slice the sign-flip-zero region into simpler spaces with fewer boundaries, just as we did with the Kermit for the sign-flip-two MHV pattern. This slicing can be achieved by realizing that both MHV and  $\overline{\text{MHV}}$  spaces are related by parity,  $Z_a \leftrightarrow W_a$ . In particular, the  $n$ -point  $\overline{\text{MHV}}$  space has an equivalent definition as

the sign-flip-two space in the  $W_a$  coordinates, i.e., two sign flips in the sequence

$$\begin{aligned}
\text{“}\overline{\text{MHV}}\text{” positivity : } & \langle ijkl \rangle > 0, \quad \text{for } i < j < k < l, \\
& \langle ABii+1 \rangle > 0, \\
& \{ \langle AB\bar{1}2 \rangle, \langle AB\bar{1}3 \rangle, \dots, \langle AB\bar{1}n \rangle \} \quad \text{has two sign flips,}
\end{aligned} \tag{2.2.30}$$

where the  $\langle AB1i \rangle$  term in the MHV sequence eq. (2.2.16) has been replaced by  $\langle AB\bar{1}i \rangle$ , and  $(\bar{1}i)$  denotes the intersection of the planes  $\bar{1} = -(n12)$  and  $\bar{i} = (i-1ii+1)$ . By expanding the intersections in the first and last brackets in this sequence, we see they are invariant under conjugation (up to a factor that only depends on the external data) and are therefore both positive as a consequence of  $\langle AB12 \rangle, \langle AB1n \rangle > 0$ . In this definition, the  $\overline{\text{MHV}}$  space is triangulated by the collection of sign-flip-two regions of eq. (2.2.30), analogous to the Kermit triangulation of the MHV space. Using the sequence of brackets in eq. (2.2.30), we can conversely define the MHV space as the single sign-flip-zero region with all  $\langle AB\bar{i}j \rangle > 0$ , for  $i < j$  (always accounting for the twisted cyclic symmetry when  $i = 1$  or  $j = n$ ).

While breaking up the MHV and  $\overline{\text{MHV}}$  spaces into smaller regions using sign flips is a useful triangulation strategy, we can also characterize them in a uniform way as the sign-flip-zero regions in eq. (2.2.16) and eq. (2.2.30) respectively. In addition to  $\langle ABii+1 \rangle > 0$  and the  $k=0$  conditions on the external data eq. (2.2.11), we get:

$$\text{alternative MHV : } \langle AB\bar{i}j \rangle > 0, \quad \text{for all } i < j, \tag{2.2.31}$$

$$\text{alternative } \overline{\text{MHV}} : \langle ABij \rangle > 0, \quad \text{for all } i < j. \tag{2.2.32}$$

As we have seen, the Kermit expansion [125] of the MHV one-loop integrand in eq. (2.2.19) is in one-to-one correspondence with the sign-flip representation of the Amplituhedron, and it provides a very natural triangulation. We call this triangulation *internal*, emphasizing that it cuts the Amplituhedron into smaller pieces by introducing internal (spurious) boundaries. Each geometric space associated to a Kermit lies inside the Amplituhedron, but in addition to *physical* (Amplituhedron) boundaries it also has a

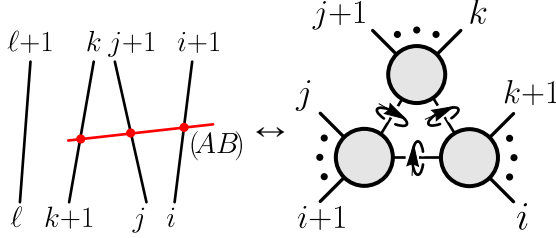
number of spurious boundaries of the form  $\langle AB1i \rangle = 0$ , which cancel geometrically when taking the collection of all Kermit. The analogs of Kermit expansions for higher  $k$  and  $L$  have been found in [64], and they involve more complicated spurious poles whose cancellations are nontrivial to demonstrate analytically.

### MHV and $\overline{\text{MHV}}$ geometry and allowed singularity structure

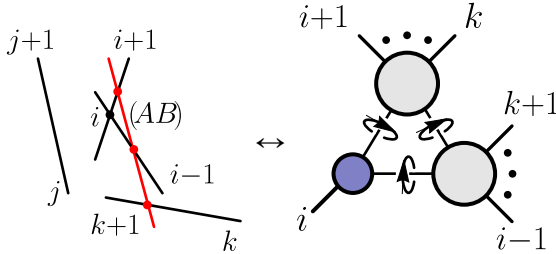
As we have laid out in section 2.2 and appendix A, taking residues of one-loop integrands in loop-momentum space is equivalent to localizing the line  $(AB)$  to special configurations with respect to the external  $(ii+1)$  lines. On the other hand, imposing a set of inequalities  $\{\langle ABX_1 \rangle > 0, \dots, \langle ABX_r \rangle > 0\}$ , where the  $X_i$  are some lines (involving external data) in  $\mathbb{P}^3$ , effectively slices the full configuration space of  $(AB)$  into smaller subspaces. A given subspace will generically contain a rather small subset of the possible special configurations associated to cuts of the integrand. The constraint that a cut-configuration of the loop line  $(AB)$  be compatible with the inequalities defining the positive geometry of interest becomes rather severe once we go deep into the cut structure to, say, codimension-four boundaries. Checking the compatibility of certain cut configurations and the geometric inequalities will then tell us which singularities are physical and which ones are spurious.

Let us illustrate this point explicitly in the case of the MHV one-loop geometry. As we discussed in eq. (2.2.16) and eq. (2.2.31), this space can be characterized by a simple set of inequalities,  $\langle ABii+1 \rangle > 0$  and  $\langle AB\bar{i}\bar{j} \rangle > 0$  (together with the conditions on the external data in eq. (2.2.10)). It is easy to verify that none of the codimension-one (eq. (2.2.8)) or two configurations (listed in eq. (A.0.4) of appendix A) violate any of these inequalities, so all of these singularities are physical. However, there are two spurious codimension-three configurations which violate the MHV inequalities: the

three-mass triple cut where  $(AB)$  intersects three non-adjacent lines,

not allowed in MHV:  , (2.2.33)

as well as the configuration where  $(AB)$  is in the plane  $(\bar{i})$  and intersects a non-adjacent line  $(kk+1)$ ,

not allowed in MHV:  . (2.2.34)

To prove that the three-mass triple cut of eq. (2.2.33) lies outside of the MHV Amplituhedron, we first consider the simplest six-point case where this cut first arises,  $\langle AB12 \rangle = \langle AB34 \rangle = \langle AB56 \rangle = 0$ . This cut can be parametrized by setting

$$\begin{aligned} (AB) &= ((Z_1 + xZ_2)34) \cap ((Z_1 + xZ_2)56) \\ &= (134) \cap (156) + x(134) \cap (256) + x(234) \cap (156) + x^2(234) \cap (256), \end{aligned} \tag{2.2.35}$$

where  $x$  parametrizes the intersection point of the lines  $(AB)$  and  $(12)$ . Because this cut is inconsistent with both the MHV and  $\overline{\text{MHV}}$  geometries, the proof that this cut configuration is spurious must follow directly from the inequalities which are valid in both spaces. For this example, these are the three inverse propagators

$$\begin{aligned} \langle AB23 \rangle &= \langle 1234 \rangle (\langle 1356 \rangle + x \langle 2356 \rangle) > 0, \\ \langle AB45 \rangle &= -(\langle 1345 \rangle + x \langle 2345 \rangle) (\langle 1456 \rangle + x \langle 2456 \rangle) > 0, \\ \langle AB16 \rangle &= \langle 1256 \rangle x (\langle 1346 \rangle + x \langle 2346 \rangle) > 0. \end{aligned} \tag{2.2.36}$$

This set of inequalities is equivalent to

$$-\frac{\langle 1345 \rangle}{\langle 2345 \rangle} < x < -\frac{\langle 1346 \rangle}{\langle 2346 \rangle} \quad \text{and} \quad x > -\frac{\langle 1356 \rangle}{\langle 2356 \rangle}. \quad (2.2.37)$$

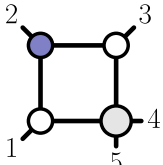
Non-trivially, the upper bound on  $x$  in the first inequality is inconsistent with the second lower bound given. Namely, by combining  $x < -\langle 1346 \rangle / \langle 2346 \rangle$  and  $x > -\langle 1356 \rangle / \langle 2356 \rangle$  we find, using the Schouten identity,

$$0 < \frac{\langle 1356 \rangle \langle 2346 \rangle - \langle 1346 \rangle \langle 2356 \rangle}{\langle 2346 \rangle \langle 2356 \rangle} = -\frac{\langle 1236 \rangle \langle 3456 \rangle}{\langle 2346 \rangle \langle 2356 \rangle} < 0, \quad (2.2.38)$$

which is a contradiction. This proof crucially depends on the simple external data positivity conditions relevant for the MHV and  $\overline{\text{MHV}}$  spaces. The general three-mass triple cut  $\langle ABii+1 \rangle = \langle ABjj+1 \rangle = \langle ABkk+1 \rangle = 0$  can be shown to be spurious by the obvious generalization of the parametrization of eq. (2.2.35), and the proof depends only on the inequalities adjacent to the cut propagators.

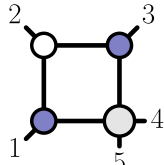
In contrast, the codimension-four leading singularities are much easier to analyze, as any inequality evaluated on such a configuration just reduces to a condition on the external data. In fact, simply demanding compatibility of the inequalities defining the MHV space eq. (2.2.31) evaluated on the leading singularity configurations listed in appendix A with the positivity constraints on the external data eq. (2.2.10) is enough to fix the positions of all MHV leading singularities to  $(AB) = (ij)$ . Said differently, any leading singularity *not* of this form will explicitly violate at least one of the inequalities defining the MHV space. For example, at five points, the line (13) is an allowed leading singularity, but its parity conjugate  $(\overline{13}) = -(512) \cap (234)$  is not.

allowed in MHV:



$(AB) = (13)$

not allowed in MHV:



$(AB) = (\overline{13})$

$$(2.2.39)$$

From the inequalities point of view, this can be clearly seen by evaluating  $\langle AB\overline{24} \rangle = \langle AB(123) \cap (345) \rangle$  on the forbidden leading singularity  $(AB) = (\overline{13})$ , which gives

$$\langle AB\overline{24} \rangle \Big|_{(\overline{13})} = -\langle (512) \cap (234) (123) \cap (345) \rangle = -\langle 1235 \rangle \langle 2345 \rangle \langle 1234 \rangle < 0, \quad (2.2.40)$$

and is incompatible with being inside the MHV Amplituhedron. This argument goes through at  $n$ -points. The leading singularities of the form  $(ij)$ , for  $i < j$ , are allowed precisely because of the nontrivial positivity conditions [54]

$$\langle AB\bar{k}\bar{\ell} \rangle|_{(ij)} = \langle ij\bar{k}\bar{\ell} \rangle > 0, \quad \text{for } i < j, \quad (2.2.41)$$

while the parity conjugate lines  $(\bar{i}\bar{j})$ , as well as all other codimension-four configurations listed in appendix A, are always inconsistent with at least one of the positivity constraints. Note that related analyses were performed in [82] in order to check admissible Landau singularities in planar  $\mathcal{N} = 4$  sYM.

#### 2.2.4 Positivity and the dual Amplituhedron

The original idea of linking scattering amplitudes to projective geometry appeared in the seminal work by Hodges [48] (which pre-dates the Amplituhedron) who showed that the six-particle NMHV tree-level amplitude can be interpreted as the *volume* of a polytope in *dual* momentum twistor space. Later it was shown that the same amplitude can also be associated with a *logarithmic differential form*,  $\Omega$ , directly in momentum twistor space. It is this picture of amplitudes as differential forms with logarithmic singularities that was later generalized to the Amplituhedron for all  $n$ ,  $k$ , and  $L$ . For many reasons, the original volume interpretation seems more fundamental than thinking about amplitudes as differential forms. This led to the conjecture of the existence of a *dual Amplituhedron* [54] whose volume calculates all scattering amplitudes in planar  $\mathcal{N} = 4$  sYM theory.

The only case for which we fully understand the volume interpretation, however, remains the NMHV tree-level amplitude. There, both the Amplituhedron and the dual Amplituhedron are certain polytopes in projective space  $\mathbb{P}^4$  which are related by the standard dualization procedure: vertices in the Amplituhedron space are mapped into faces of the dual Amplituhedron, and similarly for other boundaries (codimension  $r$  subspaces of the Amplituhedron map into codimension  $5 - r + 1$  subspaces of the dual Amplituhedron). It is not clear how to repeat the same procedure beyond NMHV

( $k > 1$ ) and/or at higher loops ( $L > 0$ ) where Amplituhedra are no longer polytopes but rather their generalizations to Grassmannians and beyond [56].

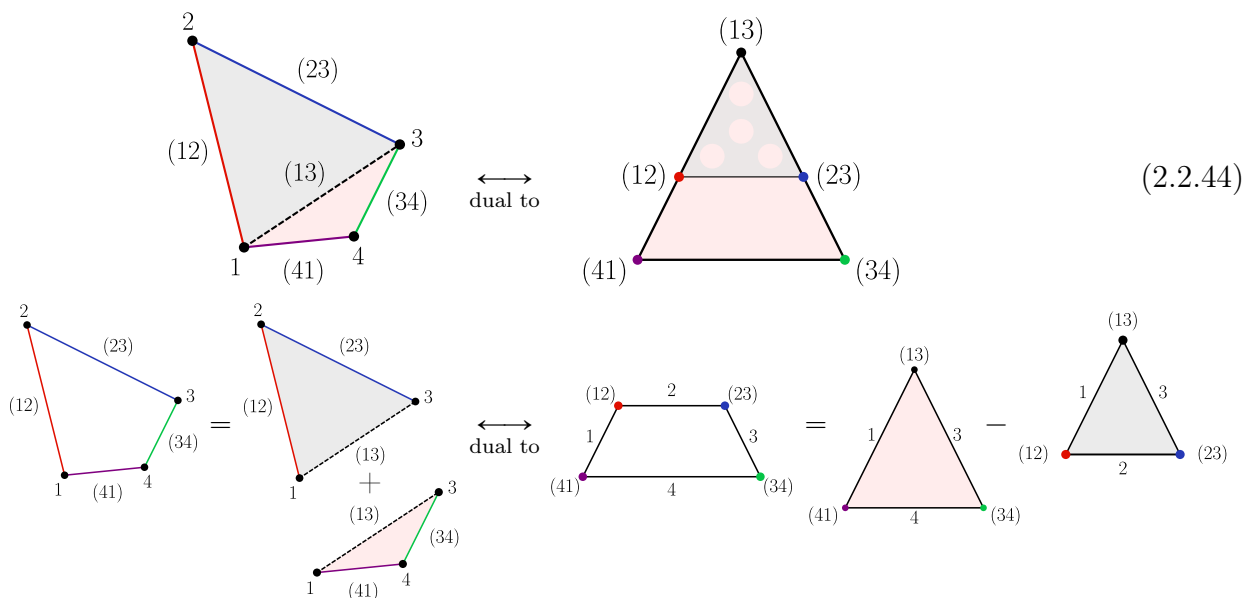
Even without an explicit definition of the dual Amplituhedron, there are two important properties which follow from its presumed existence. First, volumes are naturally *positive* and therefore, we would expect that amplitudes exhibit a similar positivity property. While the definition of the Amplituhedron is based on a set of positivity conditions eq. (2.2.10) and eq. (2.2.12), nothing a priori predicts any positivity properties of the differential form  $\Omega$ . However, if the amplitude also has a volume interpretation, then we expect that  $\Omega$  is positive in some suitable sense. Indeed, it was shown in [54] for many nontrivial examples that if we strip off the measure from  $\Omega$ , i.e.

$$\Omega^{(n,k,L)} = d\mu \omega^{(n,k,L)}, \quad (2.2.42)$$

then the integrand  $\omega^{(n,k,L)}$  (which is just the scattering amplitude) is in fact positive if evaluated inside the positive region for both  $Z_a$  and  $\mathcal{L}_i = (AB)_i$ . The positivity of  $\omega^{(n,k,L)}$  therefore serves as indirect evidence for the existence of a dual Amplituhedron and the volume interpretation of scattering amplitudes,

$$\omega^{(n,k,L)} = \int_{\tilde{\mathcal{A}}} dV. \quad (2.2.43)$$

where  $\tilde{\mathcal{A}}$  is the dual Amplituhedron space and  $dV$  is the appropriate volume form. An important clue on how to proceed in the search for the dual Amplituhedron is to investigate whether or not positivity is respected in the context of different triangulations of the Amplituhedron. Despite the fact that the full integrand  $\omega^{(n,k,L)}$  is positive inside the positive region, individual terms in e.g., the BCFW triangulation of  $\mathcal{A}_{n,k,L}$  do not have definite signs inside the positive space. While individual BCFW terms *internally* triangulate the Amplituhedron, in the dual picture, they get mapped to spaces that are partially outside of the dual Amplituhedron and therefore do not have a uniform sign. This is easiest to understand with a simple toy example of a quadrilateral in the projective plane:



The two triangles with vertices  $(123)$  and  $(134)$  triangulate the quadrilateral, but in the dual picture they correspond to triangles which lie partially outside of the dual quadrilateral. Therefore, while the triangles on the left-hand-side of (2.2.44) give an *internal* triangulation of the original space via the line  $(13)$ , in the dual picture, this corresponds to an *external* triangulation with an external triangulation point  $(13)$  that is outside the dual space. In the same sense, internal triangulations of the Amplituhedron are expected to externally triangulate the dual Amplituhedron.

In particular, the Kermit expansion of MHV amplitudes internally triangulates the one-loop Amplituhedron [56] and—following our discussion above—is expected to externally triangulate the putative dual Amplituhedron. This external triangulation of the dual space therefore suggests that individual Kermits will not be positive term-wise (after stripping the measure) despite the positivity of the full one-loop integrand. We can see this non-positivity directly by looking at the denominators of the kermit forms: each Kermit contains denominator factors like  $\langle AB1i \rangle$  which do not have a fixed sign inside the Amplituhedron. Consequently, for fixed positive external data and an arbitrary point  $(AB)$  inside the MHV one-loop Amplituhedron, the stripped forms



$\omega_n^{(i,j)}$  in eq. (2.2.19) can have arbitrary signs.

It is very natural to ask about a term-wise positive expansion of the amplitude, which geometrically would provide an internal triangulation of the putative dual Amplituhedron. While we will not definitively establish the existence of a dual Amplituhedron in this chapter, it is easy to at least find a term-wise positive expansion of the amplitude. A priori, any such candidate expansion must have only *local* poles,  $\langle ABi+1 \rangle$  as only these terms have fixed signs, and in addition the numerator factors must be uniformly positive inside the Amplituhedron. As it turns out, the right candidate is the chiral pentagon expansion [41, 50, 123]<sup>7</sup>

$$\begin{aligned}
 \omega^{(n,0,1)} &= \sum_{i < j} \omega_{ij}^{(n)} = \sum_{i < j} \text{Diagram} \\
 &= \sum_{i < j} \frac{\langle 1ijn \rangle \langle AB\bar{i}j \rangle}{\langle ABi-1i \rangle \langle ABi+1 \rangle \langle ABj-1j \rangle \langle ABj+1 \rangle \langle AB1n \rangle}.
 \end{aligned} \tag{2.2.45}$$

As a consequence of the MHV loop-positivity eq. (2.2.31), together with the positivity of external data  $\langle ijkl \rangle > 0$  (for  $i < j < k < l$ ) in eq. (2.2.11), it can be seen that all four-brackets in eq. (2.2.45) are manifestly positive, including the loop-momentum dependent part of the numerator. Based on this positivity property of individual terms, the natural conjecture is that these chiral pentagons internally triangulate the dual Amplituhedron (but externally triangulate the original Amplituhedron). In our quadrilateral analogy, this would correspond to introducing a spurious triangulation point  $(12) \cap (34)$

---

<sup>7</sup>In the representation here, we have singled out a particular propagator  $\langle AB1n \rangle$  that appears in all diagrams and will also take a special role in our geometric considerations below. Furthermore, we point out that the chiral pentagon expansion contains various “boundary” terms that correspond to one-mass, and two-mass-hard box integrands. This should be contrasted to the older representations of one-loop  $n$ -point MHV amplitudes [2] in terms of two-mass easy boxes that only match the parity-even sector at the integrand level but are of course equivalent upon loop integration.

outside the quadrilateral,

$$(2.2.46)$$

While the chiral pentagons have only physical codimension-one poles  $\langle ABii+1 \rangle$  (we also refer to them as local poles), their higher codimension singularities are not all physical. For example, the generic chiral pentagon eq. (2.2.45) has a non-zero residue at the leading singularity location  $(AB) = (ijj+1) \cap (in1)$ , which is not a physical leading singularity of MHV amplitudes and corresponds to a cut solution labeled by the following on-shell function<sup>8</sup>

$$(2.2.47)$$

As we will show, in the original Amplituhedron geometry this means that all codimension-one boundaries are given by physical  $\langle ABii+1 \rangle = 0$  singularities analogous to the lines  $(ii+1)$  in eq. (2.2.46), whereas higher codimension boundaries can be spurious (such as the spurious triangulation vertex  $(12) \cap (34)$ ). In the dual picture, some of the first boundaries of chiral pentagon spaces are spurious, analogous to the spurious triangulation line of our quadrilateral example on the right-hand-side of eq. (2.2.46).

### 2.3 Geometry of $d$ log forms

In this section we lay the groundwork for further study of the relation between positive geometry and local triangulations of the Amplituhedron. As a first step, we

<sup>8</sup>Here, we make use of on-shell functions to label solutions to on-shell conditions and not the value of field theory cuts. This dual meaning of on-shell functions is common in the literature, see e.g. [126].

need to associate a geometric region to a particular local loop-integrand form. The most natural starting point for such an endeavour is the  $d \log$  representation of local integrands.

### 2.3.1 $d \log$ forms for pentagon integrands

It is our goal to associate a “local” positive geometry to each chiral pentagon and explore how they glue together into a larger geometric object. In a subsequent step, we define these new objects and find their connection to the Amplituhedron in section 2.5. Starting from the local representation of the one-loop MHV amplitude eq. (2.2.45), our only input information is the rational pentagon integrand. Due to the natural connection between  $d \log$  forms and positive geometry, we therefore rewrite the integrands appearing in eq. (2.2.45) as  $d \log$  forms [47],

$$\Omega_{ij}^{(n)} = \langle AB d^2 A \rangle \langle AB d^2 B \rangle \omega_{ij}^{(n)} = d \log f_1 d \log f_2 d \log f_3 d \log f_4, \quad (2.3.1)$$

where we suppress the wedge notation for differential forms and  $f_j$  are ratios of four-brackets (to be specified in eq. (2.3.3)). We would like to interpret this  $d \log$  form as the form with logarithmic singularities on a region which has fixed signs of all  $f_j$ . In particular, each  $f_j$  can be either positive or negative which leads to  $2^4 = 16$  different regions that each have the same  $d \log$  form. Furthermore, the change of variables eq. (2.3.1) is not unique and there are many different looking  $d \log$  forms that all have the same rational form appearing in eq. (2.2.45).

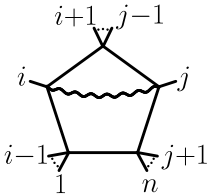
For the massless scalar box integral, which can be viewed as a particular  $n = 4$  degeneration of the chiral pentagon, there are at least two different  $d \log$  forms,

$$\begin{aligned} \Omega_{23}^{(4)} &= \begin{array}{c} 2 \\ \diagup \quad \diagdown \\ \square \\ \diagdown \quad \diagup \\ 1 \quad \quad 4 \end{array} = \frac{\langle AB d^2 A \rangle \langle AB d^2 B \rangle \langle 1234 \rangle^2}{\langle AB12 \rangle \langle AB23 \rangle \langle AB34 \rangle \langle AB14 \rangle} \\ &= d \log \frac{\langle AB12 \rangle}{\langle ABX \rangle} d \log \frac{\langle AB23 \rangle}{\langle ABX \rangle} d \log \frac{\langle AB34 \rangle}{\langle ABX \rangle} d \log \frac{\langle AB14 \rangle}{\langle ABX \rangle} \end{aligned} \quad (2.3.2)$$

where we can choose between the two solutions of the quadruple cut,  $X = (13)$  or  $X = (24)$ . For  $X = (13)$  the  $d \log$  form eq. (2.3.2) explicitly depends on  $\langle AB13 \rangle$ .

Therefore, one might worry that this spurious pole could show up in the rational form.<sup>9</sup> However, by construction, the  $d\log$  form cannot have  $\langle AB13 \rangle$  or  $\langle AB24 \rangle$  as an actual singularity. Algebraically, the absence of the spurious poles from the rational integrand derived from the  $d\log$  form eq. (2.3.2) follows from non-trivial kinematic identities.

For more complicated integrands, various alternative  $d\log$  forms for the same rational integrand might look remarkably different. This is also the case for the generic chiral pentagon we discuss next. One particular  $d\log$  form for this integrand has been written down in ref. [47] which manifestly breaks the  $ij$  flip symmetry of the diagram,

$$\begin{aligned} \Omega_{ij}^{(n)} &= \frac{\langle ABd^2A \rangle \langle ABd^2B \rangle \langle 1ijn \rangle \langle ABi\bar{j} \rangle}{\langle ABi-1i \rangle \langle ABii+1 \rangle \langle ABj-1j \rangle \langle ABjj+1 \rangle \langle AB1n \rangle} \quad (2.3.3) \\ &= d\log \frac{\langle ABi-1i \rangle}{\langle ABn1 \rangle} d\log \frac{\langle ABii+1 \rangle}{\langle ABn1 \rangle} d\log \frac{\langle ABj-1j \rangle}{\langle AB(in1) \cap \bar{j} \rangle} d\log \frac{\langle ABjj+1 \rangle}{\langle AB(in1) \cap \bar{j} \rangle}, \end{aligned}$$


with an analogous expression for  $i \leftrightarrow j$ . Here, we present a *new*  $d\log$  form for  $\Omega_{ij}^{(n)}$ :

$$\Omega_{ij}^{(n)} = d\log \frac{\langle ABi-1i \rangle}{\langle ABii+1 \rangle} d\log \frac{\langle ABj-1j \rangle}{\langle ABjj+1 \rangle} d\log \frac{\langle AB(n1i) \cap (ij\star) \rangle}{\langle AB1n \rangle} d\log \frac{\langle AB(n1j) \cap (ij\star) \rangle}{\langle AB1n \rangle}, \quad (2.3.4)$$

where  $\star$  corresponds to an *arbitrary* point in momentum twistor space. It is a highly non-trivial statement that the integrand form does not depend on the choice of  $\star$ . Let us point out that our new  $d\log$  representation in eq. (2.3.4) has two nice features: (i) it is manifestly  $ij$  symmetric, and (ii) it makes the fact that the integrand vanishes for  $(AB) \in (i-1ii+1)$  or  $(AB) \in (j-1jj+1)$  obvious since e.g. only one  $d\log$  blows up on this cut –  $\langle ABi-1i \rangle$  and  $\langle ABii+1 \rangle$  appear together in one ratio – and this is not enough to produce a non-zero residue. However, the other solution of the double cut  $\langle ABi-1i \rangle = \langle ABii+1 \rangle = 0$ , which is  $A = i$ , does produce a non-zero residue because

<sup>9</sup>The presence of spurious poles in the arguments of  $d\log$ 's is a very general feature, and in fact is relevant for understanding simplified differential equations based on  $d\log$  integrands [127].

$\langle AB(n1i) \cap (ij\star) \rangle$  also vanishes. In the simplest five-point case, the  $d$  log form reads

$$\begin{aligned}
\Omega_{24}^{(5)} &= \frac{\langle AB d^2 A \rangle \langle AB d^2 B \rangle \langle 1245 \rangle \langle AB \overline{24} \rangle}{\langle AB12 \rangle \langle AB23 \rangle \langle AB34 \rangle \langle AB45 \rangle \langle AB15 \rangle} \\
&= d \log \frac{\langle AB12 \rangle}{\langle AB23 \rangle} d \log \frac{\langle AB34 \rangle}{\langle AB45 \rangle} d \log \frac{\langle AB(512) \cap (243) \rangle}{\langle AB15 \rangle} d \log \frac{\langle AB(514) \cap (243) \rangle}{\langle AB15 \rangle},
\end{aligned} \tag{2.3.5}$$

where we have chosen the special point  $\star = 3$ .

Similar to the chiral pentagon expansion of the MHV amplitude in eq. (2.2.45), we can write an analogous formula for the  $\overline{\text{MHV}}$  amplitude where the pentagon with a wavy-line numerator is replaced by a dashed-line numerator of opposite chirality,

$$\begin{aligned}
\omega^{(n,n-2,1)} &= \sum_{i < j} \overline{\omega}_{ij}^{(n)} = \sum_{i < j} \frac{\langle 1\overline{ij}n \rangle \langle ABij \rangle}{\langle ABi-1i \rangle \langle ABii+1 \rangle \langle ABj-1j \rangle \langle ABjj+1 \rangle \langle AB1n \rangle}.
\end{aligned} \tag{2.3.6}$$

and all statements about the ‘‘MHV’’ pentagons can be readily transferred to the ‘‘ $\overline{\text{MHV}}$ ’’ pentagons as well. For completeness, we write a *novel* symmetric  $d$  log form for  $\overline{\Omega}_{ij}^{(n)}$  obtained by dualizing eq. (2.3.4),

$$\begin{aligned}
\overline{\Omega}_{ij}^{(n)} &= \frac{\langle ABi-1i \rangle \langle ABj-1j \rangle \langle AB((n1) \cap \overline{i})(\overline{\star} \cap \overline{j} \cap \overline{i}) \rangle}{\langle ABii+1 \rangle \langle ABjj+1 \rangle \langle AB1n \rangle} d \log \frac{\langle AB((n1) \cap \overline{j})(\overline{\star} \cap \overline{i} \cap \overline{j}) \rangle}{\langle AB1n \rangle},
\end{aligned} \tag{2.3.7}$$

where  $\overline{\star} = (x_1 x_2 x_3)$  is an arbitrary plane.

Besides the two chiral pentagons appearing in eq. (2.3.3) and eq. (2.3.6), there is one additional pentagon that will play an important role, namely the *parity-odd* pentagon. In momentum space its numerator is proportional to the Levi-Cevita tensor

and evaluates to zero upon integration over real Minkowski space. In momentum twistor space, the parity-odd numerator is the difference of two chiral numerators

$$N_{ij}^{\text{odd}} = \langle AB\bar{i}j\rangle\langle 1ijn\rangle - \langle ABij\rangle\langle 1\bar{i}jn\rangle. \quad (2.3.8)$$

The relative minus sign between the the wavy and dashed numerators is necessary for the integrand to be unit on all codimension-four residues; a relative plus sign would give some leading singularities equal to  $\pm 2$ , rather than  $\pm 1$ . The denominator of the parity-odd pentagon is the same as in eq. (2.3.3). The  $d\log$  form for this integral is very simple and involves only physical propagators:

$$\Omega_{ij}^{(n),\text{odd}} = d\log \frac{\langle ABi-1i\rangle}{\langle AB1n\rangle} d\log \frac{\langle ABii+1\rangle}{\langle AB1n\rangle} d\log \frac{\langle ABj-1j\rangle}{\langle AB1n\rangle} d\log \frac{\langle ABjj+1\rangle}{\langle AB1n\rangle}, \quad (2.3.9)$$

where we could also reshuffle the propagators that appear in the denominator. The fact that only propagators appear as  $d\log$  arguments also leads to a simple understanding of why this integral evaluates to zero from a differential equation point of view [127].

The difference of MHV and  $\overline{\text{MHV}}$  amplitudes is the *parity-odd* amplitude, which integrates to zero on the parity invariant contour. However, it will play a very important rôle in our further discussion. Combining the expansions eq. (2.2.45) and eq. (2.3.6), we see that the chiral numerators combine precisely into the numerator  $N_{ij}^{\text{odd}}$  of eq. (2.3.8) and we get a sum of parity-odd pentagons

$$\begin{aligned} \omega^{\text{odd}} &= \sum_{i<j} \left( \omega_{ij}^{(n)} - \bar{\omega}_{ij}^{(n)} \right) = \sum_{i<j} \left( \begin{array}{c} i+1 \quad j-1 \\ \diagup \quad \diagdown \\ i \quad \quad j \\ \diagdown \quad \diagup \\ i-1 \quad 1 \quad n \quad j+1 \end{array} - \begin{array}{c} i+1 \quad j-1 \\ \diagup \quad \diagdown \\ i \quad \quad j \\ \diagdown \quad \diagup \\ i-1 \quad 1 \quad n \quad j+1 \end{array} \right) \\ &= \sum_{i<j} \frac{N_{ij}^{\text{odd}}}{\langle ABi-1i\rangle\langle ABii+1\rangle\langle ABj-1j\rangle\langle ABjj+1\rangle\langle AB1n\rangle}. \end{aligned} \quad (2.3.10)$$

Note that all “boundary terms” (i.e.  $j = i+1$ ) cancel between the MHV and  $\overline{\text{MHV}}$  sectors in this expansion so that there are no parity-even box integrals remaining. Therefore, the sum is zero at four points, gives one parity-odd pentagon at five points, and so on.

### 2.3.2 From $d\log$ 's to geometry

In the usual Amplituhedron setup, we *start* with a positive geometry, and from it calculate the canonical form with logarithmic singularities on its boundaries. However, in our case the situation is reversed: we have the  $d\log$  form for e.g. the pentagon integrand in eq. (2.3.3) or eq. (2.3.4), but we do not a priori know the correct geometric space associated to that differential form, let alone whether or not there is even a unique answer to that question. By construction, any space defined by demanding definite signs for the *ratios* of the arguments of each  $d\log$  in e.g., eq. (2.3.4) gives *some* geometry with the appropriate canonical form. More generally, if we start with a  $d\log$  form

$$\Omega = d\log f_1 d\log f_2 d\log f_3 d\log f_4 \tag{2.3.11}$$

there are  $2^4 = 16$  geometric spaces associated to it via the inequalities

$$f_1 \leq 0, f_2 \leq 0, f_3 \leq 0, f_4 \leq 0. \tag{2.3.12}$$

Each  $d\log f_i$  factor is the correct form for both inequalities  $f_i > 0$  and  $f_i < 0$ , up to a sign. (If we did not impose any restrictions on  $f_i$ , the form would vanish as there are no boundaries.)

#### Faithful geometries and $d\log$ forms

As we have alluded to above, starting from a rational form of the integrand that only has logarithmic singularities there are often numerous ways to change variables to bring the integrand into a  $d\log$  form. For the simple four-point box integrand, we found at least two solutions specified by the choice of  $\langle ABX \rangle$  in eq. (2.3.2). Likewise, for the chiral pentagons, we also have at least two alternative  $d\log$  forms in eqs. (2.3.3) and (2.3.4). Combining this multitude of  $d\log$  forms with the 16-fold multiplicity of geometric spaces associated to a given one-loop form encoded in the choice of inequalities in eq. (2.3.12), it is not hard to imagine that the number of possible geometric spaces associated to a given integrand quickly grows. It is therefore natural to ask, whether or not there exist

any special subsets of geometries that have certain desirable properties. Here, and in the following, we are going to argue for *faithful geometries*.

What we mean by *faithful geometries* is the following: for our purposes, simply getting the correct canonical form is insufficient—we also require the correct boundary structure of the geometric space itself. Concretely, we demand that *all* boundaries of the geometry show up as poles in the form, and furthermore that these are the *only* boundaries. (Note that looking at the entries of the  $d\log$  forms can be misleading as certain entries of the  $d\log$ s are in fact not poles of the form. If one were to compute the residue on such a pole, one in fact finds zero. The simplest example of this is  $\langle ABX \rangle$  in eq. (2.3.2). This bracket is manifestly absent in the rational representation of the form so that it is clear that there is no singularity at this location.) Checking the “faithfulness” of a given geometry is more intricate and requires a detailed analysis similar in spirit to the discussion of the geometric boundaries of the kermit expansion in section 2.2.3. As we will explain shortly, there are “rare” cases of  $d\log$  forms that give rise to faithful geometries, i.e., there is at least one set of inequalities akin to (2.3.12) for which the resulting geometry *only* has the geometric boundaries appearing as singularities of the form and no others. These are the spaces of our interest in this chapter.

The presence of a boundary in the geometry which does not appear as a corresponding pole in the integrand form might seem strange, but this is in fact one of the defining features of Grassmannian geometry. As a simple example, consider the four-point box integral in eq. (2.3.2). As shown earlier, one version of the  $d\log$  form contains the  $\langle ABX \rangle = \langle AB13 \rangle$  bracket while the rational integrand form does not. This  $d\log$  form naively implies that there are  $2^4 = 16$  different geometries, reflecting the various sign choices for the four ratios of brackets. Geometrically, each choice would give rise to the same  $d\log$  form. However, these 16 geometries are all different, and some of them actually have  $\langle AB13 \rangle = 0$  as a boundary despite its absence in the differential



form. One concrete example of this occurs for the following sign choice<sup>10</sup>

$$\frac{\langle AB12 \rangle}{\langle AB13 \rangle} > 0, \quad \frac{\langle AB23 \rangle}{\langle AB13 \rangle} > 0, \quad \frac{\langle AB34 \rangle}{\langle AB13 \rangle} > 0, \quad \frac{\langle AB14 \rangle}{\langle AB13 \rangle} < 0. \quad (2.3.13)$$

We can always fix one of the brackets to have a definite sign, as the only relevant information is encoded in the ratios. Fixing the sign of  $\langle AB12 \rangle > 0$  then implies that all four-brackets appearing in eq. (2.3.13) are positive, except for  $\langle AB14 \rangle$ , which is negative. The geometric region associated to the sign choice eq. (2.3.13) still has eq. (2.3.2) as the logarithmic form, but geometrically we can now access the  $\langle AB13 \rangle = 0$  boundary without violating any of the inequalities. We can see this fact explicitly in coordinates: expanding  $Z_A = Z_3 + xZ_1 + yZ_2$ , and  $Z_B = Z_4 + zZ_1 + wZ_2$  the inequalities eq. (2.3.13) are equivalent to

$$x > 0, \quad y < 0, \quad w > 0, \quad (xw - yz) > 0. \quad (2.3.14)$$

In this parametrization we have  $\langle AB13 \rangle = -y\langle 1234 \rangle$ , so accessing the boundary corresponds to setting  $y \rightarrow 0$ . In this case, the only remaining inequality sensitive to this choice is  $xw - yz \rightarrow xw > 0$ , which is clearly consistent with  $x, w > 0$ . Therefore,  $\langle AB13 \rangle = 0$  is an accessible boundary of the geometry. Since this singularity is absent in the differential form, we conclude that this geometry is not faithful according to our definition above.

However, if we instead choose the geometric space where all ratios appearing in eq. (2.3.13) are positive, in the parametrization above the space becomes

$$x > 0, \quad y < 0, \quad w < 0, \quad (xw - yz) > 0, \quad (2.3.15)$$

i.e., we now have the opposite sign for  $w < 0$ . This time, sending  $y \rightarrow 0$  yields the three inequalities  $x > 0, w < 0$  and  $xw > 0$ , which are clearly incompatible, thus demonstrating that  $y = 0$  (and therefore  $\langle AB13 \rangle = 0$ ) is not a geometric boundary

---

<sup>10</sup>Let us note that for the ‘local spaces’ we define in this chapter, we do not insist on  $\langle ABi+1 \rangle > 0$  which was a crucial part of the Amplituhedron definition (2.2.12). We comment on this in section 2.3.3.

of the space. According to our definition above, we would call the positive geometry associated to this choice of inequalities *faithful*.

In summary, we see that each  $d \log$  form gives rise to a large set of geometric spaces (one for each sign choice of the ratios of four-brackets appearing in the  $d \log$  form) which all have the same integrand form. However, only a subset of these spaces are free of unphysical boundaries. For admissible (faithful) positive geometries, we demand that all boundaries of the space are directly reflected in the pole structure of the integrand form. This is true for the Amplituhedron, and we want to preserve this property here.

### Faithful geometries from the chiral pentagon $d \log$ form

For the generic chiral pentagon of eq. (2.3.3), we found two possible  $d \log$  forms in eqs. (2.3.3) and (2.3.4). Starting with the original  $d \log$  form in eq. (2.3.3) and checking the boundary structure of the  $2^4$  geometries arising from the respective sign choices for the entries of the  $d \log$ s, we find that *none* of these spaces gives rise to a *faithful geometry*, i.e., these spaces always have certain additional geometric boundaries that do not appear as singularities of the form and are therefore unacceptable to us.

This encourages us to consider our novel  $d \log$  form presented in eq. (2.3.4). While the rational integrand in eq. (2.3.3) does not have the spurious poles  $\langle AB(n1i) \cap (ij\star) \rangle$  or  $\langle AB(n1j) \cap (ij\star) \rangle$ , certain sign choices for the arguments of the  $d \log$  form in eq. (2.3.4) do lead to geometric spaces with boundaries when  $(AB)$  intersects the lines  $(n1i) \cap (ij\star)$  or  $(n1j) \cap (ij\star)$ . Only the special sign combinations where the spurious boundaries are geometrically absent are of our interest. In this case, there are exactly two choices of signs for the ratios of four-brackets in the  $d \log$  form eq. (2.3.4) which do have the correct boundary structure to represent a faithful geometry. The two possibilities correspond to choosing the reference point  $Z_\star$  to be either in the set  $Z_\star \in \{i+1, \dots, j-1\}$ , or  $Z_\star \in \{1, \dots, i-1\} \cup \{j+1, \dots, n\}$ .<sup>11</sup> In the first case,  $Z_\star \in \{i+1, \dots, j-1\}$ , we find a

---

<sup>11</sup>Here, we restrict ourselves to simple momentum twistor choices for  $Z_\star$  that are already part of the diagram. We do not exclude the possibility that there may exist more complicated choices that yield additional choices satisfying our boundary structure criterion. Furthermore, it is also possible

consistent geometry defined by the following set of inequalities

$$\left\{ \frac{\langle ABi-1i \rangle}{\langle ABii+1 \rangle} < 0, \frac{\langle ABj-1j \rangle}{\langle ABjj+1 \rangle} < 0, \frac{\langle AB(n1i) \cap (ij\star) \rangle}{\langle AB1n \rangle} < 0, \frac{\langle AB(n1j) \cap (ij\star) \rangle}{\langle AB1n \rangle} > 0 \right\}. \quad (2.3.16)$$

We fix the sign of  $\langle AB1n \rangle > 0$  which in turn fixes the signs for the brackets with intersections, but leaves four options for the signs of the four individual propagator-type brackets,  $\{\langle ABi-1i \rangle, \langle ABii+1 \rangle, \langle ABj-1j \rangle, \langle ABjj+1 \rangle\}$ . As a result, the first consistent chiral pentagon space is a union of four sign patterns:

$$P_{ij}^{(1)} \leftrightarrow \begin{array}{|c|c|c|c|c|c|c|} \hline \langle ABi-1i \rangle & \langle ABii+1 \rangle & \langle ABj-1j \rangle & \langle ABjj+1 \rangle & \langle AB1n \rangle & \langle ABX_i \rangle & \langle ABX_j \rangle \\ \hline - & + & - & + & + & - & + \\ \hline + & - & - & + & + & - & + \\ \hline - & + & + & - & + & - & + \\ \hline + & - & + & - & + & - & + \\ \hline \end{array} \quad (2.3.17)$$

where we denoted  $X_i = (n1i) \cap (ij\star)$  and  $X_j = (n1j) \cap (ij\star)$ .

The second consistent option we found is to pick  $\star \in \{1, \dots, i-1\}$ ,<sup>12</sup> together with the following signs for the ratios of four-brackets in the  $d \log$  form eq. (2.3.4)

$$\left\{ \frac{\langle ABi-1i \rangle}{\langle ABii+1 \rangle} < 0, \frac{\langle ABj-1j \rangle}{\langle ABjj+1 \rangle} < 0, \frac{\langle AB(n1i) \cap (ij\star) \rangle}{\langle AB1n \rangle} > 0, \frac{\langle AB(n1j) \cap (ij\star) \rangle}{\langle AB1n \rangle} > 0 \right\}. \quad (2.3.18)$$

One can check that out of the four possibilities for the signs of individual four-brackets consistent with the ratios eq. (2.3.18), only one region is actually non-empty, and we get

$$P_{ij}^{(2)} \leftrightarrow \begin{array}{|c|c|c|c|c|c|c|} \hline \langle ABi-1i \rangle & \langle ABii+1 \rangle & \langle ABj-1j \rangle & \langle ABjj+1 \rangle & \langle AB1n \rangle & \langle ABX_i \rangle & \langle ABX_j \rangle \\ \hline - & + & + & - & + & + & + \\ \hline \end{array} \quad (2.3.19)$$

When some legs of the pentagon become massless, there are degenerate configurations which allow more sign choices in the  $d \log$  form eq. (2.3.4) than in the generic case.

that there are other representations of the chiral pentagon  $d \log$  form that opens up yet more options. It would be interesting to prove exhaustively what the set of the most general geometries that can consistently be assigned to the pentagon integrand are.

<sup>12</sup>In fact, we can also choose  $\star \in \{j+1, \dots, n\}$ , for which the inequalities of the last two ratios in eq. (2.3.18) flip sign. For this option the geometric space is identical to the one defined by eq. (2.3.18). As such, it is just a different representation of the same geometry.

However, upon gluing different integrands, none of these choices lead to a global geometry which is free of spurious boundaries. We return to this point in greater detail in section 2.5 as well as appendix A.3.

### Faithful geometries from the box $d \log$ form

A particular degeneration of the chiral pentagon in eq. (2.2.45) leads to the two-mass-hard integral which arises as a special case,  $j = i+1$ . The  $d \log$  form for the general box integral is similar to eq. (2.3.2). In the context of the two-mass-hard box, it reads

$$\begin{aligned} \Omega_{ii+1}^{(n)} &= \begin{array}{c} i \qquad i+1 \\ \diagdown \quad \diagup \\ \text{---} \quad \text{---} \\ \diagup \quad \diagdown \\ i-1 \quad i+2 \\ \text{---} \quad \text{---} \\ 1 \qquad n \end{array} = \frac{\langle ABd^2A \rangle \langle ABd^2B \rangle \langle i-1ii+1i+2 \rangle \langle 1ii+1n \rangle}{\langle ABi-1i \rangle \langle ABii+1 \rangle \langle ABi+1i+2 \rangle \langle AB1n \rangle} \quad (2.3.20) \\ &= d \log \frac{\langle ABi-1i \rangle}{\langle ABX \rangle} d \log \frac{\langle ABii+1 \rangle}{\langle ABX \rangle} d \log \frac{\langle ABi+1i+2 \rangle}{\langle ABX \rangle} d \log \frac{\langle AB1n \rangle}{\langle ABX \rangle}, \end{aligned}$$

where  $X$  is one of the two solutions of the quadruple cut of the box,

$$\begin{array}{c} i \qquad i+1 \\ \circ \quad \circ \\ \diagdown \quad \diagup \\ \text{---} \quad \text{---} \\ \diagup \quad \diagdown \\ i-1 \quad i+2 \\ \circ \quad \circ \\ \text{---} \quad \text{---} \\ 1 \qquad n \end{array} \leftrightarrow X_i = (ii+1i+2) \cap (in1), \quad \text{or} \quad \begin{array}{c} i \qquad i+1 \\ \circ \quad \circ \\ \diagdown \quad \diagup \\ \text{---} \quad \text{---} \\ \diagup \quad \diagdown \\ i-1 \quad i+2 \\ \circ \quad \circ \\ \text{---} \quad \text{---} \\ 1 \qquad n \end{array} \leftrightarrow X_{i+1} = (i-1ii+1) \cap (i+1n1) \quad (2.3.21)$$

We now repeat the same exercise as for the chiral pentagon and determine the consistent positive geometries associated to this  $d \log$  form. As it turns out, fixing one of the signs of the brackets involving either  $X_i$  or  $X_{i+1}$  is sufficient to specify the space, as one inequality automatically enforces the other. Fixing  $\langle AB1n \rangle > 0$  then forces  $\langle ABX \rangle$  to have a definite sign depending on the sign of the ratio in the last  $d \log$ . We find two different consistent sign choices for the ratios of the  $d \log$ s in eq. (2.3.20), both of which have fixed signs for the  $\langle ABii+1 \rangle$  brackets of the diagram. The first region is given by:

$$B_{1i-1, i+2n}^{(1)} \leftrightarrow \begin{array}{|c|c|c|c|c|c|} \hline \langle ABi-1i \rangle & \langle ABii+1 \rangle & \langle ABi+1i+2 \rangle & \langle AB1n \rangle & \langle ABX_i \rangle & \langle ABX_{i+1} \rangle \\ \hline - & + & - & + & + & - \\ \hline \end{array} \quad (2.3.22)$$

Consistent with the statements above, let us reiterate that fixing the sign of only one of the brackets  $\langle ABX_i \rangle$  or  $\langle ABX_{i+1} \rangle$  together with the signs of the propagator brackets is sufficient to fix the region; the sign of the other bracket is implied by the rest.

The second allowed region has the same signs as in eq. (2.3.22) for the first four brackets, but the signs for  $\langle ABX_i \rangle < 0$ ,  $\langle ABX_{i+1} \rangle > 0$  are flipped.

$$B_{1i-1, i+2n}^{(2)} \leftrightarrow \begin{array}{|c|c|c|c|c|c|} \hline \langle AB_{i-1i} \rangle & \langle AB_{ii+1} \rangle & \langle AB_{i+1i+2} \rangle & \langle AB_{1n} \rangle & \langle ABX_i \rangle & \langle ABX_{i+1} \rangle \\ \hline - & + & - & + & - & + \\ \hline \end{array} \quad (2.3.23)$$

Note that the union of the two regions eq. (2.3.22) and eq. (2.3.23) constitutes a larger achiral geometric region defined only by the first four inequalities with no constraints on  $\langle ABX_i \rangle$  and  $\langle ABX_{i+1} \rangle$ . The canonical form for this achiral region trivially vanishes because four inequalities are insufficient to produce a non-trivial  $d \log$  form (simply because we cannot form four independent ratios). Therefore, this achiral space is a particular example of a zero-form space defined in subsection 2.2.1. The larger space can be sliced into two subspaces by fixing the sign of  $\langle ABX_i \rangle$ , corresponding to exactly the two chiral subspaces we found in eq. (2.3.22) and eq. (2.3.23). Because the form for the achiral space vanishes, both subspaces have the same form (up to a sign). We can once again illustrate this feature of zero-form spaces with a simple two-dimensional example in the  $xy$ -plane. The space defined by  $-\infty < x < \infty, 0 < y < b$  has zero canonical form, so cutting the space into two pieces with  $x \leq a$ , the respective canonical forms  $\Omega_{<}, \Omega_{>}$  differ only by a sign:

$$\begin{array}{ccc} \begin{array}{c} y \\ \uparrow \\ b \\ \hline \Omega = 0 \end{array} & \xrightarrow{\text{slicing}} & \begin{array}{c} y \\ \uparrow \\ b \\ \hline < > \\ \hline \Omega_{<} + \Omega_{>} = \frac{dx dy}{(x-a)y(y-b)} - \frac{dx dy}{(x-a)y(y-b)} \end{array} \end{array} \quad (2.3.24)$$

We can also use an alternative  $d \log$  form representation for the box integrand derived directly from the degeneration of the chiral pentagon eq. (2.3.4) by setting  $j = i+1$ .

For this leg configuration, the integrand form eq. (2.3.3) naïvely generates a double pole  $\langle ABii+1 \rangle$  in the denominator. However, the chiral numerator exactly cancels one power of this pole so that we end up with a two-mass-hard box. The resulting  $d \log$  form obtained by this procedure has different arguments than eq. (2.3.20), but reproduces the same rational integrand. This is in complete agreement with our earlier statements about the non-uniqueness of  $d \log$  representations.

If we repeat the exercise of subsection 2.3.2 to associate consistent geometric regions with the appropriate boundary structure to the  $d \log$  form, we find exactly the same geometric regions as in eq. (2.3.22) and eq. (2.3.23), albeit described by different inequalities. The brackets involving the lines  $X_i = (n1i) \cap (ii+1\star)$  and  $X_{i+1} = (n1i+1) \cap (ii+1\star)$  inherited from the pentagon simply provide an equivalent description of the same spaces. Once again, this simply reflects the non-uniqueness of the  $d \log$  form of an integrand, and emphasizes that demanding we get the *geometry* correct (rather than just the form) is a very strong constraint. More generally, we expect (but have no proof) that alternative  $d \log$  forms for the local integrals discussed in this section will not yield any new consistent geometries.

In addition to the two-mass hard box discussed above, the only other box topology relevant for the local expansion eq. (2.2.45) are “one-mass” boxes. The first of these arises as a boundary term when  $i = n-2, j = n-1$ . The second one-mass box is a degeneration of the pentagon when  $i = 2, j = 3$ , and can be obtained by trivial relabelling.

$$B_{1n-3} = \begin{array}{c} n-2 \quad n-1 \\ \diagdown \quad \diagup \\ \square \\ \diagup \quad \diagdown \\ n-3 \quad n \\ \vdots \quad \vdots \\ 1 \end{array}, \quad B_{4n} = \begin{array}{c} 2 \quad 3 \\ \diagdown \quad \diagup \\ \square \\ \diagup \quad \diagdown \\ 1 \quad 4 \\ \vdots \quad \vdots \\ n \end{array}. \quad (2.3.25)$$

The one-mass geometries with the correct boundary structure can be specified by imposing conditions on the propagators appearing in the diagram, as well as one bracket involving (one of) the solutions to the quadruple cut. Thus, for e.g.,  $B_{1n-3}$  in eq. (2.3.25)

we can define the space by correctly choosing the signs of

$$\{\langle ABn-3n-2\rangle, \langle ABn-2n-1\rangle, \langle ABn-1n\rangle, \langle AB1n\rangle\} \quad \text{and} \quad \langle ABn-2n\rangle. \quad (2.3.26)$$

In the two-mass hard case there was only one choice of signs for the list of propagators i.e., eq. (2.2.29) and eq. (2.3.23) differed only in the signs of the brackets  $\langle ABX_i\rangle$  and  $\langle ABX_{i+1}\rangle$ . In the one-mass case, both sign choices for the bracket  $\langle ABn-2n\rangle$  are also allowed. In addition, there are two allowed choices for the signs of the sequence of brackets in eq. (2.3.26) which are geometrically free of spurious boundaries—giving a total of *four* consistent spaces. The first two can be written compactly as

$$B_{1n-3}^{(1,2)} \leftrightarrow \begin{array}{|c|c|c|c|c|} \hline \langle ABn-3n-2\rangle & \langle ABn-2n-1\rangle & \langle ABn-1n\rangle & \langle AB1n\rangle & \langle ABn-2n\rangle \\ \hline + & - & - & + & \pm \\ \hline \end{array}, \quad (2.3.27)$$

while the second pair of solutions is

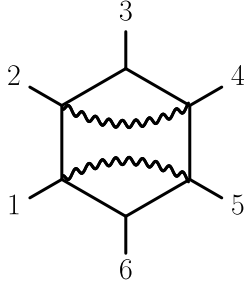
$$B_{4n}^{(3,4)} \leftrightarrow \begin{array}{|c|c|c|c|c|} \hline \langle ABn-3n-2\rangle & \langle ABn-2n-1\rangle & \langle ABn-1n\rangle & \langle AB1n\rangle & \langle ABn-2n\rangle \\ \hline - & + & - & + & \pm \\ \hline \end{array}. \quad (2.3.28)$$

In subsections 2.5.3 and 2.5.4 we consider the problem of *combining* the geometries associated to individual terms in the chiral pentagon expansion of the MHV one-loop integrand eq. (2.2.45). A priori, we have no reason to prefer any one of the individually well-defined spaces we have just constructed. Remarkably, however, as we shall demonstrate in section 2.5, it turns out that demanding a sensible global geometry whose boundary structure is identical to that of the original Amplituhedron is restrictive enough to give a *unique* choice for the one-mass, the two-mass hard, as well as the chiral pentagon spaces subject to the assumption that we treat all graph isomorphic topologies in a uniform way.

### Faithful geometries from the chiral hexagon $d\log$ form

In this subsection, we consider the problem of assigning faithful geometries to logarithmic forms more generally. The first example which goes beyond the results of

the previous two subsections is the chiral hexagon,



$$\Omega_{\text{hex}} = \frac{\langle ABd^2 A \rangle \langle ABd^2 B \rangle \langle AB\bar{24} \rangle \langle AB\bar{51} \rangle}{\langle AB12 \rangle \langle AB23 \rangle \langle AB34 \rangle \langle AB45 \rangle \langle AB56 \rangle \langle AB16 \rangle}. \quad (2.3.29)$$

To identify some candidate geometries the most natural starting point is, as we have seen, a rewriting of this integrand as a single  $d\log$  form. For integrals with more than five local poles, any such form must involve at least one ratio in which both the numerator and denominator depend quadratically on  $(AB)$ . For the hexagon of eq. (2.3.29) our starting point is a novel expression which is a single  $d\log$  form,

$$\Omega_{\text{hex}} = d\log \frac{\langle AB13 \rangle}{\langle AB23 \rangle} d\log \frac{\langle AB34 \rangle}{\langle AB45 \rangle} d\log \frac{\langle AB46 \rangle}{\langle AB56 \rangle} d\log \frac{\langle AB23 \rangle \langle AB16 \rangle}{\langle AB12 \rangle \langle AB36 \rangle}. \quad (2.3.30)$$

Demanding that the geometry defined by sign conditions on the four ratios in this expression be faithful requires that the three codimension-one loci  $\langle AB13 \rangle = 0$ ,  $\langle AB46 \rangle = 0$  and  $\langle AB36 \rangle = 0$  do not appear as boundaries of the space. There are two sign choices which accomplish this:

$$H^{(1)} = \left\{ \frac{\langle AB13 \rangle}{\langle AB23 \rangle} < 0, \frac{\langle AB34 \rangle}{\langle AB45 \rangle} < 0, \frac{\langle AB46 \rangle}{\langle AB56 \rangle} < 0, \frac{\langle AB23 \rangle \langle AB16 \rangle}{\langle AB12 \rangle \langle AB36 \rangle} > 0 \right\}, \quad (2.3.31)$$

$$H^{(2)} = \left\{ \frac{\langle AB13 \rangle}{\langle AB23 \rangle} < 0, \frac{\langle AB34 \rangle}{\langle AB45 \rangle} < 0, \frac{\langle AB46 \rangle}{\langle AB56 \rangle} > 0, \frac{\langle AB23 \rangle \langle AB16 \rangle}{\langle AB12 \rangle \langle AB36 \rangle} > 0 \right\}. \quad (2.3.32)$$

Decomposing  $H^{(i)}$  into subspaces where all brackets appearing in the ratios have fixed sign, we naïvely generate a considerable number of non-overlapping regions. Although this is indeed the case for  $H^{(2)}$ , the first solution is surprisingly equivalent to a single region described by significantly simpler inequalities

$$H^{(1)} = \left\{ \langle AB12 \rangle < 0, \langle AB23 \rangle > 0, \langle AB34 \rangle > 0, \langle AB45 \rangle < 0, \right. \\ \left. \langle AB56 \rangle > 0, \langle AB16 \rangle > 0, \langle AB14 \rangle < 0 \right\}, \quad (2.3.33)$$

which will arise in a different context in section 2.4 below.



### 2.3.3 No-go theorem for external triangulation

In all previous cases, assigning a sensible (faithful) geometric space to a given  $d \log$  form led us to consider situations where at least a subset of signs of  $\langle AB_{i+1} \rangle$  were negative. In particular, for all faithful geometries of the local integrands, we did not encounter any region for which *all* such brackets were positive. On the other hand, the Amplituhedron itself is defined with all  $\langle AB_{i+1} \rangle > 0$ , and is cut further either by the sign-flip conditions in eq. (2.2.10) or by the positivity of  $\langle AB_{\bar{i}\bar{j}} \rangle > 0$  in eq. (2.2.31). This means that all geometric regions we discussed in the context of the chiral pentagon expansion are *outside* the Amplituhedron.

It is actually very easy to see that even if there was some other  $d \log$  representation for the pentagon or boxes, with correspondingly different geometric regions, they can not possibly be even partially inside the Amplituhedron space for the following reason: In order to fix, e.g., the MHV (or  $\overline{\text{MHV}}$ ) Amplituhedron space, we need to specify  $n - 3$  conditions in addition to the positivity of all  $\langle AB_{i+1} \rangle > 0$ . While there are many equivalent ways how to express these conditions, e.g., via sign flips in the sequence  $\{\langle AB_{1i} \rangle\}_{i=2, \dots, n}$ , or via sign flips in the sequence  $\{\langle AB_{2i} \rangle\}_{i=3, \dots, n, 1}$ , or via the positivity of  $\langle AB_{\bar{i}\bar{j}} \rangle > 0$ , we always need at least  $n - 3$  of them. This number is irreducible and cannot be decreased. If we attempted to specify fewer conditions, the resulting space would lie inside the Amplituhedron, alas it would contain spurious boundaries. One example of this scenario is given by the individual sign-flip spaces associated to the BCFW Kermit eq. (2.2.19). The unique space with only physical boundaries inside the Amplituhedron is the whole Amplituhedron itself, and can not be cut into smaller spaces with purely physical boundaries.

A natural follow-up question is whether or not the Amplituhedron can be contained inside a space whose logarithmic form is given by the chiral pentagon or the box. While the logarithmic form for the Amplituhedron is generally very complicated, combining the Amplituhedron space with many other spaces outside can lead to a simpler space whose form can be as simple as that of the chiral pentagon or the box. In our two-

dimensional geometry toy example in subsection 2.2.4, this is precisely what happened in the external triangulation of the quadrilateral on the left-hand-side of eq. (2.2.46). There, adding a triangle outside the space gave rise to a larger triangle, for which the logarithmic form would be simpler than the one for the quadrilateral itself. So the question is whether or not we can replicate something similar for the Amplituhedron.

For the simplest five-point case, the answer is yes. For  $n > 5$ , however, this is no longer true and there is *no* consistent local space based on the pentagon  $d \log$  form which *contains* the Amplituhedron space. This can be understood heuristically by noting that in the  $n$ -point case, to define pentagon geometries that contain the amplitude we would need  $n - 3$  extra conditions, analogous to the intersections appearing in eq. (2.2.31). However, the  $d \log$  form of the pentagon contains only four ratios of brackets, indicating that the set of conditions defining the pentagon should not grow with  $n$ . Thus, without resorting to increasingly complicated ratios of brackets at higher multiplicities a simple pentagon space cannot possibly contain the complicated Amplituhedron. The  $n=5$  case is exceptional, as the two conditions required to cut out the Amplituhedron matches the number of conditions required to define the pentagon.

This argument suggests the chiral pentagon expansion cannot represent a geometric triangulation (internal or external) of the Amplituhedron. As we will see later in section 2.5, the chiral pentagons triangulate a different region which has only physical boundaries and has (almost) all the same properties as the Amplituhedron. However, our suspicion, for which we give evidence in section 2.6, is that the primary purpose of the pentagons is to internally triangulate the dual Amplituhedron.

## 2.4 Sign-flip regions

In this section we take a step back from the chiral pentagon expansion, and look more generally at the positive geometries which arose in the study of the local integrands, such as eqs. (2.3.17), (2.3.19), (2.3.22), (2.3.23), (2.3.27) and (2.3.28). In particular, we constructed spaces with only physical boundaries that were defined by

both positive and negative signs of various  $\langle ABi+1 \rangle$  brackets. In [128] we provided an intriguing classification of these geometries using certain sign-flip conditions which are reminiscent of, but distinct from, the sign-flip characterization of the Amplituhedron [58]. In this section we will review these results and provide further discussions and elaborate on the properties of the various sign-flip spaces.

### Classification of sign-flip regions

In the first step we discuss achiral positive spaces that are defined by imposing fixed signs for  $\langle ABi+1 \rangle$  brackets only, without further constraints on any other four-bracket. In other words, we study geometric regions defined by the following set of  $n$  signs for the sequence of brackets

$$S = \{\langle ABi+1 \rangle\}_{i \in \{1, \dots, n\}} := \{\langle AB12 \rangle, \langle AB23 \rangle, \dots, \langle AB1n \rangle\}. \quad (2.4.1)$$

From the study of the Amplituhedron, we already know of one example of such a region: the union of the MHV and  $\overline{\text{MHV}}$  one-loop spaces. The corresponding logarithmic form is the parity-odd amplitude, which is given by the sum of MHV and  $\overline{\text{MHV}}$  one-loop amplitudes in eq. (2.3.10) (defined with appropriate sign). This function integrates to zero on the parity-invariant Feynman contour. However, from a geometric point of view, it is the most natural space we can consider where all signs in  $S$  are positive,

$$S^{(0)} = \{+, +, \dots, +\}. \quad (2.4.2)$$

For obvious reasons, we also call  $S^{(0)}$  a *sign-flip-zero region* because the sequence  $S$  has no sign flips. By drawing the  $n$  points on a circle, we can represent the sign-flip-zero space as

$$S^{(0)} = \begin{array}{c} \dots \\ \dots + \dots + \dots \\ \dots + \dots + \dots \\ \dots + \dots + \dots \\ 1 \quad + \quad n-1 \\ \quad \quad \quad + \quad \quad \quad \\ \quad \quad \quad n \end{array} \quad (2.4.3)$$

where the + sign between points 1 and 2 denotes  $\langle AB12 \rangle > 0$ , and similarly for the other brackets. The only subtlety arises when we reach the arc from  $n$  to 1, where we draw a + sign to denote the positivity of  $\langle ABn\hat{1} \rangle = \langle AB1n \rangle$  in line with the twisted cyclic symmetry.

Following the same logic, we define a *sign-flip-two region* as sequence of signs

$$S_{ij}^{(2)} = \begin{array}{c} \dots \\ i+1 \quad - \quad \dots \quad - \quad j-1 \\ \vdots \\ i \quad \quad \quad \quad \quad j \\ \vdots \\ i-1 \quad + \quad \dots \quad + \quad j+1 \\ \dots \end{array}, \quad (2.4.4)$$

where the labels  $i$  and  $j$  denote the two positions where the first and second sign flip occurs, respectively. In particular, this implies that

$$\begin{aligned} \{ \langle ABi \ i+1 \rangle, \langle ABi+1 \ i+2 \rangle, \dots, \langle ABj-1 \ j \rangle < 0 \}, \\ \{ \langle ABj \ j+1 \rangle, \langle ABj+1 \ j+2 \rangle, \dots, \langle ABi-1 \ i \rangle > 0 \}, \end{aligned} \quad (2.4.5)$$

where the labels 1 and  $n$  can be in either the positive or negative regions<sup>13</sup> (appropriately taking into account the twisted cyclic symmetry as commented on above).

Next, we define a *sign-flip-four region* with  $i, k, \ell, j$  labelling the four positions where the signs in the sequence eq. (2.4.1) flip,

$$S_{ik\ell j}^{(4)} = \begin{array}{c} k+1 \quad \dots \quad \ell-1 \\ k \quad + \quad \dots \quad + \quad \ell \\ \vdots \\ k-1 \quad - \quad \dots \quad - \quad \ell+1 \\ \vdots \\ i+1 \quad - \quad \dots \quad - \quad j-1 \\ i \quad + \quad \dots \quad + \quad j \\ i-1 \quad + \quad \dots \quad + \quad j+1 \end{array} \quad (2.4.6)$$

Naïvely, we can continue to consider sequences of brackets eq. (2.4.1) with ever more sign flips. Remarkably, all higher sign-flip patterns correspond to *empty* geometric regions.

<sup>13</sup>As written, eq. (2.4.4) and eq. (2.4.5) suggest that  $i < j$  and therefore  $\langle AB1n \rangle > 0$  is in the positive region. In general, spaces  $\langle AB1n \rangle < 0$  presents no additional complications whatsoever, although we will have no use for them in this chapter.

## Sign-flip-zero regions

All the sign-flip-zero, two, and four spaces are positive geometries; as such, all of these spaces have associated canonical forms with only logarithmic singularities on all boundaries. By definition, all codimension-one boundaries of the achiral spaces defined in the previous subsection have to be of the form  $\langle AB_{ii+1} \rangle = 0$ . Naïvely, one may expect that, at  $n$  points, all such inverse propagators  $\langle AB_{12} \rangle, \dots, \langle AB_{1n} \rangle$  will indeed be boundaries of the spaces leading to very complicated canonical forms. For the sign-flip-zero space, this is true: the associated form has  $n$  poles

$$S^{(0)} = 2 \begin{array}{c} \dots \\ \dots + \dots \\ \dots + \dots \\ \dots + \dots \\ \dots + \dots \\ 1 \quad \dots \quad n-1 \\ \dots \\ \dots + \dots \\ \dots + \dots \\ \dots + \dots \\ \dots + \dots \\ n \end{array} \leftrightarrow \frac{N^{(0)}}{\langle AB_{12} \rangle \langle AB_{23} \rangle \dots \langle AB_{n-1n} \rangle \langle AB_{1n} \rangle}. \quad (2.4.7)$$

This means the complexity of the numerator of the canonical form grows with  $n$ , just as the complexity of MHV and  $\overline{\text{MHV}}$  amplitudes does. This should not be surprising, because both of these chiral amplitude spaces in fact live inside the larger achiral space  $S^{(0)}$ ! The MHV amplitude is the subspace of the achiral space defined by the additional conditions (i)  $\langle AB_{i\bar{j}} \rangle > 0$ , eq. (2.2.31), while the parity conjugate  $\overline{\text{MHV}}$  space uses (ii)  $\langle AB_{ij} \rangle > 0$ , eq. (2.2.32). It is quite nontrivial that imposing either set of these conditions does not introduce new codimension-one boundaries. In fact, it is straightforward to verify there is no way to impose a mixed set of conditions of type (i) and (ii), without at least one of these conditions becoming a boundary. Thus, we may think of the achiral space as having two components, neither of which has any spurious boundaries; for obvious reasons, we refer to these as *chiral* components.

In other words, we can cut the sign-flip-zero space defined by  $\langle AB_{ii+1} \rangle > 0$  into two chiral components which are MHV and  $\overline{\text{MHV}}$  Amplituhedra. Both of these spaces have only physical boundaries. As alluded to in subsection 2.3.3, we need to impose  $n-3$  conditions to specify either one of these spaces.

Interestingly, the achiral sign-flip zero space can be externally triangulated in terms of simpler spaces. In fact, the “parity-odd” pentagon expansion in eq. (2.3.10) exactly gives this geometric triangulation:

$$\begin{aligned}
 & \text{Circle with } n \text{ points } 1, \dots, n \text{ and plus signs between them} \\
 &= \sum_{i=2}^{n-3} \sum_{j=i+2}^{n-1} \text{Circle with } n \text{ points } 1, \dots, n \text{ and signs: } + \text{ between } 1 \text{ and } i-1, - \text{ between } i \text{ and } j, + \text{ between } j \text{ and } n, \text{ and } * \text{ between } i-1 \text{ and } i, i \text{ and } i+1, j-1 \text{ and } j, \text{ and } j \text{ and } j+1.
 \end{aligned}
 \tag{2.4.8}$$

Each parity-odd pentagon corresponds to a positive geometry with only five boundaries. The terms in the set are overlapping and provide an external triangulation of  $S^{(0)}$ . On the right-hand-side of eq. (2.4.8),  $* = + \oplus -$  instructs us to marginalize over both signs of the corresponding bracket. More details, including the derivation of (2.4.8) are given in appendix A.1. As argued above, the same procedure does not work for chiral spaces, and the chiral pentagon expansion does not provide an external triangulation of the Amplituhedron. We will get back to the precise role of this expansion in the next section.

### Sign-flip-two regions

Let us continue our discussion with the achiral sign-flip-two regions defined in eq. (2.4.4) and eq. (2.4.5). First, one can check that this space has all  $n$  codimension-one boundaries so that the logarithmic form a priori has a similar structure as the one of  $S^{(0)}$  in eq. (2.4.7), but with a different numerator.

However, something surprising happens when we slice the achiral sign-flip-two region eq. (2.4.4) into smaller components. First, similar to the sign-flip-zero case we find that the sign-flip-two region can be again cut into two chiral components without introducing spurious boundaries. Naïvely, we would expect that in order to specify each subspace we have to impose  $\mathcal{O}(n)$  additional inequalities, but in fact only a single inequality suffices; for the sign-flip-two space eq. (2.4.4) the chiral components correspond to the two signs of the bracket  $\langle ABij \rangle \gtrless 0$ , which we represent diagrammatically

as

$$S_{ij}^{(2),\pm} = \begin{array}{c} \dots \\ i+1 \quad - \quad j-1 \\ \circ \quad \circ \quad \circ \\ \langle \langle ij \rangle \rangle \geq 0 \\ \circ \quad \circ \quad \circ \\ i \quad \quad \quad j \\ + \quad \quad \quad + \\ i-1 \quad + \quad j+1 \\ \dots \end{array}, \quad \text{for } i < j. \quad (2.4.9)$$

This additional inequality is very natural as  $i$  and  $j$  are the positions where the two sign-flips occur.

Looking more closely at one of the subspaces defined by  $\langle ABij \rangle > 0$ , we find two interesting features: First, all brackets inside the “plus region” have fixed positive sign,

$$\langle ABpq \rangle > 0 \quad \text{and} \quad \langle AB\bar{p}\bar{q} \rangle > 0, \quad (2.4.10)$$

for  $p < q$  and  $p, q \in \{j, j+1, \dots, i-1, i\}$ . No similar statement is true for the indices inside the “minus region.” Second, from the collection of terms  $\langle ABpq \rangle$  inside the plus region *only* the boundary terms  $\langle ABjj+1 \rangle$  and  $\langle ABi-1i \rangle$  represent boundaries. In other words,  $\langle ABpp+1 \rangle$  for  $p \in (j+1, \dots, i-2)$  are not poles of the logarithmic form. Therefore, the canonical form for this chiral region is considerably simpler,

$$S_{ij}^{(2),+} = \begin{array}{c} \dots \\ i+1 \quad - \quad j-1 \\ \circ \quad \circ \quad \circ \\ \langle ABij \rangle > 0 \\ \circ \quad \circ \quad \circ \\ i \quad \quad \quad j \\ + \quad \quad \quad + \\ i-1 \quad + \quad j+1 \\ \dots \end{array} \leftrightarrow \frac{N_{ij}^{(2),+}}{\langle ABi-1 \rangle \langle ABi+1 \rangle \cdots \langle ABj-1j \rangle \langle ABjj+1 \rangle}. \quad (2.4.11)$$

In the general  $n$ -point case the form eq. (2.4.11) is still non-trivial and we will give a precise formula and its derivation in eq. (A.1.16) of appendix A.1. For some special cases, the structure of the form simplifies considerably. In particular, if the ‘-’ region shrinks, the number of poles decreases, as does the complexity of the form. For the special case where  $j = i+2$  there are only two negative brackets,  $\langle ABii+1 \rangle, \langle ABi+1i+2 \rangle < 0$ , which means that the chiral sign-flip-two space has only four boundaries and the logarithmic

form must be a box.

$$\begin{aligned}
 S_{ii+2}^{(2),+} &= \text{Diagram of a circle with points } i-1, i, i+1, i+2, i+3 \text{ and others. A purple line connects } i \text{ and } i+2 \text{ with } \langle ABi+2 \rangle > 0 \text{ written above it.} \\
 &\leftrightarrow \frac{\langle i-1 \ i \ i+1 \ i+2 \rangle \langle i \ i+1 \ i+2 \ i+3 \rangle}{\langle ABi-1 \ i \rangle \langle ABi+1 \ i+2 \rangle \langle ABi+1 \ i+2 \rangle \langle ABi+2 \ i+3 \rangle} \\
 &= \text{Diagram of a square with vertices } i-1, i, i+1, i+2 \text{ and } i+3 \text{ at the bottom-left corner.}
 \end{aligned}
 \tag{2.4.12}$$

If we shrink the ‘-’ region even further and consider  $j=i+1$ , the negative region consists of a single term,  $\langle ABi+1 \rangle < 0$ , i.e.,

$$\begin{aligned}
 &\text{Diagram of a circle with points } i-1, i, i+1, i+2 \text{ and others. A purple line connects } i \text{ and } i+1 \text{ with } \langle ABi+1 \rangle > 0 \text{ written above it.} \\
 &\leftrightarrow 0.
 \end{aligned}
 \tag{2.4.13}$$

Note, however, that this bracket  $\langle ABi+1 \rangle$  is exactly the one used to cut the space into chiral components. Therefore, the  $\langle ABi+1 \rangle > 0$  subspace is actually empty, i.e., the achiral space is now a single region which cannot be cut further without introducing spurious boundaries.

Above, we have discussed  $S_{ij}^{(2),+}$  where  $\langle ABij \rangle > 0$ , but the same analysis can be done for the opposite chirality where  $\langle ABij \rangle < 0$  where the rôles of  $+ \leftrightarrow -$  are interchanged. Going back to the achiral space, we divide the region into chiral components,





where we have also indicated the additional inequalities ( $\langle AB(512) \cap (241) \rangle > 0$  and  $\langle AB(514) \cap (241) \rangle > 0$ ) imposed to define the space. Similar to what we have seen above, this is one chiral subspace of a larger achiral region defined by the signs of  $\langle ABi+1 \rangle$  only. In fact, the intersections appearing in eq. (2.4.15) can be replaced by a single inequality, either

$$\langle AB25 \rangle < 0 \text{ or } \langle AB14 \rangle < 0. \quad (2.4.16)$$

to define exactly the same space as eq. (2.4.15),

$$\quad (2.4.17)$$

Note that the bracket  $\langle AB24 \rangle > 0$  is positive as a consequence of the  $\langle ABi+1 \rangle$  signs *only*. From a Schouten identity,

$$\langle \underset{-}{AB12} \rangle \langle \underset{-}{AB45} \rangle + \langle \underset{+}{AB15} \rangle \langle \underset{+}{AB24} \rangle = \langle AB14 \rangle \langle AB25 \rangle > 0, \quad (2.4.18)$$

it then follows that fixing the sign of  $\langle AB14 \rangle$  determines the sign of  $\langle AB25 \rangle$ , and vice versa. Only one of the two four-brackets is necessary to define the chiral sign-flip-four space, and the other is redundant. The five-point pentagon eq. (2.4.15) space has both signs negative, while the second chiral subspace (which corresponds to the opposite chirality pentagon diagrammatically represented by a dashed line) has both signs positive,

$$\quad (2.4.19)$$

$$\begin{array}{c} 3 \\ + \\ 2 \\ - \\ 1 \\ + \\ 5 \end{array} \begin{array}{c} 4 \\ \leftrightarrow \end{array} \frac{\langle AB24 \rangle \langle 1235 \rangle \langle 1345 \rangle}{\langle AB12 \rangle \langle AB23 \rangle \langle AB34 \rangle \langle AB45 \rangle \langle AB15 \rangle} \equiv \begin{array}{c} 3 \\ 2 \\ 1 \\ 5 \\ 4 \end{array} \quad (2.4.20)$$

The union of these two spaces is a larger achiral space whose form is the difference of the two chiral pentagons, earlier introduced as parity-odd pentagon eq. (2.3.8),

$$\begin{array}{c} 3 \\ + \\ 2 \\ - \\ 1 \\ + \\ 5 \end{array} \begin{array}{c} 4 \\ \leftrightarrow \end{array} \frac{N_{\text{odd}}}{\langle AB12 \rangle \langle AB23 \rangle \langle AB34 \rangle \langle AB45 \rangle \langle AB15 \rangle}, \quad (2.4.21)$$

where the numerator is  $N_{\text{odd}} = \langle AB\bar{24} \rangle \langle 1245 \rangle - \langle AB24 \rangle \langle 1235 \rangle \langle 1345 \rangle$ .

Our next example is the achiral six-point region which can likewise be cut into two chiral components using a single additional inequality,

$$\begin{array}{c} 3 \\ + \\ 2 \\ - \\ 1 \\ + \\ 6 \end{array} \begin{array}{c} 5 \\ = \end{array} \begin{array}{c} 3 \\ + \\ 2 \\ - \\ 1 \\ + \\ 6 \end{array} + \begin{array}{c} 3 \\ + \\ 2 \\ - \\ 1 \\ + \\ 6 \end{array}, \quad (2.4.22)$$

where, again, the signs of the “diagonal brackets” are either both positive or both negative as a consequence of a Schouten identity. Calculating the forms associated to these spaces, we find two chiral hexagons which were introduced in [123] as examples

of IR-finite integrands,

$$\begin{array}{c}
 \begin{array}{c}
 \text{3} \quad + \quad \text{4} \\
 \text{+} \quad \text{+} \\
 \text{2} \quad \text{+} \quad \text{5} \\
 \text{+} \quad \text{+} \\
 \text{1} \quad \text{+} \quad \text{6}
 \end{array}
 \leftrightarrow
 \frac{\langle AB\bar{24} \rangle \langle AB\bar{51} \rangle}{\langle AB12 \rangle \langle AB23 \rangle \cdots \langle AB16 \rangle}
 \equiv
 \begin{array}{c}
 \text{3} \\
 | \\
 \text{2} \quad \text{4} \\
 \text{---} \text{---} \text{---} \\
 | \\
 \text{1} \quad \text{5} \\
 | \\
 \text{6}
 \end{array},
 \quad (2.4.23)
 \end{array}$$

$$\begin{array}{c}
 \begin{array}{c}
 \text{3} \quad + \quad \text{4} \\
 \text{+} \quad \text{+} \\
 \text{2} \quad \text{+} \quad \text{5} \\
 \text{+} \quad \text{+} \\
 \text{1} \quad \text{+} \quad \text{6}
 \end{array}
 \leftrightarrow
 \frac{\langle AB24 \rangle \langle AB51 \rangle \langle 3456 \rangle \langle 6123 \rangle}{\langle AB12 \rangle \langle AB23 \rangle \cdots \langle AB16 \rangle}
 \equiv
 \begin{array}{c}
 \text{3} \\
 | \\
 \text{2} \quad \text{4} \\
 \text{---} \text{---} \text{---} \\
 | \\
 \text{1} \quad \text{5} \\
 | \\
 \text{6}
 \end{array}.
 \quad (2.4.24)
 \end{array}$$

Finally, we consider an additional six-point region corresponding to yet another chiral pentagon integrand:

$$\begin{array}{c}
 \begin{array}{c}
 \text{3} \quad + \quad \text{4} \\
 \text{+} \quad \text{+} \\
 \text{2} \quad \text{+} \quad \text{5} \\
 \text{+} \quad \text{+} \\
 \text{1} \quad \text{+} \quad \text{6}
 \end{array}
 \leftrightarrow
 \frac{\langle AB\bar{25} \rangle \langle 1256 \rangle}{\langle AB12 \rangle \langle AB23 \rangle \langle AB45 \rangle \langle AB56 \rangle \langle AB16 \rangle}
 \equiv
 \begin{array}{c}
 \text{3} \quad \text{4} \\
 \diagdown \quad \diagup \\
 \text{2} \quad \text{5} \\
 \text{---} \text{---} \text{---} \\
 \text{1} \quad \text{6}
 \end{array}.
 \quad (2.4.25)
 \end{array}$$

We see the same pattern as in the sign-flip-two spaces: inside the ‘+’ region the “inner boundaries” are absent; e.g., in eq. (2.4.25),  $\langle AB34 \rangle$  is not a pole of the form nor a boundary of the geometric space.

Having discussed several illuminating examples at low multiplicity, we are now

ready to present the general sign-flip-four case:

$$S_{iklj}^{(4),\pm} = \begin{array}{c} i+1 \dots j-1 \\ i \quad - \quad - \quad - \quad j \\ i-1 \quad + \quad \dots \quad + \quad j+1 \\ \dots \quad + \quad \dots \quad + \quad \dots \\ l+1 \quad + \quad \dots \quad + \quad k-1 \\ l \quad - \quad - \quad - \quad k \\ l-1 \dots k+1 \end{array} \quad (2.4.26)$$

where the large achiral region  $S_{iklj}^{(4)}$  of eq. (2.4.6) is cut into two chiral subspaces by specifying the signs of  $\langle ABi\ell \rangle$  or  $\langle ABkj \rangle$ . In one subspace they are both positive while in the other they are both negative. In addition, all signs are uniformly fixed inside the four sign sectors. For example, all brackets of the form

$$\langle ABpq \rangle, \langle AB\bar{p}\bar{q} \rangle > 0 \quad \text{for } p < q \in \{j, j+1, \dots, i\}, \quad (2.4.27)$$

are positive, whereas the analogous brackets in the “minus region” are negative. We give further details on the fixed sign structure in appendix A.2. Practically, this means that the only boundaries from each of these sectors are the ones adjacent to the sign-flip positions, so the logarithmic form has exactly eight boundaries in the general case. In fact, each chiral component can be identified with a *chiral octagon* integrand

$$\begin{array}{c} k+1 \dots \ell-1 \\ k \quad + \quad + \quad + \quad \ell \\ k-1 \quad - \quad \dots \quad - \quad \ell+1 \\ \dots \quad - \quad \dots \quad - \quad \dots \\ i+1 \quad - \quad \dots \quad - \quad j-1 \\ i \quad + \quad \dots \quad + \quad j \\ i-1 \quad + \quad \dots \quad + \quad j+1 \end{array} \longleftrightarrow \begin{array}{c} k+1 \quad \ell-1 \\ \dots \quad \dots \\ k \quad \ell \\ k-1 \quad \ell+1 \\ \dots \quad \dots \\ i+1 \quad j-1 \\ \dots \quad \dots \\ i \quad j \\ \dots \quad \dots \\ i-1 \quad j+1 \end{array}, \quad (2.4.28)$$

where the wavy and dashed lines indicate the respective numerators [123],

$$\omega_{iklj}^{(4),-} = \frac{\langle AB\bar{i}j \rangle \langle ABik \rangle \langle AB\bar{k}\ell \rangle \langle AB\ell j \rangle}{\langle ABi-1i \rangle \langle ABi+1 \rangle \langle ABk-1k \rangle \langle ABkk+1 \rangle} \times \langle AB\ell-1\ell \rangle \langle AB\ell\ell+1 \rangle \langle ABj-1j \rangle \langle ABjj+1 \rangle. \quad (2.4.29)$$

The form for the other chiral space,  $\omega_{iklj}^{(4),+}$ , for which  $\langle ABi\ell \rangle, \langle ABkj \rangle > 0$ , is obtained by flipping the wavy and dashed lines. The chiral octagons were introduced in [123] as the one-loop integrand basis elements which split the basis into parity-odd (which integrate to zero), IR-finite and IR-divergent integrands. While the expression for the integrand may look complicated, because of the special form of the numerator in the generic case the integrand is IR finite and evaluates to a simple combination of dilogarithms. It is very surprising that we see the same objects here in a very different setup as the integrand forms for maximal sign-flip regions.

The chiral octagons naturally degenerate to simpler spaces when the labels  $i, k, \ell, j$  become adjacent. Exactly the same happens with our regions as well, and we can indeed identify the pentagon and hexagon examples discussed above as boundary cases of the generic octagon.

## 2.5 Local geometries and the Amplituhedron-Prime

Having discussed various aspects of more general sign-flip spaces, let us come back to the local integrands of section 2.3 that enter the chiral pentagon expansion of the one-loop MHV amplitude, eq. (2.2.45). After a careful analysis of consistent sign patterns for the individual local geometries, we concluded in section 2.3 that there are only two faithful geometric spaces which can be associated with the general chiral pentagon eqs. (2.3.17) and (2.3.19), two choices for the two-mass-hard boxes eqs. (2.3.22) and (2.3.23), and four choices for the one-mass boxes eqs. (2.3.27) and (2.3.28), respectively.

In the next step we discuss how to glue these geometric regions together. We are going to show that only a single choice for the pentagon and box spaces is globally consistent (at all multiplicities) upon gluing. By consistency, we mean the require-

ment that there are no unphysical boundaries left in the resulting geometry akin to our discussion of *faithful geometries* in section 2.3.2. As a tool, we make use of the classification of all relevant positive geometries in terms of the sign-flip-two and four regions summarized in sections 2.4 and appendix A.1. This allows us to write a (conjectured) closed formula for the final geometric space in eq. (2.5.32).

The primary result of this section is a *new* positive geometry, which we name the *Amplituhedron-Prime*, comprised of a particular collection of chiral sign-flip-two and four regions with only physical boundaries of all codimensions. While this new space has exactly the same singularity structure as the Amplituhedron, their bulk geometries are entirely non-overlapping. This follows directly from the fact that the original Amplituhedron is comprised of a single chiral sign-flip-zero space.

### 2.5.1 Chiral regions for boxes and pentagons

We start our discussion with the five-point one-loop MHV amplitude. Specializing eq. (2.2.45) to  $n=5$ , the integrand is a sum of one chiral pentagon and two boxes,

$$\omega^{(5,0,1)} = \text{pentagon} + \text{box}_1 + \text{box}_2. \quad (2.5.1)$$

The first box in this expression, which we label as  $B_{12}$ , has four individually well-defined faithful geometries as described in eqs. (2.3.27)–(2.3.28), where the sign of the bracket  $\langle AB12 \rangle$  is unfixed. In section 2.3 we constructed the candidate spaces for the box (all of which had no spurious boundaries) by imposing conditions on  $\langle ABi+1 \rangle$  brackets as well as additional conditions involving its leading singularities. By expanding the unfixed sign  $* = + \oplus -$ , it is straightforward to identify all four choices as particular instances of sign-flip-two and four spaces described in section 2.4. For the box  $B_{12}$  we

may write the options as

$$\begin{aligned}
 B_{12}^{(1)} &= \text{Diagram 1}, & B_{12}^{(2)} &= \text{Diagram 2}, \\
 B_{12}^{(3)} &= \text{Diagram 3}, & B_{12}^{(4)} &= \text{Diagram 4}.
 \end{aligned}
 \tag{2.5.2}$$

Note that for the choice labelled  $B_{12}^{(1)}$ , the missing space where  $\langle AB_{12} \rangle < 0$  is empty. The additional inequality  $\langle AB_{35} \rangle \leq 0$  is needed to select one of the chiral components of the larger achiral space. As we stressed above, all four spaces  $B_{12}^{(i)}$  are *a priori* locally satisfactory as they have the correct boundary structure to represent the associated integral. However, this box has singularities which are absent in the MHV one-loop integrand. Indeed, we consider such singularities spurious from the point of view of the global geometry of the Amplituhedron. Thus, the manner in which  $B_{12}$  glues together with the other terms in eq. (2.5.1) must be such that all spurious singularities cancel and we are left with exactly the physical singularity structure of the MHV Amplituhedron.

The discussion of the other box integrand,  $B_{45}$ , is analogous and we once again



have four different options:

$$\begin{aligned}
 B_{45}^{(1)} &= \begin{array}{c} \text{3} \\ \text{---} \quad \text{+} \\ \text{2} \quad \text{4} \\ \text{---} \quad \text{+} \\ \text{1} \quad \text{5} \\ \text{+} \end{array} , & B_{45}^{(2)} &= \begin{array}{c} \text{3} \\ \text{---} \quad \text{+} \\ \text{2} \quad \text{4} \\ \text{---} \quad \text{*} \\ \text{1} \quad \text{5} \\ \text{+} \end{array} , \\
 B_{45}^{(3)} &= \begin{array}{c} \text{3} \\ \text{+} \quad \text{---} \\ \text{2} \quad \text{4} \\ \text{---} \quad \text{*} \\ \text{1} \quad \text{5} \\ \text{+} \end{array} , & B_{45}^{(4)} &= \begin{array}{c} \text{3} \\ \text{+} \quad \text{---} \\ \text{2} \quad \text{4} \\ \text{---} \quad \text{*} \\ \text{1} \quad \text{5} \\ \text{+} \end{array} .
 \end{aligned} \tag{2.5.3}$$

Although this suggests a total of  $4^2$  possible choices for combining the two boxes, in our analysis below we will only consider the four choices  $\{B_{12}^{(i)}, B_{45}^{(i)}\}$ . This corresponds to assigning uniform geometries to all permutations of one-mass boxes. While at five points it is possible to mix-and-match the box spaces and get a consistent global geometry, this is simply due to the degenerate kinematics and does not extend to the all multiplicity case.

For the pentagon space, we have two possibilities which are geometrically consistent, as discussed in subsection 2.3.2. In this discussion we carved out the chiral spaces via inequalities involving  $\langle AB(n1i) \cap (ij\star) \rangle$  and  $\langle AB(n1j) \cap (ij\star) \rangle$ , where  $\star$  was in either of the two sets  $\{i+1, \dots, j-1\}$  or  $\{1, \dots, i-1\}$ . However, it follows directly from the complete characterization of *all* sign-flip spaces given in section 2.4 that both solutions for the pentagon (once expanded using  $\ast = + \oplus -$ ) must be a direct sum of either sign-flip-two or four chiral spaces. For the first option eq. (2.3.17) (which corresponds

to the choice  $\star = 3$ ), the equivalent sign-flip characterization of the space is

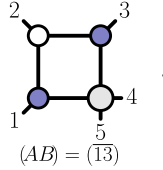
$$P_{24}^{(1)} = \begin{array}{c} \text{3} \\ \text{+} \quad \text{-} \\ \text{2} \quad \text{4} \\ \text{1} \quad \text{5} \\ \text{+} \end{array} \langle AB13 \rangle > 0 + \begin{array}{c} \text{3} \\ \text{-} \quad \text{-} \\ \text{2} \quad \text{4} \\ \text{1} \quad \text{5} \\ \text{+} \end{array} \langle AB24 \rangle > 0 + \begin{array}{c} \text{3} \\ \text{+} \quad \text{+} \\ \text{2} \quad \text{4} \\ \text{1} \quad \text{5} \\ \text{+} \end{array} \langle AB14 \rangle > 0 + \begin{array}{c} \text{3} \\ \text{-} \quad \text{+} \\ \text{2} \quad \text{4} \\ \text{1} \quad \text{5} \\ \text{+} \end{array} \langle AB35 \rangle > 0 \quad (2.5.4)$$

where for brevity we simply label the sign-flip four spaces by a single non-adjacent chord of the circle. As discussed in section 2.4 above, a single condition is always sufficient to fix this space. The second option eq. (2.3.19) corresponds to either choice of  $\star = 5$  or  $\star = 1$  and is equivalent to a single chiral sign-flip-four space:

$$P_{24}^{(2)} = \begin{array}{c} \text{3} \\ \text{+} \quad \text{+} \\ \text{2} \quad \text{4} \\ \text{1} \quad \text{5} \\ \text{+} \end{array} \langle AB14 \rangle < 0 \quad (2.5.5)$$

As a result, considering a uniform choice for the one-mass boxes eqs. (2.5.2)–(2.5.3) together with the two choices for the chiral pentagon eqs. (2.5.4)–(2.5.5) yields eight possible global geometries as a result of gluing the individual spaces. Our task is to see which (if any) of these are consistent with the *boundary structure* of the original five-point MHV Amplituhedron. This is a nontrivial constraint in spite of the fact that each individual space is free of spurious boundaries from the perspective of the individual local integrals. As described in appendix A, each local integral has many unphysical cuts from the perspective of the MHV one-loop geometry; a codimension-four example of this is the point  $(AB) = (\overline{13})$ , which is an allowed singularity of the one-mass box

$B_{45}$  and the pentagon  $P_{24}$  but is not an allowed singularity of the MHV Amplituhedron,

not allowed in MHV:  (2.5.6)

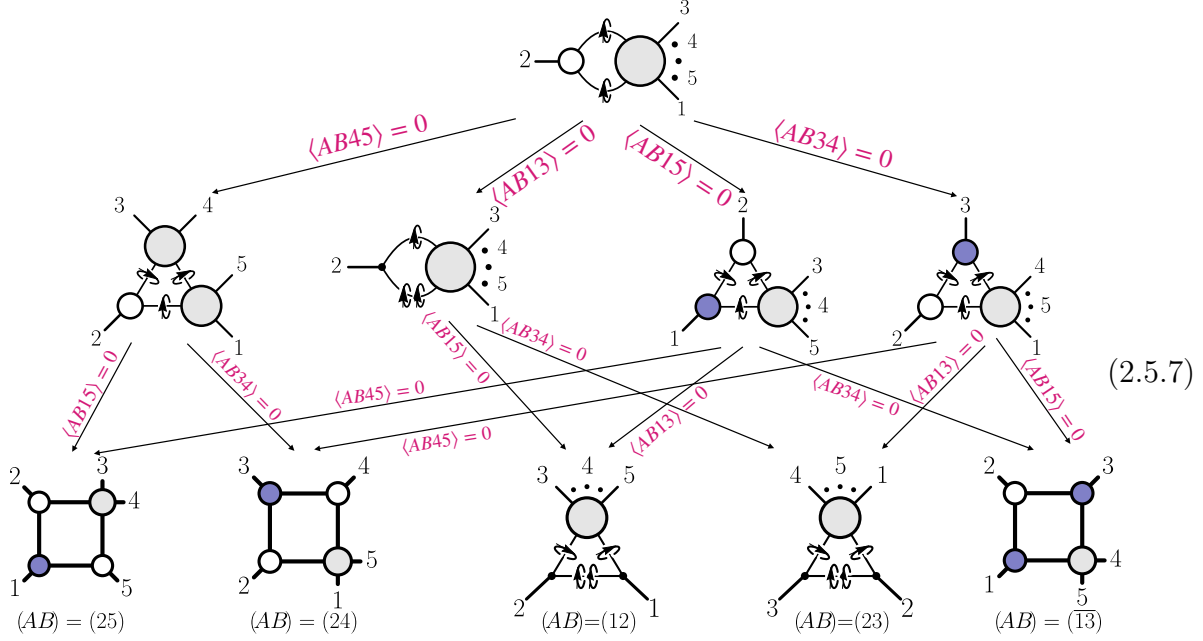
In fact, while the cancellation of leading singularities is nontrivial, there is an even stronger constraint at the level of triple cuts which we explain in detail shortly.

### 2.5.2 Two-dimensional projections

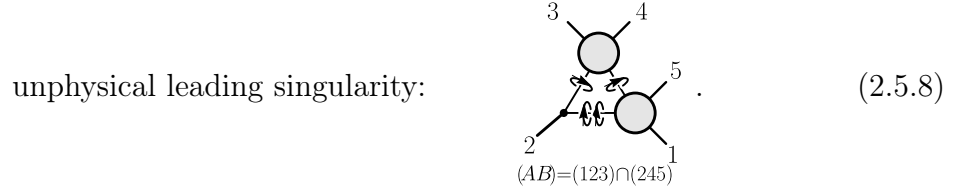
In deciding which individual geometric spaces can be consistently glued together, it is best to focus on certain two-dimensional boundaries where everything can be visualized geometrically as regions, lines, and points in the projective plane. The codimension-two boundaries of interest corresponds to configurations in momentum twistor space where the line  $(AB)$  intersects two adjacent lines  $(i-1i), (ii+1)$ . The codimension-two boundaries of this type are defined by solutions to  $\langle ABi-1i \rangle = \langle ABii+1 \rangle = 0$ .

As discussed in more detail in appendix A in eqs. (A.0.4) and (A.0.6) there are two solutions to these conditions, the first of which has the geometric interpretation that the line  $(AB)$  passes through the point  $Z_i$ . On this boundary, there are four codimension-three boundaries which correspond to setting one of the remaining three  $\langle ABjj+1 \rangle = 0$  together with one additional boundary which corresponds to setting  $\langle ABi-1i+1 \rangle = 0$ . Geometrically, this additional cut forces  $(AB)$  to also lie in the plane  $(i-1ii+1)$ . Physically, this special configuration is a collinear cut, see eq. (A.0.7). We can furthermore look at all the higher-codimension residues that are accessible for MHV and  $\overline{\text{MHV}}$  amplitudes. This can be summarized in the following picture of on-shell functions that

label the respective cut solutions [47].

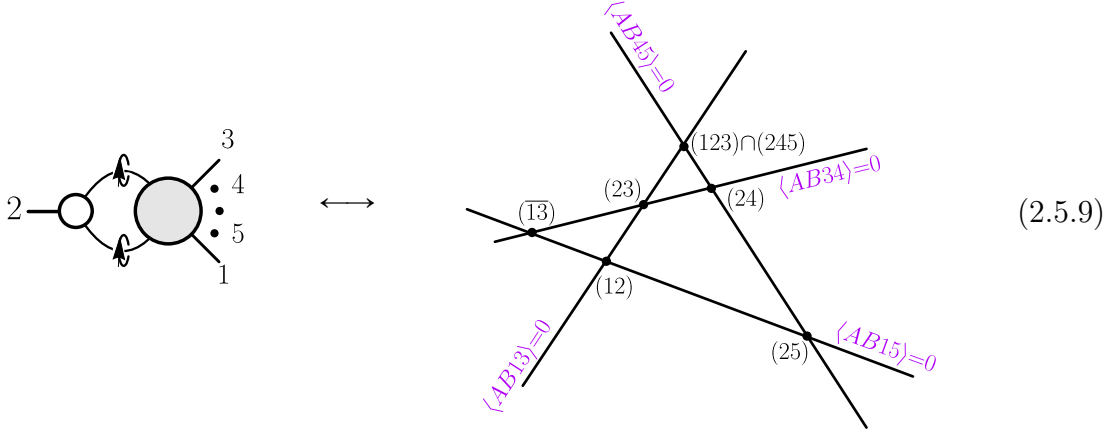


Besides the physical singularities of either MHV or  $\overline{\text{MHV}}$  amplitudes depicted in eq. (2.5.7), there is one additional unphysical leading singularity that could in principle appear in individual integrals,



However, for the local representation eq. (2.5.1), this spurious singularity is absent term-by-term. Geometrically, the content of eq. (2.5.7) can be encoded in the two-

dimensional configuration space for the line  $(AB)$  that is passing through  $Z_2$ ,



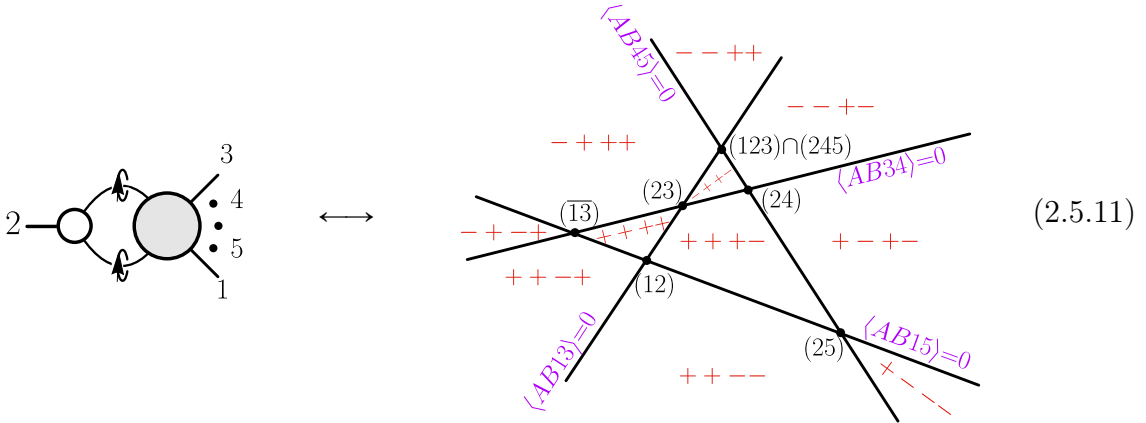
In this picture, lines correspond to codimension-three boundaries, i.e., configurations where  $(AB)$  intersects one more line in addition to passing through point  $Z_2$ . The codimension-four boundaries are the points in this picture where two lines intersect, and correspond to completely fixing all four degrees of freedom in  $(AB)$ . In other words, the line  $(AB)$  intersects two additional lines and passes through  $Z_2$ . These vertices correspond to positions of leading singularities which are accessible from the codimension-two surface where  $(AB) = (A2)$ . Note first that all triple cuts in this picture are physical, i.e., the MHV amplitude form has a non-zero residue when evaluated on all codimension-three boundaries in this picture. However, only a subset of the vertices represent actual leading singularities of the amplitude, which are what we consider physical. In particular, for the MHV amplitude only the points  $(AB) = (ij)$  are physical and all others are spurious.

The positive geometries associated to the local integrals in eqs. (2.5.2)–(2.5.5) above correspond to *regions* in the plane in eq. (2.5.9), which can be identified by the signs of brackets which are nonvanishing when evaluated on the boundary  $(AB)=(A2)$ . For  $(AB)=(A2)$ , the non-vanishing brackets of interest are

$$\{\langle AB34 \rangle, \langle AB45 \rangle, \langle AB15 \rangle, \langle AB13 \rangle\}. \quad (2.5.10)$$

Note that because this cut surface is defined by the conditions  $\langle AB12 \rangle = \langle AB23 \rangle = 0$ , all information about the signs of these two brackets is lost upon accessing the  $(AB) = (A2)$  boundary. While the first three brackets in eq. (2.5.10) are the usual  $\langle AB_{i+1} \rangle$  propagator-type boundaries, the bracket  $\langle AB13 \rangle$  corresponds to a spurious codimension-one boundary that only becomes physical *when evaluated on the support of this cut*. On the  $(AB) = (A2)$  codimension-two boundary, sign conditions on  $\langle AB13 \rangle$  are equivalent to many other expressions, e.g.,  $\langle AB\overline{24} \rangle \rightarrow -\langle AB13 \rangle \langle 2345 \rangle$ .

It is a relatively simple exercise to deduce the correspondence between regions in eq. (2.5.9) and sequences of signs for the brackets in eq. (2.5.10) by looking at the relative positions of vertices with respect to certain lines and using the positivity of the external data, eq. (2.2.11). For example, the vertex  $(AB) = (23)$  is to the left of the line  $\langle AB45 \rangle$ . Taking into account  $\langle 2345 \rangle > 0$ , we therefore conclude that the whole region to the left of the  $\langle AB45 \rangle = 0$  line corresponds to  $\langle AB45 \rangle > 0$  while the region to the right corresponds to  $\langle AB45 \rangle < 0$ . Again using the vertex  $(AB) = (23)$ , we get similar information about the regions where  $\langle AB15 \rangle \leq 0$ . For information on  $\langle AB34 \rangle$  we can use the vertex  $(AB) = (12)$ . Note that  $\langle AB13 \rangle$  vanishes for both  $(AB) = (12)$  and  $(AB) = (23)$  since both points are on this line. Instead, we can use  $(AB) = (24)$  which is on the side of  $\langle AB13 \rangle < 0$ . These arguments fix the labeling of all regions



where we simply replace the sequence of brackets eq. (2.5.10) by their respective fixed signs in a given region. Note that since the plane is projective, certain regions “wrap

around” the point at infinity and come back on the other side of the picture, and naively have all signs opposite; an example of this is region  $\{+, -, +, -\}$ , which wraps around at infinity to join with  $\{-, +, -, +\}$ . This is a simple consequence of the fact, already alluded to above in our discussion of  $d \log$  forms and geometry, that it is not the inequality  $\langle ABX \rangle > 0$  which is projectively meaningful, but rather an inequality involving a *ratio* of two four brackets,  $\langle ABX \rangle / \langle ABY \rangle > 0$ . In this context, this means that flipping all signs in the definition of a space gives a completely equivalent description of it. In eq. (2.5.11) the regions  $\{+, -, +, -\}$  and  $\{-, +, -, +\}$  are precisely the same space. Therefore, we will use the same signs for all such instances of regions which wrap around at infinity, i.e., we identify  $\{+, -, +, -\} \sim \{-, +, -, +\}$ .

Note that in eq. (2.5.11) the MHV Amplituhedron corresponds to the region labelled as  $\{+, +, +, -\}$ . This region is a quadrilateral with the four vertices (12), (23), (24) and (25) that correspond to the four physical leading singularities accessible from the  $(AB)=(A2)$  cut surface. In contrast, the  $\overline{\text{MHV}}$  region corresponds to  $\{+, +, +, +\}$  which is the triangle with vertices (12), (23), (13).

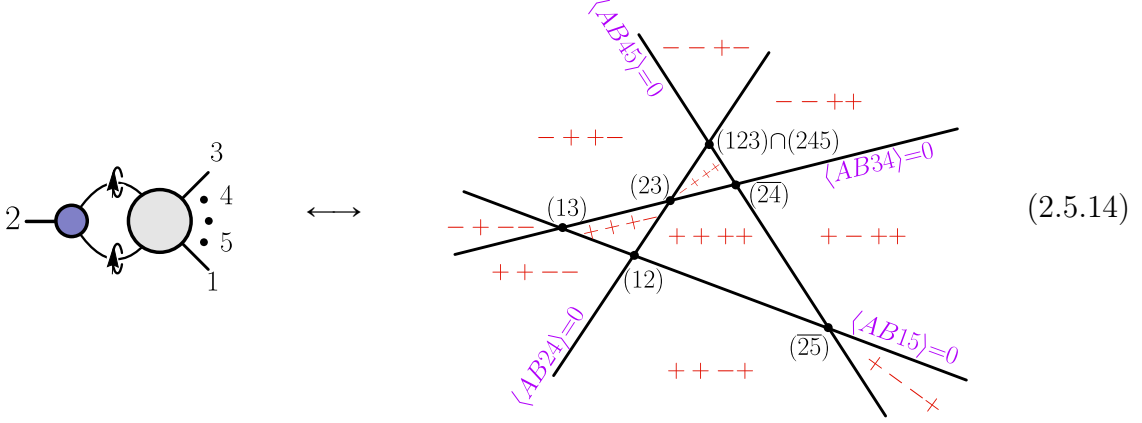
The second solution to the cut conditions  $\langle AB12 \rangle = \langle AB23 \rangle = 0$  has the geometric interpretation that the line  $(AB)$  is completely contained in the plane (123),

(2.5.12)

Starting from the on-shell function for the double-cut, we could again write down all possible higher codimension residues that are accessible from this surface. For the sake of brevity, we refrain from doing so here and proceed directly to the geometric picture for the configuration space of the line  $(AB)$  that is contained in the plane (123). Analogous to eq. (2.5.10), the accessible codimension-three boundaries

$$\{\langle AB34 \rangle, \langle AB45 \rangle, \langle AB15 \rangle, \langle AB24 \rangle\} \quad (2.5.13)$$

correspond to lines in the two-dimensional pictures. We chose a particular bracket,  $\langle AB24 \rangle$ , to indicate on which side of the *collinear boundary* the line  $(AB)$  is. As mentioned above, on support of the  $\langle AB12 \rangle = \langle AB23 \rangle = 0$  cut conditions this can be re-written in various equivalent ways. The corresponding two-dimensional picture for the configuration space of the line  $(AB) \subset (123)$  is,



where we have labeled the regions in terms of the signs of the brackets in the sequence eq. (2.5.13). The MHV Amplituhedron is the region  $\{+, +, +, -\}$  (which on this cut surface has only three vertices) while the  $\overline{\text{MHV}}$  region corresponds to  $\{+, +, +, +\}$ . Note that for the MHV geometry the entire line  $\langle AB45 \rangle = 0$  is an unphysical codimension-three boundary corresponding to the on-shell function



Geometrically, none of the physical leading singularities (vertices) lie on  $\langle AB45 \rangle = 0$ . In the same spirit, the line  $\langle AB45 \rangle = 0$  was unphysical for the  $\overline{\text{MHV}}$  Amplituhedron in the previous two-dimensional picture eq. (2.5.11).

All two-dimensional boundaries of the type where  $(AB) \subset (i-1ii+1)$  or  $(AB)$  passes through  $Z_i$  have the same geometry, and the corresponding projections can be



obtained by cyclically relabelling the above examples. In principle, there is one additional class of codimension-two boundaries where we set two non-adjacent  $\langle AB_{ii+1} \rangle$  brackets to zero, e.g.  $\langle AB_{12} \rangle = \langle AB_{34} \rangle = 0$ . This boundary, while also two-dimensional, has a significantly more complicated stratification and is not easily visualized in the projective plane. While boundaries of this form can lead to spurious higher codimension cuts which a priori could place additional constraints on gluing together local integral spaces (discussed in the following subsection 2.5.3), we find in practice that matching all simple two-dimensional projections mentioned above is sufficient to fix a unique consistent gluing of spaces into the “Amplituhedron-Prime”.

### 2.5.3 Gluing regions

While all codimension-two boundaries of the type  $(AB) \subset (i-1ii+1)$  or  $(AB) = (Ai)$  have the same geometry, in the context of the particular local expansion eq. (2.2.45) we have to consider each case separately. The reason is that our global choice of  $\langle AB_{1n} \rangle > 0$  for the local spaces introduced in section 2.3.2 breaks the cyclic symmetry of the integrand and the individual contributions are different depending on the boundary we consider.

At five points we must consider ten two-dimensional projections of the form described in section 2.5.2. For each projection, we demand that the combination of all local integrals has exactly the same *boundary* (but not necessarily bulk) structure as the original Amplituhedron, i.e., there are no spurious boundaries. In this section, we first give the answer for the correct spaces for the boxes and pentagons at five and six points, and subsequently state the result for the general  $n$ -point geometries. We only schematically illustrate how all spurious boundaries cancel for the final correct choice of geometries for the boxes and chiral pentagons on some representative two-dimensional planes. The details on how we find a unique solution (under the assumptions discussed in subsection 2.5.1) that holds for an arbitrary number of external points requires a careful analysis of multiple two-dimensional projections which is deferred to appendix A.3.

Let us briefly start with the five-point geometries, where further details are rel-

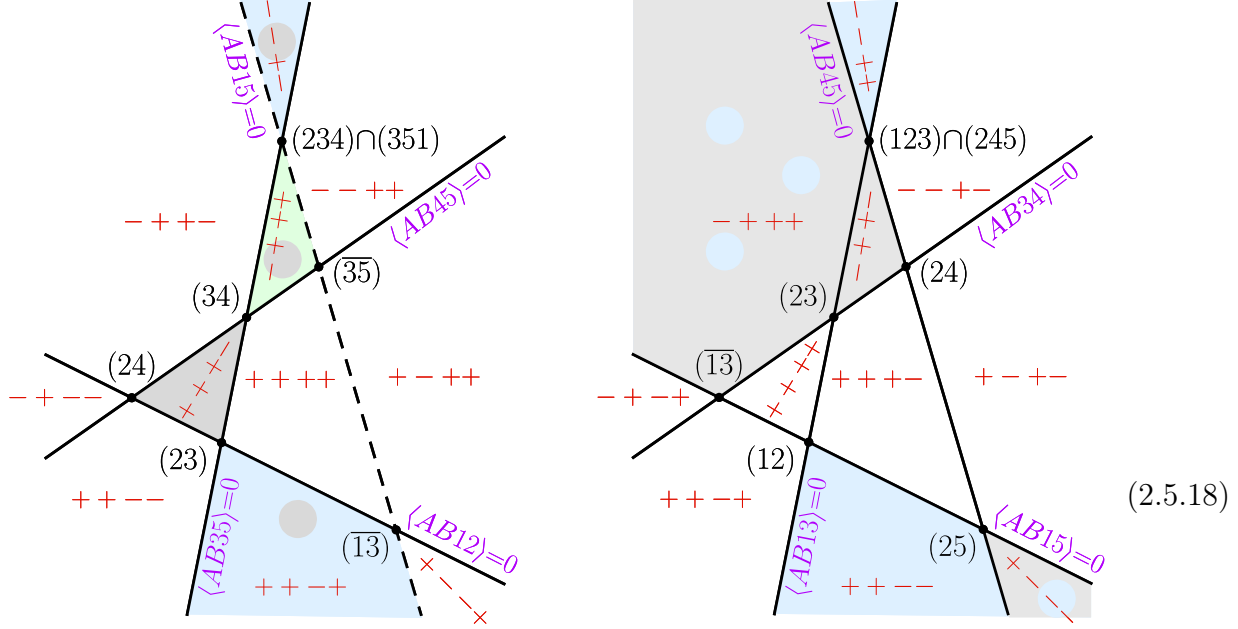
egated to appendix A.3. From eq. (2.5.1), there are two box integrands,  $B_{12}, B_{45}$ , and one chiral pentagon  $P_{24}$ , which we can a priori associate with a number of valid geometric spaces, see (2.5.2)–(2.5.5). Now we would like to combine these individual pieces into a single geometric object which has the same singularity structure as the original Amplituhedron. In order to find the consistent gluings which cancel all spurious singularities for the eight possible combinations of the box and pentagon spaces  $\{B_{12}^{(i)}, B_{45}^{(i)}, P_{24}^{(1)}, P_{24}^{(2)}\}$ , we consider projections to ten codimension-two boundaries where the loop line  $(AB)$  passes either through a point  $(AB) = (Ai)$  or is in a plane  $(AB) \subset (i-1 i i+1)$ . On these codimension-two boundaries, the configuration spaces for  $(AB)$  become the simple two-dimensional geometries of the form of eqs. (2.5.11) and (2.5.14). As discussed in section 2.5.2, in these projective pictures codimension-three boundaries are lines and codimension-four boundaries (i.e., leading singularities) are points. In order to determine the consistent global geometries, we demand that all *spurious boundaries*, i.e. boundaries that are not part of the original Amplituhedron, cancel. The result of this analysis is that, at five points, only two combinations of box and pentagon spaces survive:

$$\{B_{12}^{(2)}, B_{45}^{(2)}, P_{24}^{(1)}\}, \quad \text{and} \quad \{B_{12}^{(3)}, B_{45}^{(3)}, P_{24}^{(1)}\}. \quad (2.5.16)$$

For more details on how this was determined we refer the interested reader to appendix A.3. Of these two solutions, it is the second option,  $\{B_{12}^{(3)}, B_{45}^{(3)}, P_{24}^{(1)}\}$ , which generalizes to six and higher points, as we show in appendix A.3. Let us briefly discuss why the second option of eq. (2.5.16) is consistent on two representative two-dimensional projections. For illustrative purposes, we discuss (i) the projection where  $(AB) \subset (234)$ , and (ii) the projection where  $(AB) = (A2)$ . Physically, from the on-shell function point-of-view these correspond to,

$$(2.5.17)$$

On these two-dimensional boundaries the local spaces of eqs. (2.5.2)–(2.5.5) correspond to certain regions in the projective plane which are labeled by the signs of non-vanishing brackets in the sequences  $\{\langle AB45\rangle, \langle AB15\rangle, \langle AB12\rangle, \langle AB35\rangle\}$  and eq. (2.5.10), respectively. The (projections of the) second solution of eq. (2.5.16), which correctly generalizes to the all-multiplicity Amplituhedron-Prime, are



	$\langle AB45\rangle$	$\langle AB15\rangle$	$\langle AB12\rangle$	$\langle AB35\rangle$
$B_{12}^{(3)}$	–	+	+	+
$B_{45}^{(3)}$	+	+	–	+
$P_{24}^{(1)}$	+	+	–	+
	+	+	+	–
	–	+	+	+

	$\langle AB34\rangle$	$\langle AB45\rangle$	$\langle AB15\rangle$	$\langle AB13\rangle$
$B_{45}^{(3)}$	–	+	+	+
	–	–	+	+
$P_{24}^{(1)}$	–	+	+	+
	–	+	+	–

where we have color-coded the regions of the relevant local spaces eqs. (2.5.2)–(2.5.5) on both  $(AB)\subset(234)$  (l.h.s.) and  $(AB)=(A2)$  (r.h.s.) codimension-two boundaries. As already mentioned below eq. (2.5.11), spaces where we flip all signs lead to equivalent geometries; therefore, we only list one representative in the tables summarizing the contributing regions of each local integrand. This is why, e.g. on the l.h.s. of (2.5.18),

the pentagon  $P_{24}^{(1)}$  fills in both regions  $\{++--\} \sim \{--+-\}$  in the above left-hand-side picture. Furthermore, not all sign patterns which are present in the full local integral contribute on a given cut surface. Thus, for  $P_{24}^{(1)}$  only three of the four sign patterns in eq. (2.5.4) have access to the codimension-two boundary where  $(AB) \subset (234)$ .

In order to show the consistency of our claimed solutions eq. (2.5.16) for the local integrand spaces on this boundary, we have to identify the cancellation of the spurious  $\langle AB15 \rangle = 0$  line. In the solution  $\{B_{12}^{(3)}, B_{45}^{(3)}, P_{24}^{(1)}\}$  depicted on the left of eq. (2.5.18), we trivially see the cancellation of the entire spurious line, because the regions  $\{-+ -\}, \{-+ ++\}, \{++ -+\}$  are double-covered by parts of the pentagon spaces as well as the boxes. For the  $(AB) = (A2)$  projection depicted on the right of eq. (2.5.18), we see that after cancelling overlapping regions we are left with the union of three regions,  $\{++ --\}, \{- - ++\}$  and  $\{- + +- \}$ . While this space has the correct boundary structure, here we can see it is non-overlapping with the original Amplituhedron which is the region  $\{++ +- \}$  on this projection.

Thus, at five points there is only one consistent space for the pentagon and we may cancel all spurious boundaries using two different (uniform) choices for the boxes. Both choices have exactly the same boundaries as the original Amplituhedron and are completely satisfactory at this multiplicity. However, only one of these solutions generalizes to higher points. This can be seen directly at six points, where an additional constraint arises: our five-point choice must be compatible with (at least) one of the two spaces eqs. (2.3.22) and (2.3.23) for the two-mass hard box.

Next, we discuss the local representation of the one-loop six-point MHV integrand

$$\begin{aligned}
 \omega^{(6,0,1)} = & \begin{array}{c} \text{Diagram 1} \\ \text{Diagram 2} \\ \text{Diagram 3} \end{array} + \begin{array}{c} \text{Diagram 4} \\ \text{Diagram 5} \\ \text{Diagram 6} \end{array} + \begin{array}{c} \text{Diagram 7} \\ \text{Diagram 8} \\ \text{Diagram 9} \end{array} \\
 & + \begin{array}{c} \text{Diagram 10} \\ \text{Diagram 11} \\ \text{Diagram 12} \end{array} + \begin{array}{c} \text{Diagram 13} \\ \text{Diagram 14} \\ \text{Diagram 15} \end{array} + \begin{array}{c} \text{Diagram 16} \\ \text{Diagram 17} \\ \text{Diagram 18} \end{array} .
 \end{aligned}
 \tag{2.5.19}$$

Let us consider the six-point analog of eq. (2.5.9), i.e., the two-dimensional projection where  $(AB) \subset (234)$ .

$$\tag{2.5.20}$$

We have labeled the regions by the signs of the sequence of brackets

$$\{\langle AB45 \rangle, \langle AB56 \rangle, \langle AB16 \rangle, \langle AB12 \rangle, \langle AB35 \rangle\},
 \tag{2.5.21}$$

so that the MHV Amplituhedron is the  $\{+, +, +, +, -\}$  triangle region with vertices  $(23), (24), (34)$ . At six points there are now *two* spurious lines, defined by the conditions  $\langle AB56 \rangle = 0$  and  $\langle AB16 \rangle = 0$ . These have simple on-shell function interpretations analogous to eq. (2.5.15), but for brevity we do not write them explicitly here. In the

chiral pentagon expansion eq. (2.5.19), three terms contribute on this cut configuration:

$$\omega^{(6,0,1)} \Big|_{\text{cut}} = \begin{array}{c} \text{Diagram 1: Pentagon with vertices 1-6, wavy line between 2 and 4} \\ \text{Diagram 2: Square with vertices 1-6, diagonal from 1 to 4} \\ \text{Diagram 3: Square with vertices 1-6, diagonal from 2 to 5} \end{array} \Big|_{\text{cut}} . \quad (2.5.22)$$

This is the first example where the two-mass-hard box plays a role. We now take the generalizations of the two consistent spaces for the one-mass box and chiral pentagons from our five-point analysis eq. (2.5.16) and augment them by two options for the two-mass hard spaces, see eqs. (2.3.22) and (2.3.23). The details of this analysis can be found in appendix A.3, but roughly speaking the strategy involves consistently canceling spurious boundaries on all two-dimensional projections.

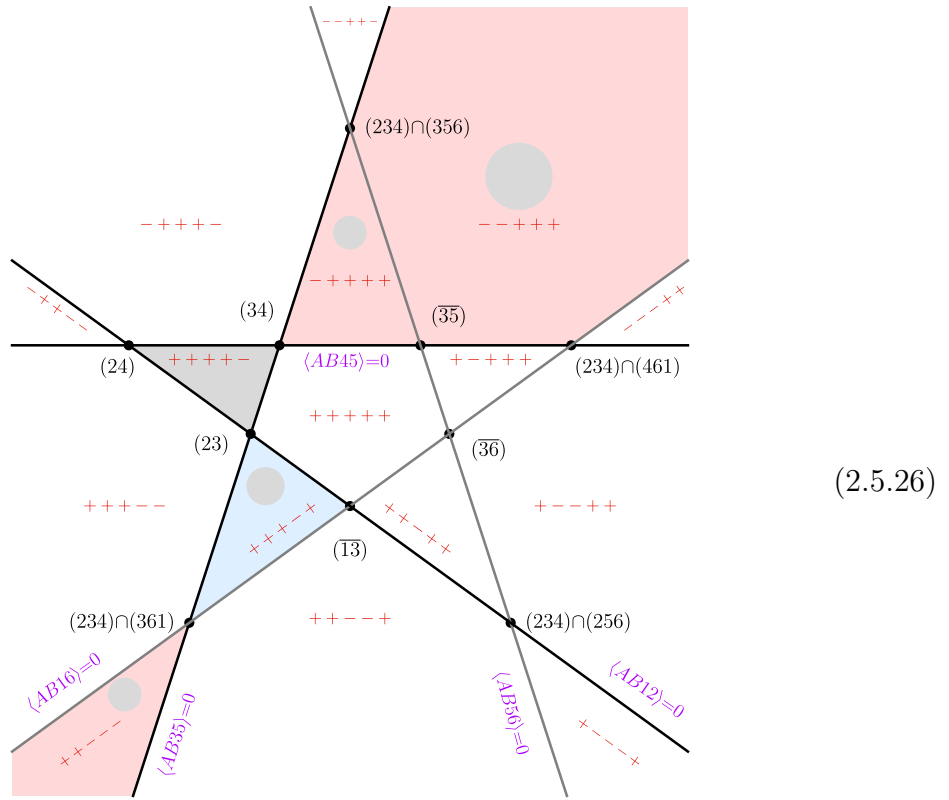
Ultimately, we find only the generalization of the second solution in eq. (2.5.16) together with the first choice  $B_{12,56}^{(1)}$  defined in eq. (2.5.29) is the *unique* (subject to the assumption that we make uniform choices for all boxes and pentagons, respectively) candidate space which is free of all spurious boundaries on all cut surfaces. For the  $(AB) \subset (234)$  projection discussed above, the relevant spaces are defined by the following by-now familiar circle diagrams:

$$B_{456}^{(3)} = 2 \begin{array}{c} \text{Circle diagram with vertices 1-6, vertical purple line from 2 to 4, label } \langle AB13 \rangle > 0 \\ \text{Signs: } 1(+), 2(+), 3(-), 4(-), 5(*), 6(+). \end{array} , \quad (2.5.23)$$

$$P_{24}^{(1)} = 2 \begin{array}{c} \text{Circle diagram 1: } \langle AB13 \rangle > 0, \text{ signs } 1(+), 2(+), 3(-), 4(-), 5(*), 6(+). \\ \text{Circle diagram 2: } \langle AB24 \rangle > 0, \text{ signs } 1(+), 2(+), 3(-), 4(-), 5(+), 6(+). \\ \text{Circle diagram 3: } \langle AB14 \rangle > 0, \text{ signs } 1(+), 2(+), 3(+), 4(+), 5(-), 6(+). \\ \text{Circle diagram 4: } \langle AB24 \rangle > 0, \text{ signs } 1(+), 2(+), 3(+), 4(+), 5(-), 6(+). \end{array} \quad (2.5.24)$$

$$\begin{array}{c}
 \begin{array}{c}
 \begin{array}{c}
 3 \quad + \quad 4 \\
 \circ \\
 \text{---} \quad \text{---} \\
 \circ \\
 * \quad \quad * \\
 \circ \\
 1 \quad + \quad 6 \\
 \langle AB(234) \cap (461) \rangle > 0
 \end{array}
 \end{array}
 \end{array}
 = 2 \quad (2.5.25)$$

Filling in the regions corresponding to the spaces defined in eqs. (2.5.23)–(2.5.25) in the two-dimensional projection eq. (2.5.20), the result is:



	$\langle AB45 \rangle$	$\langle AB56 \rangle$	$\langle AB16 \rangle$	$\langle AB12 \rangle$	$\langle AB35 \rangle$
$B_{456}^{(3)}$	+	+	+	-	+
$P_{24}^{(1)}$	+	+	+	-	+
	+	+	+	+	-
	-	+	+	+	+
	-	-	+	+	+
$B_{12,56}^{(1)}$	-	+	+	+	+
	-	-	+	+	+

Again, we see that the chiral pentagon overlaps with the one-mass and two-mass-hard box in all regions that have spurious boundaries and therefore cancels those geometrically. On this particular two-dimensional projection, we are left with the triangle with vertices (23), (24) and (34) corresponding to the MHV space. We have verified the cancellation of spurious boundaries on all other two-dimensional projections.

The five- and six-point examples heretofore considered suggest a unique conjecture for the all-multiplicity Amplituhedron-Prime. Namely, we consider the union of the one-mass box spaces eq. (2.3.28) (choosing the positive sign for the bracket involving the leading singularity), the first pentagon space eq. (2.3.17) and the first two-mass hard box space eq. (2.3.22). We give explicit formulae for these spaces in terms of the sign-flip spaces of section 2.4 in the following subsection. This encompasses all integrand topologies that enter the  $n$ -point amplitude in the chiral pentagon expansion eq. (2.2.45).<sup>14</sup> Checking higher-point generalizations of projections such as eqs. (2.5.18) and (2.5.26) is a straightforward, if tedious, exercise. At seven points, we have verified that all spurious boundaries accessible from the codimension-two configurations  $(AB) \subset (i-1ii+1)$  cancel geometrically. At eight points, we have also verified by parametrizing  $(AB)$  with four real degrees of freedom that the spurious triple cuts which cut three

<sup>14</sup>Although the fully massive chiral pentagon first appears at eight points, this generates no additional complications in our analysis.



non-adjacent propagators (which are not visible in the two-dimensional projections considered above) cancel as functions of the last remaining degree of freedom in  $(AB)$ .

### 2.5.4 Amplituhedron-Prime

In the previous subsection, we have seen that demanding a consistent gluing of spaces associated to general chiral pentagon and box integrands led to a unique definition for the individual local geometries. In terms of the original integrals appearing in the chiral pentagon expansion, we associate to the generic chiral pentagon the space eq. (2.3.17). From the results of section 2.4 it follows that the additional inequalities involving  $\langle ABX_i \rangle$  and  $\langle ABX_j \rangle$  can always be replaced by one of the conditions defining the sign-flip-two or four spaces. As such, the space in eq. (2.3.17) can be represented in terms of our sign-flip circle-diagrams as a direct sum of four spaces:

$$\begin{aligned}
 P_{ij}^{(1)} &\leftrightarrow \text{Pentagon Diagram} \leftrightarrow \text{Circle Diagram 1} + \text{Circle Diagram 2} \\
 &\quad + \text{Circle Diagram 3} + \text{Circle Diagram 4} \quad (2.5.27)
 \end{aligned}$$

The one-mass and two-mass-hard box spaces in eq. (2.3.28) and eq. (2.3.22), respectively, have the following sign-flip representations:

$$\begin{aligned}
 B_{1n-3}^{(3)} &\leftrightarrow \begin{array}{c} n-2 \quad n-1 \\ \diagdown \quad \diagup \\ \text{---} \\ \diagup \quad \diagdown \\ n-3 \quad \dots \quad 1 \quad n \end{array} \leftrightarrow \dots \begin{array}{c} n-3 \quad - \quad n-2 \\ \text{---} \\ \text{---} \\ \text{---} \\ \text{---} \\ 1 \quad + \quad n \end{array} \begin{array}{c} * \\ * \\ * \\ * \\ * \end{array} \begin{array}{c} + \\ - \\ \langle AB_{n-2n} \rangle > 0 \\ - \\ + \end{array} \end{aligned} \tag{2.5.28}$$

$$\begin{aligned}
 B_{4n}^{(3)} &\leftrightarrow \begin{array}{c} 2 \quad 3 \\ \diagdown \quad \diagup \\ \text{---} \\ \diagup \quad \diagdown \\ 1 \quad \dots \quad 4 \quad n \end{array} \leftrightarrow \begin{array}{c} 3 \quad - \quad 4 \\ \text{---} \\ \text{---} \\ \text{---} \\ 1 \quad + \quad n \end{array} \begin{array}{c} * \\ * \\ * \\ * \\ * \end{array} \begin{array}{c} + \\ - \\ \langle AB_{13} \rangle > 0 \\ - \\ + \end{array} \end{aligned}$$

$$\begin{aligned}
 B_{1i-1, i+2n}^{(1)} &\leftrightarrow \begin{array}{c} i \quad i+1 \\ \diagdown \quad \diagup \\ \text{---} \\ \diagup \quad \diagdown \\ i-1 \quad \dots \quad 1 \quad n \end{array} \leftrightarrow \begin{array}{c} i \quad + \quad i+1 \\ \text{---} \\ \text{---} \\ \text{---} \\ 1 \quad + \quad n \end{array} \begin{array}{c} * \\ * \\ * \\ * \\ * \end{array} \begin{array}{c} - \\ + \\ \langle AB_{(i-1 \ i \ i+1) \cap (i+1 \ n \ 1)} \rangle > 0 \\ - \\ + \end{array} \end{aligned} \tag{2.5.29}$$

Let us now take the chiral pentagon expansion for the five- and six-particle amplitudes of eq. (2.5.1) and eq. (2.5.19) and write it in terms of the sign-flip spaces eqs. (2.5.27)–(2.5.29). As argued in subsection 2.5.3, the resulting space is free of spurious singularities. Therefore, we call the resulting collection of geometric regions the five- and six-point *Amplituhedron-Prime*:

$$\mathcal{A}'^{(5,0,1)} = \overbrace{\begin{array}{c} P_{24}^{(1)} \\ \text{---} \\ \text{---} \\ \text{---} \\ \text{---} \\ 1 \quad + \quad 5 \end{array}}^{\begin{array}{c} 3 \\ + \quad - \\ \langle AB_{13} \rangle > 0 \\ - \\ + \end{array}} + \overbrace{\begin{array}{c} P_{24}^{(1)} \\ \text{---} \\ \text{---} \\ \text{---} \\ \text{---} \\ 1 \quad + \quad 5 \end{array}}^{\begin{array}{c} 3 \\ - \quad - \\ \langle AB_{24} \rangle > 0 \\ - \\ + \end{array}} + \overbrace{\begin{array}{c} P_{24}^{(1)} \\ \text{---} \\ \text{---} \\ \text{---} \\ \text{---} \\ 1 \quad + \quad 5 \end{array}}^{\begin{array}{c} 3 \\ + \quad + \\ \langle AB_{14} \rangle > 0 \\ - \\ + \end{array}} + \overbrace{\begin{array}{c} P_{24}^{(1)} \\ \text{---} \\ \text{---} \\ \text{---} \\ \text{---} \\ 1 \quad + \quad 5 \end{array}}^{\begin{array}{c} 3 \\ - \quad + \\ \langle AB_{35} \rangle > 0 \\ - \\ + \end{array}}$$

$$\begin{array}{c}
+ \quad \begin{array}{c} 3 \\ \circlearrowleft \\ 2 \quad + \quad 4 \\ \text{ } \quad \text{ } \quad \text{ } \\ * \quad \text{ } \quad \text{ } \\ 1 \quad + \quad 5 \end{array} \quad + \quad \begin{array}{c} 3 \\ \circlearrowleft \\ 2 \quad + \quad 4 \\ \text{ } \quad \text{ } \quad \text{ } \\ * \quad \text{ } \quad \text{ } \\ 1 \quad + \quad 5 \end{array} \\
\hline
B_{12}^{(3)} \quad \quad \quad B_{45}^{(3)}
\end{array}
\tag{2.5.30}$$

$$\begin{array}{c}
\mathcal{A}'(6,0,1) = 2 \quad \begin{array}{c} 3 \quad + \quad 4 \\ \circlearrowleft \\ * \quad \text{ } \quad \text{ } \\ 1 \quad + \quad 6 \end{array} \quad + 2 \quad \begin{array}{c} 3 \quad - \quad 4 \\ \circlearrowleft \\ * \quad \text{ } \quad \text{ } \\ 1 \quad + \quad 6 \end{array} \quad + 2 \quad \begin{array}{c} 3 \quad + \quad 4 \\ \circlearrowleft \\ * \quad \text{ } \quad \text{ } \\ 1 \quad + \quad 6 \end{array} \quad + 2 \quad \begin{array}{c} 3 \quad - \quad 4 \\ \circlearrowleft \\ * \quad \text{ } \quad \text{ } \\ 1 \quad + \quad 6 \end{array} \\
\hline
P_{35}^{(1)} \\
\hline
+ 2 \quad \begin{array}{c} 3 \quad - \quad 4 \\ \circlearrowleft \\ + \quad \text{ } \quad \text{ } \\ 1 \quad + \quad 6 \end{array} \quad + 2 \quad \begin{array}{c} 3 \quad - \quad 4 \\ \circlearrowleft \\ + \quad \text{ } \quad \text{ } \\ 1 \quad + \quad 6 \end{array} \quad + 2 \quad \begin{array}{c} 3 \quad + \quad 4 \\ \circlearrowleft \\ + \quad \text{ } \quad \text{ } \\ 1 \quad + \quad 6 \end{array} \quad + 2 \quad \begin{array}{c} 3 \quad + \quad 4 \\ \circlearrowleft \\ + \quad \text{ } \quad \text{ } \\ 1 \quad + \quad 6 \end{array} \\
\hline
P_{24}^{(1)} \\
\hline
+ 2 \quad \begin{array}{c} 3 \quad * \quad 4 \\ \circlearrowleft \\ + \quad \text{ } \quad \text{ } \\ 1 \quad + \quad 6 \end{array} \quad + 2 \quad \begin{array}{c} 3 \quad * \quad 4 \\ \circlearrowleft \\ + \quad \text{ } \quad \text{ } \\ 1 \quad + \quad 6 \end{array} \quad + 2 \quad \begin{array}{c} 3 \quad * \quad 4 \\ \circlearrowleft \\ + \quad \text{ } \quad \text{ } \\ 1 \quad + \quad 6 \end{array} \quad + 2 \quad \begin{array}{c} 3 \quad * \quad 4 \\ \circlearrowleft \\ + \quad \text{ } \quad \text{ } \\ 1 \quad + \quad 6 \end{array} \\
\hline
P_{25}^{(1)} \\
\hline
+ 2 \quad \begin{array}{c} 3 \quad * \quad 4 \\ \circlearrowleft \\ + \quad \text{ } \quad \text{ } \\ 1 \quad + \quad 6 \end{array} \quad + 2 \quad \begin{array}{c} 3 \quad * \quad 4 \\ \circlearrowleft \\ + \quad \text{ } \quad \text{ } \\ 1 \quad + \quad 6 \end{array} \quad + 2 \quad \begin{array}{c} 3 \quad * \quad 4 \\ \circlearrowleft \\ + \quad \text{ } \quad \text{ } \\ 1 \quad + \quad 6 \end{array} \quad + 2 \quad \begin{array}{c} 3 \quad * \quad 4 \\ \circlearrowleft \\ + \quad \text{ } \quad \text{ } \\ 1 \quad + \quad 6 \end{array} \\
\hline
+ 2 \quad \begin{array}{c} 3 \quad - \quad 4 \\ \circlearrowleft \\ * \quad \text{ } \quad \text{ } \\ 1 \quad + \quad 6 \end{array} \quad + 2 \quad \begin{array}{c} 3 \quad - \quad 4 \\ \circlearrowleft \\ * \quad \text{ } \quad \text{ } \\ 1 \quad + \quad 6 \end{array} \quad + 2 \quad \begin{array}{c} 3 \quad + \quad 4 \\ \circlearrowleft \\ * \quad \text{ } \quad \text{ } \\ 1 \quad + \quad 6 \end{array} \\
\hline
B_{13}^{(3)} \quad \quad \quad B_{46}^{(3)} \quad \quad \quad B_{12,56}^{(1)}
\end{array}
\tag{2.5.31}$$

In subsection 2.5.3, we have seen on various two-dimensional projections that the representation of the full space in terms of the local building blocks is massively overlapping. From the sign-flip representation in terms of the circle-diagrams in eqs. (2.5.30)–(2.5.31), this overlap is visible as many terms with the same sign patterns appear in

different building blocks. In fact, we can exploit the results of section 2.4 and expand all  $*$  =  $+$   $\oplus$   $-$  present in these spaces<sup>15</sup>, throwing out all patterns with more than four sign flips. It is easy to see that many terms appear multiple times throughout the expansion, which geometrically means the same space gets multiply-covered. If we cover a space an even number of times it cancels completely, while for an odd number of covers we are left with a single copy of the space. In the end, there is a surprisingly uniform non-overlapping description of the Amplituhedron-Prime directly in terms of the sign-flip-two and four spaces of section 2.4, which naturally generalizes to all-multiplicities. Our conjecture for the  $n$ -point, one-loop MHV Amplituhedron-Prime is<sup>16</sup>

$$\begin{aligned}
\mathcal{A}'^{(n,0,1)} = & \sum_{2 \leq i < k < \ell < j \leq n-1} \text{Diagram 1} + \sum_{2 \leq i < j \leq n-1} \text{Diagram 2} \\
& + \sum_{2 \leq i < j \leq n-1} \text{Diagram 3}
\end{aligned} \tag{2.5.32}$$

Extending the five and six-point analysis of section 2.5 to test our all- $n$  expression eq. (2.5.32) is a straightforward exercise. We demand that all spurious boundaries present in the individual sign-flip spaces disappear upon gluing. Just as in the five and six-point examples, the spurious codimension-three boundaries are

- (1)  $(AB) \subset (i-1ii+1)$  and  $(AB)$  cuts  $(jj+1)$ ,
- (2) triple cuts of non-adjacent propagators,  $\langle ABii+1 \rangle = \langle ABjj+1 \rangle = \langle ABkk+1 \rangle = 0$

<sup>15</sup>After expanding all  $*$  in the two-mass-hard box (2.5.29) into a collection of spaces with definite signs for all  $\langle ABii+1 \rangle$ , we can relate these spaces to the chiral sign-flip regions in (2.4.9) and (2.4.26).

<sup>16</sup>Note that in the sum on the second line the term where  $j = i+1$  is an empty space as it simultaneously requires both  $\langle ABij \rangle > 0$  and  $\langle ABij \rangle < 0$ .

We have verified at seven points that all spurious boundaries of type (1) and (2) are absent from the final space. We also performed extensive numerical checks at eight (and higher) points that eq. (2.5.32) satisfies many nontrivial constraints. In principle, we could repeat the exercise of section 2.5 at higher points and attempt to find all positive geometries which consistently glue together. Our conjecture is that the unique spurious-boundary free combination is equivalent to (after cancelling overlapping regions) the result eq. (2.5.32). Note that it is clear by construction, that our new Amplituhedron-Prime space is externally triangulated by the chiral pentagon expansion.

Since the spaces constituting the Amplituhedron-Prime are always defined by (at least) one inequality of the form  $\langle ABii+1 \rangle < 0$ , the bulk of this new geometry is entirely non-overlapping with the original Amplituhedron. At the same time, it has only physical boundaries and exactly the same integrand form as the Amplituhedron. This construction demonstrates there are multiple positive spaces which can be associated with loop integrands in planar  $\mathcal{N} = 4$  sYM and the Amplituhedron of [56] is only a particular example (albeit possibly the most canonical one).

It is also interesting to note that while the chiral pentagon expansion externally triangulates the Amplituhedron-Prime, it also plays an even more natural role in the presumptive dual geometry. We will argue in section 2.6 that the chiral pentagons *internally* triangulate the (yet-to-be discovered) dual Amplituhedron.

As an aside, investigating the structure of eq. (2.5.32) more carefully, we note the absence of certain sign-flip regions, such as

(2.5.33)

While eq. (2.5.32) does provide the complete definition of the Amplituhedron-Prime

space, it is an expansion in terms of elementary regions and it would be desirable to find some more uniform definition, much like the definition of the MHV one-loop Amplituhedron in eq. (2.2.31). One can verify that the following definition is equivalent to eq. (2.5.32): the Amplituhedron-Prime is the space of all lines  $(AB)$  which satisfy

$$\begin{aligned} \{\langle AB12\rangle, \langle AB23\rangle, \dots, \langle ABn-1n\rangle\} \text{ has even number of sign flips} \\ \{\langle AB1n\rangle > 0, \langle ABi_1n\rangle > 0, \langle ABi_1i_{-1}\rangle > 0, \langle ABi_2i_{-1}\rangle < 0\}, \end{aligned} \tag{2.5.34}$$

where  $i_{1,2}$  is the position of the first (second) sign flip and  $i_{-1}$  that of the last sign flip.

The final two conditions in the second line of (2.5.34) are empty for the third term in eq. (2.5.32) which only has two sign flips. Also, the representative spaces (2.5.33) of terms that do *not* appear in (2.5.32) are ruled out by the first condition in (2.5.34) which only includes brackets up to  $\langle ABn-1n\rangle$  and does not “wrap around” to  $\langle AB1n\rangle$ . While the definition in eq. (2.5.34) is very simple, we do not quite understand its deeper meaning at the moment and leave a detailed investigation to future work.

Note that the chiral pentagon expansion of eq. (2.5.27) singles out the the line  $(n1)$  as special, as does our definition of the Amplituhedron-Prime, where  $\langle AB1n\rangle > 0$  is the only uniformly positive quantity throughout the space. While the  $d\log$  form for the whole space is cyclic, the space is obviously not, as can be seen in eq. (2.5.32). By using the chiral pentagon expansion with  $(ii+1)$ , rather than  $(1n)$ , fixed, we can construct  $n$  other Amplituhedron-Prime spaces by cyclically shifting eq. (2.5.32).

### Relation between $\mathcal{A}$ and $\mathcal{A}'$

The results of this subsection suggests a natural question: how is the Amplituhedron-Prime  $\mathcal{A}'$  related to the original Amplituhedron space  $\mathcal{A}$ ? They are non-overlapping positive geometries which have only physical boundaries and the same canonical form. Therefore, it must be possible to identify a collection of zero-form spaces (with no spurious boundaries) which can be added to  $\mathcal{A}'$  to directly yield  $\mathcal{A}$ .

As it turns out, identifying the correct zero-form space which relates  $\mathcal{A}$  and  $\mathcal{A}'$  is nontrivial, and at the moment we have no closed-form expression for this space.

However, the process is relatively straightforward for the simplest case of the four-point one-loop integrand, as we will now demonstrate. While the Amplituhedron is the space given by  $\langle AB_{ii+1} \rangle > 0$  and  $\langle AB_{13} \rangle < 0$ , the Amplituhedron-Prime is given by a single term from the second sum in eq. (2.5.32),

$$\mathcal{A}^{(4,0,1)} = 1 \begin{array}{c} 2 \\ \text{+} \quad \text{+} \\ \text{+} \quad \text{+} \\ \langle AB_{13} \rangle < 0 \\ \langle AB_{23} \rangle < 0 \\ \text{+} \quad \text{+} \\ 4 \end{array} 3, \quad \mathcal{A}'^{(4,0,1)} = 1 \begin{array}{c} 2 \\ \text{-} \quad \text{+} \\ \text{+} \quad \text{-} \\ \langle AB_{13} \rangle > 0 \\ \langle AB_{23} \rangle > 0 \\ \text{+} \quad \text{-} \\ 4 \end{array} 3. \quad (2.5.35)$$

Starting with  $\mathcal{A}'$ , we first add the achiral space

$$\mathcal{B}_1 = 1 \begin{array}{c} 2 \\ \text{-} \quad \text{+} \\ \text{+} \quad \text{-} \\ 4 \end{array} 3, \quad (2.5.36)$$

which effectively flips the sign of  $\langle AB_{13} \rangle$  in  $\mathcal{A}'$ . Next, we add a combination of chiral spaces  $\mathcal{B}_2$  which is defined

$$\mathcal{B}_2 = \left\{ \frac{\langle AB_{12} \rangle}{\langle AB_{34} \rangle} > 0, \langle AB_{23} \rangle > 0, \langle AB_{14} \rangle > 0, \langle AB_{13} \rangle < 0 \right\}, \quad (2.5.37)$$

and obtain  $\mathcal{A}$  as a result. Expanding  $\mathcal{B}_2$  in terms of sign-flip-spaces, we have

$$\mathcal{A}^{(4,0,1)} = \mathcal{A}'^{(4,0,1)} + 1 \begin{array}{c} 2 \\ \text{-} \quad \text{+} \\ \text{+} \quad \text{-} \\ 4 \end{array} 3 + 1 \begin{array}{c} 2 \\ \text{-} \quad \text{+} \\ \text{+} \quad \text{-} \\ \langle AB_{13} \rangle < 0 \\ \langle AB_{23} \rangle < 0 \\ \text{+} \quad \text{-} \\ 4 \end{array} 3 + 1 \begin{array}{c} 2 \\ \text{+} \quad \text{+} \\ \text{+} \quad \text{+} \\ \langle AB_{13} \rangle < 0 \\ \langle AB_{23} \rangle < 0 \\ \text{+} \quad \text{+} \\ 4 \end{array} 3. \quad (2.5.38)$$

Note that even in this simple example, it is actually quite non-trivial that the spaces with vanishing form we add have only physical boundaries. In particular, if we had

flipped the sign of  $\langle AB23 \rangle$  in the definition of  $\mathcal{B}_2$  in eq. (2.5.37), the resulting space would still have zero form, but would have the spurious boundary where  $\langle AB13 \rangle = 0$ .

As our conjecture is that  $\mathcal{A}'$  has only physical boundaries, the geometric difference between  $\mathcal{A}$  and  $\mathcal{A}'$  must be a collection of zero-form spaces with physical boundaries only. Finding the exact combination becomes very laborious at higher points, and we do not have a closed formula for it. However, as discussed in the motivations of section 2.1 and as we will see in the details of section 2.6, the real purpose in life of the chiral pentagons is to triangulate the dual Amplituhedron, where both  $\mathcal{A}$  and  $\mathcal{A}'$  are mapped under dualization.



## 2.6 Triangulation of the dual Amplituhedron

In the previous section we have seen that the chiral pentagons externally triangulate the Amplituhedron-Prime, which is free of all spurious boundaries, has the same canonical form as the Amplituhedron, but is geometrically distinct. In fact, both the  $\mathcal{A}$  and  $\mathcal{A}'$  spaces only intersect on various codimension boundaries. While the Amplituhedron-Prime is certainly an interesting positive geometry in its own right, we believe that the real purpose of the chiral pentagon expansion is more directly associated with the internal triangulation of the *dual Amplituhedron*.

This belief was first raised in [54] based on the simple observation that the chiral pentagon forms are positive when evaluated inside the Amplituhedron region, and therefore provide a term-wise positive expansion for the MHV one-loop integrand. In this picture, the positivity of the loop integrand is reminiscent of the volume interpretation of the dual Amplituhedron. The volume is naturally a positive function of (real) geometric data (momentum twistors) and slicing this volume into smaller pieces via internal triangulation preserves a term-wise positivity.

For the simplest  $k = 1$  tree Amplituhedron the dualization procedure is well understood and involves a simple map between polytopes and their duals. However, for  $k > 1$  tree-level (and all loop-level amplituhedra) the geometries become non-polytopal, and in these cases the dualization procedure has not been defined as of yet. While we do not give a complete solution of this problem in this chapter, in this section we provide a more direct link between the chiral pentagon expansion and the yet-to-be-found dual one-loop MHV Amplituhedron.

In subsection 2.5.3 we considered a significant subset of simple codimension-two faces of the MHV one-loop Amplituhedron. In these pictures, we localize two degrees of freedom of the line  $(AB)$ , so that the resulting projection can be viewed as a point (and polygons) on the projective plane. Although the correct dual of the fully off-shell line  $(AB)$  is not known, we can avoid this problem by working directly on codimension-two surfaces which reduce to the projective plane  $\mathbb{P}^2$ . By exploiting the elementary geomet-

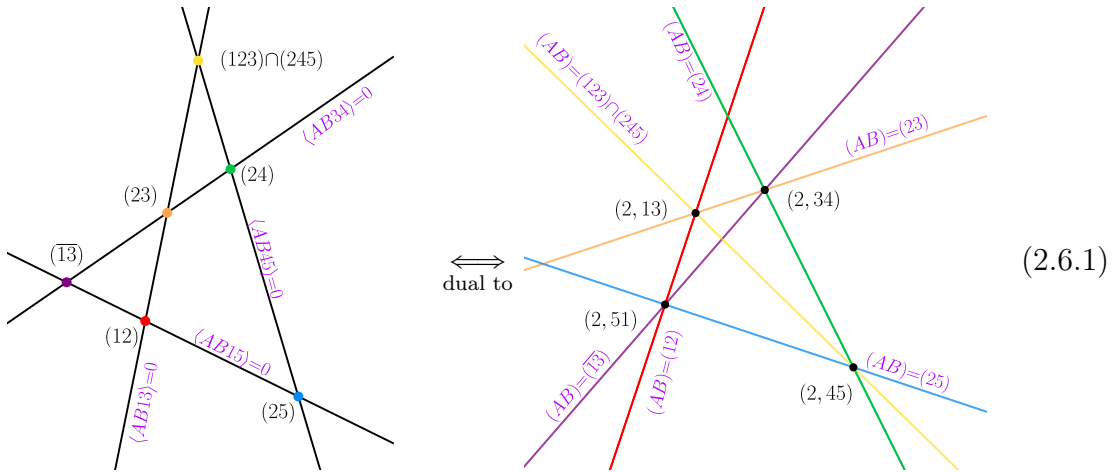
rical fact that polygons dualize to polygons, we can explicitly construct the associated codimension-two boundaries of the dual Amplituhedron by mapping points $\leftrightarrow$ lines, in a precise way that we outline below. On these dual codimension-two boundaries, we show that the chiral pentagon expansion corresponds to an internal triangulation of the dual of the MHV Amplituhedron.

### 2.6.1 Dualizing polygons

As discussed in section 2.5.3 there are two different codimension-two boundaries which reduce to the geometry of a point inside a polygon on  $\mathbb{P}^2$ : either we localize the line  $(AB)$  in a plane  $(i-1ii+1)$  or it passes through the point  $Z_i$ .

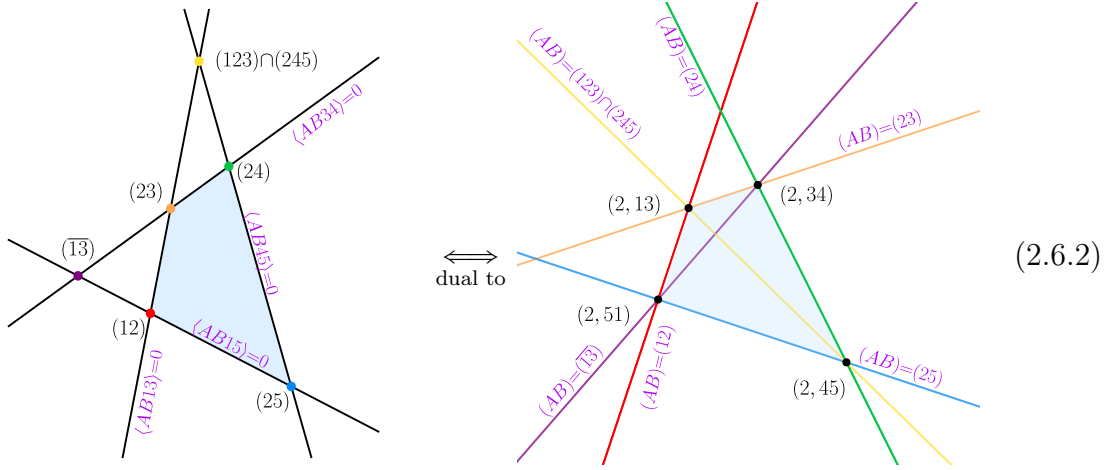
In order to connect the chiral pentagons and the dual Amplituhedron, we dualize the  $\mathbb{P}^2$  geometries of subsection 2.5.3. In fact, these projections are structurally identical to the toy model of appendix A.1; only the labelling of the points and lines is different. Dualizing a polygon is a straightforward procedure and yields another (dual) polygon; this was discussed in the (pre-)Amplituhedron context in [50].

We begin with the five-point codimension-two boundary (2.5.9) where  $(AB)$  passes through  $Z_2$ . The dualization procedure maps points $\leftrightarrow$ lines. Thus, the vertices (leading singularities) in the original projection become the edges of the dual polygon, while the codimension-one boundaries  $\langle ABii+1 \rangle = 0$  become the vertices in the dual space. The dualization of eq. (2.5.9) is



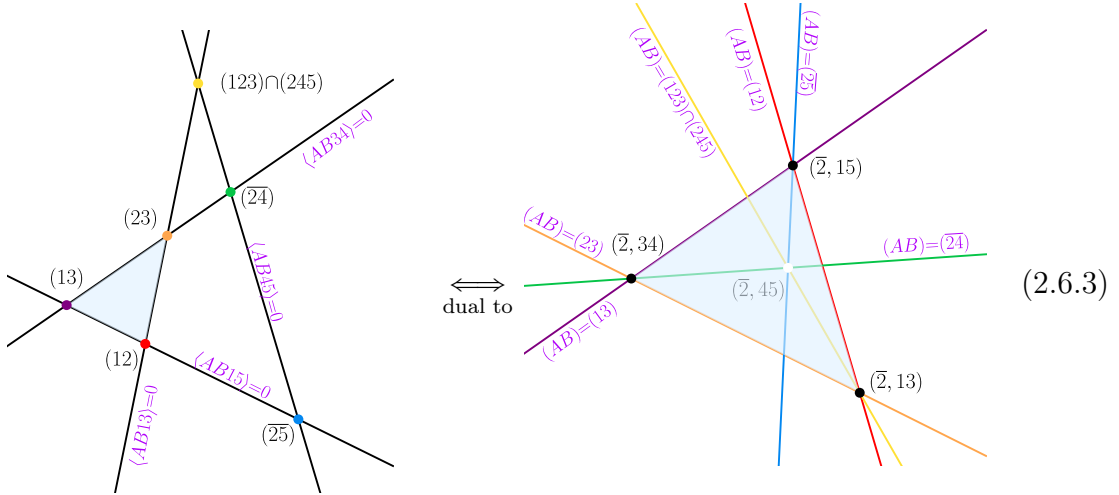
where we use the notation that e.g.,  $(2, 51)$  corresponds to  $(AB)$  passing through  $Z_2$  and cutting the line (15). We have also color-coded the leading singularities (and their dual lines) to direct the eye of the reader. For example, the red vertex (leading singularity)  $AB = (12)$  in the left figure gets mapped to the red line in the right figure. Note that we label the dual picture with conditions imposed on the line  $(AB)$ , despite the fact that this projection is actually describing the localization of some dual line  $(\widetilde{AB})$  to an associated codimension-two boundary. From this perspective, it is crucial that the space of  $(AB)$  lines is four-dimensional, so the dual of a two-dimensional geometry is another two-dimensional geometry! This gives a concrete way of constructing the faces of the dual geometry. Ideally, in the dual picture we would like to dispense with  $(AB)$  altogether and identify the regions and boundaries in the projection with the signs of some brackets, à la  $\langle \widetilde{AB} \dots \rangle \geq 0$ ; however, we do not yet know the constraints which  $(\widetilde{AB})$  should satisfy. Nevertheless, the simple structure of the dualization on these two-dimensional projections allows us to take a region in the original space and find the corresponding region in the dual space just by working in the original  $(AB)$  space, using a very simple prescription. The rule is that any line which intersected the region in the original space corresponds to a point in the dual space; moreover, that point must be outside the dual region. Similarly, a line which was outside the region in the original space maps to a point which must be inside the dual region. These simple rules suffice to uniquely determine the image of any region in the dual space. As an example, the dual of the Amplituhedron in the above example where  $(AB)$  passes through  $Z_2$  is

the light-blue shaded region on the right-hand-side of:



In particular, the spurious leading singularities  $(\overline{13})$  and  $(123)\cap(245)$ , which are outside the original Amplituhedron on the left, map to lines in the dual space which pass through the dual Amplituhedron on the right.

The parity conjugate projection, where  $(AB)$  lies in the plane  $(123)$ , is a slightly less trivial example of the correct dualization procedure

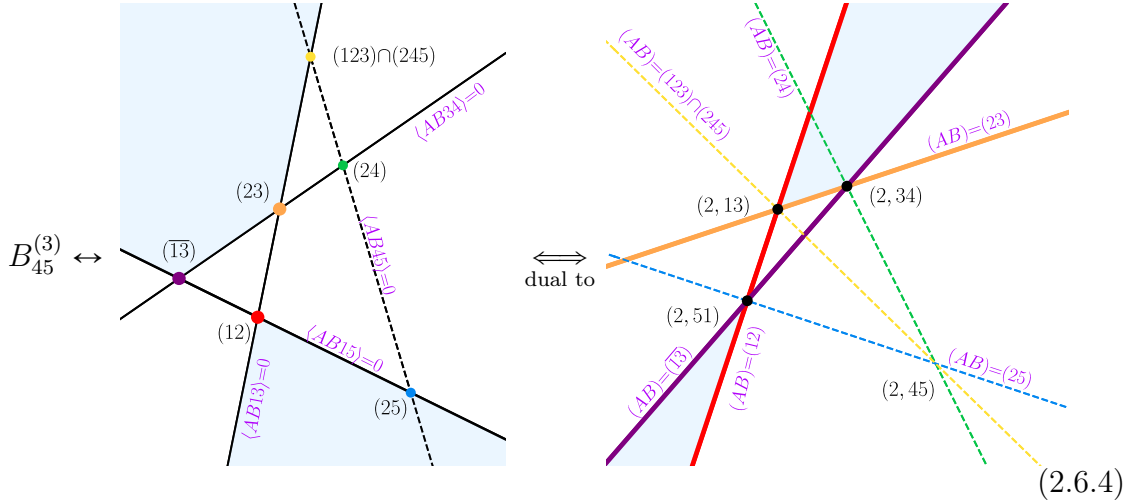


The relative positions of lines/vertices in the dual picture on the right merit an explanation. Once again, the shaded region is the (dual) Amplituhedron, indicated primarily for illustrative purposes. In this case, the spurious leading singularities  $(\overline{24})$ ,  $(\overline{25})$  and  $(123)\cap(245)$  must all pass through the dual Amplituhedron region. Our convention

throughout this chapter has been to assign the Amplituhedron to a region with finite area. To maintain this convention here requires the vertex  $(\bar{2}, 45)$ , which denotes the codimension-three boundary where the line  $(AB)$  lies in the plane  $(123)$  and cuts  $(45)$ , to lie *inside* the triangle bounded by the edges corresponding to the accessible MHV leading singularities. On this cut surface, these are  $(AB) = \{(12), (13), (23)\}$ . Importantly, the point  $(\bar{2}, 45)$  is spurious, so it is not included in the amplitude region; to indicate this, we use an empty (white) vertex. All similar codimension-two boundaries (at five points) are obtained by simply relabeling the above examples.

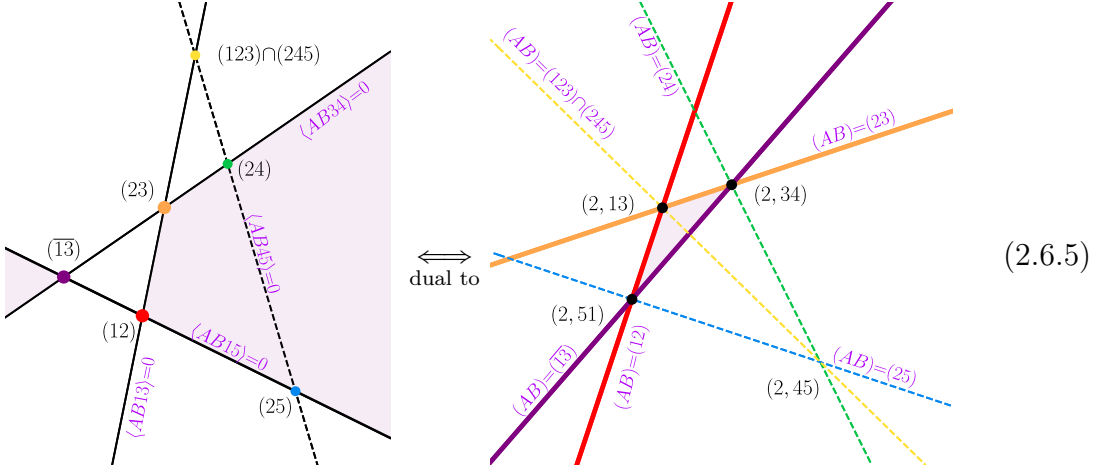
### 2.6.2 Dual spaces of chiral pentagons

Having introduced the dual two-dimensional projections, we now turn to identifying the image of the boxes and chiral pentagons under dualization using the prescription discussed above. Let us return to the five-point case, where the amplitude is a sum of two boxes and a single pentagon, c.f. eq. (2.5.1). Using the results of section 2.5.3 and appendix A.3, we can identify the dual regions corresponding to the projection summarized in eq. (A.3.1), where  $(AB) = (A2)$ . The box space  $B_{45}^{(3)}$  relevant for the Amplituhedron-Prime and its naïve dualization are



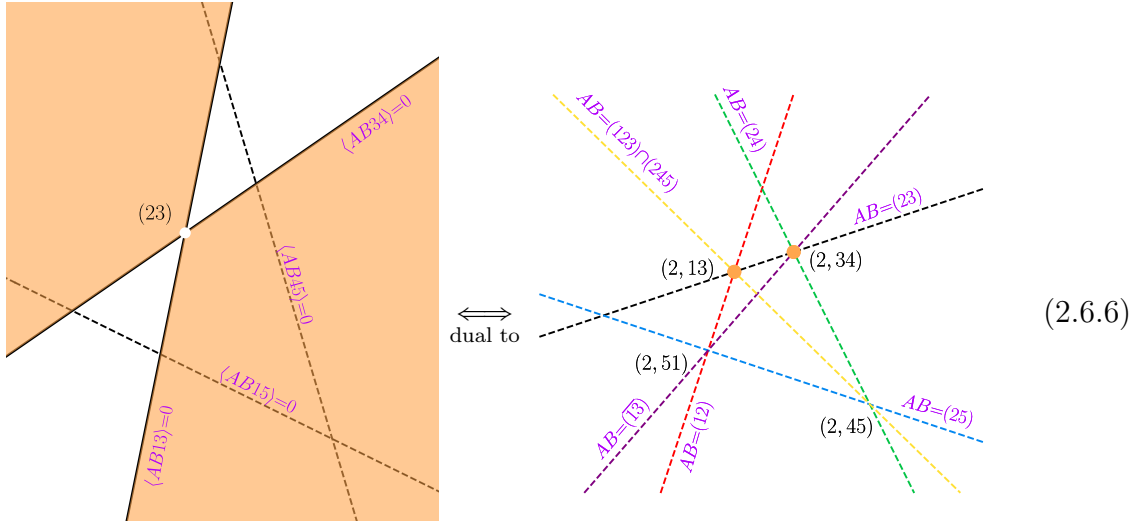
This seems to suggest that the dual of the Amplituhedron-Prime is *not* an internal triangulation of the dual Amplituhedron as the dual of the  $B_{45}^{(3)}$  box region naively lies outside of the dual of the Amplituhedron in the right figure of (2.6.4). However, there

is a critical feature of the dualization which has been neglected in eq. (2.6.4): namely, the *lower-dimensional boundaries* in the original projection on the left-hand-side, which map under dualization to infinite wedges in the dual picture on the right. The cavalier treatment of the lines and vertices on the left-hand-sides of eq. (2.6.4) causes no issue from the perspective of the canonical forms because any less-than-full-rank subspace of  $\mathbb{P}^3$  has vanishing form. However, these same boundaries play a pivotal role in the dual picture because they dualize to larger spaces with nonzero (in fact, infinite) volume. Note that while the dual of a line is a point, the dual of a line *segment* is an infinite wedge (with two codimension-one boundaries in the dual) defined by the two leading singularities which bookend the line segment. Thus, the right-hand-side of eq. (2.6.4) only represents the bulk component of the dualization and is incomplete. In fact, there is a simpler way of identifying the correct dual spaces which exploits the fact that zero-form spaces dualize to lower-dimensional boundaries. First, we can identify the region which dualizes to the triangle with vertices  $(2, 51)$ ,  $(2, 13)$  and  $(2, 34)$ , with *all boundaries* included:

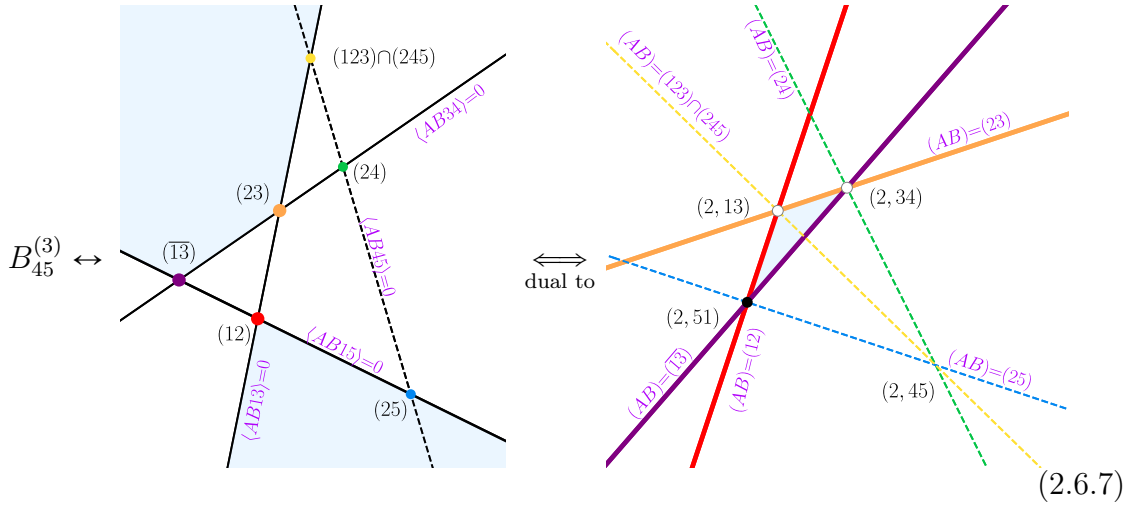


In the dual picture, we use filled vertices to indicate these are included as boundaries of the region. Now, the box space on the left-hand-side of eq. (2.6.4) can be related to the left-hand-side of eq. (2.6.5) by adding a zero-form wedge in the original space,

namely

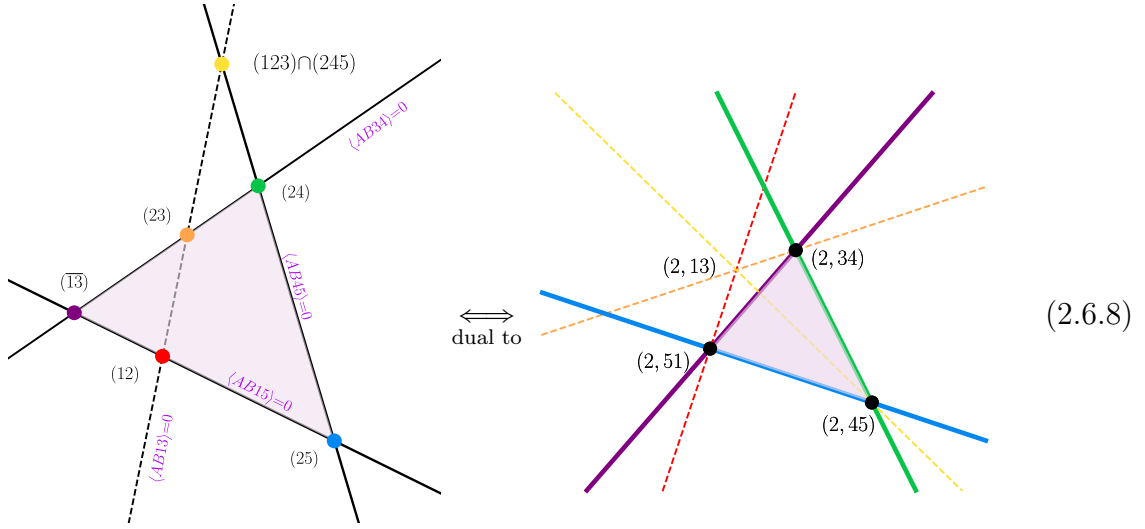


We use a white vertex to indicate that this point is *excluded* from boundary of the region. In the dual picture, we draw “dashed” lines to indicate that only the two orange vertices constitute the dual region. Therefore, the dualization of the box space of the left-hand-side of eq. (2.6.4) is the internal triangle with precisely this edge absent,

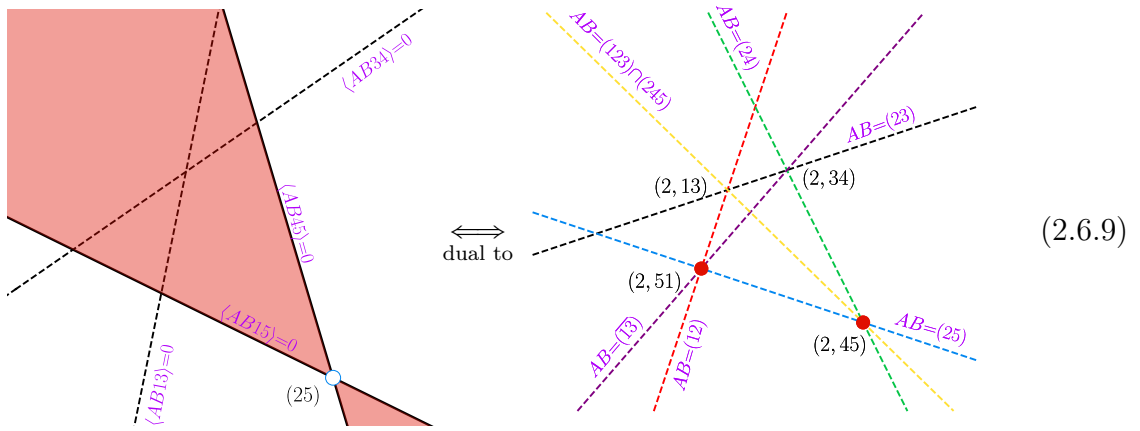


The dualization of both pentagon spaces (A.3.2) on the boundary where  $(AB) = (A2)$  can be constructed in a similar fashion. Similarly to (2.6.5), we first identify the region

in the original space which maps to the second internal triangle of the dual space:

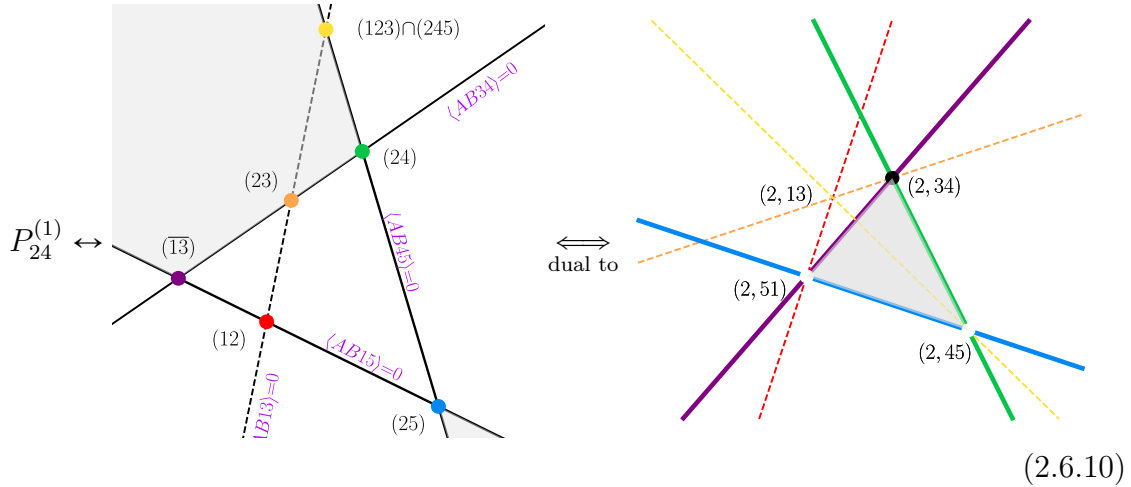


The pentagon space  $P_{24}^{(1)}$ , relevant for the Amplituhedron-Prime, can be related to eq. (2.6.8) by the addition of the zero form region





so the correct dualization for the pentagon  $P_{24}^{(1)}$  is



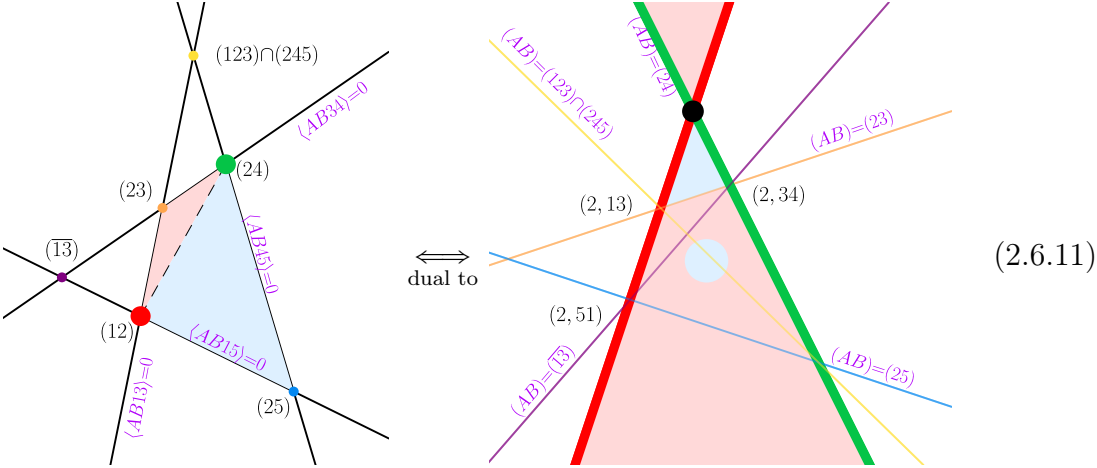
For reference, the dualization for the alternative pentagon space  $P_{24}^{(2)}$  is the same dual bulk region, but with the vertices  $(2, 51)$  and  $(2, 34)$  missing.

### 2.6.3 Two-dimensional triangulations

The chiral pentagon expansion triangulated the Amplituhedron-Prime space  $\mathcal{A}'$ . Since the logarithmic forms for  $\mathcal{A}$  and  $\mathcal{A}'$  are equal, by definition, their dual spaces have the same volume. Thus, a priori in the dual pictures  $\mathcal{A}$  and  $\mathcal{A}'$  can only differ by zero-volume lower-dimensional boundaries which are dual to zero-form wedges in the original space. In fact, the same argument suggests that *any* choice of individual box and pentagon geometries must match the dual Amplituhedron up to possibly its vertices and edges. To demonstrate this correspondence explicitly, we carefully account for all lower-dimensional boundaries in the dualization procedure. As discussed in the previous subsection, these line segments dualize to infinite wedges which dramatically affect the resulting dual region. In general, it is easiest to understand the dualization by utilizing zero form regions in the original two-dimensional projection.

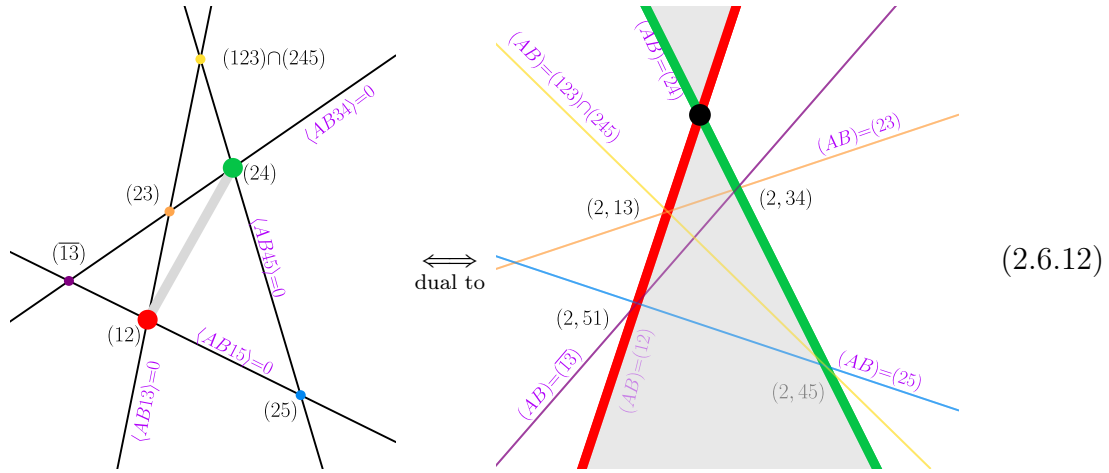
Let us now compare the behavior of the Kermit eq. (2.2.19) and chiral pentagon eq. (2.3.3) expansions in the original and dual two-dimensional projections. As shown in section 2.2, the Kermit representation is by construction an internal triangulation of the Amplituhedron. By the schematic arguments of section 2.1, the expectation is

that internal triangulations map to external triangulations of the dual, and vice versa. We now establish this for the Kermit expansion at five points on the boundary when  $(AB)$  passes through  $Z_2$ . On this cut, the Kermit's triangulate the quadrilateral using the line  $\langle AB14 \rangle = 0$ . *Excluding* this line from consideration, the naïve dualization reads

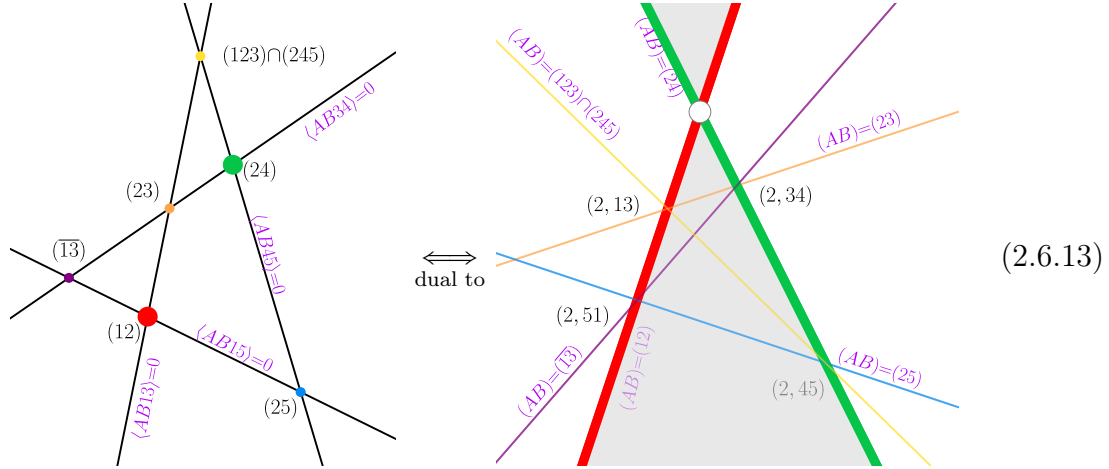


We see that just as in eq. (2.6.4) the space remaining is not the quadrilateral representing the dual Amplituhedron. The issue here is the same as in the naïve dualization attempt of the previous subsection: we have been glib about the lower-dimensional boundaries in the original space. Specifically, in the example on the left-hand-side of eq. (2.6.11), the segment of the line  $\langle AB14 \rangle = 0$  between the points (12) and (24) dualizes to an infinite wedge with exactly these two codimension-one dual boundaries. To account for this in the dual picture requires that we add the dual of this line segment

to our naïve picture eq. (2.6.11), i.e.,



To be clear, this picture includes both the points (12), (24) as well as the line segment itself. Including this boundary with both Kermit regions eq. (2.6.11), we double-cover the points (12) and (24). Thus, to recover the dual space we must add these points back, without the line segment in between them. The dual of this piece is, by completeness, the wedge in eq. (2.6.12) minus the single point (2, 14):

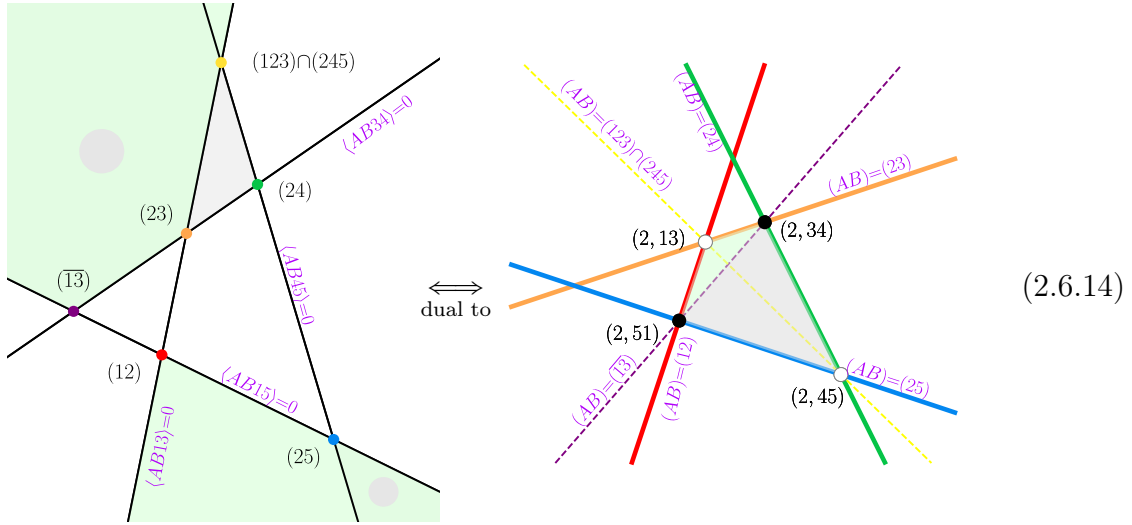


The net effect of these subtleties on our naïve picture eq. (2.6.11) is the addition of the infinite wedge eq. (2.6.13), which gives exactly the dual Amplituhedron.

(An alternative resolution to this problem is to include the triangulation line with one of the Kermit regions but not the other. Upon removing the extra point (14) in the dual space, we recover exactly the same (up to relabelling) external triangulation as

in the motivational example of eq. (2.2.44). This is sensible from a purely geometrical perspective. However, from the point of view of canonical forms it seems more natural to include the triangulation line *with* its endpoints in both terms, as both forms do have nonzero residues on this boundary.)

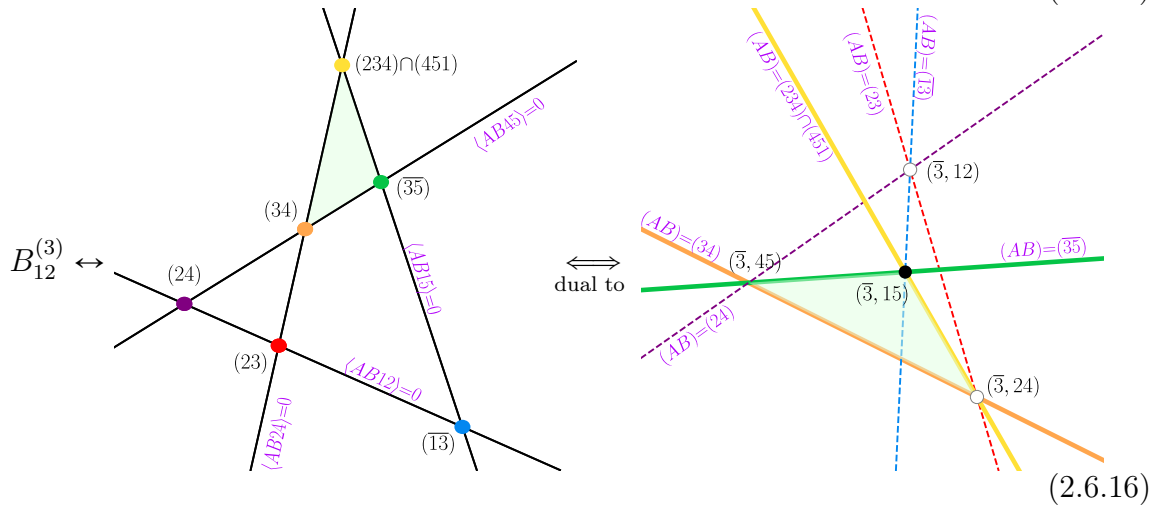
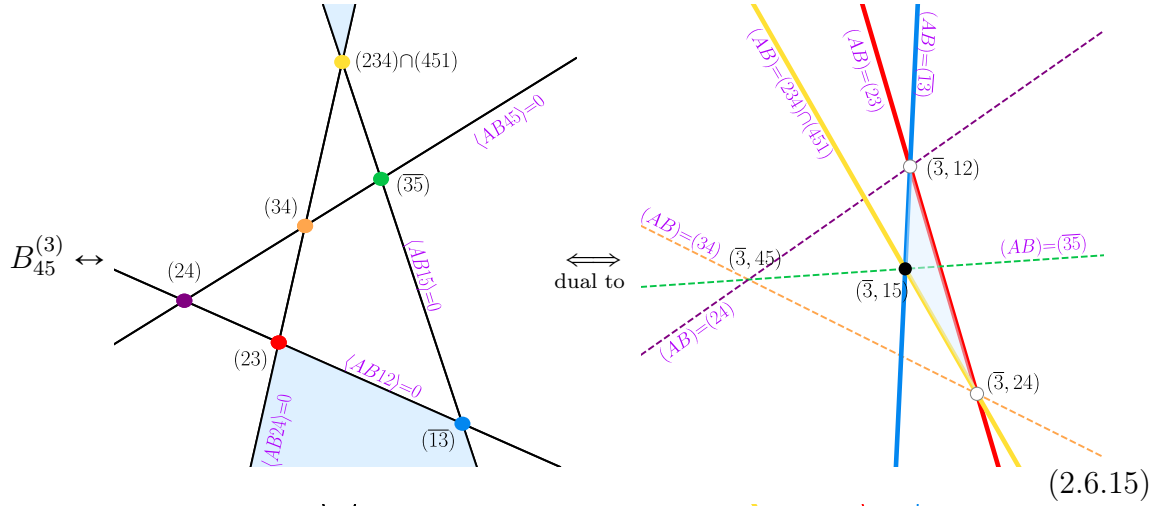
Using the results of eq. (2.6.7) and eq. (2.6.10), we see that the dual of the Amplituhedron-Prime on this cut surface triangulates the dual of the Amplituhedron, *except for the two vertices* (2, 13) *and* (2, 45), i.e.,

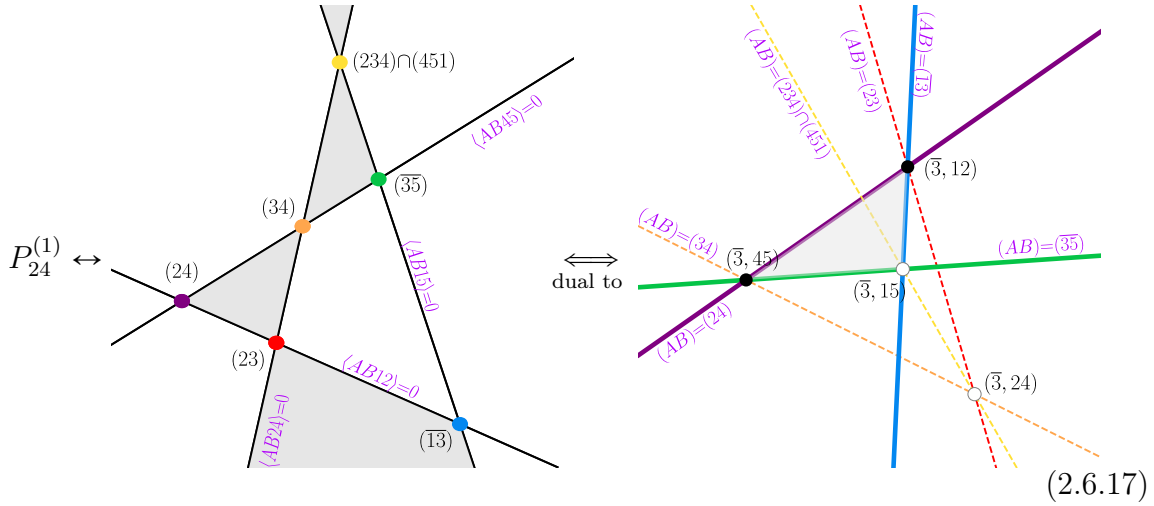


Note that the original non-overlapping regions with fixed signs of  $\langle ABij \rangle$  brackets are now overlapping in the dual space. Therefore, it is very non-trivial that the regions corresponding to chiral pentagons triangulate internally the dual Amplituhedron without any overlaps.

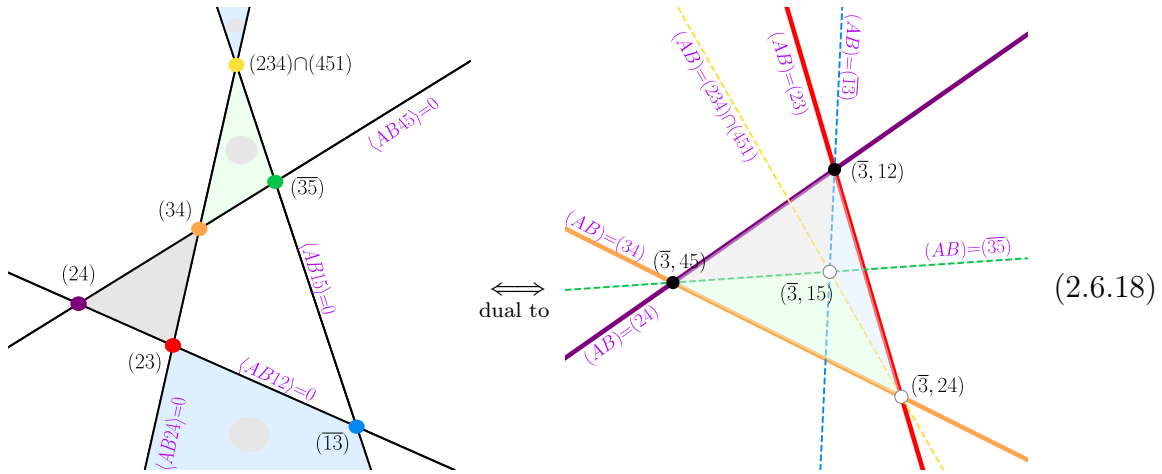
The fact that the logarithmic forms for Amplituhedron and Amplituhedron-Prime are identical means that their (conjectured) dual spaces have the same volume and are identical up to spaces which have zero volume. This matches the result of eq. (2.6.14), where we can see that  $\mathcal{A}$  and  $\mathcal{A}'$  differ by lower-dimensional boundaries. This line of reasoning is also suggestive of an ambiguity in the definition of the Amplituhedron-Prime. Namely, we are always free to add any spaces which have zero form (such as the infinite wedge of eq. (2.6.6)) because in the dual space they correspond to zero-volume lines or points.

To provide additional evidence that the Amplituhedron-Prime dualizes to an internal triangulation of the (bulk) dual Amplituhedron, we can repeat the above exercise for the cut surface  $(AB) \subset (234)$  which was analyzed in eq. (2.5.18). For the Amplituhedron-Prime, all three local integrals contribute:





Hence the dual of the Amplituhedron-Prime triangulates the dual Amplituhedron, up to a single vertex  $(\bar{3}, 24)$  on the two-dimensional projection where  $(AB) \subset (234)$ ,



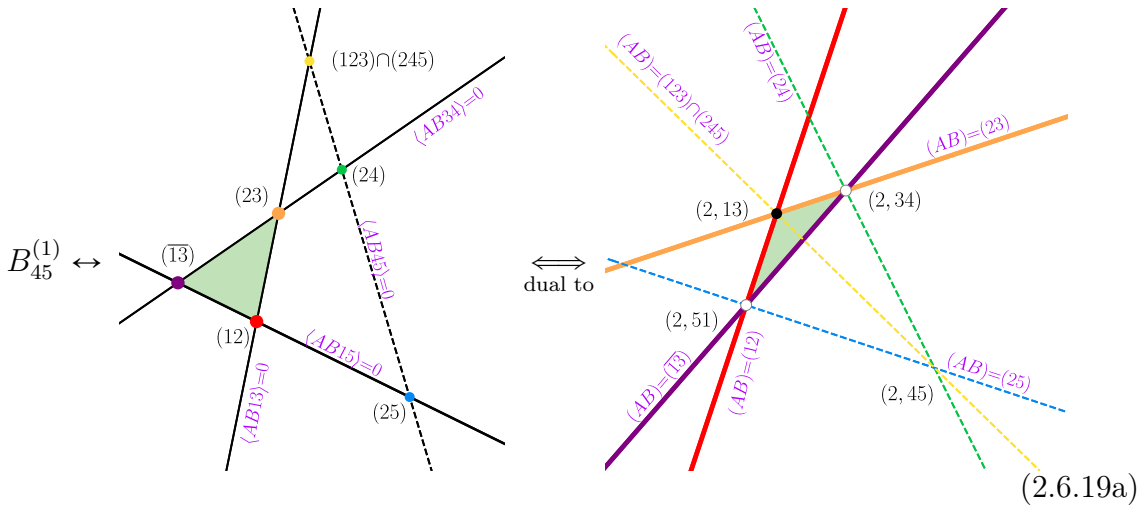
We have exhaustively verified for all remaining five and six point two-dimensional projections where  $(AB) = (Ai)$  or  $(AB) \subset (i-1ii+1)$  that the Amplituhedron-Prime internally triangulates the dual Amplituhedron up to contributions with zero-volume. In fact, in retrospect this conclusion would follow immediately from the existence of a spurious-boundary-free, zero-form space  $\mathcal{B}$  which connects  $\mathcal{A}$  and  $\mathcal{A}'$  through  $\mathcal{A} = \mathcal{A}' + \mathcal{B}$ . We wrote down an explicit expression for  $\mathcal{B}$  at four points in eq. (2.5.38) and, although we do not have an explicit formula for this space at  $n$ -points, we see no *conceptual* obstruction which would preclude its existence. We leave an explicit

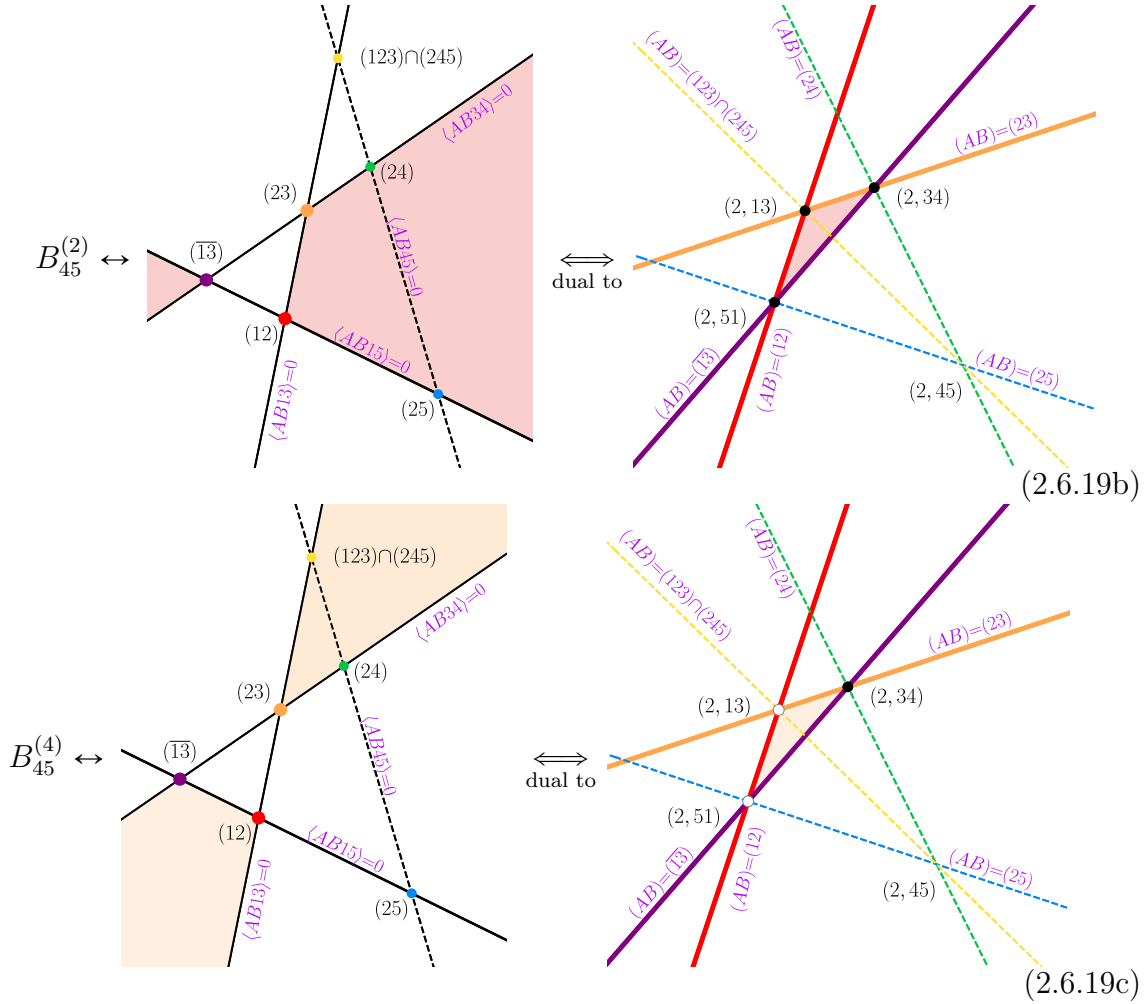
construction of the zero-form space connecting the Amplituhedron and Amplituhedron-Prime to future work.

### Rigidity of the dual space

We have seen in the previous discussion that a single  $d$  log form gives rise to various positive geometries. We emphasized the importance of *faithful geometries* in section 2.3.2, where all boundaries of the geometric space appear as poles in the  $d$  log form. Furthermore, we used these geometries to interpret the chiral pentagon expansion as external triangulation of Amplituhedron-Prime in eq. (2.5.32). From our discussion it is clear, that all these spaces have different geometries, but one can naturally ask about the duals of the positive spaces which originate from the same  $d$  log form.

Here, we explicitly discuss different box spaces for the one-mass box  $B_{45}$  summarized in eq. (2.5.3). We can dualize these spaces on the two-dimensional boundary where the line  $(AB)$  passes through  $Z_2$ , c.f. (2.5.11) and (2.6.1). We repeat the same exercise from section 2.6.1 for the three alternative box spaces appearing in eq. (A.3.1) even though they are irrelevant for the Amplituhedron-Prime. Because these additional box spaces are all equivalent to eq. (2.6.5) up to a zero-form region in the original two-dimensional projection, they all map to the same internal piece of the dual Amplituhedron *up to lower-dimensional boundaries*. Indeed, the results of dualization for the alternative box spaces are, using the coloring convention of eq. (A.3.1):





This makes perfect sense because the positive geometries differ by spaces with vanishing form (wedges on the two-dimensional boundaries) which get mapped to points and lines in the dual two-dimensional geometry. Therefore, from the point of view of the dual Amplituhedron, it does not matter which positive geometry we use for a given  $d \log$  form, it always represents the same dual geometry. This simply follows from the fact that the regions with vanishing  $d \log$  form map to lower-dimensional objects in the dual which have zero volume.

Therefore, it is natural to expect that while the positive geometries  $\mathcal{A}$  and  $\mathcal{A}'$  are different, the putative dual Amplituhedron is unique, and the chiral pentagons triangulate it internally. We gave some evidence for this claim in this section.



## 2.7 Conclusion

In this chapter we discussed various positive geometries in the context of the one-loop Amplituhedron and its variants. We have shown that for external data satisfying the MHV positivity conditions (2.2.11), there are a number of further interesting positive geometries besides the original MHV and  $\overline{\text{MHV}}$  Amplituhedra. In section 2.4, we classified all these spaces using topological sign-flip properties which are reminiscent of, but distinct from, the sign-flip definition of the Amplituhedron [58]. Furthermore, we showed that these positive spaces can be used to give a geometric interpretation of the chiral pentagon expansion of the one-loop MHV amplitude of eq. (2.2.45). In particular, the chiral pentagons externally triangulate a new Amplituhedron-Prime space (2.5.32) which is a non-overlapping twin of the original Amplituhedron with only physical boundaries and the same logarithmic form. Finally, in section 2.6, we made more precise the statement that the chiral pentagon expansion can also be interpreted as the internal triangulation of the yet-to-be found dual Amplituhedron. We were able to demonstrate the internal triangulation of the dual on certain two-dimensional boundaries of the full space where the geometry reduces to that of polygons for which a dualization prescription exists. Exploring other two-dimensional boundaries of non-polygonal form, as well as three-dimensional boundaries and the role of internal triangulations, should bring us to the ultimate goal of the discovery of the dual Amplituhedron space.

# Chapter 3

## Integrands of Less-Supersymmetric Yang-Mills at One Loop

### 3.1 Introduction and Overview

Important recent progress in our understanding of scattering amplitudes in quantum field theory originated from considering the structure of loop amplitudes at the level of the *integrand* whose analytic structure is determined by unitarity in terms of *on-shell* processes.

The origins of generalized unitarity [2, 3, 129] are extremely simple to understand: loop integrands, being rational differential forms on the space of loop momenta, can be expanded into a basis of such forms with coefficients that are loop-momentum independent. For any process in any particular quantum field theory and at any fixed loop order and spacetime dimension, the space of *all* scattering amplitude integrands (arbitrary multiplicity and external particle content) spans a finite-dimensional space of ‘master’ integrands. Once these integrands are integrated they can be recycled for arbitrary scattering amplitudes of interest in the theory.

A familiar illustration of the power of this idea is the ‘no-triangle property’ for amplitudes in maximally supersymmetric Yang-Mills and gravity at one loop [130–133]. Specifically, this means that all amplitudes in these theories are expressible in a basis of

‘scalar box’ integrals (those that scale like four propagators at infinite loop momentum). This basis was called  $\mathfrak{B}_4^{(4)}$  in ref. [134], and it is a classic result of Passarino and Veltman [135] that all one loop *integrals* involving more than four-propagators can be expanded into those with four or fewer. Thus, at one-loop in these theories, the scalar box integrals suffice for representing all scattering amplitudes.

More generally, the size of the basis required to represent amplitudes in a quantum field theory remains an important and open question. For example, it is known that scattering amplitudes in both the Standard Model and pure Yang-Mills are expressible in terms of the basis of integrands  $\mathfrak{B}_0$ —integrands that scale like a loop-independent constant at infinite momentum—which is the basis described by OPP in ref. [136, 137]; but it is not known whether this is the *smallest* space of loop integrands needed to express amplitudes in these theories.

In this chapter, we consider the case of one-loop amplitudes in less-than-maximally supersymmetric ( $1 \leq \mathcal{N} < 4$ ) Yang-Mills theory (‘sYM $_{\mathcal{N}}$ ’). We show that these amplitudes can be expressed in the space  $\mathfrak{B}_2^{(4)}$ —the space of integrands with ‘bubble’ power-counting in four dimensions. We do this by constructing a particular, *prescriptive* [138] basis for  $\mathfrak{B}_2^{(4)}$  with several special features, and show how amplitudes in sYM $_{\mathcal{N}}$  can be represented in this basis.

More precisely, we focus on scattering amplitudes of pure  $\mathcal{N} = 1, 2$  vector multiplets without additional matter. In terms of on-shell multiplets, one can label on-shell scattering states in terms of helicity super-multiplets [139]. In the planar limit, we expect a well-defined notion of the *integrand* due to the fact that planarity, or equivalently (leading) color ordering, induces a fixed cyclic ordering of the external momenta of the scattering states, which in turn allows us to define unique labels for the loop-variables to any order in perturbation theory. These variables are given either by choosing an origin of loop-momentum space, going to dual coordinates [27], or (in strictly four spacetime dimensions) introducing momentum twistors [48], all of which have played a major role in recent developments for maximally supersymmetric amplitudes, and beyond. One

key advantage of the global labels that originated in  $\mathcal{N}=4$  sYM arises from multiple different definitions of the integrand, either in terms of a standard diagrammatic representation or via loop-level on-shell recursion relations [125]. For less-supersymmetric amplitudes in the planar limit, these recursion relations should exist, but are associated with various subtleties [92].

The computation of one-loop amplitudes (including non-supersymmetric ones) has a long tradition partially inspired by the precision needs for particle collider observables. Previous amplitudes constructions mostly rely on the basis of known scalar one-loop *integrals* where the integral coefficients can either be obtained from the integrand reduction of Feynman diagrams or generalized unitarity cuts. These methods have been implemented in a number of useful numerical computer codes, see e.g. [140–143]. The unitarity approach has the advantage of being also suitable for a fully analytic calculation as demonstrated in the seminal work by Bern, Dixon, Dunbar, and Kosower [3], where one-loop MHV amplitudes in  $\mathcal{N}=1$  sYM were explicitly computed for arbitrary multiplicity. Furthermore, NMHV amplitudes are known from similar computations [144–147], and e.g. [148–150] for additional relevant one-loop amplitudes. Crucially, the above mentioned methods rely on post-integration results and commonly drop the massless bubble coefficients in the integrand construction and fix them a posteriori by matching to the expected IR or UV singularities of scattering amplitudes. Alternatively, ref. [151] fixes supersymmetric Yang-Mills integrands with matter multiplets running in the loop via the Bern Carrasco Johansson (BCJ) color-kinematic dual representations, see also [152] for a non-supersymmetric BCJ computation for different matter fields running in the loop.

In contrast, one goal of this chapter is to uniquely define the one-loop *integrands* for less than maximally ( $1 \leq \mathcal{N} \leq 4$ ) supersymmetric Yang-Mills theory (the pure Yang-Mills case has new features which we leave for future work). The situation is significantly different from the case of maximal supersymmetry because of the presence of poles at infinity as indicated by having triangles and bubbles in the one-loop expansion. We

show that the standard cuts considered in the context of generalized unitarity fix the integrand up to massless bubbles contributions. These terms integrate to zero but are nevertheless important at the integrand-level; and we illustrate two choices of contours which can be used to fix their coefficients.

## Organization and Outline

This chapter is organized as follows. In section 3.2, we review the ingredients of basis-integrand construction and the role of prescriptivity [138]. We describe our particular choice of basis for  $\mathfrak{B}_2^{(4)}$  in section 3.2.2, and highlight how it is stratified by its UV/IR structure and its transcendental weight in section 3.2.2.3.

Because the basis we construct is prescriptive, the coefficient of every integrand is a ‘leading singularity’ in field theory: i.e. the integral of the amplitude along some particular compact contour (at one loop, always a ‘residue’). In less-than-maximally supersymmetric Yang-Mills theory, leading singularities require more information to specify than in  $\mathcal{N} = 4$  sYM. We review these ingredients in section 3.3. In particular, we find that one loop amplitude integrands in sYM $_{\mathcal{N}}$  can be represented as a combination of the corresponding amplitude integrands in  $\mathcal{N} = 4$  sYM (which have better power-counting), plus corrections involving only those diagrams with so-called ‘non-singlet’ helicity flow. In section 3.3.2, we discuss some subtleties that arise in the case of leading singularities associated with massless bubble integrals, and suggest two natural paths to defining a unique integrand.

In section 3.4, we apply our diagonalized bubble power-counting basis of integrands to write down a closed formula for all-multiplicity MHV amplitudes in section 3.4.2. We further illustrate these ideas with a particular six-point NMHV amplitude integrand in section 3.4.3, and discuss how this representation of amplitudes *manifests* the finiteness of many observables in these theories before concluding in section 3.5.

Finally, in appendix B we provide full details for our integral basis, and each basis element’s result from loop integration. These results, as well as the all-multiplicity MHV amplitude integrand, are also provided as ancillary files attached to [153].

### 3.2 A Prescriptive, Bubble Power-Counting Basis at One Loop

The fundamental principle behind generalized unitarity [2, 3, 129] is that loop amplitude integrands  $\mathcal{A}$  are elements of a vector space of differential forms on the space of loop momenta; as such, they may be expanded into a *basis*  $\mathfrak{B}$  (large enough that  $\mathcal{A} \subset \mathfrak{B}$ ) of such forms,

$$\mathcal{A} = \sum_{\mathfrak{b}_i \in \mathfrak{B}} c_i \mathfrak{b}_i, \quad (3.2.1)$$

where the coefficients  $c_i$  are loop-momentum-independent ‘on-shell’ functions determined by *generalized unitarity*: i.e. the left and right-hand sides of eq. (3.2.1) agree on all contour integrals which ‘encircle’ loop-dependent Feynman propagators.

In principle, an *arbitrary* spanning set of Feynman integrands (rational differential forms involving some number of Feynman propagators and arbitrary functions of loop momenta in the numerators) can be chosen for a basis in (3.2.1). In this case, the determination of the coefficients  $c_i$  amounts to a problem of linear algebra: suppose that one has some spanning set of integration contours  $\{\Omega_j\}$  on which the *period matrix*

$$\oint_{\Omega_j} \mathfrak{b}_i =: \mathbf{M}_{i,j} \quad (3.2.2)$$

were known or determined to be full-rank. Then the coefficients of amplitudes  $a_i$  would be determined by the system of equations

$$\begin{aligned} a_j := \oint_{\Omega_j} \mathcal{A} &= \oint_{\Omega_j} \left( \sum_{\mathfrak{b}_i \in \mathfrak{B}} c_i \mathfrak{b}_i \right) = \sum_{\mathfrak{b}_i \in \mathfrak{B}} c_i \left( \oint_{\Omega_j} \mathfrak{b}_i \right) = \sum_i c_i \mathbf{M}_{i,j} \\ \Rightarrow c_j &= \sum_i a_i \cdot [\mathbf{M}^{-1}]_{i,j}. \end{aligned} \quad (3.2.3)$$

Typically, the cycles chosen to determine coefficients are those involving as many ‘residue’ contours as possible—those which encircle a number of Feynman propagators, poles at infinity, collinear regions, and so-on. Because these contours enclose physical poles, the periods of *amplitude integrands*  $a_j$  defined in (3.2.3) are called *lead-*

ing singularities [126] and can be determined in terms of on-shell (tree) amplitudes. The story of these coefficients is one with a very rich history.

Setting aside the potential computational complexity involved in inverting the period matrix  $\mathbf{M}_{i,j}$  defined in (3.2.2), it is worth emphasizing that most *seemingly natural* choices for bases of master integrands (those involving some Feynman graph’s worth of propagators and a spanning-set of ‘Lorentz-invariant scalar products’ in their numerators) lead to very poor integrals—ones that can deeply obscure many interesting and important features of scattering amplitudes. Thus, it is worthwhile to try and find a *good* set of integrands for any basis.

### 3.2.1 Brief Review of Prescriptive Integrand Bases for Amplitudes

A *prescriptive* integrand basis is one chosen to be cohomologically *dual* to a spanning set of maximal-dimensional compact contours of integration. That is, a basis is prescriptive provided that there exists a set of compact, maximal-dimensional integration contours  $\{\Omega_j\}$  such that

$$\oint_{\Omega_j} \mathbf{b}_i = \delta_{i,j}. \quad (3.2.4)$$

When this is the case, the coefficients  $c_i$  of the amplitude integrand (3.2.1) are *leading singularities* of field theory because the inversion of the period matrix (3.2.2) is trivial:

$$c_i = a_i := \oint_{\Omega_i} \mathcal{A}. \quad (3.2.5)$$

Prescriptive integrand bases have been shown to possess many desirable properties. In particular, they often evaluate to *pure* functions (those satisfying nilpotent systems of differential equations, see e.g. [154, 155]), and hence are comparatively easy to integrate.

To be clear, prescriptive integrand bases are fairly straightforwardly to construct. Starting from an arbitrary basis of loop integrands  $\mathfrak{B}^0$  and an arbitrary spanning-set of contour integrals  $\{\Omega_j\}$ <sup>1</sup>, a prescriptive basis can be obtained according a simple ‘rotation’ of the basis:

---

<sup>1</sup>The contours of integration are understood to fully localize the loop momentum. Therefore the

$$\mathfrak{b}_i := \sum_k [\mathbf{M}^{-1}]_{i,k} \mathfrak{b}_k^0 \quad \text{where} \quad \mathbf{M}_{k,j} := \oint_{\Omega_j} \mathfrak{b}_k^0. \quad (3.2.6)$$

It should be clear how important the role of the cycle basis is in the above discussion: different choices of contours  $\{\Omega_j\}$  can result in strikingly different bases of integrands. Thus, there is relatively little uniqueness here. For our particular purposes in this work, we chose a maximal subset of contours to expose IR and UV divergences, resulting in a basis stratified by divergences. As stressed previously, this choice is by no means unique and one could think about alternative bases inspired by other physical or mathematical properties.

In what follows, we review the elements involved in defining a particular set of Feynman integrands for a basis—as defined by (some proxy for) ‘power-counting’. Then we illustrate the kinds of choices made for a dual set of cycles, and how these choices affect the resulting integrand basis.

### 3.2.2 Defining a Bubble Power-Counting Basis $\mathfrak{B}_2^{(4)}$

As described in ref. [134], one can construct a basis of ‘bubble-power-counting’ integrands at one loop as follows. Start with any Feynman graph involving some number of  $p \geq 2$  propagators and consider the vector space of loop-dependent polynomials in the numerator

$$[\ell]^{(p-2)} \quad \text{with} \quad [\ell]^q := \text{span}_{Q_i \in \mathbb{R}^d} \left\{ (\ell - Q_1)^2 \cdots (\ell - Q_q)^2 \right\}. \quad (3.2.7)$$

That is,  $[\ell]^q$  represents that linear span of all  $q$ -fold products of inverse propagators. Thus, the space of  $\mathfrak{B}_2$  is defined as the linear span of all Feynman integrals with  $p$  propagators and a product of  $p-2$  inverse propagators in the numerator.

Graphically, if we use

---

integral coefficients are determined by purely algebraic manipulations. In the absence of sufficiently many propagators, the contours might involve encircling arbitrary reference points, see e.g. [138] for more details which is comparable to the one-loop methods of [136, 156]. These procedures are in contrast to spinor integration methods to extract one-loop coefficients, e.g. [157].



$$\frac{\text{---}\circ\text{---}}{\ell} := \frac{[\ell]}{\ell^2}, \quad (3.2.8)$$

to denote the vector space of inverse-propagators times some propagator, then

$$\mathfrak{B}_2 := \text{span} \left\{ \text{---}\circ\text{---}, \text{---}\triangle\text{---}, \text{---}\square\text{---}, \text{---}\text{pentagon}\text{---}, \text{---}\text{hexagon}\text{---}, \text{---}\text{heptagon}\text{---}, \dots \right\}. \quad (3.2.9)$$

As described in ref. [134], this space is finite dimensional for any fixed spacetime dimension (or multiplicity). In four dimensions, all integrands involving more than four propagators are expressible in terms of those with four or fewer. In particular, the basis  $\mathfrak{B}_2^{(4)}$  is spanned by the following vector spaces of loop integrands:

$$\begin{aligned} & \text{---}\square\text{---} \quad (A, B, C, D) \quad := \frac{[\ell]^2}{\ell^2(\ell + p_A)^2(\ell + p_{AB})^2(\ell + p_{ABC})^2}, \\ & \text{---}\triangle\text{---} \quad (A, B, C) \quad := \frac{[\ell]^1}{\ell^2(\ell + p_A)^2(\ell + p_{AB})^2}, \quad \text{and} \quad \text{---}\circ\text{---} \quad (A, B) \quad := \frac{1/2}{\ell^2(\ell + p_A)^2}. \end{aligned} \quad (3.2.10)$$

Throughout this chapter, we always leave implicit the factor of ‘ $d^4\ell$ ’ in these integration measures. For each set of leg distributions, these spaces of integrands have rank (in four-dimensions) of  $20 = 2 + 18$ ,  $6 = 3 + 3$ , and 1, respectively. What we mean by this, for example, is that the 6-dimensional vector space  $[\ell]^1$  of loop-dependent numerators for the triangle integrands can be viewed as spanned by 3 ‘top-level’ degrees of freedom and 3 contact terms—one numerator for each of the 3 inverse-propagators appearing in the graph. Similarly, of the 20-dimensional vector space  $[\ell]^2$  of numerators for the box integrands, all but 2 can be spanned by contact terms:  $\binom{4}{2} = 6$  double-contact terms (with one degree of freedom each), and  $\binom{4}{1} = 4$  single contact terms with 3 top-level degrees of freedom each. Labeling only the top-level degrees of freedom for

each denominator topology (those numerators not spanned by the contact terms of the integral) , our bubble power-counting basis consists of **2** numerators per box, **3** numerators per triangle, and a single numerator per bubble, denoted by  $\mathcal{I}_{A,B,C,D}^i$ ,  $\mathcal{I}_{A,B,C}^I$ , and  $\mathcal{I}_{A,B}$ , respectively. We may represent each of these integrands graphically as follows:

$$\text{Box}(i) \Leftrightarrow \frac{\mathbf{n}_{A,B,C,D}^i(\ell)}{\ell_a^2 \ell_b^2 \ell_c^2 \ell_d^2}, \quad \text{Triangle}(I) \Leftrightarrow \frac{\mathbf{n}_{A,B,C}^I(\ell)}{\ell_a^2 \ell_b^2 \ell_c^2}, \quad \text{Bubble} \Leftrightarrow \frac{1/2}{\ell_a^2 \ell_b^2} \quad (3.2.11)$$

where  $i \in \{1, 2\}$  indexes the **top-level** degrees of freedom of each box, and  $I \in \{1, 2, 3\}$  indexes the **top-level** degrees of freedom of each triangle. To be clear, the sets  $\{A\}, \dots$  represent arbitrary *non-empty* collections of external momenta flowing into the vertex, with  $p_A := \sum_{a \in A} p_a$  and  $s_A := p_A^2 = (\sum_{a \in A} p_a)^2$ .

Later on, we will have reason to distinguish between sets of external momenta that are ‘massive’ (sets consisting of more than one massless leg) from those which are massless. When  $\{A\}$  consists of a single element, we will denote it by  $a := \{a\} = \{A\}$ , and similarly for the other momenta labels. More generally, we refer to ‘ $a$ ’ as the *first* label in the set  $\{A\} := \{a, \dots\}$ , and so-on. Due to our focus on planar (color-ordered) amplitudes, the sets are endowed with a natural ordering of external legs.

To determine the specific numerators for the basis, we start from a spanning set of contours and fix the precise numerators according to the prescriptivity condition (3.2.4). It is worth emphasizing how the particular numerators are chosen using these conditions. For example, in the case of box-integrands, two particular numerators are chosen not simply by the condition

$$\oint_{\Omega_{A,B,C,D}^j} \mathcal{I}_{A,B,C,D}^i = \delta_{i,j}, \quad (3.2.12)$$

but *also* by the requirement that it vanish on all triangle-topology contours of its contact terms

$$\oint_{\Omega_{(A+B),C,D}^J} \mathcal{I}_{A,B,C,D}^i = \oint_{\Omega_{A,(B+C),D}^J} \mathcal{I}_{A,B,C,D}^i = \oint_{\Omega_{A,B,(C+D)}^J} \mathcal{I}_{A,B,C,D}^i = \oint_{\Omega_{(D+A),B,C}^J} \mathcal{I}_{A,B,C,D}^i = 0; \quad (3.2.13)$$

and similarly for all the contours for its bubble-topology, double-contact terms:

$$\oint_{\Omega_{(A+B+C),D}} \mathcal{I}_{A,B,C,D}^i = \oint_{\Omega_{A,(B+C+D)}} \mathcal{I}_{A,B,C,D}^i = \oint_{\Omega_{B,(C+D+A)}} \mathcal{I}_{A,B,C,D}^i = \oint_{\Omega_{(D+A+B),C}} \mathcal{I}_{A,B,C,D}^i = \oint_{\Omega_{(A+B),(C+D)}} \mathcal{I}_{A,B,C,D}^i = \oint_{\Omega_{(D+A),(B+C)}} \mathcal{I}_{A,B,C,D}^i = 0. \quad (3.2.14)$$

Thus, of the  $\text{rank}([\ell]^2) = 2+18$  degrees of freedom required to specify the basis numerators  $\mathbf{n}_{A,B,C,D}^i$ , only **2** are fixed by (3.2.12), while  $3 \times 4$  of the remaining degrees of freedom are determined by (3.2.13) and  $6 \times 1$  are fixed by the analogous equations (3.2.14) for bubble contact-terms. This is what we mean by saying that an integrand basis  $\mathfrak{B}_2^{(4)}$  is *dual* to a spanning set of particular cycles.

Of course, in order to construct *specific* integrand numerators, we must specify the contour conditions which define the basis prescriptively as described above. We do this in the following subsection. However, it should be clear that, independent from the precise contour definition, scattering amplitude integrands in this basis will be represented according to

$$\mathcal{A} = \sum_{A,B,C,D} \sum_{i=1}^2 a_{A,B,C,D}^i \mathcal{I}_{A,B,C,D}^i + \sum_{A,B,C} \sum_{I=1}^3 a_{A,B,C}^I \mathcal{I}_{A,B,C}^I + \sum_{A,B} a_{A,B} \mathcal{I}_{A,B} \quad (3.2.15)$$

where

$$a_{A,B,C,D}^i := \oint_{\Omega_{A,B,C,D}^i} \mathcal{A}, \quad a_{A,B,C}^I := \oint_{\Omega_{A,B,C}^I} \mathcal{A}, \quad a_{A,B} := \oint_{\Omega_{A,B}} \mathcal{A}. \quad (3.2.16)$$

To be any more specific, we must specify the contour conditions which define our basis prescriptively.

### 3.2.2.1 A Spanning Set of Maximal-Dimension Contours

It is interesting to note that the basis of bubble power-counting integrands in four dimensions can be viewed as  $\mathfrak{B}_2^{(4)} \simeq \mathfrak{B}_3^{(4)} \oplus \mathfrak{B}_2^{(3)}$ . That is, we may consider the new

integrands in  $\mathfrak{B}_2^{(4)}$  relative to those of  $\mathfrak{B}_3^{(4)}$  to be those associated with a bubble power-counting basis in *three* dimensions—merely *reinterpreted* in four dimensions. This is also motivated by the fact that all the new integrals required have less than maximal transcendental weight when integrated in  $4D$ , but would be of maximal-weight in  $3D$ ; these weight drops are related to the presence of double-poles when the integrands are interpreted in  $4D$ . Provided the integrands of  $\mathfrak{B}_3^{(4)}$  are full-weight, they will automatically be diagonal with respect to the integrands in  $\mathfrak{B}_2^{(3)}$ —that is, they will vanish on all contours involving double-poles.

The basis elements *without* double-poles—those of  $\mathfrak{B}_3^{(4)} \subset \mathfrak{B}_2^{(4)}$ —are easiest to discuss, which is why we start with their defining contours. The basis elements in this category are the chiral boxes  $\mathcal{I}_{A,B,C,D}^i$  as well as the scalar triangle integrands  $\mathcal{I}_{A,B,C}^{I=1}$ . All other basis elements have double-poles at infinity and will be considered momentarily in section 3.2.2.1. A summary of our defining set of contours is also provided in Table B.1 of appendix B.1.

The contours defining the chiral box integrands can be represented graphically according to:

$$\Omega_{A,B,C,D}^i := \left\{ \begin{array}{c} \begin{array}{ccc} B & & C \\ \diagdown & & / \\ \bullet & \text{---} & \bullet \\ \diagup & & \diagdown \\ A & & D \end{array} & , & \begin{array}{ccc} B & & C \\ \diagdown & & / \\ \bullet & \text{---} & \bullet \\ \diagup & & \diagdown \\ A & & D \end{array} \end{array} \right\}; \quad (3.2.17)$$

these are simply the contours encircling the two solutions  $\{\ell_1^*, \ell_2^*\}$  to the quadruple-cut equations  $\ell_a^2 = \ell_b^2 = \ell_c^2 = \ell_d^2 = 0$ . Only the box integrals have four-propagators to have a non-vanishing contour integral on such a cut, and each box integrand involves a unique set of such propagators; as such, all other basis elements automatically vanish on these contours.

The chirality of box-integrand contours can be seen more clearly in cases where massless corners are present, for which we may indicate the parity of the contour using blue or white vertices. For example, we denote the three-mass box contours as

$$\Omega_{a,B,C,D}^i := \left\{ \begin{array}{c} \text{Diagram 1: A square loop with vertices } B \text{ (top-left), } C \text{ (top-right), } D \text{ (bottom-right), and } a \text{ (bottom-left). Blue arrows indicate a clockwise contour. A blue circle is at vertex } a \text{ with } \ell = \ell_1^*. \\ \text{Diagram 2: A square loop with vertices } B \text{ (top-left), } C \text{ (top-right), } D \text{ (bottom-right), and } a \text{ (bottom-left). Red arrows indicate a clockwise contour. A red circle is at vertex } a \text{ with } \ell = \ell_2^*. \end{array} \right\}, \quad (3.2.18)$$

which highlights that these contours involve  $\ell_1^* = \lambda_a \tilde{\lambda}_X$  and  $\ell_2^* = \lambda_X \tilde{\lambda}_a$ , respectively, and the precise form of  $\lambda_X$  and  $\tilde{\lambda}_X$  is irrelevant for the moment.

Next, consider the contours for the *scalar* triangle integrands. Most interesting are the cases where there is at least one massless leg, since the associated dual basis integrands can have IR singularities. For example, we define the two-mass scalar-triangle integrals' contours by

$$\Omega_{a,B,C}^{I=1} := \begin{array}{c} \text{Diagram: A triangle with vertices } B \text{ (top), } C \text{ (right), and } a \text{ (bottom). A circle is at vertex } a. \text{ A contour is shown with arrows.} \end{array}, \quad (3.2.19)$$

where the circle is a graphical notation for the collinearity condition  $\ell_a \sim p_a$  imposed in addition to the triple cut  $\ell_a^2 = \ell_b^2 = \ell_c^2 = 0$ . Let us mention that this particular contour is spurious [101], and thus no scattering amplitude has support here. Furthermore, demanding that the chiral box integrands vanish on  $\Omega_{a,B,C}^{I=1}$  guarantees that they are free of this particular collinear singularity associated with IR divergences.

A similar discussion also applies for the scalar one-mass triangle contour  $\Omega_{a,b,C}^{I=1}$  (see subsection 3.2.2.2 for further details). The contour choice in Table B.1 for the scalar triangles renders all boxes *locally* IR-finite as in [158] by demanding that the chiral box integrands vanish in all collinear or soft regions of loop-momentum space. This choice leads to the same numerators that have been described in the context of  $\mathcal{N}=4$  sYM in [53]. Our integrated results, summarized in tab. B.3 are also related to the IR finite integrals discussed in [145].

## Defining Contours for Lower-Weight Integrands

The second class of basis integrands and their associated contours involves certain double-poles at infinite loop momentum. These are the objects we turn to now.

The key observation to define a bubble power-counting basis in four dimensions is that  $\mathfrak{B}_2^{(4)} \simeq \mathfrak{B}_3^{(4)} \oplus \mathfrak{B}_2^{(3)}$ . That is, the additional integrands needed, relative to a triangle power-counting basis in four dimensions, are scalar bubbles and triangle integrals with single-inverse-propagator loop-dependence in their numerators which define  $\mathfrak{B}_2^{(3)}$ ; both of these are *naturally* defined in three dimensions—and for more than merely pragmatic reasons.

Consider for example the scalar bubble integral. With the appropriate normalization of the numerator in terms of powers of  $s_A$ , the bubble integrates to a pure weight-one function in either two or three dimensions. Moreover, it is possible to write it as a wedge-product of  $d\log$ -differential forms in either case: (for a more detailed discussion, see e.g. [127, 159])

$$\begin{aligned} I_{A,B}^{(D=2)} &= \int \bar{d}^2 \ell \frac{1}{2} \frac{s_A}{\ell_a^2 \ell_b^2} = \frac{1}{4} \int \bar{d}\log \frac{\ell_a^2}{\ell_b^2} \wedge \bar{d}\log \frac{(\ell_a - \ell_a^*)^2}{(\ell_a - \tilde{\ell}_a^*)^2} \\ I_{A,B}^{(D=3)} &= \int \bar{d}^3 \ell \frac{1}{2} \frac{\sqrt{s_A}}{\ell_a^2 \ell_b^2} = \frac{1}{4} \int \bar{d}\log \ell_a^2 \wedge \bar{d}\log \ell_b^2 \wedge \bar{d}\log \frac{\ell \cdot q}{\ell \cdot \bar{q}} \end{aligned} \tag{3.2.20}$$

where, in the two-dimensional bubble,  $\ell_a^*$  and  $\tilde{\ell}_a^*$  are the two solutions to the maximal cut equation  $\ell_a^2 = \ell_b^2 = 0$  and the bubble has no pole at infinity,  $\ell \rightarrow \infty$ . The three-dimensional bubble is slightly more complicated and has a single pole at  $\ell \rightarrow \infty$ . This can be thought of as a dual conformal triangle in  $D = 3$  where one of the dual points is taken to be infinity [127]. In suitable coordinates (embedding space), infinity is treated on the same footing as any other point which makes this analysis very clear. Here, we refrain from introducing embedding coordinates (see [160]) and work in momentum space directly which leads to the appearance of the two null-vectors  $q$  and  $\bar{q}$  normalized by  $q \cdot \bar{q} = 1$  which are defined by the relations  $q \cdot p_A = \bar{q} \cdot p_A = 0$ . (Technically, this is easiest to implement by choosing light-cone coordinates transverse to  $p_A$ . Furthermore, the  $d\log$  form remains valid for massive internal propagators where  $\ell_{a,b}^2 \rightarrow \ell_{a,b}^2 - m^2$  which

will become important for our discussion in  $D=4$ .) In  $D=3$ , we consider for example the triple cut of the bubble which encircles the two propagators and furthermore encloses the odd combination (parity-even) of simple poles at  $\ell \rightarrow \infty$  which is clear from the  $d \log$  form in  $3D$  where one cuts the two propagators  $\ell_a^2 = \ell_b^2 = 0$  and then encircles the parity-even combination of  $\ell \cdot q = 0$  and  $\ell \cdot \bar{q} = 0$ . In three dimensions, this is a leading singularity of the scalar bubble integrand.

In contrast, in four dimensions, the scalar bubble integrand has a double-pole—signaling a weight-drop in the resulting integral [99, 100]. This is reflected in the fact that the bubble can be written explicitly by decomposing the four-dimensional space of loop-momenta into a three-dimensional subspace and one additional direction, say  $\ell^i$  orthogonal to the momentum  $p_A$  (as well as  $q, \bar{q}$ ) entering the bubble and to the three-dimensional slice. This effectively means that we can think about the  $4D$  bubble as a  $3D$  bubble where the propagators become massive, with mass  $m^2 := (\ell^i)^2$ . Since our  $3D$   $d \log$  form was valid for internal massive legs, we find

$$I_{A,B}^{(D=4)} = \int \bar{d}^3 \ell \bar{d} \ell^i \frac{1}{2} \frac{\sqrt{s_A}}{\ell_a^2 \ell_b^2} = \frac{1}{4} \int \bar{d} \log \ell_a^2 \wedge \bar{d} \log \ell_b^2 \wedge \bar{d} \log \frac{\ell \cdot q}{\ell \cdot \bar{q}} \wedge \bar{d} \ell^i, \quad (3.2.21)$$

so that the triple-cut residue results in a ‘double-pole at infinity’: an integrand which is *independent* of the remaining loop integration parameter.

$$\oint_{\substack{\ell_a^2 = \ell_b^2 = 0 \\ \vec{\ell} \rightarrow \infty \\ (\text{odd})}} \bar{d}^4 \vec{\ell} \frac{1}{\ell_a^2 \ell_b^2} \propto \int \bar{d} \ell^i, \quad (3.2.22)$$

where  $\ell^i$  is whatever component of  $\vec{\ell}$  *not* eliminated in the three integration cycles. Thus, for this integrand the differential of the form ‘ $\bar{d} \ell^i$ ’ looks like a *total derivative* on the cut. Moreover, this differential form has a double-pole at infinity. Unlike  $\bar{d} \log$ ,  $\bar{d} \ell^i$  is *not* scale invariant and thus the coefficient of the double-pole is not uniquely defined. As this example should make clear, the particular component for the final integration, say  $\ell^i$ , is completely arbitrary: any three components of  $\vec{\ell}$  can be eliminated in the first integrations, always resulting in an integrand of the form  $\bar{d} \ell^i$  in the remaining

variable. Thus, there is no *particular* double-pole: there is a three-dimensional (four-dimensional, modulo rescaling) family of such double-poles. Perhaps a more invariant way of describing a bubble integrand in four dimensions would be to start with the fact that in three dimensions, it is purely polylogarithmic: it is a  $d\log$ -form. Going from three to four dimensions amounts to appending a trivial  $d\ell^i$  onto this polylogarithmic three-form.

To be clear, the bubble integral is polylogarithmic on *any* three-dimensional subspace chosen—which we may denote as  $(\ell^i)^\perp$  for any component  $\ell^i$  of  $\vec{\ell}$ . Considering that  $\ell^i := \ell^\mu \cdot e_\mu^i$  for some basis vector  $e_\mu^i$ , it is clear that we can view the complementary space as the solutions to  $\ell \cdot p_X = 0$  for any  $p_X$ . For reasons of simplicity, it turns out to be beneficial to take  $p_X$  to be null. In this construction, we define a three-dimensional subspace of loop momenta according to

$$\vec{d}^4\ell \mapsto \vec{d}^3\hat{\ell} \quad \text{where} \quad \hat{\ell} \in (p_X)^\perp. \quad (3.2.23)$$

Noting that the null-space  $(p_X)^\perp$  of  $p_X$  is defined by  $\ell \cdot p_X = 0$ , we see that this can be interpreted more concretely as:

$$\vec{d}^3\hat{\ell} := \vec{d}^4\ell \delta(\ell \cdot p_X). \quad (3.2.24)$$

Although this three-dimensional subspace depends on  $p_X$ , we will choose the *same* subspace for all integrands with double-poles. Thus, when we say that  $\mathfrak{B}_2^{(4)} \simeq \mathfrak{B}_3^{(4)} \oplus \mathfrak{B}_2^{(3)}$ , we consider the basis  $\mathfrak{B}_2^{(3)}$  to be defined as in (3.2.23) for all integrands and consider contours to be taken over *this* three-dimensional space  $\hat{\ell}$ .

### 3.2.2.2 Illustrations of the Resulting Numerators in the Basis

In order to make some of the abstract definitions of the previous subsections more concrete, we consider a few illustrative examples that highlight all relevant features. The complete list of one-loop basis integrands with bubble power-counting is summarized



in Table B.2 of appendix B.2. First, we consider the two-mass-easy box integrands

$$\begin{array}{c} B \\ \diagup \quad \diagdown \\ \ell_c \quad c \\ \diagdown \quad \diagup \\ \ell_b \quad i \\ \diagup \quad \diagdown \\ \ell_d \quad \ell_a \\ \diagdown \quad \diagup \\ a \quad D \end{array} \leftrightarrow \mathcal{I}_{a,B,c,D}^i := \frac{\mathbf{n}_{a,B,c,D}^i}{\ell_a^2 \ell_b^2 \ell_c^2 \ell_d^2} \quad \text{with} \quad \begin{cases} \mathbf{n}_{a,B,c,D}^{i=1} := \llbracket p_a, \ell_b, \ell_c, p_c \rrbracket \\ \mathbf{n}_{a,B,c,D}^{i=2} := \llbracket \ell_b, \ell_c, p_c, p_a \rrbracket \end{cases} \quad (3.2.25)$$

where we use the kinematic bracket conventions from [161, 162] to denote contractions of momenta

$$\llbracket a_1, a_2, \dots, c_1, c_2 \rrbracket := \left[ (a_1 \cdot a_2)^\alpha{}_\beta \cdots (c_1 \cdot c_2)^\gamma{}_\alpha \right], \quad (3.2.26)$$

where  $(a_1 \cdot a_2)^\alpha{}_\beta := a_1^{\alpha\dot{\alpha}} \epsilon_{\dot{\alpha}\dot{\gamma}} a_2^{\dot{\gamma}\gamma} \epsilon_{\gamma\beta}$  and  $a^{\alpha\dot{\alpha}} := a^\mu \sigma_\mu^{\alpha\dot{\alpha}}$  are ‘ $2 \times 2$ ’ four-momenta, defined via the Pauli matrices. The ‘ $\llbracket \dots \rrbracket$ ’ object may be more familiar to some readers if written equivalently as ‘ $\text{tr}_+[\dots]$ ’, are linear in their arguments, and satisfy the following identities

$$\llbracket a_1, a_2, \dots, c_1, c_2 \rrbracket = \llbracket c_2, c_1, \dots, a_2, a_1 \rrbracket = \llbracket c_1, c_2, a_1, a_2, \dots \rrbracket. \quad (3.2.27)$$

Often, they may be simplified using

$$\llbracket \dots, x, A, A, y, \dots \rrbracket = s_A \llbracket \dots, x, y, \dots \rrbracket, \quad \text{with} \quad \llbracket \square \rrbracket = 2. \quad (3.2.28)$$

The two chiral<sup>2</sup>-box numerators are normalized to unity on the following maximal-dimensional cycles

$$\begin{array}{c} B \\ \diagup \quad \diagdown \\ \ell_c \quad c \\ \diagdown \quad \diagup \\ \ell_b \quad 1 \\ \diagup \quad \diagdown \\ \ell_d \quad \ell_a \\ \diagdown \quad \diagup \\ a \quad \ell = \ell_1^* \\ D \end{array}, \quad \begin{array}{c} B \\ \diagup \quad \diagdown \\ \ell_c \quad c \\ \diagdown \quad \diagup \\ \ell_b \quad 2 \\ \diagup \quad \diagdown \\ \ell_d \quad \ell_a \\ \diagdown \quad \diagup \\ a \quad \ell = \ell_2^* \\ D \end{array}, \quad (3.2.29)$$

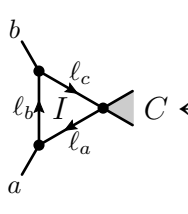
where  $\ell_1^*$  and  $\ell_2^*$  are the two solutions to the maximal cut equations of the box  $\ell_a^2 = \ell_b^2 = \ell_c^2 = \ell_d^2 = 0$  and the white and blue vertices in the contour prescription in (3.2.29) indicates the chirality of the solution at that vertex. In particular  $\ell_1^* \sim \lambda_a \tilde{\lambda}_X$  and

<sup>2</sup>Chiral numerators have also appeared elsewhere in the literature with further remarks on special analytic and IR properties, including at higher loops [163, 164] and in non-supersymmetric YM theory [165].

$\ell_2^* \sim \lambda_X \tilde{\lambda}_a$ . Due to the chirality of the solution and the order of the momenta in the brackets of  $\mathbf{n}_{a,B,c,D}^i$  in (3.2.25), the integrand basis elements are diagonal on the respective contours. In order to claim that our basis is truly prescriptive, it remains to be checked that both integrand basis elements vanish on all other defining contours summarized in Table B.1 in appendix B.

First, we should note that the chiral boxes scale at infinity like scalar triangle integrals, i.e. they have at most *single* poles at  $\ell \rightarrow \infty$ . This implies that these integrands trivially vanish on all contours that involve the instruction of taking a double-pole at infinity. This implies that the chiral boxes vanish on all defining contours for chiral triangles (to be discussed in detail shortly) as well as on the bubble-integral contours. The only remaining question is therefore associated with the defining contours for the scalar triangle subtopologies  $\Omega_{a,B,C}^1$  in the language of Table B.1. For the example considered above, all triangle subtopologies have one massless leg. Our particular choice of the one-mass scalar-triangle contour involves the collinear limit around the massless corner of the triangle. Fortunately, the chiral box numerators in (3.2.25) vanish in the collinear limit where  $\ell_a \varphi_{p_a}$  or  $\ell_c \varphi_{p_c}$  due to the properties of  $\llbracket \cdot \cdot \cdot \rrbracket$ . Crucially, the fact that these chiral boxes have only single poles at  $\ell \rightarrow \infty$  together with the fact that they vanish in the collinear regions  $\ell_a \varphi_{p_a}$  or  $\ell_c \varphi_{p_c}$  renders these objects both UV and IR finite. These integrands have been integrated in [53] and for the convenience of the reader we give their result in terms of polylogarithms in Table B.3.

A second illustrative example to consider is the one-mass triangle sector



$$\leftrightarrow \begin{cases} \mathbf{n}_{a,b,C}^{I=1} := -s_C \\ \mathbf{n}_{a,b,C}^{I=2} := \frac{1}{2\llbracket p_a - p_b, p_X \rrbracket} (2\llbracket p_a, \ell_b, p_b, p_X \rrbracket + \ell_b^2 \llbracket p_a - p_b, p_X \rrbracket) \\ \mathbf{n}_{a,b,C}^{I=3} := \frac{1}{2\llbracket p_a - p_b, p_X \rrbracket} (2\llbracket p_X, p_a, \ell_b, p_b \rrbracket + \ell_b^2 \llbracket p_a - p_b, p_X \rrbracket) \end{cases} \quad (3.2.30)$$

The chiral numerators  $\mathbf{n}_{a,b,C}^{I=2,3}$  are written in a way to make the collinear and UV properties manifest. In particular, the ordering of momenta in  $\llbracket p_a, \ell_b, p_b, p_X \rrbracket$  and its con-

jugated version guarantees that these integrand elements are IR finite in the collinear regions  $\ell_b \not\sim p_a, p_b$  as well as in the soft region  $\ell_b \sim 0$ .

These integrands in (3.2.30) are constructed to be dual to the following defining contours

$$\Omega_{a,b,C}^I := \left\{ \begin{array}{c} \text{Diagram 1: Triangle with vertices } a, b, C. \text{ A dashed line from } b \text{ to } a \text{ has a loop with a dot.} \\ \text{Diagram 2: Triangle with vertices } a, b, C. \text{ A blue loop with a dot and } \ell_1^* \rightarrow \infty \text{ (double-pole).} \\ \text{Diagram 3: Triangle with vertices } a, b, C. \text{ A red loop with a dot and } \ell_2^* \rightarrow \infty \text{ (double-pole).} \end{array} \right\} \quad (3.2.31)$$

where the first contour  $\Omega_{a,b,C}^{I=1}$  represents the soft-collinear leading singularity that sets  $\ell_b = 0$  and uniquely selects the scalar one-mass triangle. (All box integrands are chiral and their numerators guarantee the vanishing in the soft-collinear configuration.)

The chiral contours  $\Omega_{a,b,C}^{I=2,3}$  warrant some further explanation. This is the first time in our discussion where we have to deal with the double-poles at infinity that are naturally associated with a weight drop at the integrated level. These were discussed abstractly in section 3.2.2.1 and we would like to concretely give our definition for the chiral one-mass triangles here. The way to think about the chiral contours such as  $\Omega_{a,b,C}^{I=2}$  that involve the double-pole at infinity is as follows. First, one projects  $\ell_a$  into a particular direction

$$\frac{\llbracket \ell_a, p_X \rrbracket}{\llbracket p_a - p_b, p_X \rrbracket} = 0, \quad (3.2.32)$$

which leaves us with a three-dimensional surface for  $\ell_a$  perpendicular to the above projection constraint. The particular normalization of the projection (3.2.32) is related to our choice of projection and enters in the overall normalization of our integrand. The remaining three parameters of  $(\ell_a)^\perp$  are then fixed on the triple-cut  $\ell_a^2 = \ell_b^2 = \ell_c^2 = 0$ . Together with the projection condition (3.2.32), the three on-shell constraints therefore localize all four degrees of freedom of  $\ell_a$ . There are two different solutions to the constraints which we denote by  $\ell_{1,\infty}^*$  and  $\ell_{2,\infty}^*$ , where the additional subscript signals that we are interested in the leading behavior of  $\ell \rightarrow \infty$ . Taking into account the proper

Jacobian factor  $\mathcal{J}$ , our numerators evaluated on the leading singularity solutions are unit

$$\left. \frac{\mathbf{n}_{a,b,C}^{I=2}}{\mathcal{J}} \right|_{\ell_a=\ell_{1,\infty}^*} = 1, \quad \left. \frac{\mathbf{n}_{a,b,C}^{I=3}}{\mathcal{J}} \right|_{\ell_a=\ell_{1,\infty}^*} = 0, \quad \left. \frac{\mathbf{n}_{a,b,C}^{I=2}}{\mathcal{J}} \right|_{\ell_a=\ell_{2,\infty}^*} = 0, \quad \left. \frac{\mathbf{n}_{a,b,C}^{I=3}}{\mathcal{J}} \right|_{\ell_a=\ell_{2,\infty}^*} = 1. \quad (3.2.33)$$

One additional point worth discussing is the explicit presence of the bubble-contact term  $+\ell_b^2$  in the definition of our one-mass chiral triangle numerators  $\mathbf{n}_{a,b,C}^{I=2,3}$ . This term is there in order to have the chiral triangles vanish on the massive bubble contour  $\Omega_{a+b,C}$ , which we define presently.

Consider the generic massive bubble topology  $\Omega_{A,B}$ . Just as in the chiral triangle sector, we begin by projecting  $\ell_a$  onto the three-dimensional subspace

$$\frac{\llbracket \ell_a, p_X \rrbracket}{\llbracket p_A, p_X \rrbracket} = 0. \quad (3.2.34)$$

Next, two additional degrees of freedom are fixed by localizing to the bubble cut  $\ell_a^2 = \ell_b^2 = 0$ . In fact, there are two solutions to these three combined conditions, which we may denote as  $\ell_1^*, \ell_2^*$ . (If one parametrizes  $\ell_a$  in a basis of spinors involving the null momentum  $p_X$ , these two solutions are *chiral* and involve loop momenta proportional to either  $\lambda_X$  or  $\tilde{\lambda}_X$ , as we illustrate more explicitly in section 3.4.2.) The final degree of freedom is fixed on the double-pole at infinity, with the bubble integral normalized on the parity-even combination of these two evaluations.

The downside of the explicit presence of this bubble contact term is that the chiral triangles are rendered UV divergent. In principle, one could avoid this feature by explicitly removing the bubble contribution. However, this would come at the cost that the resulting basis would no longer be dual to a particular choice of contours, rendering the basis *non*-prescriptive. This would have the effect that in the representation of an amplitude, the coefficients of bubbles, say, would need to be the difference of bubble-cut leading singularities and whatever pollution arises from the triangle integrals.

Of course, one could start from a prescriptive basis to determine coefficients simply and then rotate into a non-prescriptive one in order to highlight other aspects of

interest—such as a better separation between UV and IR divergent integrands. We should note in passing that we have in fact constructed such a possibly preferential basis—one in which the *only* UV-divergent integrals are the bubbles, and for which all integrals are pure. Such choices, however, are far from unique, and leave open the generally broad questions of aesthetic and technical preferences, and so we leave such potentially illuminating rotations to future work.

### Bubble Integrands and Integrals Involving Massless Legs

Most of the integrand and contour definitions are conceptually very simple, although the exact details and choices made required a nontrivial amount of work. There is however, one additional cases that is often neglected: bubbles involving massless external legs:



The diagram shows a bubble with two internal lines forming a loop. The top line is labeled  $\ell_b$  and the bottom line is labeled  $\ell_a$ . An external leg labeled  $a$  enters from the left, and an external leg labeled  $B$  exits to the right. The vertex where  $B$  exits is shaded. The equation number (3.2.35) is to the right of the diagram.

In dimensional regularization, this integral is somewhat special in the sense that it is scaleless and integrates to zero in a nontrivial way. UV and IR divergences cancel one another in the form  $0 = \frac{1}{\epsilon_{\text{UV}}} - \frac{1}{\epsilon_{\text{IR}}}$ . In traditional generalized unitarity constructions, these terms are neglected at first and a tentative amplitude is computed. Once one separates UV from IR divergences, e.g. by introducing a mass regulator, one can compare the resulting IR or UV divergences of the tentative amplitude to general expectations and ultimately adjust the coefficients of these massless bubbles to match the expected results. We come back to this point in more detail in subsection [3.3.2](#).

From the viewpoint of prescriptivity and basis-building, however, these integrals pose no subtlety whatsoever: they are defined in exactly the same ways as the massive bubble integrands—except that the collinear condition is imposed on the three-point vertex instead of taking a residue at infinity—thereby highlighting the region of loop-momentum space that is responsible for these integrals’ IR divergences.

**Table 3.1.** Properties of basis integrands defined in  $\mathfrak{B}_3^{(4)} \subset \mathfrak{B}_2^{(4)}$ . All these integrals are *pure* and weight-2 in transcendentality when integrated in  $(4-2\epsilon)$  dimensions.

	$\mathcal{I}_{A,B,C,D}^i$	$\mathcal{I}_{a,B,C,D}^i$	$\mathcal{I}_{a,b,C,D}^i$	$\mathcal{I}_{a,B,c,D}^i$	$\mathcal{I}_{A,B,C}^1$	$\mathcal{I}_{a,B,C}^1$	$\mathcal{I}_{a,b,C}^1$
locally-finite	✓	✓	✓	✓	✓	—	—
IR-divergent (UV-finite)	—	—	—	—	—	✓	✓

What is genuinely subtle, however, is the meaning of leading singularities defined on such a contour—which affects the coefficients of these integrands in the representation of amplitudes. We review this issue in some detail in section 3.3.2, and pose two possible definitions one may take for these coefficients.

### 3.2.2.3 Stratification of UV/IR Structure and Transcendental Weight

The discussion of the previous subsection 3.2.2.2 should have made clear that our prescriptive basis integrands have certain desirable features both from an UV and IR point of view, related to the presence or absence of double-poles at infinity, or (soft-)collinear poles, respectively. Of course, being one-loop integrals, by now it is straight forward to explicitly check these integrand-level statements by simply integrating all basis elements. The results of the loop integration (in dimensional regularization) for every integrand in our basis is given in Table B.3.

It is worth highlighting several interesting features. In the decomposition of the basis  $\mathfrak{B}_2^{(4)} \simeq \mathfrak{B}_3^{(4)} \oplus \mathfrak{B}_2^{(3)}$ , the integrands in the  $\mathfrak{B}_3^{(4)}$  subspace are all pure, weight-2 functions that are free of any regions of UV-divergence; moreover, only the scalar triangle integrals involving massless legs are IR divergent—all others are *locally* finite. These general features are summarized in Table 3.1.

In contrast, all those integrands in the  $\mathfrak{B}_2^{(3)}$  subspace are weight-one functions when evaluated in  $4-2\epsilon$  dimensions (as is natural for having maximal weight in  $3D$ ). All but one class evaluates to a pure function. These general features of these integrals are

summarized in Table 3.2.

As discussed above, it is possible to alter the basis of integrands to improve the IR/UV properties of the basis. For example, it is easy to render the integrands  $\mathcal{I}_{a,B,C}^{2,3}$  pure or to make all triangle integrands UV-finite. However, this rotation of the basis would seem to be in conflict with prescriptivity, and make it harder to directly determine the coefficients of an amplitudes in the new basis.

### 3.3 Leading Singularities in $\mathcal{N} \leq 4$ Super Yang-Mills Theory

Having discussed the integrand basis construction at length, we now comment on the second key building block in the generalized unitarity expansion of the amplitude which are the coefficient functions. As discussed in section 3.2.2.1, all defining contours are of maximal dimension so that the coefficients of our basis integrands are simply leading singularities. In this section, we give details on how to compute these leading singularities in less (than maximally) supersymmetric theories.

The description of on-shell (super-)states for amplitudes in  $\mathcal{N} < 4$  super Yang-Mills theory are best implemented by considering the states to be truncations of those in  $\mathcal{N} = 4$ . This was described in detail in ref. [139], but is worth reviewing. We denote the fields related by supersymmetry to the (+)-helicity gluon by an ordered list (of length 0 to length  $\mathcal{N}$ ) of indices  $I \in \{1, \dots, \mathcal{N}\}$ ; similarly, we can label the fields related by supersymmetry to the (-)-helicity gluon by the complements of the previous labels

	$\mathcal{I}_{A,B,C}^2$	$\mathcal{I}_{A,B,C}^3$	$\mathcal{I}_{a,B,C}^{2,3}$	$\mathcal{I}_{a,b,C}^{2,3}$	$\mathcal{I}_{A,B}^1$	$\mathcal{I}_{a,B}^1$
locally-finite	✓	—	—	—	—	—
UV-divergent (IR-finite)	—	✓	✓	✓	✓	—
UV- and IR-divergent	—	—	—	—	—	✓

**Table 3.2.** Properties of basis integrands defined in  $\mathfrak{B}_2^{(3)} \subset \mathfrak{B}_2^{(4)}$ . All these integrals are weight-1 in transcendentality when integrated in  $(4-2\epsilon)$  dimensions; only  $\mathcal{I}_{a,B,C}^{2,3}$  are impure.

within the set  $\{1, \dots, 4\}$ . Thus, a (+)-helicity gluon always has a label of  $\{\}$  and (-)-helicity gluon always has a label of  $\{1, 2, 3, 4\} =: \overline{\{\}}$ ; similarly, the  $(+\frac{1}{2})$ -helicity fermions are labeled by sets  $\{I\}$  with  $I \in \{1, \dots, \mathcal{N}\}$  while the  $(-\frac{1}{2})$ -helicity fermions are labelled by  $\overline{\{I\}} := \{1, 2, 3, 4\} \setminus \{I\}$ ; and similarly for the rest of the states in the theory. Labeling the states in this way, every (non-vanishing) amplitude involves the same number  $k$  of each of the indices  $\{1, 2, 3, 4\}$  corresponding to an  $N^{k-2}$ MHV super-amplitude.

This scheme makes it obvious that for any amount of supersymmetry, the external states can be labelled as particular instances of those of  $\mathcal{N} = 4$ —the only difference being in the selection rule for which  $R$ -charge labels are allowed among the external states. These selection rules have the effect of *requiring* that the indices  $\{\mathcal{N}+1, \dots, 4\}$  *all* appear in the labels of some subset of  $k$  external states for an  $N^{k-2}$ MHV amplitude. This amounts to a truncation of some  $\mathcal{N} = 4$  super-function.

Thus, all processes in an  $N^{k-2}$ MHV amplitude (or on-shell function) must specify precisely  $k$  states related by supersymmetry to the (-)-helicity gluon. These are simply ‘helicity’ amplitudes in the case of ‘pure’ ( $\mathcal{N} = 0$ ) Yang-Mills theory; but the same  $\binom{n}{k}$  distinguished labels are required for all component amplitudes for any degree of supersymmetry (other than maximal).

This can be encoded graphically in an on-shell diagram by *orienting* all its edges. We choose to use an incoming arrow to denote the  $\binom{n}{k}$  states related to the (-)-helicity gluons (incoming at the vertex), and outgoing arrows to denote those related to the (+)-helicity gluons (incoming at a vertex). For example, the three-point super-amplitudes in  $\text{sYM}_{\mathcal{N}}$  would require *orientations* as in



$$(3.3.1)$$

To be clear, these amplitudes may be defined in terms of coherent states as follows:



$$\begin{aligned}
\mathcal{A}_3^{(i)} &:= \text{diagram} \quad := \frac{[ab]^{4-\mathcal{N}}}{[ia][ab][bi]} \delta^{1 \times \mathcal{N}} ([ab] \tilde{\eta}_i^I + [bi] \tilde{\eta}_a^I + [ia] \tilde{\eta}_b^I) \delta^{2 \times 2}(\lambda \cdot \tilde{\lambda}) \\
\mathcal{A}_3^{(i,j)} &:= \text{diagram} \quad := \frac{\langle ij \rangle^{4-\mathcal{N}}}{\langle ij \rangle \langle ja \rangle \langle ai \rangle} \delta^{2 \times \mathcal{N}} (\lambda_i^\alpha \tilde{\eta}_i^I + \lambda_j^\alpha \tilde{\eta}_j^I + \lambda_a^\alpha \tilde{\eta}_a^I) \delta^{2 \times 2}(\lambda \cdot \tilde{\lambda})
\end{aligned} \tag{3.3.2}$$

in terms of Grassmann variables  $\tilde{\eta}_i^I$  for  $I \in \{1, \dots, \mathcal{N}\}$ . The generalization to MHV amplitudes is extremely natural:

$$\mathcal{A}_{n,0}^{(i,j)} := \frac{\langle ij \rangle^{4-\mathcal{N}}}{\langle 12 \rangle \langle 23 \rangle \dots \langle n1 \rangle} \delta^{2 \times \mathcal{N}}(\lambda \cdot \tilde{\eta}) \delta^{2 \times 2}(\lambda \cdot \tilde{\lambda}) \tag{3.3.3}$$

where

$$\delta^{2 \times \mathcal{N}}(\lambda \cdot \tilde{\eta}) := \delta^{2 \times \mathcal{N}} \left( \sum_a \lambda_a^\alpha \tilde{\eta}_a^I \right) \tag{3.3.4}$$

is the super-momentum-conserving  $\delta$ -function and  $\delta^{2 \times 2}(\lambda \cdot \tilde{\lambda}) := \delta^{2 \times 2}(\sum_{a=1}^n \lambda_a^\alpha \tilde{\lambda}_a^{\dot{\alpha}})$  encodes overall momentum conservation. More generally, an  $N^{k-2}$ MHV superfunction (such as a leading singularity) in  $\mathcal{N} = 4$  super Yang-Mills is related to  $\binom{n}{k}$  *oriented* superfunctions in sYM $_{\mathcal{N}}$  according to

$$f(\lambda, \tilde{\lambda}) \delta^{k \times 4}(C \cdot \tilde{\eta}) \Rightarrow f^{(i_1, \dots, i_k)} := f(\lambda, \tilde{\lambda}) \det(c_{i_1}, \dots, c_{i_k})^{4-\mathcal{N}} \delta^{k \times \mathcal{N}}(C \cdot \tilde{\eta}), \tag{3.3.5}$$

where  $C$  represents the  $k \times n$  ‘boundary-measurement’ matrix [47] and  $\{i_r\}$  label the negative helicity super-multiplets. Just as in the three-point amplitudes given above, any decorated on-shell diagram must be oriented such that each  $N^{k-2}$ MHV tree-amplitude appearing at a vertex has  $k$  ‘sources’—i.e., incoming arrows.

### 3.3.1 Decorated On-Shell Diagrams: Singlet vs. Non-Singlet

There is a marked difference between on-shell functions in maximally supersymmetric Yang-Mills and its less supersymmetric cousins. This is primarily a result of the distinction between so-called ‘singlet’ and ‘non-singlet’ helicity configurations. In the former case, the  $R$ -charges of the external states uniquely determine those of the internal states running through the loop, regardless of the amount of supersymmetry.

All such singlet on-shell diagrams are therefore  $\mathcal{N}$ -independent and therefore equal to (truncations of)  $\mathcal{N} = 4$  super-functions and may be immediately recycled. In contrast, when there are oriented loops of ‘helicity’ in an on-shell diagram, we must sum over all the states in the supermultiplet which clearly depends on  $\mathcal{N}$ .

A prototypical example of a non-singlet decorated on-shell function is the following four-point box diagram with external states  $\{2, 4\}$  are taken as incoming:

$$\begin{array}{c} \text{Diagram with red square and } \pm \end{array} := \begin{array}{c} \text{Diagram with clockwise arrows} \end{array} + \begin{array}{c} \text{Diagram with counter-clockwise arrows} \end{array} . \quad (3.3.6)$$

For each of the two possible ‘helicity’ flows through the graph (each involving a sum over states), it is not difficult to determine the corresponding on-shell function by direct computation. In particular, we find:

$$\begin{array}{c} \text{Diagram with clockwise arrows} \end{array} = \mathcal{A}_{4,0}^{(2,4)} \varphi^{4-\mathcal{N}}, \quad \begin{array}{c} \text{Diagram with counter-clockwise arrows} \end{array} = \mathcal{A}_{4,0}^{(2,4)} (1-\varphi)^{4-\mathcal{N}} \quad (3.3.7)$$

where we have defined the cross-ratio

$$\varphi := \frac{\langle 14 \rangle \langle 23 \rangle}{\langle 13 \rangle \langle 24 \rangle} . \quad (3.3.8)$$

Thus, the decorated on-shell diagram (3.3.6) is, for  $1 \leq \mathcal{N} < 4$ ,

$$\begin{array}{c} \text{Diagram with red square and } \pm \end{array} = \mathcal{A}_{4,0}^{(2,4)} \left[ \varphi^{4-\mathcal{N}} + (1-\varphi)^{4-\mathcal{N}} \right] . \quad (3.3.9)$$

When  $\mathcal{N} = 4$ , the equation above over-counts the sum over states by 2 as both directions of helicity flow are included in the same coherent state. Furthermore, eq. (3.3.9) is valid for *entire* super-amplitudes: replacing the pre-factor (the gluonic component of the

MHV tree amplitude) by the superamplitude gives the correct answer for all components such that the  $R$ -charges of particles  $\{1, 3\}$  are in the ‘+’ multiplet (related to  $g^+$  by some number of supersymmetry generators  $\tilde{Q}_I$ ’s).

Another example which is directly relevant for the all-multiplicity MHV amplitude presented in section 3.4 is the generic two-mass easy box cut where the states related to the negative helicity gluons have particle label  $i, j$ . It is easy to verify that the only non-singlet configuration in this case is when both  $i$  and  $j$  are each in a distinct massive corner:

$$\begin{array}{c}
 \begin{array}{ccc}
 \begin{array}{c} i \\ \nearrow \\ \bullet \\ \searrow \\ a \end{array} & \begin{array}{c} \text{---} \\ \square \\ \text{---} \\ \bullet \\ \nearrow \\ j \end{array} & \begin{array}{c} c \\ \nearrow \\ \bullet \\ \searrow \\ j \end{array} \\
 \text{---} \\ \square \\ \text{---} \\ \bullet \\ \nearrow \\ a
 \end{array}
 \end{array}
 :=
 \begin{array}{c}
 \begin{array}{ccc}
 \begin{array}{c} i \\ \nearrow \\ \bullet \\ \searrow \\ a \end{array} & \begin{array}{c} \text{---} \\ \square \\ \text{---} \\ \bullet \\ \nearrow \\ j \end{array} & \begin{array}{c} c \\ \nearrow \\ \bullet \\ \searrow \\ j \end{array} \\
 \text{---} \\ \square \\ \text{---} \\ \bullet \\ \nearrow \\ a
 \end{array}
 \end{array}
 +
 \begin{array}{c}
 \begin{array}{ccc}
 \begin{array}{c} i \\ \nearrow \\ \bullet \\ \searrow \\ a \end{array} & \begin{array}{c} \text{---} \\ \square \\ \text{---} \\ \bullet \\ \nearrow \\ j \end{array} & \begin{array}{c} c \\ \nearrow \\ \bullet \\ \searrow \\ j \end{array} \\
 \text{---} \\ \square \\ \text{---} \\ \bullet \\ \nearrow \\ a
 \end{array}
 \end{array}
 .
 \end{array}
 \quad (3.3.10)$$

A straightforward calculation yields the result

$$\begin{array}{c}
 \begin{array}{ccc}
 \begin{array}{c} i \\ \nearrow \\ \bullet \\ \searrow \\ a \end{array} & \begin{array}{c} \text{---} \\ \square \\ \text{---} \\ \bullet \\ \nearrow \\ j \end{array} & \begin{array}{c} c \\ \nearrow \\ \bullet \\ \searrow \\ j \end{array} \\
 \text{---} \\ \square \\ \text{---} \\ \bullet \\ \nearrow \\ a
 \end{array}
 \end{array}
 =
 \mathcal{A}_{n,0}^{(i,j)}
 \left[
 \left(
 \frac{\langle a i \rangle \langle c j \rangle}{\langle a c \rangle \langle i j \rangle}
 \right)^{4-\mathcal{N}}
 +
 \left(
 1 - \frac{\langle a i \rangle \langle c j \rangle}{\langle a c \rangle \langle i j \rangle}
 \right)^{4-\mathcal{N}}
 \right].
 \quad (3.3.11)$$

On-shell diagrams of either the triangle or bubble type may be computed in an analogous fashion; the structure of the result is depends on whether the cut is singlet or non-singlet. As mentioned in section 3.2, the evaluation of field theory on triangle and bubble contours involves double-poles at infinity and requires a projection of the loop momentum onto a particular direction. Pragmatically, one can always derive such contour integrals from the double and triple-cuts of standard unitarity. We illustrate this feature for the massive MHV bubble coefficients in section 3.4.2.

### 3.3.2 Generalized Unitarity for Massless Bubble Coefficients

For gauge theories with  $\mathcal{N} < 3$  supersymmetry, there is an important subtlety associated with loop integrand and cut topologies which define the massless bubble integrals. If only interested in the integrated amplitudes, these coefficients may be ignored as all such integrands integrate to zero (in dimensional regularization). However,

if one were interested in disentangling the UV and IR structure of an amplitude, they play an important role. As such, their coefficients can be determined post-integration by the requirement that this behavior is correct (see e.g. [139, 166, 167]).

To see this subtlety, consider the two-particle, massless cuts of an amplitude. For any  $N^k$ MHV degree (and any assignments of external helicities), there always exists one singlet and one non-singlet configuration depending on the parity of the three-particle vertex:

$$\left\{ a \rightarrow \text{bubble}, a \rightarrow \text{bubble}^{\pm} \right\} \text{ or } \left\{ a \leftarrow \text{bubble}^{\pm}, a \leftarrow \text{bubble} \right\}. \quad (3.3.12)$$

The singlet cuts are always unambiguous and finite (and in fact always equal to truncated superfunctions of  $\mathcal{N} = 4$  due to the helicity selection rules described above). This allows one to compute such cuts directly from any valid representation of the maximally supersymmetric amplitudes (including unitarity based representations). Since e.g. unitarity based representations of maximally supersymmetric amplitudes do not include any bubble topologies at all, the finiteness of the singlet bubble cuts is clear. In contrast, the *non-singlet* cuts are unfortunately always *ill-defined*—as they generally diverge. Thus, there is no obvious meaning to these cuts in field theory, making it difficult to compute the leading singularities corresponding to the massless bubble contours: there always exists *some* branch of the bubble-cut on which the amplitude diverges. Similar observations were also made in e.g. [168] from a string theory perspective.

Of course, the massless bubble integrals in our basis have been defined by contours not merely taking the co-dimension 2 residue of the bubble cut, but a contour accessing the double-pole at infinity which starts from the collinear triple-cut in loop-momentum space—the region in which

$$\ell_a^* = \alpha p_a, \quad \ell_b^* = (1 + \alpha) p_a. \quad (3.3.13)$$

If this contour were viewed as arising as a co-dimension one residue taken along the well-defined (singlet) triple-cut in every case, then because all such cuts are equal to

(truncations of) their  $\mathcal{N} = 4$  equivalents, no amplitudes would have support on these double poles. This would suggest that every massless bubble coefficient should be identically zero. This is the first option we consider.

While this choice for interpretation is ensured to match field theory functionally on all of the well-defined (singlet) massless bubble-cuts, it turns out that it fails to match the conventional UV-structure of amplitudes (as deduced using the logic of e.g. [139, 166, 167]). In particular, it leads to representations of one-loop amplitudes that exactly misses the standard answer by a multiple of the tree amplitude times the sum of massless bubble integrals.

Perhaps this missing contribution could be attributed to some (however unconventional) renormalization ‘scheme’. And it may prove that ignoring all massless bubble contributions turns out to lead to better (more elegant in some way, perhaps) strategies at higher loops. But we must leave such speculation to future work.

However, there is another way to interpret the leading singularities corresponding to these collinear cuts. Namely, it seems natural to associate the collinear configuration as equivalent to a massless bubble on an external leg, as in:

$$\begin{array}{c} a \text{---} \bigcirc \text{---} b \\ \text{---} \bigcirc \end{array} := a \text{---} \bigcirc \text{---} \bigcirc \text{---} b \quad \Rightarrow \quad a \text{---} \bigcirc \text{---} b \quad . \quad (3.3.14)$$

This interpretation naturally suggests that we should view the value of field theory evaluated on these contours directly as the tree amplitude as in [169]. This also reproduces the standard result for one-loop amplitudes’ UV and IR structure, and certainly seems like an appropriate ‘convention’ for defining these bubble coefficients. This is the prescription used in the expressions generated for our concrete examples given in the ancillary files for this work in [153].

These kinds of subtleties are much more abundant in pure ( $\mathcal{N} = 0$ ) Yang-Mills theory, the amplitudes of which are known to require worse power-counting in their bases. While we can certainly define a prescriptive basis  $\mathfrak{B}_0$  to express these amplitudes, the coefficients of tadpoles and constants seem intrinsically ambiguous and for similar

reasons. There have been some recent proposals for how to deal with tadpoles [170] (see also [171]); however, all these proposals begin from some prior knowledge of the loop integrand—i.e. start from the (literal) sum of Feynman diagrams in some gauge and using some regularization scheme. This does lead to specific coefficients for any integrand in a basis even as ugly as  $\mathfrak{B}_0$ , but it does not provide a gauge-invariant, cut-level definition of the coefficients in terms of on-shell, tree-level scattering data. (But see e.g. [172] for some interesting ideas in that direction at higher loops that relies on a particular on-shell renormalization scheme.) Naturally, we must leave such questions—important though they are—to future work.

### 3.4 Amplitude Integrands for $\mathcal{N} \leq 4$ Super Yang-Mills Theory

The derivation of a diagonalized basis of integrands in section 3.2 has an immediate application: namely, the construction of prescriptive representations of  $1 \leq \mathcal{N} \leq 4$  sYM amplitudes. Achieving this amounts to the computation of the coefficient of each basis element—that is, field theory evaluated on the contours defining the basis.

As discussed in section 3.3.1, there are essentially two cases to consider for each coefficient, depending on the helicity configuration of interest. For a given on-shell diagram, if there is only a single allowed internal helicity flow—i.e., a ‘singlet’ configuration where the external helicities uniquely specify the internal helicity states—then the on-shell function is identical for sYM for *any*  $\mathcal{N}$ . By virtue of the fact that the  $\mathcal{N} = 4$  integrand is free of all poles at infinity, this implies that for all ‘singlet’ cuts, the coefficient of every basis element defined on contours involving infinite loop momentum necessarily vanishes.

For the ‘non-singlet’ configurations where there are multiple allowed helicity configurations, sYM for  $\mathcal{N} < 4$  can have support on single (and double) poles at infinity and the associated coefficients are generically non-vanishing (and non-trivial).

In this section, we illustrate the procedure outlined above with two concrete examples: the all-multiplicity MHV ( $\mathcal{A}_{n,1\text{-loop}}^{(i,j)}$ ) and the six-point split-helicity NMHV

$(\mathcal{A}_{6,1\text{-loop}}^{(4,5,6)})$  one-loop integrands.

### 3.4.1 General Structure of Amplitude Integrands

The general form of a one-loop amplitude integrand expressed in the bubble-power-counting basis defined in section 3.2 is,

$$\mathcal{A} = \sum_{A,B,C,D} \sum_{i=1}^2 a_{A,B,C,D}^i \mathcal{I}_{A,B,C,D}^i + \sum_{A,B,C} \sum_{I=1}^3 a_{A,B,C}^I \mathcal{I}_{A,B,C}^I + \sum_{A,B} a_{A,B} \mathcal{I}_{A,B} \quad (3.4.1)$$

where the coefficients of each basis element are defined as

$$a_{A,B,C,D}^i := \oint_{\Omega_{A,B,C,D}^i} \mathcal{A}, \quad a_{A,B,C}^I := \oint_{\Omega_{A,B,C}^I} \mathcal{A}, \quad a_{A,B} := \oint_{\Omega_{A,B}} \mathcal{A}. \quad (3.4.2)$$

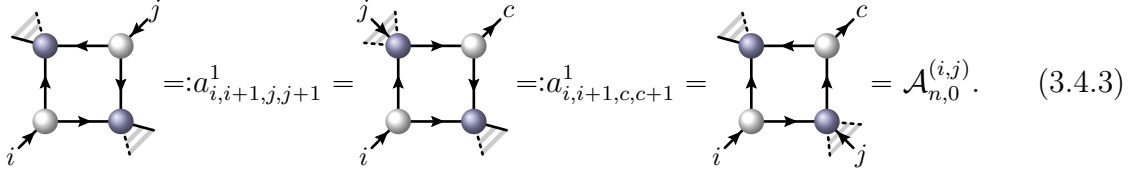
The box coefficients  $a_{A,B,C,D}^i$  are defined on the two quad-cut leading singularities i.e., field theory evaluated on the two solutions to  $\ell_a^2 = \ell_b^2 = \ell_c^2 = \ell_d^2 = 0$ . For any singlet configuration, these leading singularities are simply truncations of those defined in  $\mathcal{N} = 4$ ; for the non-singlet configurations, there is a modification resulting from the helicity flow as described above.

Regardless of supersymmetry, all one-mass triangle integrands with scalar numerators have coefficients  $a_{a,b,C}^1$  because are defined on the composite ‘soft-collinear’ residue where one internal leg is set to zero on which amplitudes always have support. Moreover, and just as in maximal sYM, the residue of field theory is always equal to the tree amplitude (as this reflects the only universal IR divergence at one loop); that is,  $a_{a,b,C}^1 = \mathcal{A}_{n,0}$ . For similar reasons, the coefficients of all two-mass scalar triangles are always zero:  $a_{a,B,C}^1 = 0$ .

The non-singlet cuts of amplitudes *can* generally lead to support on double-poles at infinity, resulting in non-trivial coefficients for triangles with loop-dependent numerators. For any singlet cuts, these coefficients are all zero. The same is true for the all bubble contours defined on double-poles at infinity. Thus, these coefficients depend strongly on how the helicity-flow at each vertex amplitude of the cut flows into the graph, and varies depending on which of the  $\binom{n}{k}$  external legs are taken to have ‘incoming’ helicity.

### 3.4.2 *Exempli Gratia*: MHV Amplitude Integrands

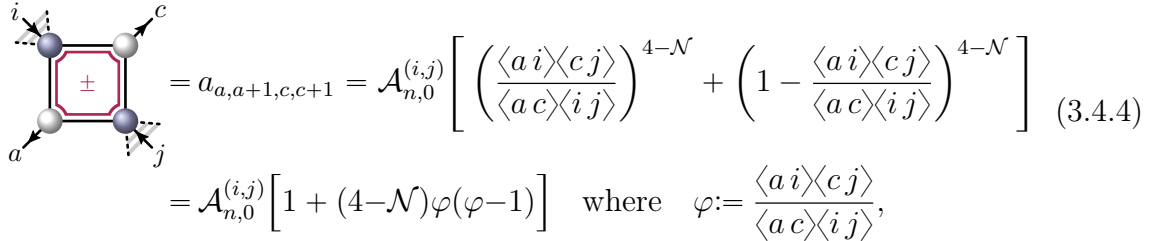
We can illustrate how these considerations work in the concrete case of MHV amplitudes ( $k=2$ ) in  $\mathcal{N} = 1, 2$  super Yang-Mills theory. As with maximal supersymmetry, the only box cuts which have non-vanishing support for these amplitudes are  $\Omega_{a,B,c,D}^1$ —the (chiral) two-mass-easy contours (and their one-mass degenerations). Of these, most contours admit only a singlet configuration of internal helicity—namely,



$$=:a_{i,i+1,j,j+1}^1 = =:a_{i,i+1,c,c+1}^1 = = \mathcal{A}_{n,0}^{(i,j)}. \quad (3.4.3)$$

All of these leading singularities are equal to the tree-level MHV amplitude  $\mathcal{A}_{n,0}^{(i,j)}$ .

Among the two-mass-easy boxes, there is only one case which admits a non-singlet configuration, see eq. (3.3.10). This example was already encountered in section 3.3, and leads to the coefficient

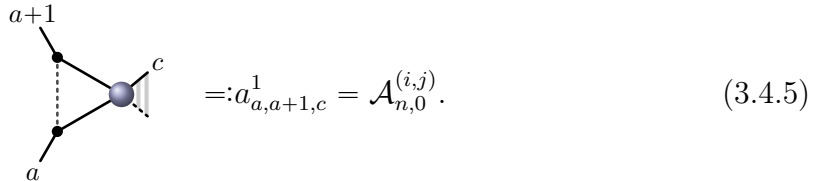


$$= a_{a,a+1,c,c+1} = \mathcal{A}_{n,0}^{(i,j)} \left[ \left( \frac{\langle a i \rangle \langle c j \rangle}{\langle a c \rangle \langle i j \rangle} \right)^{4-\mathcal{N}} + \left( 1 - \frac{\langle a i \rangle \langle c j \rangle}{\langle a c \rangle \langle i j \rangle} \right)^{4-\mathcal{N}} \right] \quad (3.4.4)$$

$$= \mathcal{A}_{n,0}^{(i,j)} \left[ 1 + (4-\mathcal{N})\varphi(\varphi-1) \right] \quad \text{where} \quad \varphi := \frac{\langle a i \rangle \langle c j \rangle}{\langle a c \rangle \langle i j \rangle},$$

where the final equality follows from the binomial expansion of the exponents in the first line and is valid only for  $\mathcal{N} = 1, 2$ .

Turning now to the triangle configurations, we may start with the scalar one-mass contours, on which all amplitudes have support equal to the tree:



$$=:a_{a,a+1,c}^1 = \mathcal{A}_{n,0}^{(i,j)}. \quad (3.4.5)$$



(We have neglected to indicate any helicity information from the left-hand-side for the simple reason that *every* one-mass scalar triangle has the same coefficient, regardless of the helicity configuration under consideration.)

For the two triangle integrals elements normalized on double-poles, there are just three classes of leg distributions with non-singlet helicity configurations leading to non-zero coefficients. By directly evaluating field theory on the corresponding contours, we find that these non-vanishing coefficients are:

$$\begin{aligned}
\begin{array}{c} \text{Diagram 1: Triangle with legs } i, j, c \text{ and internal lines } a, b \\ \text{Diagram 2: Triangle with legs } i, j, c \text{ and internal lines } a, b \\ \text{Diagram 3: Triangle with legs } i, j, c \text{ and internal lines } a, b \end{array} \Rightarrow \begin{aligned} a_{a,i,C}^2 &:= \mathcal{A}_{n,0}^{(i,j)} (4-\mathcal{N}) \frac{\langle ic \rangle \langle ja \rangle \langle iX \rangle \langle ja \rangle}{\langle ij \rangle \langle ca \rangle \langle ij \rangle \langle Xa \rangle} \left( 1 - \frac{\llbracket p_a, p_X \rrbracket}{\llbracket p_i, p_X \rrbracket} \right), \\ a_{i,b,C}^3 &:= \mathcal{A}_{n,0}^{(i,j)} (4-\mathcal{N}) \frac{\langle bj \rangle \langle iX \rangle \langle bj \rangle \langle ii-1 \rangle}{\langle ij \rangle \langle bX \rangle \langle ij \rangle \langle bi-1 \rangle} \left( 1 - \frac{\llbracket p_b, p_X \rrbracket}{\llbracket p_i, p_X \rrbracket} \right), \\ a_{a,B,C}^2 &:= \mathcal{A}_{n,0}^{(i,j)} (4-\mathcal{N}) \frac{1}{2} \frac{[Xa] \langle c-1c \rangle}{\langle a|p_B|X \rangle \langle c-1a \rangle \langle ca \rangle} \left( \frac{\langle ia \rangle \langle ja \rangle}{\langle ij \rangle} \right)^2. \end{aligned} \end{aligned} \tag{3.4.6}$$

Finally, among the massive bubble contours, the only ones with non-singlet helicity flow are those for which  $\{i, j\}$  are on opposite sides of the bubble. These coefficients turn out to be

$$\begin{array}{c} \text{Diagram: Massive bubble with legs } i, j \text{ and internal lines } a, b \end{array} \Rightarrow a_{A,B} := \mathcal{A}_{n,0}^{(i,j)} (4-\mathcal{N}) \frac{\langle a-1a \rangle \langle b-1b \rangle}{\langle ij \rangle^2} \left[ \frac{\langle iX \rangle^2 \langle jX \rangle^2}{\langle a-1X \rangle \langle aX \rangle \langle b-1X \rangle \langle bX \rangle} + \frac{\langle i|p_A|X \rangle^2 \langle j|p_A|X \rangle^2}{\langle a-1|p_A|X \rangle \langle a|p_A|X \rangle \langle b-1|p_A|X \rangle \langle b|p_A|X \rangle} \right]. \tag{3.4.7}$$

The massless bubble coefficients  $a_{a,B}$  were discussed at length in section 3.3.2 and—as emphasized there—we have two options: either  $a_{a,B} = 2(\mathcal{N}-4)\mathcal{A}_{n,0}^{(i,j)}$  or  $a_{a,B} = 0$ .

It is worth clarifying how the massive bubble coefficients  $a_{A,B}$  in eq. (3.4.7) may be obtained by a straightforward computation. It is convenient to evaluate field theory

on the bubble contour by first computing the two-parameter non-singlet bubble cut, which was in fact given already in [139] and may be written as,

$$\begin{array}{c} i \\ \swarrow \\ \text{---} \bullet \\ \searrow \\ a \end{array} \begin{array}{c} \text{---} \bullet \\ \swarrow \\ \text{---} \oplus \text{---} \\ \searrow \\ \text{---} \bullet \\ \swarrow \\ b \\ \searrow \\ j \end{array} = \mathcal{A}_{n,0}^{(i,j)} \frac{\langle a-1 a \rangle \langle b-1 b \rangle (\langle i \ell_a \rangle \langle j \ell_b \rangle)^{4-\mathcal{N}} + (\langle i \ell_b \rangle \langle \ell_a j \rangle)^{4-\mathcal{N}}}{J \langle i j \rangle^2 \langle a-1 \ell_a \rangle \langle a \ell_a \rangle \langle b-1 \ell_b \rangle \langle b \ell_b \rangle}. \quad (3.4.8)$$

A parametrization of  $\ell_a, \ell_b$  which is particularly convenient for the projection onto  $[[\ell_a, p_X]] = 0$  is given by

$$\begin{aligned} \ell_a &= \left[ s_A \left( \frac{1}{[[p_X, p_A]]} - \alpha \right) \lambda_{\mathbf{X}} + \beta (p_A \cdot \tilde{\lambda}_{\mathbf{X}}) \right] \left[ \tilde{\lambda}_{\mathbf{X}} + \frac{\alpha}{\beta} (p_A \cdot \lambda_{\mathbf{X}}) \right], \\ \ell_b &= \left[ -\alpha s_A \lambda_{\mathbf{X}} + \beta (p_A \cdot \tilde{\lambda}_{\mathbf{X}}) \right] \left[ \tilde{\lambda}_{\mathbf{X}} - \frac{1}{\beta} \left( \frac{1}{[[p_X, p_A]]} - \alpha \right) (p_A \cdot \lambda_{\mathbf{X}}) \right]. \end{aligned} \quad (3.4.9)$$

The Jacobian of the bubble cut in this parametrization is simply  $J = \beta$ , while the projection condition  $[[\ell_a, p_X]] = 0$  has two solutions,  $\lambda_{\ell_a} \sim \lambda_{\mathbf{X}}$  and  $\tilde{\lambda}_{\ell_a} \sim \tilde{\lambda}_{\mathbf{X}}$ , which correspond to  $\beta \rightarrow 0$  and  $\beta \rightarrow \infty$ , respectively. Our bubble contour prescription amounts to evaluating (3.4.8) on (3.4.9), taking the residue at either  $\beta \rightarrow 0$  or  $\beta \rightarrow \infty$ , and extracting the coefficient of the double-pole at  $\alpha \rightarrow \infty$ . We define the bubble leading singularity to be the even combination of these two field-theory evaluations, which are precisely the two terms appearing in (3.4.7).

The basis of integrands and the collection of non-vanishing coefficients in (3.4.4), (3.4.3), (3.4.6), (3.4.6) and (3.4.7), together with a prescription for the massless bubble coefficients, constitutes the MHV one-loop amplitude integrand in the form of (3.4.1). Combining all terms, one can (numerically) check that the  $p_X$  dependence drops out of the integrand via a nontrivial cancellation between all terms.

Using the tabulated integration rules found in appendix B.3, we find the  $n$ -point MHV integral to be of the form,

$$\begin{aligned} \int \bar{d}^{4-2\epsilon} \ell \mathcal{A}_{n,1(-\text{loop})}^{(i,j)} &=: -\mathcal{A}_{n,0}^{(i,j)} \left[ n \left( \frac{1}{\epsilon^2} + \frac{1}{\epsilon} \log(\mu^2) + \frac{1}{2} \log(\mu^2)^2 \right) \right. \\ &\quad \left. + \left( \frac{1}{\epsilon} + \log(\mu^2) + 2 \right) \left( (4-\mathcal{N}) - \sum_{a=1}^n \log(s_{a,a+1}) \right) \right. \\ &\quad \left. + \hat{\mathcal{A}}_{n,1}^{(i,j)} \right] + \mathcal{O}(\epsilon). \end{aligned} \quad (3.4.10)$$

Here, the expression  $\widehat{\mathcal{A}}_{n,1}^{(i,j)}$  is implicitly defined to be the UV- and IR-finite part of the one-loop amplitude divided by the tree amplitude.

It is worth remarking that while the expression in (3.4.10) is *correct*, it is not entirely manifest in our representation. In particular, the expression on the second line does not follow *manifestly* from the basis we have constructed. Nevertheless, we have explicitly checked its correctness.

### 3.4.3 *Exempli Gratia*: a Six-Point NMHV Amplitude Integrand

As another example of prescriptive unitarity with bubble power-counting, we consider the six-particle split-helicity NMHV amplitude integrand with particles  $\{4, 5, 6\}$  to be those related by supersymmetry generators to negative helicity states.

First, it is easy to see that for the particular helicity configuration we've considered, *every* non-vanishing box diagram is of the singlet type. This implies that the box coefficients are given by extracting the  $(\tilde{\eta}_4)^4(\tilde{\eta}_5)^4(\tilde{\eta}_6)^4$  component of the  $R$ -invariants appearing in the  $\mathcal{N}=4$  superamplitude.

Just as in the MHV example discussed above, the coefficients of the one-mass scalar triangles is always the tree amplitude,  $\mathcal{A}_{6,1\text{-loop}}^{(4,5,6)}$ . It turns out that the non-vanishing chiral triangle and bubble coefficients, can all be expressed compactly in terms of the following two superfunctions ( $R$ -invariants)

$$\begin{aligned} f_1 &:= \frac{\langle 6|p_{45}|3\rangle^{4-\mathcal{N}}}{\langle 12\rangle[45]\langle 2|p_{34}|5\rangle s_{345}\langle 6|p_{45}|3\rangle\langle 61\rangle[34]} \delta^{3\times\mathcal{N}}(C_1\cdot\tilde{\eta}) \delta^{2\times 2}(\lambda\cdot\tilde{\lambda}), \\ f_3 &:= \frac{\langle 4|p_{56}|1\rangle^{4-\mathcal{N}}}{\langle 34\rangle[61]\langle 4|p_{56}|1\rangle s_{561}\langle 2|p_{16}|5\rangle\langle 23\rangle[56]} \delta^{3\times\mathcal{N}}(C_3\cdot\tilde{\eta}) \delta^{2\times 2}(\lambda\cdot\tilde{\lambda}), \end{aligned} \quad (3.4.11)$$

$$\text{where } C_1 := \begin{pmatrix} \lambda_1^1 & \lambda_2^1 & \lambda_3^1 & \lambda_4^1 & \lambda_5^1 & \lambda_6^1 \\ \lambda_1^2 & \lambda_2^2 & \lambda_3^2 & \lambda_4^2 & \lambda_5^2 & \lambda_6^2 \\ 0 & 0 & [45][53][34] & 0 & & \end{pmatrix}, \quad C_3 := \begin{pmatrix} \lambda_1^1 & \lambda_2^1 & \lambda_3^1 & \lambda_4^1 & \lambda_5^1 & \lambda_6^1 \\ \lambda_1^2 & \lambda_2^2 & \lambda_3^2 & \lambda_4^2 & \lambda_5^2 & \lambda_6^2 \\ [56] & 0 & 0 & 0 & [61][15] & \end{pmatrix}. \quad (3.4.12)$$

In terms of these two superfunctions, we find that the non-vanishing non-singlet cuts for this amplitude give rise to the following non-vanishing coefficients:

$$\begin{aligned}
& \begin{array}{c} \text{Diagram 1} \\ \text{Diagram 2} \end{array} \Rightarrow a_{3,4,\{5,6,1,2\}}^2 := (4-\mathcal{N}) \frac{[[p_3-p_4, p_X]]}{\langle X3 \rangle [4X]} \left( f_1 \frac{\langle 6|p_{12}|4 \rangle}{\langle 6|p_{12}|3 \rangle} - f_3 \frac{\langle 3|p_{56}|1 \rangle}{\langle 4|p_{56}|1 \rangle} \right) \\
& \Rightarrow a_{6,1,\{2,3,4,5\}}^3 := (4-\mathcal{N}) \frac{[[p_6-p_1, p_X]]}{\langle X1 \rangle [6X]} \left( f_1 \frac{\langle 1|p_{45}|3 \rangle}{\langle 6|p_{45}|3 \rangle} - f_3 \frac{\langle 4|p_{23}|6 \rangle}{\langle 4|p_{23}|1 \rangle} \right)
\end{aligned} \tag{3.4.13}$$

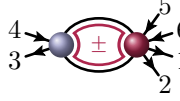
$$\begin{aligned}
& \begin{array}{c} \text{Diagram 1} \\ \text{Diagram 2} \end{array} \Rightarrow a_{2,\{3,4\},\{5,6,1\}}^2 := (4-\mathcal{N}) f_3 \frac{1}{2} \frac{\langle 24 \rangle \langle 2|p_{34}|1 \rangle [X2]}{\langle 2|p_{34}|X \rangle \langle 4|p_{56}|1 \rangle} \\
& \Rightarrow a_{2,\{3,4,5\},\{6,1\}}^2 := (4-\mathcal{N}) f_1 \frac{1}{2} \frac{\langle 26 \rangle \langle 2|p_{16}|3 \rangle [X2]}{\langle 2|p_{16}|X \rangle \langle 6|p_{45}|3 \rangle}
\end{aligned} \tag{3.4.14}$$

$$\begin{array}{c} \text{Diagram} \Rightarrow a_{5,\{6,1\},\{2,3,4\}}^3 := (4-\mathcal{N}) f_3 \frac{1}{2} \frac{[15] \langle 4|p_{16}|5 \rangle \langle X5 \rangle}{\langle 4|p_{56}|1 \rangle \langle X|p_{16}|5 \rangle} \end{array} \tag{3.4.15}$$

$$\begin{array}{c} \text{Diagram} \Rightarrow a_{5,\{6,1,2\},\{3,4\}}^3 := (4-\mathcal{N}) f_1 \frac{1}{2} \frac{[35] \langle 6|p_{34}|5 \rangle \langle X5 \rangle}{\langle 6|p_{45}|3 \rangle \langle X|p_{34}|5 \rangle} \end{array}$$

$$\begin{aligned}
& \begin{array}{c} \text{Diagram 1} \\ \text{Diagram 2} \end{array} \Rightarrow a_{\{2,3,4\},\{5,6,1\}} := \frac{(4-\mathcal{N}) f_3}{\langle 4|p_{561}|1 \rangle} \left[ \frac{\langle 24 \rangle \langle 2|[p_{561}, p_X] p_{561}|1 \rangle}{\langle 2|p_{561} p_X|2 \rangle} \right. \\
& \quad \left. + \frac{\langle 4|p_{561}|5 \rangle [1|[p_X, p_{561}]|5]}{[5|p_X p_{561}|5]} \right] \\
& \Rightarrow a_{\{3,4,5\},\{6,1,2\}} := \frac{(4-\mathcal{N}) f_1}{\langle 6|p_{345}|3 \rangle} \left[ \frac{\langle 26 \rangle \langle 2|[p_{345}, p_X] p_{345}|3 \rangle}{\langle 2|p_{345} p_X|2 \rangle} \right. \\
& \quad \left. + \frac{\langle 6|p_{345}|5 \rangle [5|[p_X, p_{345}]|3]}{[5|p_X p_{345}|5]} \right]
\end{aligned} \tag{3.4.16}$$

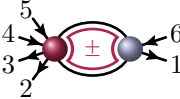
where we introduced a ‘commutator’  $\langle a|[p_A, p_B]p_C|b\rangle := \langle a|p_A p_B p_C|b\rangle - \langle a|p_B p_A p_C|b\rangle$  to write more compact expressions for the bubble-integrand coefficients. The final two non-zero bubble massive bubble coefficients are:



$$\Rightarrow a_{\{3,4\},\{5,6,1,2\}} :=$$

$$(4-\mathcal{N}) \left\{ \left[ \frac{\langle 6|p_{12}|4\rangle \llbracket p_3-p_4, X \rrbracket}{\langle X3\rangle[4X]} - \frac{\langle 6|p_{34}|5\rangle [3|[p_X, p_{34}]|5]}{[5|p_X p_{34}|5]} \right] \frac{f_1}{\langle 6|p_{45}|3\rangle} \right. \quad (3.4.17)$$

$$\left. + \left[ \frac{\langle 3|p_{56}|1\rangle \llbracket p_3-p_4, X \rrbracket}{\langle X3\rangle[4X]} - \frac{\langle 2|p_{34}|1\rangle \langle 2|[p_X, p_{34}]|4\rangle}{\langle 2|p_{34}p_X|2\rangle} \right] \frac{f_3}{\langle 4|p_{56}|1\rangle} \right\}$$



$$\Rightarrow a_{\{6,1\},\{2,3,4,5\}} :=$$

$$(4-\mathcal{N}) \left\{ \left[ \frac{\langle 1|p_{45}|3\rangle \llbracket p_6-p_1, X \rrbracket}{\langle X6\rangle[1X]} + \frac{\langle 2|p_{16}|3\rangle \langle 2|[p_X, p_{16}]|6\rangle}{\langle 2|p_{16}p_X|2\rangle} \right] \frac{f_1}{\langle 6|p_{12}|3\rangle} \right. \quad (3.4.18)$$

$$\left. + \left[ \frac{\langle 4|p_{23}|6\rangle \llbracket p_6-p_1, X \rrbracket}{[X6]\langle 1X\rangle} + \frac{\langle 4|p_{16}|5\rangle [1|[p_X, p_{16}]|5]}{[5|p_X p_{16}|5]} \right] \frac{f_3}{\langle 4|p_{23}|1\rangle} \right\}$$

Plugging these coefficients into the expansion of the amplitude in eq. (3.4.1), we obtain the integrand for the six-point split-helicity NMHV amplitude integrand with particles 4, 5 and 6 being related by supersymmetry to negative helicity gluons.

### 3.4.4 Finite Observables at One Loop

It is widely appreciated that four-dimensional scattering amplitudes for massless particles are problematic due to the presence of long-distance (infrared) divergences associated to low energy (soft) or unresolved collinear radiation, see e.g. [173]. For inclusive enough physical observables such as cross-sections, all such divergences cancel when real radiation effects are taken into account consistently as a consequence of the KLN theorem [174, 175] in QED and its generalizations. Another example of an IR-finite observable is the energy-energy correlation function, see e.g. [176, 177]. The IR structure of general gauge theories is still an important subject of current study; both formally (see e.g. [178, 179]) as well as phenomenologically in the form of efficient IR subtraction schemes for high-precision predictions for collider observables [180–184].

From an amplitudes perspective, it is possible to determine which diagrams can contribute to IR divergences and which ones remain finite. This analysis amounts to investigating all soft and collinear regions of a given diagram, taking into account potential numerator factors that can dampen IR singularities. It turns out that the situation is especially simple for one-loop integrals where one can easily account for all possible singular regions which suffices for the present discussion. For general gauge theories, the infrared structure has been completely understood up to two-loop order by Catani [185] with numerous subsequent progress, see e.g. [186–191].

The universality of IR divergences of gauge theory scattering amplitudes at one loop implies that all divergences should be proportional to the tree amplitude. Together with the requirement that UV divergences in a renormalizable gauge theory should be canceled by appropriate counter terms also implies that the one-loop UV divergences is also proportional to the tree-level amplitude. Motivated by this discussion, we can organize the  $n$ -particle one-loop amplitude in the following form:

$$\begin{aligned} \mathcal{A}_{n,1} &=: \mathcal{A}_{n,1}^{\text{fin}} + \mathcal{A}_{n,0} (\mathcal{I}_{\text{div}}^{\text{UV}} + \mathcal{I}_{\text{div}}^{\text{IR}}) \\ &=: \mathcal{A}_{n,0} \left( \widehat{\mathcal{A}}_{n,1}^{\text{fin}} + \mathcal{I}_{\text{div}}^{\text{UV}} + \mathcal{I}_{\text{div}}^{\text{IR}} \right) \quad \text{with} \quad \widehat{\mathcal{A}}_{n,1} := \mathcal{A}_{n,1} / \mathcal{A}_{n,0}, \end{aligned} \tag{3.4.19}$$

where we suppress the explicit helicity-labels of the (super-)amplitudes as well as the MHV-degree  $k$ . The universality of IR divergences is more general than the specific one-loop example discussed above and is encoded in the following factorization formula (see e.g. [191, 192]) for massless parton scattering amplitudes

$$\mathcal{A}_n(\{p_i\}, \alpha_s) = Z_n(\{p_i\}, \mu, \alpha_s) \mathcal{A}_n^{\text{fin}}(\{p_i\}, \mu, \alpha_s) \tag{3.4.20}$$

where all IR singularities are factorized in  $Z_n$  in the form of poles in dimensional regularization  $\epsilon = (D - 4)/2$ . The above equation depends on a factorization scale  $\mu$  and the running coupling constant  $\alpha_s := \alpha_s(\mu^2)$ .

Motivated by this decomposition, it is natural to introduce the IR-finite ratio function where the universal IR singularities cancel. A priori, we can write the ratio of two

$n$ -point amplitudes  $\mathcal{A}_n^{(a)}$ , and  $\mathcal{A}_n^{(b)}$  to all orders in perturbation theory:

$$\mathcal{P}_n^{(a,b)} = \frac{\mathcal{A}_n^{(a)}}{\mathcal{A}_n^{(b)}}. \quad (3.4.21)$$

In maximally supersymmetric theories, there is only a single independent super amplitude for a given  $N^{(k-2)}$ MHV sector and one takes IR finite ratios between amplitudes of different  $k$  charge. In this case, the labels ‘ $a$ ’ and ‘ $b$ ’ denote the respective  $k$ -charge of the amplitudes and it is common to always divide by the  $k=2$  MHV amplitude and denote the resulting ratio function by  $\mathcal{P}_n^{(k)}$ . The IR-finiteness of  $\mathcal{P}_n^{(k)}$  underlies several important features of the integrated results for the maximally supersymmetric theory, including dual conformal invariance [25–27, 193, 194]. These simplifications, together with a number of conceptual and technological advances enabled Dixon and collaborators to obtain function level results to very high loop order, see e.g. [15, 195, 196].

For the  $\mathcal{N} = 1, 2$  supersymmetric amplitudes under consideration, we can furthermore take nontrivial ratios of (super-) amplitudes within the same  $N^{(k-2)}$ MHV  $k$  sector due to the distinction between the positive and negative helicity gluon supermultiplet and write e.g.

$$\mathcal{P}_4^{(2)} = \frac{\mathcal{A}_4^{(2)}(1^-, 2^-, 3^+, 4^+)}{\mathcal{A}_4^{(2)}(1^-, 2^+, 3^-, 4^+)} =: \frac{\mathcal{A}_4^{(1,2)}}{\mathcal{A}_4^{(1,3)}}, \quad (3.4.22)$$

where the  $\pm$  labels the relevant supermultiplet of particle  $i$ . We omit labeling the ratios by the individual helicities of the contributing amplitudes to avoid cluttering the equations and introduced the shorthand notation  $\mathcal{A}_n^{(i,j)}$  for MHV amplitudes to indicate the position of the negative helicity supermultiplets.

All ratios can be expanded perturbatively in the coupling constant  $g$  and yield IR-finite quantities at each order in perturbation theory, e.g. up to two-loop order we find

$$\begin{aligned} \mathcal{P}_n^{(a,b)} &=: \frac{\mathcal{A}_{n,0}^{(a)} + \alpha_s \mathcal{A}_{n,1}^{(a)} + \alpha_s^2 \mathcal{A}_{n,2}^{(a)} + \mathcal{O}(\alpha_s^3)}{\mathcal{A}_{n,0}^{(b)} + \alpha_s \mathcal{A}_{n,1}^{(b)} + \alpha_s^2 \mathcal{A}_{n,2}^{(b)} + \mathcal{O}(\alpha_s^3)} = \mathcal{P}_{n,0}^{(a,b)} + \alpha_s \mathcal{P}_{n,1}^{(a,b)} + \alpha_s^2 \mathcal{P}_{n,2}^{(a,b)} + \mathcal{O}(\alpha_s^3) \\ &= \frac{\mathcal{A}_{n,0}^{(a)}}{\mathcal{A}_{n,0}^{(b)}} + \alpha_s \frac{\left( \mathcal{A}_{n,0}^{(b)} \mathcal{A}_{n,1}^{(a)} - \mathcal{A}_{n,0}^{(a)} \mathcal{A}_{n,1}^{(b)} \right)}{\left[ \mathcal{A}_{n,0}^{(b)} \right]^2} + \end{aligned} \quad (3.4.23)$$

$$+ \alpha_s^2 \frac{\left( \left[ \mathcal{A}_{n,0}^{(b)} \right]^2 \mathcal{A}_{n,2}^{(a)} - \mathcal{A}_{n,0}^{(b)} \mathcal{A}_{n,0}^{(a)} \mathcal{A}_{n,2}^{(b)} + \mathcal{A}_{n,0}^{(a)} \left[ \mathcal{A}_{n,1}^{(b)} \right]^2 - \mathcal{A}_{n,0}^{(b)} \mathcal{A}_{n,1}^{(b)} \mathcal{A}_{n,1}^{(a)} \right)}{\left[ \mathcal{A}_{n,0}^{(b)} \right]^3} + \mathcal{O}(\alpha_s^3),$$

where we indicate the loop order of various quantities by an additional subscript. The formulae for the ratio of amplitudes in the same MHV sector follow trivially from the above results. In the presentation above, the various factors of the tree-level amplitudes  $\mathcal{A}_{n,0}^{(b)}$  and  $\mathcal{A}_{n,0}^{(a)}$  ensure a uniform helicity weight of all terms in the perturbatively expanded form version of the ratio function. It is often convenient to divide out certain helicity-dependence by removing the tree-level amplitude and work instead with  $\widehat{\mathcal{A}}_n$  to define

$$\begin{aligned} \widehat{\mathcal{P}}_n^{(a,b)} &= \frac{1 + \alpha_s \widehat{\mathcal{A}}_{n,1}^{(a)} + \alpha_s^2 \widehat{\mathcal{A}}_{n,2}^{(a)} + \mathcal{O}(\alpha_s^3)}{1 + \alpha_s \widehat{\mathcal{A}}_{n,1}^{(b)} + \alpha_s^2 \widehat{\mathcal{A}}_{n,2}^{(b)} + \mathcal{O}(\alpha_s^3)} = \widehat{\mathcal{P}}_{n,0}^{(a,b)} + \alpha_s \widehat{\mathcal{P}}_{n,1}^{(a,b)} + \alpha_s^2 \widehat{\mathcal{P}}_{n,2}^{(a,b)} + \mathcal{O}(\alpha_s^3) \\ &= 1 + \alpha_s \left( \widehat{\mathcal{A}}_{n,1}^{(a)} - \widehat{\mathcal{A}}_{n,1}^{(b)} \right) + \alpha_s^2 \left( \widehat{\mathcal{A}}_{n,2}^{(a)} - \widehat{\mathcal{A}}_{n,2}^{(b)} + \left[ \widehat{\mathcal{A}}_{n,1}^{(b)} \right]^2 - \widehat{\mathcal{A}}_{n,1}^{(a)} \widehat{\mathcal{A}}_{n,1}^{(b)} \right) + \mathcal{O}(\alpha_s^3). \end{aligned} \quad (3.4.24)$$

At one-loop, the IR and UV finiteness of the ratio function is easy to see. From general expectations (and confirmed by our explicit calculation below), both the UV- and IR-divergent parts of the one-loop amplitudes must be proportional to the tree-level amplitudes as in (3.4.19). Working with the rescaled quantities, we see that the universal factor  $\mathcal{I}_{\text{div}}^{\text{IR/UV}}$  cancels in the difference (3.4.24). Similar arguments also lead to the finiteness of the higher-loop ratio functions.

We may illustrate how this works for the simplest example involving four particles. Before taking the ratios, we give the integrated results for the individual amplitudes ( $\mathcal{N} = 1, 2$ )

$$\begin{aligned} \widehat{\mathcal{A}}_{4,1}^{(1,2)} &= \frac{4}{\epsilon^2} - \frac{1}{\epsilon} \left[ (4 - \mathcal{N}) + 2 \log \frac{s}{\mu^2} + 2 \log \frac{t}{\mu^2} \right] \\ &\quad - 2(4 - \mathcal{N}) + \pi^2 + \log^2 \frac{s}{t} + (4 - \mathcal{N}) \log \frac{t}{\mu^2} + \log^2 \frac{s}{\mu^2} + \log^2 \frac{t}{\mu^2} \end{aligned} \quad (3.4.25)$$

$$\begin{aligned} \widehat{\mathcal{A}}_{4,1}^{(1,3)} &= \frac{4}{\epsilon^2} - \frac{1}{\epsilon} \left[ (4 - \mathcal{N}) + 2 \log \frac{s}{\mu^2} + 2 \log \frac{t}{\mu^2} \right] \\ &\quad - \frac{(4 - \mathcal{N})s}{u} \left[ -2 + \log \frac{t}{\mu^2} \right] - \frac{(4 - \mathcal{N})t}{u} \left[ -2 + \log \frac{s}{\mu^2} \right] \end{aligned} \quad (3.4.26)$$



$$+ \frac{s^{4-\mathcal{N}} + t^{4-\mathcal{N}} + (-u)^{4-\mathcal{N}}}{2(-u)^{4-\mathcal{N}}} \left[ \pi^2 + \log^2 \frac{s}{t} \right] + \log^2 \frac{s}{\mu^2} + \log^2 \frac{t}{\mu^2}$$

in terms of the usual Mandelstam variables  $s := (p_1 + p_2)^2, t := (p_2 + p_3)^2, u := (p_1 + p_3)^2$ . In the one-loop ratio function of (3.4.24), we are supposed to take the difference of the two amplitudes. Both the UV and IR divergences cancel in this difference and we find for  $\mathcal{N} = 1, 2$  that

$$\hat{\mathcal{A}}_{4,1}^{(1,2)} - \hat{\mathcal{A}}_{4,1}^{(1,3)} = \frac{(4 - \mathcal{N})t}{2u^2} \left[ s \left( \pi^2 + \log^2 \frac{s}{t} \right) + 2u \log \frac{s}{t} \right], \quad (3.4.27)$$

where standard Mandelstam invariants  $s, t, u$  satisfy  $s + t + u = 0$ . As advertised, this result is IR and UV finite, but of mixed transcendental weight. Compared to the individual amplitudes, the ratio is considerably simpler and does not depend on the dimensional-regularization scale  $\mu^2$  anymore.

Going to higher point is also feasible by inserting the integral values for each of our basis integrands that are summarized in Table B.3 of appendix B.3. At five points, the results depend on five independent Mandelstam invariants which leads to more complicated looking results. Since all ingredients are provided with this work, we refrain from writing explicit results here. In general, however, the fact that these ratio functions are UV- and IR-finite follows directly from the general form (3.4.10).

### 3.5 Conclusion

In this chapter, we computed one-loop amplitude integrands in color-ordered less-than-maximally supersymmetric ( $1 \leq \mathcal{N} < 4$ ) Yang-Mills theory ('sYM $_{\mathcal{N}}$ ') in the context of generalized unitarity. We constructed a *prescriptive* bubble power-counting integrand basis, and showed how the coefficients of MHV and NMHV amplitudes can be calculated using contour integrals that are dual to that basis.

While the box, triangle, and massive bubble integral coefficients can be extracted in a standard manner, there is an important subtlety in the case of massless bubbles. This topology is traditionally ignored in unitarity-based approaches due to the fact that scalar massless bubble integrals evaluate to zero in dimensional regularization. In

contrast, in this chapter, it was our primary objective to construct a well-defined *integrand*. This forces us to specify a prescription for the massless bubble coefficients as well. Here, we have presented two distinct possibilities that appear well motivated from field theory and on-shell function considerations: (a) choose collinear cuts or (b) choose singlet double cuts which are the same for any amount of supersymmetry, including  $\mathcal{N}=4$  where these cuts are unambiguously defined. In the first scenario, the massless bubble coefficients are fixed to be tree-level amplitudes. The resulting integrand correctly reproduces both the expected IR and UV divergences upon integration. In the second scenario, we get zero coefficients for the massless bubbles and the integrand has improved behavior at infinity on singlet cuts. While both approaches are justified, each exhibits a different structure for the resulting integrands for amplitudes. We leave it to future work to investigate which of the two directions is preferred from the point of view of defining the *unique*  $\mathcal{N}<4$  sYM integrand beyond one loop.

Having a unique integrand is essential for the formulation of loop-level recursion relations (see e.g. [93]), or attempts to reproduce it as a certain differential form on a positive geometry. Therefore, our work is a crucial first stepping stone for a possible extension of amplituhedron-like geometric objects [56] beyond planar maximally supersymmetric Yang-Mills theory.

# Chapter 4

## Non-planar BCFW Grassmannian Geometries

### 4.1 Introduction

We have seen enormous progress in our understanding of scattering amplitudes in the planar  $\mathcal{N} = 4$  sYM by now. A key question is if some of the developments can be generalized beyond the planar sector of  $\mathcal{N} = 4$  sYM perturbative S-matrix. Naively, planarity is essential, as it implies a cyclic ordering of the amplitude without which we can not talk about dual conformal symmetry, integrability methods, positive Grassmannian, or Amplituhedron. Nevertheless, surprisingly many of the properties indeed survive beyond the planar limit evidencing that the new ideas extend to the full  $\mathcal{N} = 4$  sYM. For instance, the absence of poles at infinite momenta in the multi-loop non-planar integrands indicates that the analog of dual conformal symmetry for full  $\mathcal{N} = 4$  sYM should exist [99–101, 162, 197–200]. The study of non-planar amplitudes in  $\mathcal{N} = 4$  sYM also pertains to a larger question of the role of planarity in the study of scattering amplitudes. Understanding how to do without planar variables and cyclic symmetry is crucial for addressing open questions in perturbative gravity where the graviton amplitudes are intrinsically non-planar. And indeed there are many intriguing properties of graviton amplitudes such as color-kinematics duality [6–8], surprisingly

compact formulas for tree-level amplitudes [201–208] or enhanced UV behavior of loop amplitudes [209–213], all of which suggest new formulations for amplitudes extend beyond the planar sector.

One interesting class of non-planar objects studied extensively in the past are on-shell diagrams. These gauge invariant functions appear as discontinuities of loop amplitudes across branch-cuts, where all intermediate particles are taken to be on-shell. There exists a fundamental connection between on-shell diagrams in quantum field theory and Grassmannian geometry. For an  $n$ -point  $N^{k-2}$ MHV amplitude, each planar on-shell diagram corresponds to a cell of the positive Grassmannian  $G_+(k, n)$ , whereas a generic non-planar diagram is associated with a general cell in  $G(k, n)$  without any positivity properties. The non-planar on-shell diagrams were partially classified in a series of papers [102, 104]. But much remains to be understood about non-planar on-shell diagrams. On-shell diagrams can be computed as products of tree-level amplitudes from the definition. The same expressions are also reproduced as canonical differential forms associated with the corresponding cells in  $G(k, n)$ . In  $\mathcal{N} = 4$  sYM, the canonical forms are simple “dlog”-forms in both the planar and non-planar cases. However, while the expressions for planar on-shell diagrams are invariant under dual super-conformal (and also Yangian) symmetry, the non-planar on-shell diagrams have no such symmetry a priori. It is natural to ask if, and under what conditions, any part of the dual conformal symmetry survives in the non-planar sector.

A hopeful starting point for investigating the problem of residual symmetry is the special class of on-shell diagrams which serve as the building blocks in the BCFW representation of scattering amplitudes. The tree-level BCFW recursion relations for cyclically ordered amplitudes can be realized diagrammatically in terms of on-shell diagrams, where each term in the recursion corresponds to one (or multiple) on-shell diagrams. These on-shell diagrams are not generic, as they originate from gluing simpler diagrams, representing the two subamplitudes separated by an additional “BCFW bridge”. A very simple application of the recursion relations for gluons allows us to

write very compact formulas for  $\mathcal{N} = 4$  sYM tree-level amplitudes. In the usual implementation of BCFW recursions, we use exclusively adjacent shifts, i.e. BCFW bridges attached to two adjacent legs, leading to highly efficient expansions in *planar* on-shell diagrams with manifest Yangian symmetry. But there is no preventing us from choosing non-adjacent legs for BCFW shifts; with such choices, the recursion relations give rise to expansions in terms of generally non-planar on-shell diagrams.

In this chapter we initiate a systematic study of the connection between non-planar on-shell diagrams arising in the context of non-adjacent BCFW shifts and the Grassmannian geometry. We identify the *BCFW cells* in the Grassmannian  $G(k, n)$  associated with these diagrams by looking at configurations of  $n$  points in  $\mathbb{P}^{k-1}$  as encoded in the representative  $C$ -matrices. While not retaining the cyclicity and convexity of their planar counterparts, the configurations underlying the non-planar on-shell diagrams generated by non-adjacent BCFW shifts turn out to form a surprisingly simple subset. We also find a new way to extract the on-shell functions directly from the Grassmannian configurations, bypassing the standard procedures of computation. The key insight, drawn from analyses of the geometry of MHV amplitudes and Parke-Taylor factors in the kinematic space, is to make connection between constrained Grassmannian configurations and singularities in external kinematic data. Exploiting this correspondence we present a closed-form formula of non-adjacent BCFW representation of tree-level amplitudes in terms of certain non-planar on-shell functions analogous to the familiar planar R-invariants. Using the Kleiss-Kuijf (KK) relations we show that the non-planar on-shell functions can be expressed as linear combinations of their planar counterparts, which is reminiscent of a similar statement for the MHV on-shell diagrams [102]. We mainly focus on NMHV amplitudes, but also show some  $N^2$ MHV examples and outline the generalization for any  $k$ .

The paper is organized as follows: In section 2, we review the connection between tree-level BCFW recursion and the cells in the positive Grassmannian. In section 3, we propose a new holomorphic formula for planar BCFW on-shell functions, extracted di-

rectly from the Grassmannian geometry as viewed in the kinematical space. In section 4, we identify the non-planar Grassmannian geometries associated with non-adjacent BCFW terms in the NMHV amplitudes. In section 5, we obtain the on-shell functions for these non-planar geometries which extend the formula in section 3 into a new type of objects, and show that they nevertheless can be re-expressed as a linear combination of planar  $R$ -invariants with different orderings. In section 6, we further exploit the geometric picture and find a holomorphic dlog-form representation of the on-shell functions directly in the kinematical space. In section 7, we extend the NMHV discussion in sections 3-6 to the  $N^2$ MHV amplitudes and beyond. We end with the conclusions and outlook in section 8.

## 4.2 Background: From BCFW to Positive Geometry

We consider the  $n$ -pt gluon  $N^k$ MHV scattering amplitudes in  $\mathcal{N} = 4$  sYM theory. (Note that at tree-level, gluon amplitudes are identical for any number of supersymmetries  $\mathcal{N}$ , so the maximal supersymmetry is here mainly for book-keeping reasons. ) At tree-level, we can decompose the amplitude as a sum of cyclically ordered amplitudes,

$$\mathcal{A}_n^{(k)} = \sum_{\pi} \text{Tr}(T^{a_1} T^{a_2} \dots T^{a_n}) A_n^{(k)}(1, 2, \dots, n), \quad (4.2.1)$$

where the sum is over all permutations modulo cyclic. We focus on the amplitude  $A_n^{(k)} \equiv A_n^{(k)}(1, 2, \dots, n)$  with a canonical ordering, which can be calculated using Britto-Cachaz-Feng-Witten (BCFW) recursion relations. We perform a BCFW shift,

$$\lambda_{\hat{i}} = \lambda_i + z\lambda_j, \quad \tilde{\lambda}_{\hat{j}} = \tilde{\lambda}_j - z\tilde{\lambda}_i, \quad (4.2.2)$$

under which the amplitude  $A_n^{(k)}(z)$  develops a dependence on the shift parameter. Since it scales like  $A_n^{(k)}(z) = \mathcal{O}(1/z)$  for  $z \rightarrow \infty$ , we can use the Cauchy formula to reconstruct the original amplitude  $A_n^{(k)} = A_n^{(k)}(z=0)$ ,

$$\oint \frac{A_n^{(k)}(z) dz}{z} = 0 \Rightarrow A_n^{(k)} = - \sum_j \text{Res}_{z=z_j} \left[ \frac{A_n^{(k)}(z)}{z} \right]. \quad (4.2.3)$$

Based on tree-level unitarity, all poles of  $A_n^{(k)}(z)$  correspond to  $P_k(z)^2 = 0$  where  $P_k$  is a (shifted) sum of adjacent external momenta, and the residues are products of lower-point amplitudes with shifted momenta,

$$A_n^{(k)} = \sum_P \frac{A_{n_L}^{(k_L)} A_{n_R}^{(k_R)}}{P^2}, \quad (4.2.4)$$

where  $n_L + n_R = n - 2$ ,  $k_L + k_R = k - 1$ , and we sum over all factorization channels where particle  $i$  is on the left side and particle  $j$  on the right side. For *adjacent* BCFW shifts, namely  $(n1)$  shift,

$$\lambda_{\hat{n}} = \lambda_n + z\lambda_1, \quad \tilde{\lambda}_{\hat{1}} = \tilde{\lambda}_1 - z\tilde{\lambda}_n, \quad (4.2.5)$$

the expression (4.2.4) simplifies to a sum over the single index  $j$ ,

$$A_n^{(k)} = \sum_j \frac{A_{n_L}^{(k_L)}(\hat{1}, 2, \dots, j, I) A_{n_R}^{(k_R)}(I, j+1, \dots, \hat{n})}{P^2}, \quad (4.2.6)$$

where the on-shell momentum  $P$  of the internal line is given by

$$P_I = \frac{(P)|n]\langle 1|(P)}{\langle 1|P|n]}, \quad \text{where } P = p_1 + \dots + p_j. \quad (4.2.7)$$

The adjacent BCFW recursion relations provide highly efficient representations of the tree-level amplitude involving a minimal number of terms. Furthermore, they preserve the cyclic ordering of external legs required for introducing momentum twistor variables [48]. In the case of  $\mathcal{N} = 4$  sYM the adjacent BCFW expansions are then term-wise Yangian invariant, making this hidden symmetry of tree-level amplitudes manifest.

#### 4.2.1 From BCFW to On-shell Diagrams

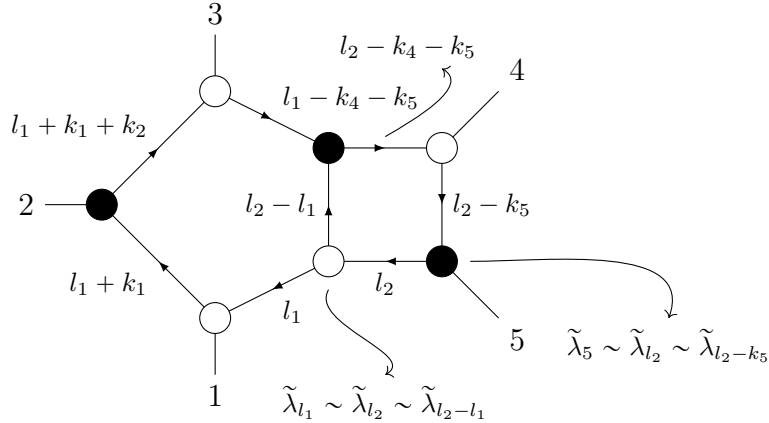
BCFW recursion relations have a natural diagrammatic realization in terms of *on-shell diagrams*. An on-shell diagram is built from 3-point massless amplitudes connected with on-shell edges. There are two types of 3-particle massless amplitudes, represented by black and white black and white 3-pt vertices in the graph, which corresponds to

MHV and  $\overline{\text{MHV}}$  helicity configuration, resp. In  $\mathcal{N} = 4$  sYM theory, all the various 3-pt amplitudes are packaged into two elementary superfunctions<sup>1</sup>

$$\begin{array}{ccc}
 \begin{array}{c} 1 \quad 2 \\ \diagdown \quad / \\ \circ \\ / \\ 3 \end{array} & = & \frac{\delta^4(P)\delta^4(Q)}{[12][23][31]}, \\
 \begin{array}{c} 1 \quad 2 \\ \diagdown \quad / \\ \bullet \\ / \\ 3 \end{array} & = & \frac{\delta^4(P)\delta^4(Q)}{\langle 12 \rangle \langle 23 \rangle \langle 31 \rangle}.
 \end{array} \tag{4.2.8}$$

Gluing these elementary building blocks together generate more complicated objects that we call on-shell diagrams.

Functions corresponding to such graphs are called on-shell functions; they have the physical interpretation as residues of multi-loop integrands that computes discontinuities of loop amplitudes across branch-cuts, where all intermediate particles taken to be on-shell. If the *cuts* conditions localize all the loop variables, and impose no further constraints on external kinematics, e.g.



$$\begin{aligned}
 l_1^2 &= (l_1 + k_1)^2 = (l_1 + k_1 + k_2)^2 = (l_1 + k_1 + k_2 + k_3)^2 \\
 &= (l_2 - k_4 - k_5)^2 = (l_2 - k_5)^2 = l_2^2 = (l_2 - l_1)^2 = 0
 \end{aligned} \tag{4.2.9}$$

we call the on-shell function (diagram) a *leading singularity*. In this case  $L = 4n_I$  where  $L$  is the number of loops and  $n_I$  number of internal propagators in the diagram;

<sup>1</sup>While we are primarily interested in  $\mathcal{N} = 4$  sYM here, let us mention in the passing that on-shell diagrams can be defined for any quantum field theory. If we work in another theory, we just replace these expressions by other 3-point amplitudes. For theories with less than maximal supersymmetry, we need to add arrows on all legs indicating the helicities



in other words, all  $4L$  degrees of freedom in  $L$  off-shell loop momenta  $\ell_i$  are fixed by cut conditions. Note that the cuts conditions admit two sets of solutions for loop momenta  $\ell_i$  and this information is also encoded in the diagram through collinearities of  $\lambda, \tilde{\lambda}$  in each vertex.

To compute the on-shell function, we take the product of all three-point amplitudes in the diagram as evaluated on the cut solution and dress it with the Jacobian factor  $J$  resulting from the elimination of internal variables.

$$= \frac{1}{J} \prod_i^7 \mathcal{A}_i^{\text{tree}} \quad (4.2.10)$$

Having introduced the on-shell diagrams, let us quickly review how to use them to implement BCFW recursion. The BCFW shift (4.2.2) of any on-shell object is furnished by a *BCFW bridge*. If we denote the  $n$ -point amplitude  $A_n$  by a grey blob schematically, then the  $(n1)$ -shifted amplitude  $A_n(z)$  corresponds to attaching the following BCFW bridge:

$$\mathcal{A}_n = \quad \mathcal{A}_n(z) = \quad (4.2.11)$$

Taking a residue of  $A_n(z)$  corresponds to removing one internal edge from the diagram on the right. The Cauchy formula (4.2.3) is then the statement that all the diagrams

with one edge by removed sum to zero (see [214] for details).

$$\partial \left[ \text{blob with bridge} \right] = \left[ \text{blob without bridge} \right] + \sum_{j=2}^{n-2} \left[ \text{blob split with bridge} \right] = 0 \quad (4.2.12)$$

Thus we can then express the unshifted amplitude  $A_n$  which corresponds to removing the edge in the BCFW bridge) as a sum of all the other on-shell diagrams, which are given by gluing together lower-point amplitudes (grey blobs) with the addition of the same BCFW bridge ( $n1$ ). Note that each grey blob in itself represents a sum of on-shell diagrams which are obtained recursively.

Let us look at a few examples. At 4-point and 5-point, the MHV amplitudes are represented by a single on-shell diagram.

$$\mathcal{A}_4^{k=2} = \frac{\delta^4(P)\delta^4(Q)}{\langle 12 \rangle \langle 23 \rangle \langle 34 \rangle \langle 41 \rangle} \quad \mathcal{A}_5^{k=2} = \frac{\delta^4(P)\delta^4(Q)}{\langle 12 \rangle \langle 23 \rangle \langle 34 \rangle \langle 45 \rangle \langle 51 \rangle} \quad (4.2.13)$$

This extends to  $n$ -point MHV as BCFW recursion only contains one term at each order.

$$\mathcal{A}_n^{k=2} = \text{Diagram} = \frac{\delta^4(P)\delta^4(Q)}{\langle 12 \rangle \langle 23 \rangle \cdots \langle n1 \rangle} \quad (4.2.14)$$

Beyond MHV, BCFW recursion decompose the amplitude into multiple on-shell diagrams. For instance, the 6-point NMHV can be expressed as

$$\mathcal{A}_6^{k=3} = \text{Diagram 1} + \text{Diagram 2} + \text{Diagram 3} \quad (4.2.15)$$

where we recognize the 4pt MHV and 5pt MHV building blocks embedded in the 6pt NMHV diagrams, with additional BCFW bridges. We will study these BCFW terms in great details later.

Before proceeding further, let us make two important remarks. First, if we choose adjacent BCFW shifts exclusively at each order of recursion, we only get planar on-shell diagrams; non-planar on-shell diagrams arise when non-adjacent legs are shifted. Second, the set of all on-shell diagrams relevant for the BCFW recursion relations (planar or non-planar) is a (particularly simple) subset of all leading singularities.

#### 4.2.2 From On-Shell Diagrams to Grassmannian Geometry

On-shell diagrams also appear in combinatorics and algebraic geometry as *plabic graphs* and are related to the cells of Grassmannian  $G(k, n)$ , where  $k$  and  $n$  specify the underlying helicity configuration and the number of external legs respectively. To each *planar* plabic graph we can associate a cell in the *positive Grassmannian*  $G_+(k, n)$ , represented by a  $(k \times n)$  real matrix  $C$  modulo  $GL(k)$  transformations which has all

main  $(k \times k)$  ordered minors being positive. The plabic graph provides a particular way to parameterize the matrix via *boundary measurement*. Specifically, a boundary measurement gives a set of variables  $\alpha_i$ 's labelling the edges of the graph; when these variables are real with definite signs, the  $C$ -matrix has all main minors positive. The *top cell* of  $G_+(k, n)$  has maximal  $k(n-k)$  dimensionality and is parameterized  $k(n-k)$  of parameters; all other cells are lower-dimensional boundaries of the top cell where some parameters are sent to zero – in the plabic graph, this corresponds to removing edges. See [214] for more details.

As an example, we can show the same diagram from the previous section. It corresponds to a *top cell* of  $G_+(2, 5)$ , and a particular positive parametrization of the  $(2 \times 5)$  matrix found using boundary measurements is as follows:

$$C = \begin{pmatrix} 1 & \alpha_1 + \alpha_2\alpha_6 & \alpha_6 & \alpha_3\alpha_6 & 0 \\ 0 & \alpha_2\alpha_5\alpha_6 & \alpha_5\alpha_6 & \alpha_4 + \alpha_3\alpha_5\alpha_6 & 1 \end{pmatrix}. \quad (4.2.16)$$

For  $\alpha_k > 0$  all  $(2 \times 2)$  ordered minors are positive.

A cell in the positive Grassmannian  $G_+(k, n)$  is a space with boundaries and an example of the *positive geometry* [60]. The geometry can be interpreted as a  $k$ -plane spanned by the rows of  $C$  in  $n$ -dimensions subject to positivity constraints on its parameters. But it is illuminating to view the  $C$ -matrix instead as a collection of  $n$  columns vectors  $\vec{P}_i$  in the projective space  $\mathbb{P}^{k-1}$

$$C = \begin{pmatrix} * & * & * & * & \dots & * \\ * & * & * & * & \dots & * \\ \vdots & \vdots & \vdots & \vdots & \vdots & \vdots \\ * & * & * & * & \dots & * \end{pmatrix} \rightarrow \left( \vec{P}_1 \ \vec{P}_2 \ \vec{P}_3 \ \vec{P}_4 \ \dots \ \vec{P}_n \right), \quad (4.2.17)$$

Modding out the scale from each vector

$$\vec{P}_i = \lambda_i P_i \quad \text{with } \lambda_i > 0 \quad (4.2.18)$$

$P_i$  then describes a point in the projective space and the cell in  $G_+(k, n)$  can be interpreted as a particular configuration of  $n$  points in the projective space  $\mathbb{P}^{k-1}$ . Let us consider the  $k = 2$  and  $k = 3$  scenarios explicitly.

$k = 2$ , **MHV case** The projective space is just  $\mathbb{P}^1$ , ie. projective line, and each  $P_i$  is a point on this projective line:

$$P_i = \begin{pmatrix} 1 & x_i \end{pmatrix} \quad (4.2.19)$$

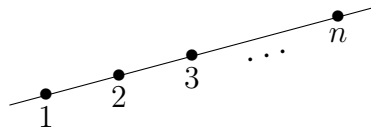
The  $(2 \times 2)$  minor of  $\vec{P}_i$  then reduces to

$$(ij) = |\vec{P}_i \vec{P}_j| = \lambda_i \lambda_j \begin{vmatrix} 1 & 1 \\ x_i & x_j \end{vmatrix} = \lambda_i \lambda_j (x_j - x_i) \quad (4.2.20)$$

Positivity of all such ordered minors,  $(ij) > 0$  for  $j > i$  implies an ordering of parameters  $x_i$ ,

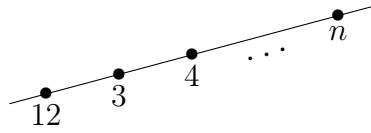
$$x_1 < x_2 < x_3 < \dots < x_n \quad (4.2.21)$$

Geometrically, this corresponds to  $n$  ordered points on a projective line,



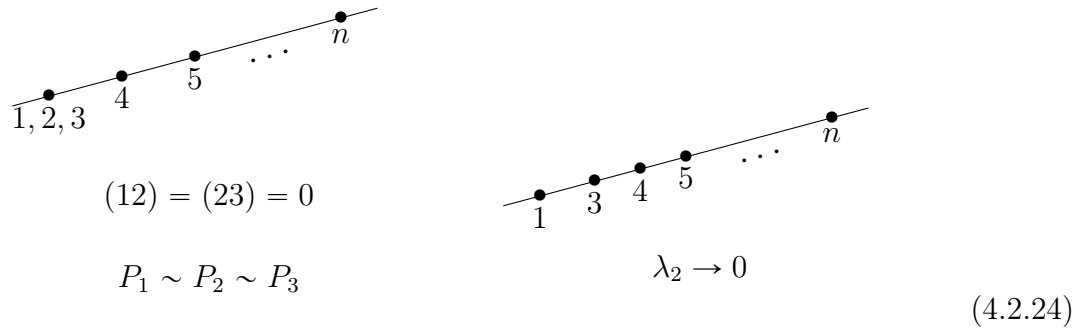
$$(4.2.22)$$

The boundaries of this geometry are lower dimensional cells which correspond to sending some of the consecutive minors  $(i i+1) = 0$ . Sending one minor to zero, for example,  $(12) = \lambda_1 \lambda_2 (x_2 - x_1) = 0 \rightarrow x_1 = x_2$ , corresponds to merging two adjacent two points



$$(12) = 0 \quad (4.2.23)$$

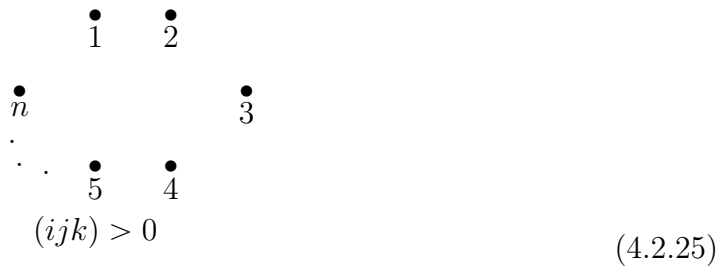
Sending another minor  $(j\ j+1) = 0$  would merge respective points and we can continue this process by probing lower and lower dimensional boundaries. We can also send the overall factor  $\lambda_i \rightarrow 0$  and delete the point  $i$  point completely. This gives us two types of codimension-2 boundaries,



$$\begin{array}{ccc}
 \begin{array}{c} \bullet \\ \bullet \\ \bullet \\ \bullet \\ \bullet \\ \dots \\ \bullet \\ n \end{array} & & \begin{array}{c} \bullet \\ \bullet \\ \bullet \\ \bullet \\ \bullet \\ \dots \\ \bullet \\ n \end{array} \\
 \begin{array}{c} 1, 2, 3 \\ 4 \\ 5 \\ \dots \\ n \end{array} & & \begin{array}{c} 1 \\ 3 \\ 4 \\ 5 \\ \dots \\ n \end{array} \\
 (12) = (23) = 0 & & \lambda_2 \rightarrow 0 \\
 P_1 \sim P_2 \sim P_3 & & \\
 & & (4.2.24)
 \end{array}$$

Note that we can only remove point  $i$  if  $P_i$  is already identified with other  $P_j$  (either  $P_{i-1}$  or  $P_{i+1}$ ), otherwise the dimensionality of the configuration would decrease by 2, rather than 1. This continues to even lower dimensional boundaries when we merge or delete more points.

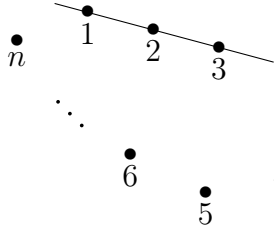
$k = 3$ , **NMHV case** The Grassmannian geometry is configurations of  $n$  points in  $\mathbb{P}^2$ , the generic configuration corresponding to the  $(3n - 9)$ -dimensional top cell are arranged as



$$\begin{array}{ccc}
 \bullet & & \bullet \\
 1 & & 2 \\
 \bullet & & \bullet \\
 n & & 3 \\
 \cdot & & \cdot \\
 \cdot & & \cdot \\
 \bullet & & \bullet \\
 5 & & 4 \\
 (ijk) > 0 & & \\
 & & (4.2.25)
 \end{array}$$

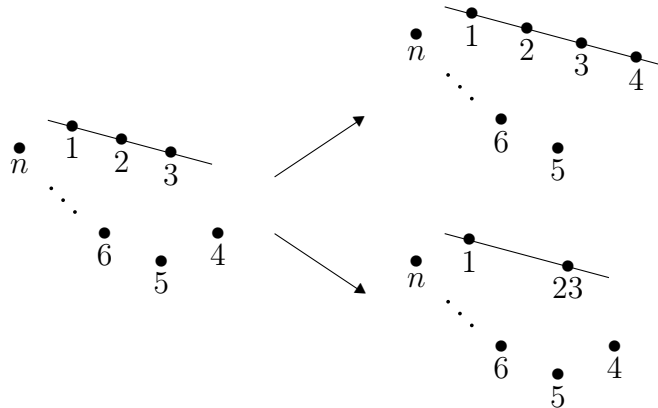
The convexity of the configuration follows from the positivity of all  $(3 \times 3)$  consecutive minors. Sending consecutive minors  $(i-1\ i\ i+1) = 0$  places three adjacent points on

the same line, for instance



$$(123) = 0, \text{ otherwise } (ijk) > 0 \tag{4.2.26}$$

Similarly, setting another consecutive minor  $(j-1 j j+1) = 0$ , places the respective triplet of points on a line. When two overlapping minors both vanish, e.g. in the above example further setting  $(234) = 0$ , we get two solutions: either all points 1, 2, 3 and 4 are on the same line or points 2 and 3 coincide.



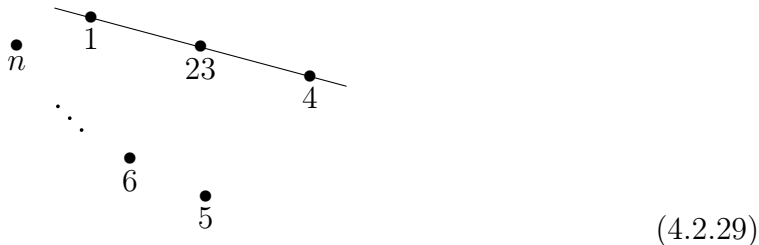
$$\Rightarrow (234) = 0 \text{ has two solutions.} \tag{4.2.27}$$

This can be also understood algebraically. When  $(123) = 0$  we can express  $P_3 = \alpha P_1 + (1 - \alpha)P_2$  and the minor  $(234)$  factorizes,

$$(234) = -\frac{\lambda_2}{\lambda_1} \alpha (124). \tag{4.2.28}$$

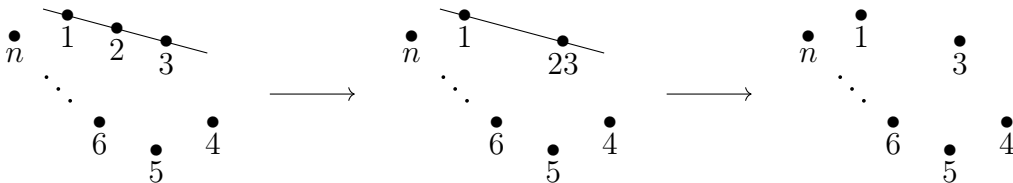
Now we can either set  $(124) = 0$  to access the first configuration or set  $\alpha = 0$  to access the second. Note that unlike in the MHV case where merging two points is achieved by imposing a single constraint, we need two constraints in the NMHV case. In addition

we have an overlapping case where  $(124) = \alpha = 0$ ,



which is  $(3n-12)$ -dimensional, ie. codimension-3 configuration.

We can also consider removing a point completely. If we remove a point directly by sending  $\lambda_i \rightarrow 0$  the dimensionality of the configuration would drop by 3. Hence, in order to eliminate a point, we must first put this point on a line with at least two other points, then merge it with an adjacent point before finally removing it.



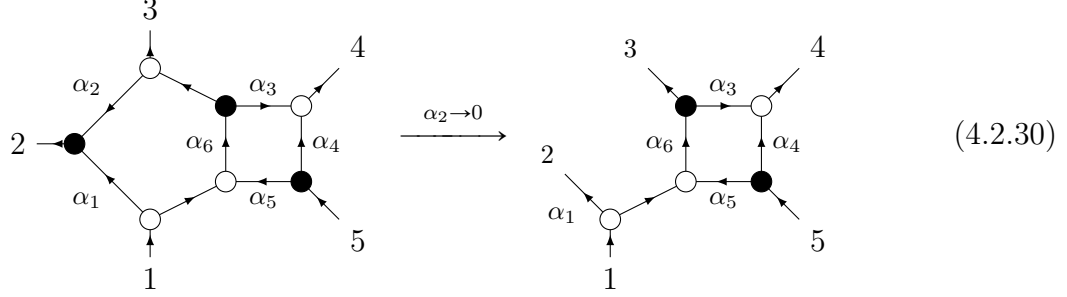
Iteratively these procedures allow us to access all lower-dimensional cells of  $G_+(3, n)$ .

The discussion above generalizes to higher  $k$ . The top cell of  $G_+(k, n)$  with all consecutive minors positive corresponds to a generic convex configuration of  $n$  points in  $\mathbb{P}^{k-1}$ . Any lower-dimensional cell results from moving some of these points to lower-dimensional spaces (eg. on special planes, lines, etc) or removing some of them completely, which can be achieved by iteratively sending consecutive minors to zero and keeping in mind that minors can factorize wherein we get multiple solutions. For more details see [42, 214].

Going back to the plabic graphs: assessing lower-dimensional boundaries by sending one of the edge variables to zero corresponds to removing that edge from the graph. Hence, the plabic graphs provide natural *stratifications* of the positive Grassmannian



$G_+(k, n)$ . In our  $G_+(2, 5)$  example, we can make minor (12) vanish by setting  $\alpha_2 = 0$  to vanish and the resulting plabic graph describes  $2n-5$  dimensional cell in  $G_+(2, 5)$ .



As we already know, this corresponds to merging points 1, 2 as shown in (4.2.23) in the geometric picture.

### 4.2.3 Canonical dlog forms

For a top cell in  $G_+(k, n)$  we can associate a canonical differential form

$$\Omega_{n,k}^{\text{top}} = \frac{d^{k \times n} C}{\text{vol}[GL(k)]} \frac{1}{(12 \dots k)(23 \dots k+1)(n1 \dots k-1)} \quad (4.2.31)$$

where we wedge all the (differentials of) parameters of the  $C$ -matrix modulo  $GL(k)$  redundancy. The denominator contains the product of all *consecutive minors* which specify the codim-1 boundaries of the top cell. The canonical form  $\Omega_{n,k}$  for a lower dimensional cell is obtained by taking subsequent residues of (4.2.31) where we set the corresponding minors to zero,

$$\Omega_{n,k} = \frac{d^{k \times n} C}{\text{vol}[GL(k)]} \frac{1}{(12 \dots k)(23 \dots k+1)(n1 \dots k-1)} \Bigg|_{(\text{minors})=0} \quad (4.2.32)$$

Let us look at some simple examples. For  $G_+(2, n)$  the canonical form for the top form is

$$\Omega_{n,k=2}^{\text{top}} = \frac{d^{2 \times n} C}{\text{vol}[GL(2)]} \frac{1}{(12)(23)(34) \dots (n1)}. \quad (4.2.33)$$

To get the canonical form associated with the cell (4.2.23), we take the residue on  $(12) = 0$ . This can be achieved by setting  $x_1 = x_2$  in the partial parametrization (4.2.19):

$$\Omega_{n,k=2} = \frac{d^{2 \times n-1} C}{\text{vol}[GL(2)]} \frac{1}{\lambda_1(23)(34) \dots (n2)}. \quad (4.2.34)$$

Similarly, starting from the top form of  $G_+(3, n)$

$$\Omega_{n,k=3}^{\text{top}} = \frac{d^{3 \times n} C}{\text{vol}[GL(3)]} \frac{1}{(123)(234)(345) \dots (n12)}. \quad (4.2.35)$$

we get for the codimension-2 cell corresponding to the second configuration in (4.2.27)

$$\Omega_{n,k=3} = \frac{d^{3 \times n - 2} C}{\text{vol}[GL(3)]} \frac{1}{\lambda_2(134)(345)(456) \dots (n13)}. \quad (4.2.36)$$

by eliminating two degrees of freedom in vector  $\vec{P}_2$ .

We can write these canonical forms explicitly using any parametrization  $\{x_i\}$  of the  $C$ -matrix, obtaining for a  $m$ -dimensional cell

$$\Omega_{n,k} = F(x_1, x_2, \dots, x_m) dx_1 \dots dx_m, \quad (4.2.37)$$

where  $F(x_1, x_2, \dots, x_m)$  is a rational function. With a proper choice of parameterization, the canonical form reduces to a simple *dlog form*,

$$\Omega_{n,k} = \frac{d\alpha_1}{\alpha_1} \frac{d\alpha_2}{\alpha_2} \dots \frac{d\alpha_m}{\alpha_m} = d\log(\alpha_1) \wedge d\log(\alpha_2) \dots \wedge d\log(\alpha_m). \quad (4.2.38)$$

making it possible to access the form for a lower-dimensional cell as a simple residue about  $\alpha_i = 0$ . The edge variables  $\{\alpha_i\}$  given by the boundary measurement of the plabic graph are one such convenient choice. Note that by explicitly parameterizing the  $C$ -matrix, we have assumed a particular gauge-fixing of  $GL(k)$  in (4.2.32). We have traded the manifest  $GL(k)$  gauge invariance of (4.2.32) for exposing that all singularities of the form  $\Omega_n^k$  are *logarithmic* in (4.2.38).

#### 4.2.4 Dual formulation

There is a direct connection between on-shell diagrams we defined in (4.2.10) and the canonical forms for the cells in the positive Grassmannian. For any on-shell diagram in a given theory, the superfunction as computed by gluing 3-pt amplitudes has the

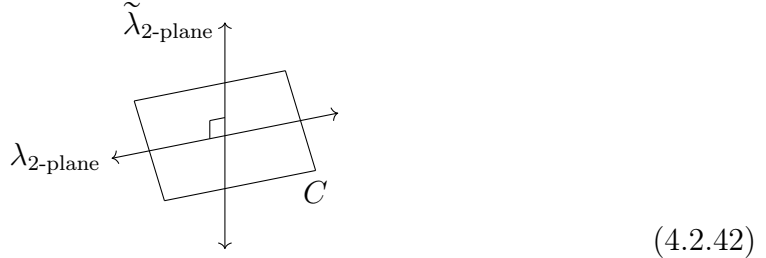
following Grassmannian integral representation<sup>2</sup>,

$$\mathcal{F}_{n,k}(\lambda, \tilde{\lambda}, \tilde{\eta}) = \int \Omega_{n,k} \delta^{k \times 2}(C \cdot \tilde{\lambda}) \delta^{2 \times (n-k)}(C^\perp \cdot \lambda) \delta^{k \times \mathcal{N}}(C \cdot \tilde{\eta}) \quad (4.2.40)$$

The specific choice of the differential form  $\Omega$  is theory-dependent. For the  $\mathcal{N} = 4$  sYM theory, this is a canonical dlog form (4.2.38). The differential form  $\Omega$  is also known for  $\mathcal{N} < 4$  sYM [214] and supergravity [94, 95]. The  $\delta$ -functions in (4.2.40) play an important role as they relate the edge variables  $\alpha_i$  and the kinematics  $\lambda_i, \tilde{\lambda}_i, \tilde{\eta}_i$ . The bosonic  $\delta$ -functions have a clear geometric interpretation. Thinking of both  $\lambda, \tilde{\lambda}$  as 2-planes in  $n$ -dimensions:

$$\lambda = \begin{pmatrix} \lambda_1^{\alpha=1} & \lambda_2^{\alpha=1} & \dots & \lambda_n^{\alpha=1} \\ \lambda_1^{\alpha=2} & \lambda_2^{\alpha=2} & \dots & \lambda_n^{\alpha=2} \end{pmatrix}, \quad \tilde{\lambda} = \begin{pmatrix} \tilde{\lambda}_1^{\dot{\alpha}=1} & \tilde{\lambda}_2^{\dot{\alpha}=1} & \dots & \tilde{\lambda}_n^{\dot{\alpha}=1} \\ \tilde{\lambda}_1^{\dot{\alpha}=2} & \tilde{\lambda}_2^{\dot{\alpha}=2} & \dots & \tilde{\lambda}_n^{\dot{\alpha}=2} \end{pmatrix} \quad (4.2.41)$$

The first set of  $\delta$ -functions constrain the  $k$ -plane  $C$  to be orthogonal to the 2-plane  $\tilde{\lambda}$ , in other words, the  $(n-k)$ -plane  $C^\perp$  contains  $\tilde{\lambda}$ ; the second set of  $\delta$ -functions says  $C$  contains the 2-plane  $\lambda$ . Together these  $\delta$ -functions imply the orthogonality of 2-planes  $\lambda$  and  $\tilde{\lambda}$ ,



which is precisely the statement of momentum conservation in the  $n$ -dimensional (particle) space.

$$\delta^4(P) \equiv \delta^{2 \times 2}(\lambda \cdot \tilde{\lambda}). \quad (4.2.43)$$

---

<sup>2</sup>All integrals are to be evaluated as contour integrals, i.e.

$$\int \frac{dx}{x} \delta(x - x_0) = \frac{1}{x_0}. \quad (4.2.39)$$

Furthermore, with  $\lambda \subset C$ , the Grassmann  $\delta$ -functions in (4.2.40) impose the super-momentum conservation (along with additional constraints on  $\tilde{\eta}$  for  $k > 2$ )

$$\delta^{2\mathcal{N}}(Q) \equiv \delta^{2 \times \mathcal{N}}(\lambda \cdot \tilde{\eta}) \quad (4.2.44)$$

Out of the  $2n$  bosonic  $\delta$ -functions,  $(2n - 4)$  constraints are available for localizing the integral. We can always use part of the  $\delta(C^\perp \cdot \lambda)$  constraints to fix the first two rows of the  $C$ -matrix to  $\lambda$ ,

$$C = \begin{pmatrix} \lambda_1^{(1)} & \lambda_2^{(1)} & \lambda_3^{(1)} & \dots & \lambda_n^{(1)} \\ \lambda_1^{(2)} & \lambda_2^{(2)} & \lambda_3^{(2)} & \dots & \lambda_n^{(2)} \\ * & * & * & \dots & * \end{pmatrix} \cdot = \begin{pmatrix} \lambda \\ C^* \end{pmatrix} \quad (4.2.45)$$

then factor out the momentum and super-momentum conserving explicitly from the remaining  $\delta$ -functions,

$$\delta^{k \times 2}(C \cdot \tilde{\lambda}) \delta^{k \times \mathcal{N}}(C \cdot \tilde{\eta}) = \delta^4(P) \delta^{2\mathcal{N}}(Q) \times \delta^{(k-2) \times 2}(C^* \cdot \tilde{\lambda}) \delta^{(k-2) \times \mathcal{N}}(C^* \cdot \tilde{\eta}). \quad (4.2.46)$$

The residual constraints only involving  $(k-2) \times n$  matrix  $C^*$ . Depending on the dimensionality of the Grassmannian cell, the full integral will evaluate to one the following

- if  $m = 2n - 4$ : ordinary superfunctions. All degrees of freedom of the  $C$ -matrix are precisely fixed by the  $\delta$ -function constraints. This is exactly the case of on-shell diagrams that appear in the BCFW recursion relations, and in general all leading singularities fall into this category.
- if  $m > 2n - 4$ : differential forms with unfixed parameters. The remaining degrees of freedom can be interpreted as components of loop momenta  $\ell_i$  not determined by cuts.
- if  $m < 2n - 4$ : singular limits of superfunctions, where the external kinematics are subject to additional constraints

Let us go back to our example of on-shell diagram (4.2.10). In  $\mathcal{N} = 4$  sYM this diagram evaluates to

$$\mathcal{F}_{2,k=5} = \frac{1}{J} \prod_j A_{3pt} = \int \Omega_{5,k=2} \delta^{2 \times 2}(C \cdot \tilde{\lambda}) \delta^{3 \times 2}(C^\perp \cdot \lambda) \delta^{2 \times 4}(C \cdot \tilde{\eta}) \quad (4.2.47)$$

The  $C$ -matrix is a 2-plane in 5-dimensions which must contain another 2-plane  $\lambda$ . We can set  $C = \lambda$  trivially. The other two  $\delta$ -functions reproduce momentum and supermomentum conservation and we get as expected

$$\mathcal{F}_{2,k=5} = \frac{\delta^{2 \times 2}(\lambda \cdot \tilde{\lambda}) \delta^{2 \times 4}(\lambda \cdot \tilde{\eta})}{\langle 12 \rangle \langle 23 \rangle \langle 34 \rangle \langle 45 \rangle \langle 51 \rangle} \quad (4.2.48)$$

Note that if we were to use the edge variables provided by the plabic graph, we would not get the solution in the form of  $C = \lambda$ . Instead we would find, for instance,

$$C = \begin{pmatrix} 1 & 0 & \frac{\langle 14 \rangle}{\langle 12 \rangle} & \frac{\langle 15 \rangle}{\langle 12 \rangle} & \cdots & \frac{\langle 1n \rangle}{\langle 12 \rangle} \\ 0 & 1 & \frac{\langle 24 \rangle}{\langle 21 \rangle} & \frac{\langle 25 \rangle}{\langle 21 \rangle} & \cdots & \frac{\langle 2n \rangle}{\langle 21 \rangle} \end{pmatrix} \quad (4.2.49)$$

this is related to  $C = \lambda$  by a  $GL(2)$  transformation. The two matrices represents the same point in the Grassmannian, only parameterized with different gauge-fixing schemes. The expression (4.2.47) obviously does not depend on the choice of the  $GL(2)$  fixing and we always get the same result.

#### 4.2.5 Cells for NMHV Tree-level Amplitudes

Now we turn our attention to NMHV tree-level amplitudes, which will be our main focus throughout this chapter. The Grassmannian cells appearing in the BCFW construction of tree amplitudes are always  $(2n - 4)$ -dimensional. Since in the NMHV case, the top cell of  $G_+(3, n)$  has the dimensionality  $3n - 9$ , the relevant cells for the amplitude must be of co-dimension  $n - 5$ . In other words, they are obtained from the top cell by imposing  $n - 5$  constraints (on consecutive minors).

The 5-point case is trivial. The BCFW representation contains only a single term, which is a parity conjugate of the 5-pt MHV amplitude. There is no constraint to be imposed – the single BCFW term directly corresponds to the top cell of  $G(3, 5)$  and

the generic convex configuration of five points in  $\mathbb{P}^2$ . The first interesting case appear at 6-point where the BCFW representation of the amplitude, using the (61) shift for instance, consists of three on-shell diagrams (4.2.15). Each diagram represents an 8-dimensional configuration in  $G_+(3, 6)$  with one constraint impose on a configuration of six points in  $\mathbb{P}^2$ ,

$$(4.2.50)$$

The first term has minor  $(123) = 0$  as reflected by points 1, 2 and 3 lying on the same line in the picture. Solving the  $\delta$ -function constraints we get the form of the  $C$ -matrix,

$$C = \begin{pmatrix} \lambda_1^{(1)} & \lambda_2^{(1)} & \lambda_3^{(1)} & \lambda_4^{(1)} & \lambda_5^{(1)} & \lambda_6^{(1)} \\ \lambda_1^{(2)} & \lambda_2^{(2)} & \lambda_3^{(2)} & \lambda_4^{(2)} & \lambda_5^{(2)} & \lambda_6^{(2)} \\ 0 & 0 & 0 & [56] & [64] & [45] \end{pmatrix}, \quad (4.2.51)$$

The superfunction (4.2.40) then takes a particularly simple form,

$$\mathcal{R}_1 = \frac{\delta^4(P)\delta^8(Q)\delta^4([56]\tilde{\eta}_4 + [64]\tilde{\eta}_5 + [45]\tilde{\eta}_6)}{s_{123}\langle 12\rangle\langle 23\rangle[45][56]\langle 1|23|4\rangle\langle 3|45|6\rangle}, \quad (4.2.52)$$

where we denoted  $\langle 1|23|4\rangle \equiv \langle 12\rangle[24] + \langle 13\rangle[34]$ . All other expressions are related by cyclic shifts  $\mathcal{R}_1 \rightarrow \mathcal{R}_{i+1}$  where we just relabel  $k \rightarrow k + i$ . The 6-point tree-level amplitude is then given by

$$\mathcal{A}_6^{(3)} = \mathcal{R}_1 + \mathcal{R}_3 + \mathcal{R}_5. \quad (4.2.53)$$

If we perform the BCFW recursion relation with the shift (12), we get a different set of on-shell diagrams. They are constructed in the same way, but the BCFW bridge attached is now (12), rather than  $(n1)$ . The set of three Grassmannian configurations

is following,

$$(4.2.54)$$

The superfunction for each configuration can be again obtained from  $\mathcal{R}_1$  by a cyclic shift,

$$\mathcal{A}_6^{(3)} = \mathcal{R}_2 + \mathcal{R}_4 + \mathcal{R}_6. \quad (4.2.55)$$

The equality of (4.2.53) and (4.2.55) is guaranteed by the Global Residue Theorem (GRT) for the superfunction associated with the top cell of  $G_+(3, 6)$  (which has an extra parameter  $z$  and vanishes for  $z \rightarrow \infty$ ).

Going to higher points BCFW recursion expands the amplitude as a sum of two types of on-shell diagrams:

$$(4.2.56)$$

The first type of on-shell diagrams corresponds to the factorizations of the NMHV amplitude into two MHV amplitudes; each MHV blob corresponds to a single on-shell diagram; gluing them with the BCFW bridge makes an NMHV on-shell diagram. It is not hard to see every diagram thus constructed corresponds to a Grassmannian

configuration where all  $n$  points are localizes on three lines:

$$(4.2.57)$$

This is indeed  $2n - 4$  dimensional configuration whose  $C$ -matrix has vanishing minors:

$$(123) = (234) = \dots = (i-2 \ i-1 \ i) = (i+1 \ i+2 \ i+3) = \dots = (n-3 \ n-2 \ n-1) = 0 \quad (4.2.58)$$

while all other minors  $(ijk) > 0$ . Note that none of the points are merged with another or removed with these constraints.

The second term in (4.2.56) corresponds to a *sum* of on-shell diagrams which arise from the factorization of the amplitude into a  $(n-1)$ -pt NMHV and a 3-point  $\overline{\text{MHV}}$  amplitude. It can also be interpreted as adding particle  $n$  to the  $(n-1)$ -pt NMHV amplitude via an  $k$ -preserving inverse-soft factor. Suppose we have found the diagrammatic expansion of the  $(n-1)$ -point NMHV amplitude via recursion (4.2.56), then adding the inverse-soft factor corresponds to adding point  $n$  between  $n-1$  and  $1$  for every Grassmannian configuration underlying the  $(n-1)$ -point NMHV amplitude, which involve  $n-1$  points distributed on three lines with special point  $1$  on the intersection of two lines

$$(4.2.59)$$



The resulting configurations have points  $n$  and  $n-1$  on the same line. They complement the first set of on-shell diagrams (4.2.57) where point  $n-1$  is on a different line than point  $n$ .

Indeed if we consistently use the same shift on the lower-point NMHV amplitudes (e.g. for the subamplitude  $A(I, \hat{1}, 2, 3, \dots, i)$  on the factorization channel we use (I1) shift in the recursion), we obtain a closed-form solution for general  $n$ -point NMHV amplitudes as a sum over a special set of configurations

$$\mathcal{A}_n^{\text{NMHV}} = \sum_{i,j} \text{Diagram} \quad (4.2.60)$$

where all  $n$  points are localized on three lines and each line has at least two points on it. Each configuration is characterized by 3 labels: the first label 1 (as 1 in the  $(n1)$  shift used above) specifying the “center” of the configuration, the other two labels  $i$  and  $j$  specifying the “boundary”, where  $i \geq 2$ ,  $i+2 \leq j \leq n-1$  ensures that at least two points are on each line. The Grassmannian cell (and also the permutation) can be easily read off from the configuration:

$$\begin{aligned} (123) &= (234) = \dots = (i-2 \ i-1 \ i) = (i+1 \ i+2 \ i+3) = \dots (j-2 \ j-1 \ j) = \\ &= (j+1 \ j+2 \ j+3) = \dots (n-1 \ n \ 1) = 0 \quad \text{while all others } (ijk) > 0 \end{aligned} \quad (4.2.61)$$

The corresponding superfunction  $\mathcal{F}$  is

$$\mathcal{R}_{1,i+1,j+1} = \text{Diagram} = \frac{\delta^4(P)\delta^8(Q)}{\langle 12 \rangle \langle 23 \rangle \dots \langle n1 \rangle} \times R[1, i, i+1, j, j+1], \quad (4.2.62)$$

where we have used the first points on each line in the general configuration (4.2.60) to label the expression. We also introduce the R-invariant in the momentum twistor space

$$R[a, b, c, d, e] = \frac{(\eta_a \langle bcde \rangle + \eta_b \langle cdea \rangle + \eta_c \langle deab \rangle + \eta_d \langle eabc \rangle + \eta_e \langle abcd \rangle)^4}{\langle abcd \rangle \langle bcde \rangle \langle cdea \rangle \langle deab \rangle \langle eabc \rangle}, \quad (4.2.63)$$

where  $\eta_k$  are the momentum twistor Grassmann variables [43, 44]. This representation makes both the superconformal and the dual superconformal symmetries (and hence the Yangian symmetry) manifest. For our purpose, we rewrite the  $R$ -invariant in the momentum space,

$$R[1, i, i+1, j, j+1] = \frac{\langle i i+1 \rangle \langle j j+1 \rangle \cdot \delta^4(\Xi_{1, i+1, j+1})}{P_2^2 \langle 1 | P_1 P_2 | j \rangle \langle 1 | P_1 P_2 | j+1 \rangle \langle 1 | P_3 P_2 | i \rangle \langle 1 | P_3 P_2 | i+1 \rangle}, \quad (4.2.64)$$

where we denoted

$$P_1 = p_2 + \dots + p_i, \quad P_2 = p_{i+1} + \dots + p_j, \quad P_3 = p_{j+1} + \dots + p_n, \quad (4.2.65)$$

such that  $P_1 + P_2 + P_3 + p_1 = 0$ . Pictorially  $P_1, P_2, P_3$  are the collections of points on each of the three lines:

(4.2.66)

The argument of the super delta function  $\delta^4(\Xi_{1, i+1, j+1})$  is given by

$$\Xi_{1, i+1, j+1} \equiv \sum_{k \in P_2} \langle k | P_2 P_3 | 1 \rangle \tilde{\eta}_k + \sum_{j \in P_3} P_2^2 \langle 1 j \rangle \tilde{\eta}_j. \quad (4.2.67)$$

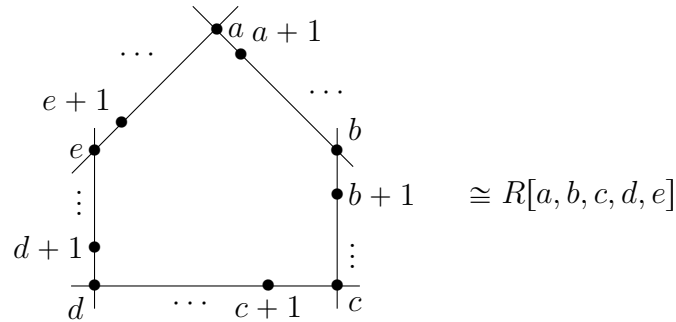
Note that this formula does not depend on the ordering in sets  $P_1, P_2$  and  $P_3$  on the respective lines. This will be very important in the next section when we discuss non-adjacent BCFW recursion. As might be evident, the expression (4.2.67) only depends

on Grassmann variables  $\tilde{\eta}$ s from lines  $P_2$  and  $P_3$ . Thus we can use super-momentum conservation to rewrite it in an equivalent form when  $P_1 \leftrightarrow P_3$  (reflection of the picture),

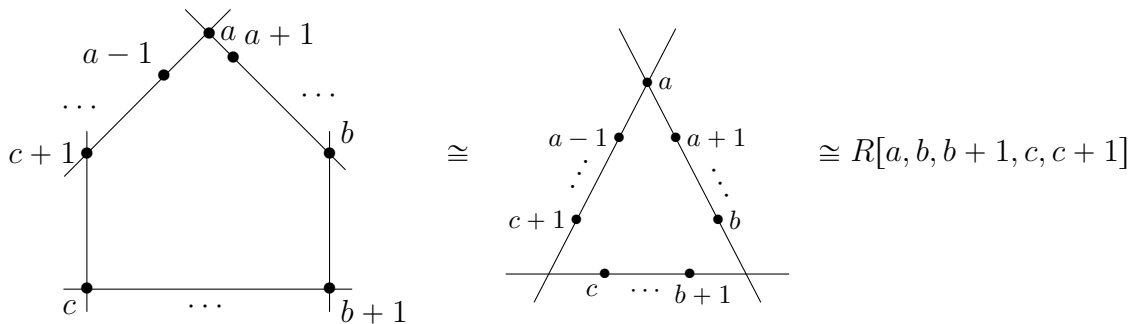
$$\Xi_{1,i+1,j+1} \equiv \sum_{k \in P_2} \langle k | P_2 P_1 | 1 \rangle \tilde{\eta}_k + \sum_{j \in P_1} P_2^2 \langle 1 j \rangle \tilde{\eta}_j. \quad (4.2.68)$$

The set of all BCFW terms generated by adjacent shifts is a subset of all *planar* on-shell diagrams of dimensionality  $2n - 4$  (which are leading singularities). For a general leading singularity, the  $(2n - 4)$ -dimensional cell in  $G_+(3, n)$  corresponds to a configuration of  $n$  points in  $\mathbb{P}^2$  located on five lines,

$$(4.2.69)$$



Any term which appears in the context of adjacent BCFW recursion is a special case, where two of the lines have exactly two points and we get the configuration discussed earlier,



$$(4.2.70)$$

**Recap:** Let us close the section with a summary of a few important points in the discussion

- Each BCFW term is a sum of on-shell diagrams.
- Each on-shell diagram corresponds to a  $2n-4$  dimensional cell in  $G_+(k, n)$  with a super-function that can be calculated using (4.2.40).
- Each cell in  $G_+(k, n)$  is characterized by a configuration of  $n$  points in  $\mathbb{P}^{k-1}$  with only consecutive constraints.
- For MHV,  $k = 2$ , the amplitude is given by the top cell of  $G_+(2, n)$  which describes  $n$  ordered points on a projective line  $\mathbb{P}^1$ , and the superfunction reproduces a famous Parke-Taylor formula.
- For NMHV,  $k = 3$ , the amplitude is given by a collection of co-dimension  $(n-5)$  cells in  $G_+(3, n)$ . These cells describe configurations of  $n$  points in  $\mathbb{P}^2$  localized on three lines and the superfunctions are the  $R$ -invariants with special labels.

It is worth repeating that having the Grassmannian configurations, we can easily reconstruct the  $C$ -matrix and calculate the associated superfunction (4.2.40). Therefore, we focus mainly on these geometries here.

### 4.3 Holomorphic expressions for BCFW terms

The  $\delta$ -functions constraints in (4.2.40) provide a map between the Grassmannian space and the kinematic space through  $C \cdot \tilde{\lambda} = C^\perp \cdot \lambda = 0$ . In this section we will recast the Grassmannian geometries of  $C$ -matrices in the space of  $\lambda$  (we refer to it as holomorphic space). We will see that the interpretation of the geometry in the kinematic space lead to new, intuitive representations of BCFW terms.

As a trivial example of the  $\lambda$ -geometry, consider the case of  $k = 2$  MHV geometry. In this case  $C = \lambda$  we identify the  $C$ -matrix with the 2-plane spanned by  $\lambda$ , and the positive Grassmannian geometry can be directly interpreted as the  $\lambda$ -geometry, that is,  $\vec{P}_k = \lambda_k$  – the column vector  $\vec{P}_k$  for each point on the projective line  $\mathbb{P}^1$  is equal to the

kinematic variable  $\lambda$ .

$$\begin{array}{ccc}
 \begin{array}{c} \bullet \\ \bullet \\ \bullet \\ \dots \\ \bullet \\ 12 \end{array} & & \begin{array}{c} \bullet \\ \bullet \\ \bullet \\ \dots \\ \bullet \\ 1 \end{array} \\
 \begin{array}{c} \bullet \\ \bullet \\ \bullet \\ \dots \\ \bullet \\ 3 \end{array} & & \begin{array}{c} \bullet \\ \bullet \\ \bullet \\ \dots \\ \bullet \\ 3 \end{array} \\
 \begin{array}{c} \bullet \\ \bullet \\ \bullet \\ \dots \\ \bullet \\ 4 \end{array} & & \begin{array}{c} \bullet \\ \bullet \\ \bullet \\ \dots \\ \bullet \\ 4 \end{array} \\
 \dots & & \dots \\
 \begin{array}{c} \bullet \\ \bullet \\ \bullet \\ \dots \\ \bullet \\ n \end{array} & & \begin{array}{c} \bullet \\ \bullet \\ \bullet \\ \dots \\ \bullet \\ n \end{array} \\
 (12) = \langle 12 \rangle = 0 & & \lambda_2 \rightarrow 0 \\
 \lambda_2 = \alpha \lambda_1 & & \\
 & & (4.3.1)
 \end{array}$$

Merging points 1 and 2 sets the minor  $(12) = 0$  and this is the same as  $\langle 12 \rangle \rightarrow 0$ . Removing the point 2 from the picture corresponds to sending  $\lambda_2 \rightarrow 0$  and so on.

For  $k > 2$  the connection between the  $C$ -matrix and kinematical constraints on  $\lambda$ ,  $\tilde{\lambda}$  is not straightforward. We need to solve the conditions  $C \cdot \tilde{\lambda} = C^\perp \cdot \lambda = 0$ , express the  $C$  matrix using  $\lambda$ ,  $\tilde{\lambda}$  and evaluate minors of the  $C$  matrix. Let us look at a 6-pt NMHV configuration associated with discussed earlier:

$$\begin{array}{ccc}
 & \bullet & \\
 & 1 & \\
 & \bullet & \\
 \bullet & & \bullet \\
 6 & & 2 \\
 & & \bullet \\
 & & 3 \\
 & \bullet & \bullet \\
 & 5 & 4 \\
 & & \\
 & & (4.3.2)
 \end{array}$$

This is a 8-dimensional cell with  $(123) = 0$ . Solving for  $C$  from the delta functions we get explicit form (4.2.51). We can evaluate remaining minors:

$$(234) = \langle 23 \rangle [56], \quad (345) = \langle 3 | 45 | 6 \rangle, \quad (456) = s_{123}, \quad (561) = \langle 1 | 23 | 4 \rangle, \quad (612) = \langle 12 \rangle [45]$$

Let us look at  $(234) = 0$ , which has two solutions (4.2.27): 1, 2, 3, 4 on the same line or merging points 2, 3. While the first one sends  $[56] = 0$ , the latter corresponds to  $\langle 23 \rangle = 0$ . Similarly,  $(612) = 0$  puts points 6, 1, 2, 3 on a line ( $[45] = 0$ ) or merges 1, 2 ( $\langle 12 \rangle = 0$ ). We can see that merging points on the 1, 2, 3 line gives  $\langle 12 \rangle = 0$  or  $\langle 23 \rangle = 0$  which resembles the  $C = \lambda$  correspondence for the  $k = 2$  geometry. The other boundaries are more complicated and there is no obvious pattern in these singularities. For instance, putting 3, 4, 5 on a line by  $(345) = 0$  sends  $\langle 3 | 45 | 6 \rangle = 0$  which is hard to

interpret. Furthermore the poles are no longer holomorphic  $\langle ab \rangle = 0$  like in the MHV case, ie. they generally depend on both  $\lambda$  and  $\tilde{\lambda}$ .

Nevertheless, our intention is to make a direct connection between the Grassmannian geometry and the kinematical space. The motivation comes from the analysis of the BCFW term (4.2.57), which originates as the product of two MHV amplitudes,

$$\begin{array}{c} \hat{n} \\ \diagdown \\ (2) \\ \diagup \\ n-1 \end{array} \text{ --- } \overset{I}{(2)} \begin{array}{c} \diagup \\ (2) \\ \diagdown \\ \hat{1} \end{array} \text{ --- } 2 \\ \begin{array}{c} \vdots \\ | \\ i+1 \\ \vdots \end{array} \quad \begin{array}{c} | \\ i \\ \vdots \end{array}$$

$$= A_{k=2}^{\text{tree}}(i+1, i+2, \dots, n-1, \hat{n}, I) \times \frac{1}{(P_2 + p_n)^2} \times A_{k=2}^{\text{tree}}(I, \hat{1}, 2, \dots, i-1, i). \tag{4.3.3}$$

Here we denote  $P_1 = p_2 + \dots + p_i$  and we also define  $P_2 = p_{i+1} + \dots + p_{n-1}$ . Momentum conservation implies  $P_1 + P_2 + p_1 + p_n = 0$ . The BCFW shift parameter is fixed to

$$z = \frac{(P_1 + p_1)^2}{\langle 1|P_1|n \rangle}, \tag{4.3.4}$$

and the shifted spinors  $\lambda_{\hat{n}}$ ,  $\tilde{\lambda}_{\hat{1}}$  and internal momentum  $p_I$  are given by

$$\lambda_{\hat{n}} = \frac{\langle 1|P_1 P_2}{\langle 1|P_1|n \rangle}, \quad \tilde{\lambda}_{\hat{1}} = \frac{P_1 P_2 |n]}{\langle 1|P_1|n \rangle}, \quad p_I = \frac{1}{\langle 1|P_1|n \rangle} (P_2 |n]) (\langle 1|P_1). \tag{4.3.5}$$

In this notation the spinor  $\langle 1|P_1 P_2$  is equal to

$$\langle 1|P_1 P_2 = \sum_{i \in P_1} \sum_{j \in P_2} \langle 1i \rangle [ij] \lambda_j \tag{4.3.6}$$

Note that the division of  $p_I$  into  $\lambda_I$  and  $\tilde{\lambda}_I$  is ambiguous. We see that the BCFW term (4.3.3) is the product of two MHV amplitudes with an additional pole  $\frac{1}{(P_2 + p_n)^2}$ .

Therefore, we can modify the Grassmannian configuration for (4.2.57) as

$$\mathcal{R}_{1,i+1,n} = \begin{array}{c} \begin{array}{c} \diagup \quad \diagdown \\ \bullet 1 \\ \diagdown \quad \diagup \\ \bullet n \quad \bullet 2 \\ \vdots \quad \vdots \\ \bullet \dots \quad \bullet i \\ \vdots \quad \vdots \\ \bullet \hat{n} \quad \bullet I \\ \diagdown \quad \diagup \\ \bullet n \quad \bullet 1 \dots i + 1 \\ \vdots \quad \vdots \\ \bullet \hat{n} \quad \bullet n \quad \bullet 1 \end{array} \\ \underbrace{\hspace{10em}}_{P_2} \end{array} \quad (4.3.7)$$

where we added two extra points  $\hat{n}$  and  $I$  in the picture. Note these points originate as certain special momenta  $p_{\hat{n}}$  and  $p_I$  but now we associate them with points in the Grassmannian geometry.

Let us take a closer look at the geometry: we have now points  $1, 2, \dots, i, I$  on the first line, points  $I, i+1, \dots, n-1, \hat{n}$  on the second line and points  $\hat{n}, n, 1$  on the third line. It is obvious that the two MHV amplitudes in (4.3.3) correspond to configurations of points on the first two lines in (4.3.7), but it is not that clear what to do with the third line and  $1/(P_2 + p_n)^2$  pole. Let us make the connection precise now.

We start with the expression for the  $\mathcal{R}_{1,i+1,j+1}$  and rewrite it as

$$\begin{aligned} \mathcal{R}_{1,i+1,n} &= \frac{\tilde{\Delta}_{1,i+1,n}}{\langle 12 \rangle \dots \langle i-1 \ i \rangle \langle i+1 \ i+2 \rangle \dots \langle n-2 \ n-1 \rangle \langle i | P_2 | n \rangle \langle i+1 | P_2 | n \rangle \langle n-1 | P_2 P_1 | 1 \rangle (P_2 + p_n)^2 P_2^2}, \end{aligned} \quad (4.3.8)$$

where

$$\tilde{\Delta}_{1,i+1,n} = \delta^4(P) \delta^8(Q) \delta^4(\tilde{\Xi}_{1,i+1,n}), \quad (4.3.9)$$

and the reduced argument of the delta function is

$$\tilde{\Xi}_{1,i+1,n} = \sum_{k \in P_2} \langle k | P_2 | n \rangle \tilde{\eta}_k + P_2^2 \tilde{\eta}_n = \frac{1}{\langle 1n \rangle} \Xi_{1,i+1,n}. \quad (4.3.10)$$

Looking at the denominator we can now clearly identify Parke-Taylor factors for MHV amplitudes on two of the lines which now also involve points  $\hat{n}$  and  $I$ ,

$$PT(1, 2, \dots, i-1, i, I) \times PT(i+1, i+2, \dots, \hat{n}, I) \quad (4.3.11)$$

where the Parke-Taylor factors are defined as usual,

$$PT(a_1, a_2, \dots, a_m) = \frac{1}{\langle a_1 a_2 \rangle \langle a_2 a_3 \rangle \dots \langle a_m a_1 \rangle}. \quad (4.3.12)$$

Note that all the mixed poles come from *holomorphic* poles involving  $\lambda_I$  and  $\lambda_{\hat{n}}$ ,

$$\langle i I \rangle \doteq \langle i | P_2 | n \rangle, \quad \langle i+1 I \rangle \doteq \langle i+1 | P_2 | n \rangle, \quad \langle n-1 \hat{n} \rangle \doteq \langle n-1 | P_2 P_1 | 1 \rangle, \quad \langle \hat{n} I \rangle \doteq P_2^2 \quad (4.3.13)$$

We have ignored any factor of  $\langle 1 | P_1 | n \rangle = -\langle 1 | P_2 | n \rangle$  to some power in the above equation; as noted before, the splitting  $p_I$  into  $\lambda_I$  and  $\tilde{\lambda}_I$  is ambiguous which produces some particular power of  $\langle 1 | P_1 | n \rangle = -\langle 1 | P_2 | n \rangle$  from the Jacobian. This will be accounted for in the end. Furthermore, there is a factor  $1/(P_2 + p_n)^2$  which does not originate from either of the Parke-Taylor factors, but can be interpreted as

$$\langle n \hat{n} \rangle = \langle 1 | P_1 P_2 | n \rangle = (P_2 + p_n)^2 \langle 1 n \rangle. \quad (4.3.14)$$

In fact, noticing that  $\langle 1 \hat{n} \rangle = \langle 1 n \rangle \langle 1 | P_1 | n \rangle$ , we can easily check all the remaining factors conspire to make another Parke-Taylor factor for the MHV amplitude living on the third line with points  $1, n, \hat{n}$ :

$$\frac{1}{\langle 1 n \rangle \langle n \hat{n} \rangle \langle \hat{n} 1 \rangle}. \quad (4.3.15)$$

Taking everything together we conclude that the  $\mathcal{R}_{1,i+1,n}$  can be rewritten as the product of three Parke-Taylor factors living on the three lines that form the Grassmannian geometry

$$\mathcal{R}_{1,i+1,n} = PT(1, \dots, i, I_1) PT(I_1, i+1, \dots, n-1, I_2) PT(I_2, n, 1) \times \langle 1 | P_1 p_n | 1 \rangle^3 \tilde{\Delta}_{1,i+1,n}, \quad (4.3.16)$$

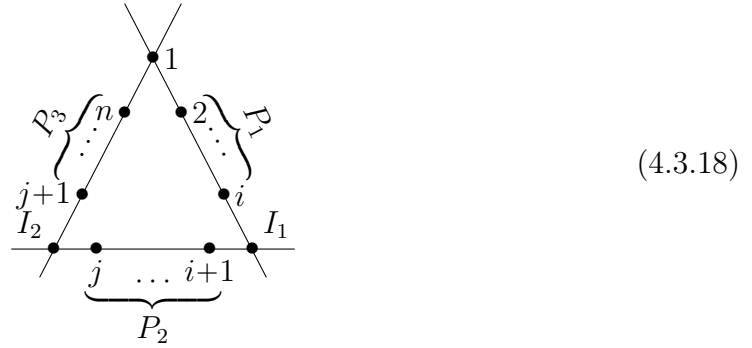


where we have introduced two points  $I_1, I_2$ , instead of  $I, \hat{n}$ , with fixed form for their  $\lambda$ -spinors,

$$\lambda_{I_1} = P_2|n], \quad \lambda_{I_2} = \langle 1|P_1P_2. \quad (4.3.17)$$

Note that in the formula (4.3.16) we have a product of three Parke-Taylor factors, rather than the full MHV amplitudes. So far we have merely rewritten  $\mathcal{R}_{1,i+1,n}$  in a particular way. But, importantly, there is a clear pattern in the formula (4.3.16) that immediately generalize to the more general R-invariants  $\mathcal{R}_{1,i+1,j+1}$ , for which the interpretation using BCFW shifts is absent.

In the general configuration we have  $n$  points living on all three lines,



and  $\mathcal{R}_{1,i+1,j+1}$  is given by the product of Parke-Taylor factor on three lines, with labels indicated in the picture,

$$\begin{aligned} \mathcal{R}_{1,i+1,j+1} = & PT(1, \dots, i, I_1) PT(I_1, i+1, \dots, j, I_2) PT(I_2, j+1, \dots, n, 1) \\ & \times \langle 1|P_1P_3|1\rangle^3 \Delta_{1,i+1,j+1} \end{aligned} \quad (4.3.19)$$

where  $P_1 = p_2 + \dots + p_i$ ,  $P_2 = p_{i+1} + \dots + p_j$  and  $P_3 = p_{j+1} + \dots + p_n$ . The auxiliary spinors  $\lambda_{I_1}, \lambda_{I_2}$  are given by

$$\lambda_{I_1} = \langle 1|P_3P_2, \quad \lambda_{I_2} = \langle 1|P_1P_2 \quad (4.3.20)$$

and  $\Delta_{1,i+1,j+1}$  is just given by the delta functions in (4.2.62),

$$\Delta_{1,i+1,j+1} = \delta^4(P) \delta^8(Q) \delta^4(\Xi_{1,i+1,j+1}) \quad (4.3.21)$$

Our expression (4.3.19) reproduces (4.2.62). The salient feature of the new formula is that all mixed poles in  $\mathcal{R}_{1,i+1,j+1}$  appear as simple holomorphic poles involving  $\lambda_{I_1}$  and  $\lambda_{I_2}$ . The introduction of points  $I_1, I_2$  prime the original configuration of  $n$  points in Grassmannian cell  $G_+(3, n)$  for a kinematical interpretation. Merging two points, which corresponds to sending certain consecutive minor of the  $C$ -matrix to zero, turns into statement about  $\langle ab \rangle = 0$ , ie.  $\lambda_a \sim \lambda_b$  for two points  $a, b$  on one of the three lines with points  $1, 2, \dots, i, I_1$  and  $I_1, i+1, \dots, j, I_2$  and  $I_2, j+1, \dots, n, 1$ . This is trivially true for the points  $1, \dots, n$  but quite remarkably this also extends to all merging involving points  $I_1$  and  $I_2$  which lead to more complicated non-holomorphic poles,

$$\langle ab \rangle = 0 \qquad \langle I_2 j \rangle = \langle 1 | P_1 P_2 | j \rangle = 0 \qquad (4.3.22)$$

As an example, let us look at the 8-point configuration  $\mathcal{R}_{1,4,7}$ .

$$(4.3.23)$$

Following the above procedure we can build the superfunction from three Parke-Taylor factors

$$\mathcal{R}_{1,4,7} = PT(1, 2, 3, I_1) PT(I_1, 4, 5, 6, I_2) PT(I_2, 7, 8, 1) \cdot \langle 1 | (23)(78) | 1 \rangle^3 \Delta_{1,4,7} \qquad (4.3.24)$$

$$= \frac{\Delta_{1,4,7}}{\langle 12 \rangle \langle 23 \rangle \langle 3|(456)(78)|1 \rangle \langle 1|(78)(56)|4 \rangle \langle 45 \rangle \langle 56 \rangle \langle 1|(23)(45)|6 \rangle s_{456} \langle 1|(23)(456)|7 \rangle \langle 78 \rangle \langle 81 \rangle}$$

with

$$\lambda_{I_1} = \langle 1|(78)(456), \quad \lambda_{I_2} = \langle 1|(23)(456). \quad (4.3.25)$$

As a side note, while all we need is the  $\lambda$ -part of  $I_1, I_2$  in the context of Yang-Mills theory, for the purpose of extending the same positive geometry picture to other theories we may try to upgrade them to full momenta. To do this, we have to ensure that momentum conservation is respected on each of the three lines. First, we can determine the  $\tilde{\lambda}$ s for  $I_1$  and  $I_2$  uniquely from the momentum conservation,

$$\tilde{\lambda}_{I_1} = \frac{\langle 1|P_1}{\langle 1|P_1 P_3|1 \rangle}, \quad \tilde{\lambda}_{I_2} = \frac{\langle 1|P_3}{\langle 1|P_3 P_1|1 \rangle}, \quad (4.3.26)$$

where we can again see the normalization factor  $\langle 1|P_1 P_3|1 \rangle$ . In this case we get a momentum conservation  $p_{I_1} + p_{I_2} + p_{i+1} + \dots + p_j = 0$ . On the other two lines, momentum  $p_1$  is split into two parts  $p_1 = p_1^a + p_1^b$ , where both momenta share the same  $\lambda_1$  but differ in  $\tilde{\lambda}$  parts such that momentum conservation  $-p_{I_2} + P_3 + p_1^a = 0$  and  $-p_{I_1} + P_1 + p_1^b = 0$  is respected.

#### 4.4 Non-adjacent BCFW recursion and non-planar positive geometry

The main goal of this chapter is to explore the space of non-planar on-shell diagrams that arise in BCFW recursion relations with non-adjacent shifts in the context of  $\mathcal{N} = 4$  sYM. We consider a non-adjacent BCFW shift  $(k1)$ ,

$$\lambda_{\hat{k}} = \lambda_k + z\lambda_1, \quad \tilde{\lambda}_{\hat{1}} = \tilde{\lambda}_1 - z\tilde{\lambda}_k, \quad \tilde{\eta}_{\hat{1}} = \tilde{\eta}_1 + z\eta_k \quad (4.4.1)$$

which gives rise to an expansion of tree-level amplitudes in terms of building blocks that are superconformal invariant.

$$A_n^{(k)} = \sum_{i,j} \hat{k} \begin{array}{c} i \\ \vdots \\ \circ \\ \vdots \\ j+1 \end{array} \text{---} \begin{array}{c} i+1 \\ \vdots \\ \circ \\ \vdots \\ j \end{array} \hat{1} \quad (4.4.2)$$

However, for general  $k$ , the dual super conformal invariance of the  $\mathcal{N} = 4$  sYM amplitude is broken in the individual terms as the cyclic ordering of points is spoiled. Nonetheless, we can still represent these terms by *non-planar on-shell diagrams*

$$(4.4.3)$$

where each blob can recursively be expressed in terms of trivalent planar graphs. For example, one of the non-planar on-shell diagrams in the BCFW expansion of 6pt NMHV amplitude using (51) shift is

$$(4.4.4)$$

While on-shell diagrams that are planar correspond to cells in the positive Grassmannian  $G_+(k, n)$ , an arbitrary non-planar diagram corresponds to a certain cell in (the non-positive part of)  $G(k, n)$ . Specifically, for each non-planar on-shell diagram we can construct the  $C$ -matrix via the boundary measurement. The rules are the same as in the planar case: label the edge variables (here face variables can not be used), choose a perfect orientation and calculate the entries of the  $C$ -matrix. For the example above we get

$$C = \begin{pmatrix} 1 & 0 & 0 & -\alpha_2\alpha_5\alpha_6\alpha_7 & -\alpha_1 - \alpha_2\alpha_5\alpha_6\alpha_7\alpha_8 & -\alpha_2\alpha_7 \\ 0 & 1 & 0 & -(\alpha_2 + \alpha_3)\alpha_5\alpha_6 & -(\alpha_2 + \alpha_3)\alpha_5\alpha_6\alpha_8 & -\alpha_2 \\ 0 & 0 & 1 & -(\alpha_4 + \alpha_5) & -\alpha_5\alpha_8 & 0 \end{pmatrix} \quad (4.4.5)$$

This  $C$ -matrix does not have any obvious positivity properties, ie. there is no choice of signs for edge variables  $\alpha_i$  such that all main minors are positive.

The lack of positive coordinates does not prevent us from calculating the on-shell functions for the BCFW term (4.4.4) using the dual formulation (4.2.40) for the on-shell diagram (4.4.4), which gives the same result as direct evaluation of the product of two MHV amplitudes with  $1/P^2$  pole,

$$\mathcal{F} = \frac{A_4(3, 4, \hat{5}, I)A_4(I, 6, \hat{1}, 2)}{s_{345}} \quad (4.4.6)$$

where  $\lambda_{\hat{5}}$  and  $\tilde{\lambda}_{\hat{1}}$  being the shifted momenta and  $I$  the internal on-shell leg.

Unlike the planar case, where the cells have a simple combinatorial characterization and are understood to be associated with stratification of the positive Grassmannian, much remains to be understood about the connection between non planar on-shell diagrams and the Grassmannian in general. In what follows, we find the Grassmannian geometry for non-adjacent BCFW terms. In other words, we identify a particular subspace in  $G(k, n)$  associated with the non-planar on-shell diagrams which appear in the context of non-adjacent BCFW recursion relations. This is a generalization of the connection between on-shell diagrams/plabic graphs and the cells of the positive Grassmannian  $G_+(k, n)$  into the non-planar sector, at least for the special set of BCFW cells identified. We start with a review of the MHV case which was worked out in [102] before discussing the new results on the NMHV non-planar cells.

### 4.4.1 MHV amplitudes

It was shown in [102] that any non-planar MHV on-shell diagram evaluates to a linear combination of Parke-Taylor factors with coefficients +1. For instance:

$$\begin{aligned}
 &= PT(1, 2, 3, 4, 5, 6) + PT(1, 2, 4, 5, 6, 3) + PT(1, 4, 2, 5, 6, 3) \\
 &\quad + PT(1, 4, 5, 6, 2, 3) + PT(1, 4, 6, 2, 3, 5) + PT(1, 4, 6, 2, 5, 3) \\
 &\quad + PT(1, 6, 2, 3, 4, 5). \tag{4.4.7}
 \end{aligned}$$

This statement follows from the fact that the whole  $G(2, n)$  Grassmannian can be decomposed into positive Grassmannians  $G_+(2, n)$  with various orderings, and holds for arbitrary complicated MHV diagrams which are associated with a cell in  $G(2, n)$ .

This is obvious from the geometric picture. The real Grassmannian  $G(2, n)$  can be represented as a collection of  $n$  points on the projective line  $\mathbb{P}^1$  (with no restrictions). Obviously, any configuration of these points has a certain ordering, so any point in  $G(2, n)$  is also in one of the positive Grassmannians  $G_+(2, n)$  (with a particular ordering). An arbitrary non-planar on-shell diagram then corresponds to a union of  $G_+(2, n)$  with different orderings.

The non-adjacent BCFW recursion relations produce a special class of non-planar on-shell diagrams. We expect this class to be particularly simple because in the recursion we have only one type of factorization diagram into  $(n-1)$ -point MHV amplitude and 3-point  $\overline{\text{MHV}}$  amplitude (the latter necessarily involve leg 3 instead of 1).

Let us start our discussion with the (31) shift. At 4-point there are two contributing

terms:

$$A_4 = \begin{array}{c} \hat{3} \\ \diagdown \\ \textcircled{1} \\ \diagup \\ 2 \end{array} \text{---} I \text{---} \begin{array}{c} 4 \\ \diagup \\ \textcircled{2} \\ \diagdown \\ \hat{1} \end{array} + \begin{array}{c} 4 \\ \diagdown \\ \textcircled{1} \\ \diagup \\ \hat{3} \end{array} \text{---} I \text{---} \begin{array}{c} \hat{1} \\ \diagup \\ \textcircled{2} \\ \diagdown \\ 2 \end{array} \quad (4.4.8)$$

Following the discussion in Section 2, both factorization diagrams are inverse soft factors on the 3-point amplitude  $A(124)$ . The first diagram then evaluates to  $-A(1324)$  and the second to  $-A(1342)$ , and the underlying Grassmannian geometry are just two different configurations of points on the projective line. So in this case each diagram is one particular fixed ordering of points on a line in  $\mathbb{P}^1$ .

$$\begin{array}{c} 1 \\ \bullet \\ \diagdown \\ 3 \\ \bullet \\ \diagdown \\ 2 \\ \bullet \\ \diagdown \\ 4 \\ \bullet \end{array} + \begin{array}{c} 1 \\ \bullet \\ \diagdown \\ 3 \\ \bullet \\ \diagdown \\ 4 \\ \bullet \\ \diagdown \\ 2 \\ \bullet \end{array} \quad (4.4.9)$$

At 5-point we get again two factorization diagrams,

$$A_5 = \begin{array}{c} \hat{3} \\ \diagdown \\ \textcircled{1} \\ \diagup \\ 2 \end{array} \text{---} I \text{---} \begin{array}{c} 4 \\ \diagup \\ \textcircled{2} \\ \diagdown \\ \hat{1} \end{array} + \begin{array}{c} 4 \\ \diagdown \\ \textcircled{1} \\ \diagup \\ \hat{3} \end{array} \text{---} I \text{---} \begin{array}{c} 5 \\ \diagup \\ \textcircled{2} \\ \diagdown \\ 2 \end{array} \quad (4.4.10)$$

The first diagram adds points 3 between 1 and 2 in an ordered amplitude  $A(1245)$  and leads to  $-A(13245)$ , while for the evaluation of the second diagram we need to use the representation (4.4.9), and we get  $-A(13425) - A(13452)$ . Note that in the first diagram  $\hat{1}$  and  $I$  are adjacent while in the second diagram they are non-adjacent. The formula for the amplitude is then

$$A_{5,2} = -A(13245) - A(13425) - A(13452) \quad (4.4.11)$$

This easily generalizes to the  $n$ -pt case, the BCFW recursion using (31) shift gives,

$$A_{n,2} = - \sum_{j=3}^n A(134 \dots j \ 2 \ j+1 \dots n) \quad (4.4.12)$$

This is just a formal way to write that we start with the  $(n-1)$  labels  $1, 3, 4, 5, \dots, n$  and we insert label 2 anywhere between  $3, \dots, n$ . In order to show that this equal to the original Parke-Taylor factor  $A(123 \dots n)$  we use a U(1) decoupling identity,

$$\sum_j A(13 \dots j 2 j+1 \dots n) = 0 \quad (4.4.13)$$

where we sum over all possible positions of the label 2.

It is easy to see that for the general  $(k1)$  shift the BCFW recursion relations contain two terms,

$$A_n = \begin{array}{c} \widehat{k} \\ \diagdown \\ \textcircled{1} \\ \diagup \\ k-1 \end{array} \overset{I}{\text{---}} \begin{array}{c} k+1 \\ | \\ \vdots \\ n \\ \textcircled{2} \\ | \\ \vdots \\ 2 \\ | \\ k-2 \end{array} \widehat{1} \quad + \quad \begin{array}{c} k+1 \\ \diagdown \\ \textcircled{1} \\ \diagup \\ \widehat{k} \end{array} \overset{I}{\text{---}} \begin{array}{c} k+2 \\ | \\ \vdots \\ n \\ \textcircled{2} \\ | \\ \vdots \\ 2 \\ | \\ k-1 \end{array} \widehat{1} \quad (4.4.14)$$

Each term is one particular on-shell diagram

$$A_n = \begin{array}{c} k \\ \bullet \\ \diagdown \\ \textcircled{1} \\ \diagup \\ k-1 \end{array} \begin{array}{c} \textcircled{1} \\ | \\ n \\ | \\ \textcircled{2} \\ | \\ \vdots \\ k-2 \end{array} \mathcal{A}_{n-1}^{\text{MHV}} \quad + \quad \begin{array}{c} k \\ \bullet \\ \diagdown \\ \textcircled{1} \\ \diagup \\ k+1 \end{array} \begin{array}{c} \textcircled{2} \\ | \\ \vdots \\ n \\ \textcircled{1} \\ | \\ \vdots \\ k+2 \end{array} \mathcal{A}_{n-1}^{\text{MHV}} \quad (4.4.15)$$

and they evaluate to

$$t_1 = (-1)^k \sum_{\sigma \in \Sigma_1} A(1 k k-1 \sigma), \quad t_2 = (-1)^k \sum_{\sigma \in \Sigma_2} A(1 k k-1 \sigma) \quad (4.4.16)$$

where  $\Sigma_1 = \{2, \dots, k-2\}^T \sqcup \{k+1, \dots, n\}$  and  $\Sigma_2 = \{2, \dots, k-1\}^T \sqcup \{k+2, \dots, n\}$ . Here  $\sqcup$  denotes the shuffle product of two orderings while the superscript  $T$  denotes the reversal of an ordering. The corresponding geometry is just given by a union of  $G_+(2, n)$ s with a particular ordering given by the ordering of the Parke-Taylor factor



in the sum. For the amplitude we get

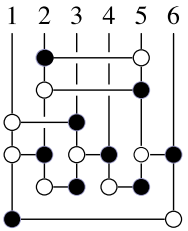
$$A_{n,2} = - \sum_{\sigma} A(1 k \sigma_{2\dots k-1, k+1\dots n}) \quad (4.4.17)$$

where we sum over all Parke-Taylor factors with indices  $1, k$  being adjacent and over all permutations of other labels which keep labels  $k-1, \dots, 2$ , resp.  $k+1, \dots, n$  relatively ordered. The fact that this is equal to a single Parke-Taylor factor with canonical ordering  $A(123\dots n)$ , is the famous Kleiss-Kuijf (KK) relation [215].

Note that the on-shell diagrams we got in the context of BCFW recursion relations formed a subset of all diagrams, and only special labels appeared in the linear combinations of Parke-Taylor factors (4.4.16). However, as noted earlier any on-shell diagram evaluates to some combination of Parke-Taylor factors and the underlying geometry is just a union of ordered points on a projective line. The first case where non-adjacent BCFW shifts lead to something qualitatively new is at the NMHV level.

#### 4.4.2 NMHV amplitudes

For  $k > 2$  the non-planar on-shell diagrams are completely new on-shell functions, which can not be obtained by relabeling of planar on-shell functions,  $\mathcal{R}$ -invariants and their higher  $k$  generalizations, or any linear combinations of them. To see what is new, we can look at an 8-dimensional non-planar on-shell diagram of  $G(3, 6)$



$$= \frac{\langle 12 \rangle [64] \delta^{3 \times 4} (C^* \cdot \tilde{\eta}) \delta^{2 \times 2} (\lambda \cdot \tilde{\lambda})}{\langle 13 \rangle [56] \langle 1|5+6|4 \rangle \langle 2|4+5|6 \rangle (\langle 23 \rangle [56] \langle 1|5+6|4 \rangle - \langle 12 \rangle [45] \langle 3|4+5|6 \rangle)}$$

(4.4.18)

Note the pole  $\langle 23 \rangle [56] \langle 1|56|4 \rangle - \langle 12 \rangle [45] \langle 3|45|6 \rangle$  does not factorize, and can not be simplified. This is a new type of singularity of purely origin that would never show up in the planar on-shell diagrams. It also implies that the non-planar loop amplitudes have new kinematical poles (in external momenta) which do not arise in the planar limit.

This on-shell diagram is one of all the inequivalent 8-dimensional cells of  $G(3, 6)$  (i.e. leading singularities) identified in [104], where new type of on-shell functions with more complicated poles were found. The authors of [104] also classified all inequivalent 9-dimensional top cells of  $G(3, 6)$ , but their underlying Grassmannian geometry (if any) is still unclear.

In this chapter we initiate the exploration of non-planar Grassmannian geometry by looking at the BCFW on-shell diagrams (we also refer to them as BCFW cells) which are expected to form a particular simple subset of all non-planar on-shell diagrams. Our goal is to identify the Grassmannian geometry for these special cells. Specifically, for each diagram parameterized by some  $G(3, n)$  matrix, we want to associate a (generally non-convex) configuration of  $n$  points in  $\mathbb{P}^2$  to it. Once identified, this configuration sets the signs of all minors needed to define the subspace in  $G(3, n)$  corresponding to the on-shell diagram.

### Five point amplitude

Let us start with the simplest 5-point case. Note that for the adjacent BCFW shift, say (51), we only had one BCFW diagram which was interpreted geometrically as

$$(4.4.19)$$

This is nothing else than the convex configuration of five points, ie. top cell of  $G_+(3, 5)$ . The three lines we chose to draw are arbitrary as no three points are on a single line.

For the non-adjacent BCFW shift (41) we get a sum of two terms,

$$(4.4.20)$$

Let us look at the first term, by definition this is equal to

$$\frac{A^{k=2}(3, \hat{4}, 5, I) A^{k=2}(I, \hat{1}, 2)}{s_{12}} \quad (4.4.21)$$

Using the procedure from the previous section, the first MHV amplitude  $A^{k=2}(3, \hat{4}, 5, I)$  corresponds to a line with  $3, \hat{4}, 5, I$  (in this ordering), the second MHV amplitude gives a line  $I, 1, 2$ , and the point 4 is on the line  $1, \hat{4}$ . Similar analysis can be done for the second BCFW term, and we get two configurations

$$(4.4.22)$$

Note that points  $I, \hat{4}$  are not part of the original set of points and do not participate in the positivity/negativity constraints on the minors of the  $C$ -matrix.

## Grassmannian cells and positivity conditions

Now we want to identify the cells in  $G(2, 5)$  which correspond to the two configurations (4.4.22). The configuration on the right is simple, it is just a usual positive Grassmannian top cell with an ordering 1, 5, 2, 3, 4, and hence satisfies  $(ijk) > 0$  where  $i, j, k$  respect this ordering.

$$\begin{array}{llll}
 (152) > 0 & (123) > 0 & (523) > 0 & (234) > 0 \\
 (153) > 0 & (124) > 0 & (524) > 0 & \\
 (154) > 0 & (134) > 0 & (534) > 0 & 
 \end{array} \tag{4.4.23}$$

The configuration on the left is more interesting, and it is a genuinely new non-planar  $G(2, 5)$  cell. The points 1, 2, 3, 4 form a convex configuration and hence  $(123)$ ,  $(124)$ ,  $(134)$ ,  $(234) > 0$ . If point 5 was next to 3 (say to the left), we would have  $(125)$ ,  $(135)$ ,  $(235)$ ,  $(154)$ ,  $(354)$ ,  $(254) > 0$  and this would be still just a top cell of  $G_+(3, 5)$  with ordering 1, 2, 3, 5, 4. However, moving the point 5 away from 3 to a different segment of the line changes the signs:

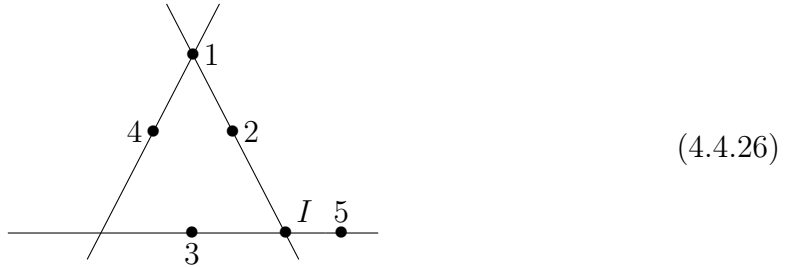
$$\begin{array}{llll}
 (123) > 0 & (234) > 0 & (235) > 0 & \mathbf{(254) \leq 0} \\
 (124) > 0 & (125) > 0 & \mathbf{(154) < 0} & \\
 (134) > 0 & (135) > 0 & (354) > 0 & 
 \end{array} \tag{4.4.24}$$

We see that two signs flipped: point 5 is now to the left of the line  $(41)$ , hence  $(415) = (154) < 0$ , and 5 can be on either side of the line  $(24)$  depending on the exact positions of 2, 4, hence  $(254)$  can have any sign and it does not impose any condition. Here we should remind the reader that each column of the  $C$ -matrix can be always rescaled without changing the Grassmannian cell. Hence, we can flip  $(j) \rightarrow -(j)$  for any

column and the configuration of points is still the same. Therefore, in (4.4.24) we can flip  $(5) \rightarrow -(5)$  and get

$$\begin{aligned}
 (123) > 0 \quad (234) > 0 \quad (235) < 0 \quad (254) \leq 0 \\
 (124) > 0 \quad (125) > 0 \quad (154) > 0 \\
 (134) > 0 \quad (135) > 0 \quad (354) < 0
 \end{aligned}
 \tag{4.4.25}$$

and it should correspond to the same configuration. It is not hard to see that these signs of minors are reproduced by



which is indeed the same configuration when we wrap 5 around infinity and come back on the right segment. As a result, drawing a point on the left or right outer segments are equivalent as (4.4.24) and (4.4.26) are the same configurations corresponding to the same non-planar cells in  $G(2, 5)$ .

At 5-point, there are really only two inequivalent BCFW shifts: adjacent  $(51)$  and next-to-adjacent  $(41)$ ; all others are related by cyclicity. But at higher points, we have a general  $(k1)$  shift. Below, we first study the next-to-adjacent shift  $(n-11)$  before considering a general case.

### Six-Point Amplitude

Let us consider the calculation of the 6-pt NMHV amplitude using  $(51)$  BCFW shift. We get four terms where the amplitude factorizes into two MHV amplitudes and two

other terms where it factorize into a 5-pt NMHV and a 3-pt  $\overline{\text{MHV}}$  amplitudes.

$$(4.4.27)$$

As before, we can easily express these BCFW terms as non-planar on-shell diagrams. The first term, for instance, is given by a single on-shell diagram:

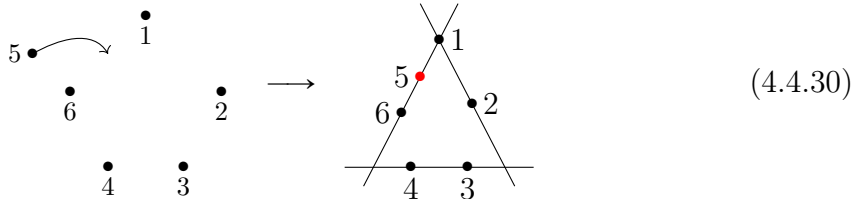
$$(4.4.28)$$

and similarly for the three other terms in (4.4.27) of this type. They are just products of two MHV amplitudes with shifted labels, and we can construct the Grassmannian geometry in the same way as for the 5-pt amplitude,

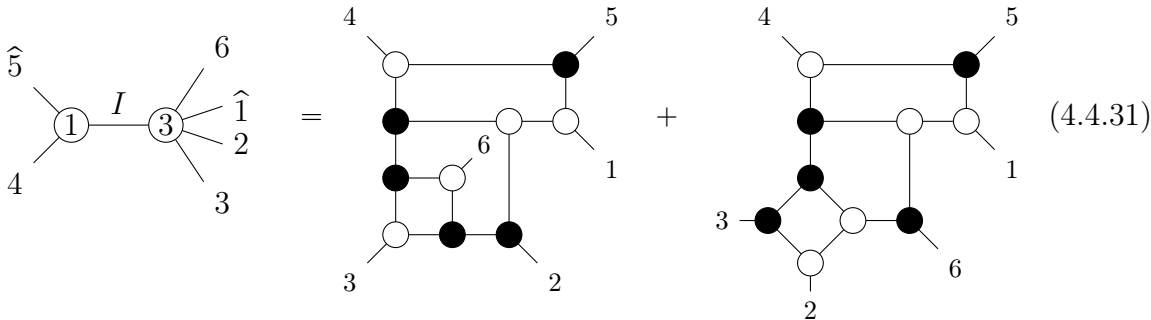
$$(4.4.29)$$

The last two terms of the form  $\mathcal{A}_3^{(1)} \otimes \mathcal{A}_5^{(3)}$  have the interpretation of (holomorphic) inverse soft-factors, and the associated configurations can be obtained by adding point

5 to some fixed configurations of points 1, 2, 3, 4, 6. Now the resulting geometry does depend on how we recurse the 5pt NMHV amplitude, whether two adjacent or non-adjacent legs in the sub-amplitude are chosen for BCFW shift. To get a closed form formula, which generalizes for any  $n$  and any  $(k1)$  shift, we use the  $(I1)$  shift, ie. the legs which are shifted in the 6-pt recursion are also used to represent the 5-pt amplitude. For the bottom left term in (4.4.27),  $(I1)$  shift is an adjacent shift, and we start with the configuration for the top cell of  $G_+(3, 5)$  with labels 1, 2, 3, 4, 6 and add point 5 between 1 and 6. We got a positive Grassmannian cell in  $G_+(3, 6)$  with minor  $(156) = 0$  while all others being positive.



For the last term of (4.4.27), the  $(I1)$  shift is a non-adjacent shift with which we get a representation of the 5pt NMHV amplitude  $A_5^{k=3}(1, 2, 3, 4, 6)$  as in (4.4.20) as a sum of two on-shell diagrams



each of them is associated with one 8-dimensional cell in  $G(3, 6)$ . Adding point 5

between 4 and 1, we get a sum of two configurations

$$(4.4.32)$$

As before, we can easily read off the signs of all  $(3 \times 3)$  minors and hence fully determine the 8-dimensional cell in  $G(3, 6)$ . For the first configuration in (4.4.32) it is

$$(4.4.33)$$

The second diagram is just a usual cell in  $G_+(3, 6)$  with an ordering 1, 6, 2, 3, 4, 5 and  $(145) = 0$ , as also suggested by the right on-shell diagram in (4.4.31). However, as we will see later we can also interpret this term as a configuration

$$(4.4.34)$$

This means that the planar on-shell diagram on the right of (4.4.31) can be associated either with the cell in  $G_+(3, 6)$  or to the cell (4.4.34) in  $G(3, 6)$ . In both cases, we get the same canonical form (up to a sign). The union of these two cells in  $G(3, 6)$  is a space with arbitrary signs of any  $(ij6) \leq 0$  (ie. point 6 can be anywhere on that line) and vanishing form.



### All- $n$ expansion

We can extend this procedure to higher points using the next-to-adjacent  $(n-1\ 1)$  shift. The amplitude either factorizes into a product of two multi-particle MHV amplitudes or a product between an  $(n-1)$ -pt NMHV amplitude and a 3-pt  $\overline{\text{MHV}}$  amplitude

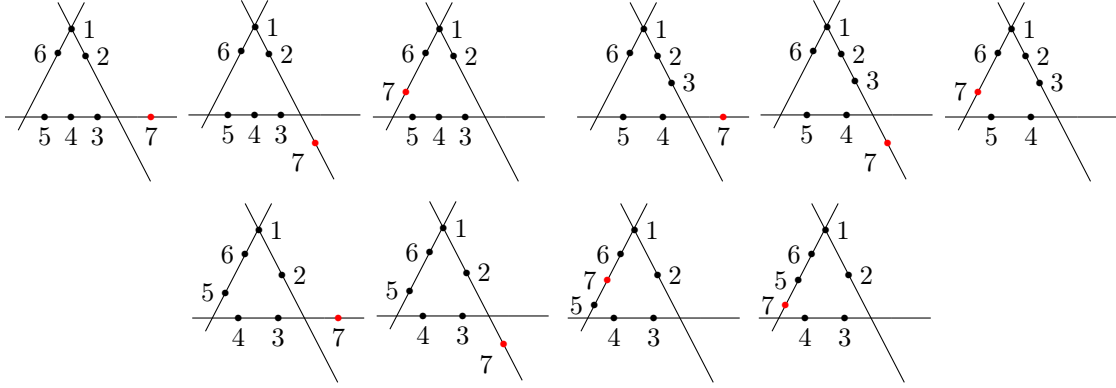
$$\widehat{n-1} \text{---} \textcircled{2} \overset{I}{\text{---}} \textcircled{2} \text{---} \widehat{1} \qquad \widehat{n-1} \text{---} \textcircled{1} \overset{I}{\text{---}} \textcircled{2} \text{---} \widehat{1} \quad (4.4.35)$$

Each BCFW term of the form MHV  $\times$  MHV, as in the adjacent case, is given by one on-shell diagram associated with a particular cell of  $G(3, n)$ , describing a single configuration of points where all except point  $n-1$  are ordered on two lines (with different orderings) and the point  $n-1$  is on another line. By contrast, every BCFW term of the form  $(n-1\text{-pt NMHV}) \times (3\text{-pt } \overline{\text{MHV}})$  gives rise to a sum of on-shell diagrams, and correspondingly, a collection of configurations of  $n$  points on three lines; all of these terms nicely complement the first type of configurations. Overall the  $n$ -pt NMHV amplitude is a sum over all configurations where points  $1, 2, 3, \dots, n-1$  are ordered on three lines, exactly as in the  $(n-1)$ -pt NMHV amplitude using adjacent shift  $(n-1\ 1)$ , but in addition we insert point  $n$  on one of the three lines at an arbitrary position – denoted by a circle:

$$A_n^{k=3} = \sum_{\sigma_n} \sum_{i,j} \text{Diagram} \quad (4.4.36)$$

Note that points  $1$  and  $n-1$  are adjacent on the third line in all the configurations, and points  $i, j$  marking the borders are such that there are at least two points on each line. Each configuration corresponds to an generally non-planar on-shell diagram, and

the particular cell in  $G(3, n)$  associated with it is defined by a set of inequalities which can be read off directly from the configuration. For illustration, we show below all 10 configurations for the 7-pt NMHV amplitude using (61) shift:

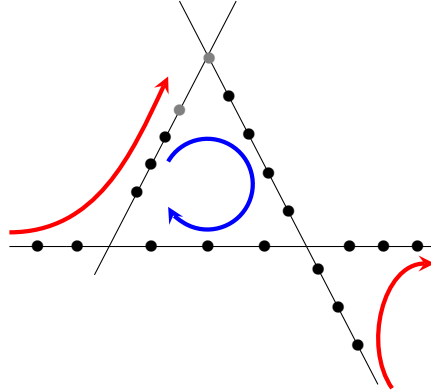


For the general shift  $(k1)$ , we proceed in the same way and find the following expression

$$A_n^{k=3} = \sum_{\substack{i,j,l,m \\ \sigma(j+1 \dots k-1; m+1 \dots n)}} \delta \left( \begin{array}{c} \left. \begin{array}{c} j+1 \dots k-1 \\ m+1 \dots n \end{array} \right\} k \\ \left. \begin{array}{c} 1 \\ 2 \\ \dots \\ i \end{array} \right\} \delta \\ j \dots i+1 \quad l \quad l+1 \dots m \\ \dots \\ k+1 \end{array} \right) \quad (4.4.37)$$

Here again we have  $n$  points on three lines distributed as follows: points 1 and  $k$  are fixed in adjacent positions on the third line; all other points are grouped into two ordered sets  $S_1 = \{2, 3, \dots, k-1\}$  and  $S_2 = \{k+1, \dots, n\}$ , and distributed among three

lines. Schematically we denote the internal orderings as



(4.4.38)

where blue represents  $S_1$  while red represents  $S_2$ . In fact, because of projectivity, the picture is invariant under switching blue and red points. The set  $S_1$  further splits into three pieces:  $\{2, \dots, i\}$  on the first line,  $\{i+1, \dots, j\}$  on the second line and  $\{j+1, \dots, k-1\}$  on the third line. Similarly the second set  $S_2$  splits into  $\{k+1, \dots, l\}$  on the first line (to the right),  $\{l+1, \dots, m\}$  on the second line (horizontal) and  $\{m+1, \dots, n\}$  on the third line (to the left). On the first two lines the two sets do not interact – they belong to distinct segments, and fixing the splitting points  $i, j$ , resp.  $l, m$  determines the configuration on these two lines completely. On the third line, points from  $S_1$  and  $S_2$  both sets are mixed together while keeping the relative orderings within their respective subsets  $\{j+1, \dots, k-1\}$  and  $\{m+1, \dots, n\}$ . This means that even after fixing  $i, j, l, m$  we get multiple configurations from various ordering of points on the third line. In (4.4.37) we sum over all the possible configurations.

To demonstrate how the points are distributed on the third line, consider an example for a general  $(k1)$  shift where we have points  $k-2, k-1$  from  $S_1$  and points  $n-1, n$  from  $S_2$  to be distributed on that line. This gives us following configurations on the

third line,

(4.4.39)

To get a full geometry we decorate them with a (fixed) configuration of points on the first two lines. As an explicit example, consider the 8-pt configurations for the (51) shift. For some choices of  $i, j, l, m$  we end up with only one configuration for the third line

(4.4.40)

but for another choice  $i = 1, j = 2, l = 6, m = 7$  we get three different terms,

(4.4.41)

To get the amplitude we have to sum over all possible choices of  $i, j, l, m$  and subsequent distributions of the remaining points on the third line. Note that for the adjacent shift  $(n1)$ ,  $S_2$  is empty and we get a usual representation (4.2.60), while for the next-to-adjacent shift  $(n-11)$ ,  $S_2 = \{n\}$  and we reproduce the formula (4.4.36).

We can also explicitly identify the cells in  $G(3, 8)$  by fixing signs of minors. For example, for the first figure in (4.4.2) we get

$$\begin{aligned}
(123) > 0 & \quad (134) > 0 & \quad (146) < 0 & \quad (167) < 0 & \quad (237) < 0 & \quad (256) < 0 & \quad (347) = 0 & \quad (457) > 0 \\
(124) > 0 & \quad (135) > 0 & \quad (147) < 0 & \quad (168) > 0 & \quad (238) > 0 & \quad (258) < 0 & \quad (348) > 0 & \quad (458) < 0 \\
(125) > 0 & \quad (136) < 0 & \quad (148) > 0 & \quad (178) > 0 & \quad (245) > 0 & \quad (267) < 0 & \quad (357) > 0 & \quad (467) < 0 \\
(126) = 0 & \quad (137) < 0 & \quad (156) < 0 & \quad (234) > 0 & \quad (246) < 0 & \quad (268) > 0 & \quad (358) < 0 & \quad (478) < 0 \\
(127) < 0 & \quad (138) > 0 & \quad (157) < 0 & \quad (235) > 0 & \quad (247) < 0 & \quad (345) > 0 & \quad (367) < 0 & \quad (567) < 0 \\
(128) > 0 & \quad (145) > 0 & \quad (158) = 0 & \quad (236) < 0 & \quad (248) > 0 & \quad (346) < 0 & \quad (378) < 0 & \quad (568) > 0 \\
(578) > 0 & & & & & & & & 
\end{aligned} \tag{4.4.42}$$

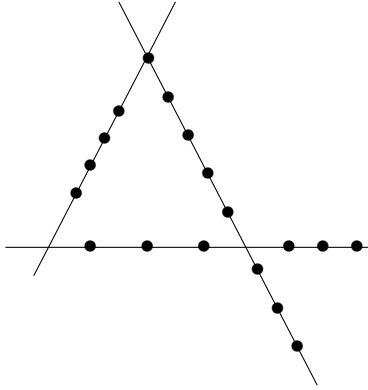
where we skipped the minors which signs are not completely fixed. As before, we can wrap points 6 and/or 7 around infinity which flips signs of all minors with 6 and/or 7, but the cell in  $G(3, 8)$  remains unchanged.

In summary, all non-planar on-shell diagrams arising from non-adjacent BCFW recursion relations for NMHV amplitudes correspond to cells in the Grassmannian  $G(3, n)$  and describe configurations of  $n$  points located on three lines. For the adjacent shift  $(n1)$  these configurations are all convex, corresponding to  $(2n-4)$ -dimensional cells in  $G_+(3, n)$ , while for a general shift the configurations subsume two independent orderings  $S_1, S_2$ . As expected, these geometries, despite being non-planar (or non-convex), are simpler than the general case of on-shell diagrams and cells in  $G(3, n)$ . We have seen earlier in (4.2.69) that, even in the planar case, the geometry of a general  $(2n-4)$ -dimensional cell involve  $n$  points on *five* different lines in  $\mathbb{P}^2$ , but here all points are restricted to be on *three* lines. It would be very interesting to find a compact

combinatorial description of these non-planar cells. Unlike the planar case, where a single permutation  $\pi(1, 2, \dots, n)$  specified the cell completely, the above discussion suggests that there should be at least two different permutations  $\pi_1, \pi_2$  involved.

## 4.5 Non-planar tree-level $R$ -invariants

In the last section, we found a correspondence between the terms in non-adjacent BCFW recursion relation and Grassmannian geometries for NMHV amplitudes, ie. configurations of  $n$  points in  $\mathbb{P}^2$ . We showed that these  $n$  points are localized on three lines:



(4.5.1)

We refer to these  $(2n-4)$ -dimensional subspaces in the Grassmannian  $G(3, n)$  as *non-planar BCFW cells*. This is the most general configuration we would get in any BCFW recursion relation, for any shift and any choice of representation of the lower-point NMHV amplitudes in (4.2.59). As we showed in the previous section, making consistent choices for shifts gives us a particularly simple and compact representation of the amplitude (4.4.37) which is a direct generalization of the expansion in terms of cells in  $G_+(3, n)$  with the adjacent shift (4.2.60). Nonetheless even if we make arbitrary choices for the lower-point geometries, we never get anything more complicated than (4.5.1), only that labeling the collection of terms that enter the BCFW formula for the NMHV amplitude is more complicated.

In this section, we discuss the superfunctions associated with these configurations. In other words, we are to find an analog of  $\mathcal{R}_{1,i+1,j+1}$  (4.3.19), the  $\mathcal{R}$ -covariant which

is associated with the general planar BCFW configuration (4.3.18). This is a laborious but in principle straightforward exercise. These configurations arise in the analysis of individual terms in the BCFW recursion relations, and each of them is tied to a particular non-planar on-shell diagram, as we showed in Section 4.4. We can compute the diagram either using (4.2.40) or by directly taking the product of 3-point amplitudes with a proper Jacobian to get the superfunction  $\mathcal{F}_\gamma(\lambda, \tilde{\lambda}, \tilde{\eta})$ . For instance, for the diagram (4.4.4) we studied earlier, the Grassmannian configuration is

(4.5.2)

and plugging the  $C$ -matrix (4.4.5) obtained from boundary measurement into (4.2.40) we get

$$\mathcal{F}_\gamma = \frac{\Delta \cdot \langle 1|26|5 \rangle}{s_{345} \langle 12 \rangle \langle 16 \rangle [34] [45] \langle 2|34|5 \rangle \langle 6|34|5 \rangle \langle 1|26|3 \rangle}, \quad (4.5.3)$$

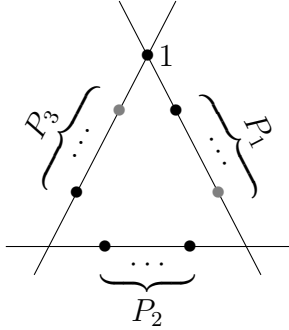
where the super  $\delta$ -functions are

$$\Delta = \delta^4(P) \delta^4(Q) \delta^4(\tilde{\Xi}) \quad \text{with} \quad \tilde{\Xi} = [45]\tilde{\eta}_3 + [53]\tilde{\eta}_4 + [34]\tilde{\eta}_5. \quad (4.5.4)$$

We make two observations here. First, the kinematical part of (4.5.3) looks different from 6-point  $\mathcal{R}$ -invariants, it has more poles and a numerator factor. On the other hand, the fermionic  $\delta$ -function is identical to the planar case (up to relabeling). This is true in general for a simple but simple reason: the argument of the fermionic  $\delta$ -function  $\delta^4(\Xi)$  in (4.2.67) (or  $\delta^4(\tilde{\Xi})$  in the special boundary case) is agnostic of the orderings of points within a line, only the partition into three sets  $P_1, P_2, P_3$  matters.

For the planar  $\mathcal{R}$ -invariant  $\mathcal{R}_{1,i+1,j+1}$  (4.2.67), we used  $\Xi_{1,i+1,j+1}$  to denote this

argument, which could have also been represented as

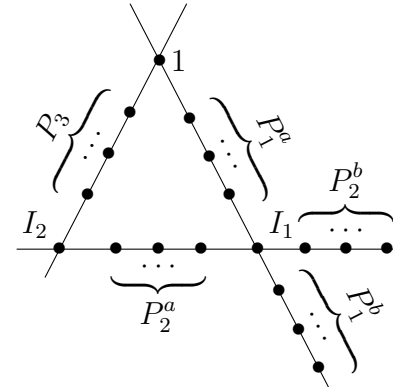


$$\Xi_{1,P_2,P_3} \equiv \sum_{k \in P_2} \langle k | P_2 P_3 | 1 \rangle \tilde{\eta}_k + \sum_{j \in P_3} P_2^2 \langle 1 j \rangle \tilde{\eta}_j, \quad (4.5.5)$$

where we list  $P_2, P_3$  explicitly ( $P_1$  is just a complement). For the non-planar generalization, indicating the boundary points is insufficient, and we need to use the more comprehensive symbol in order to specify the sets  $P_2, P_3$ .

#### 4.5.1 Non-planar $\mathcal{R}$ -invariant

In analogy with the definition of the  $\mathcal{R}$ -invariant  $\mathcal{R}_{1,i+1,j+1}$  associated with the convex configuration (4.6.19), we define the *non-planar  $\mathcal{R}$ -invariant* associated with a general non-convex configuration arising from the non-adjacent BCFW recursion,



$$\mathcal{R}_{1,P_1^a,P_1^b,P_2^a,P_2^b,P_3} = \quad (4.5.6)$$

In general, the points are completely unordered and we do need to specify all five subsets  $P_1^a, P_1^b, P_2^a, P_2^b, P_3$  including their internal orderings. While the non-planar  $\mathcal{R}$ -invariant can be a very complicated kinematical function, the actual form is surprisingly simpler. The  $\delta$ -functions are given by

$$\Delta_{1,P_2,P_3} = \delta^4(P) \delta^8(Q) \delta^4(\Xi_{1,P_2,P_3}) \quad (4.5.7)$$



where  $\Xi_{1,P_2,P_3}$  was defined in (4.5.5). Here we denote

$$P_1 = P_1^a \cup P_1^b, \quad P_2 = P_2^a \cup P_2^b \quad (4.5.8)$$

As noted above, the super  $\delta$ -function neither depends on the ordering of points, nor on the split of  $P_2$  into  $P_2^a, P_2^b$ , and is analogous to  $\Delta_{1,i+1,j+1}$  which appeared in the  $\mathcal{R}$ -invariant.

More surprisingly, the bosonic function takes exactly the same form as its planar counterpart (4.3.19), given by the product of three Parke-Taylor factors

$$\begin{aligned} \mathcal{R}_{1,\{P_1^a,P_1^b\},\{P_2^a,P_2^b\},P_3} &= PT(1, P_1^a, I_1, P_1^b) \times PT(I_2, P_2^a, I_1, P_2^b) \times PT(I_2, P_3, 1) \\ &\times \langle 1|P_2P_3|1\rangle^3 \cdot \Delta_{1,P_2,P_3} \end{aligned} \quad (4.5.9)$$

The  $\lambda$  spinors for  $I_1, I_2$  are given by the same formulae (4.3.20),

$$\lambda_{I_1} = \langle 1|P_3P_2, \quad \lambda_{I_2} = \langle 1|P_1P_2. \quad (4.5.10)$$

The only difference between (4.5.9) and (4.3.19) is that points 1,  $I_1$ , and  $I_1, I_2$  are not adjacent and that leads to more types of poles that involve  $I_1$  and  $I_2$ . Also, in the planar case (4.3.19) the factor  $\langle 1|P_2P_3|1\rangle^3$  always canceled against poles from the Parke-Taylor factors and  $\mathcal{R}_{1,i+1,j+1}$  never had any numerator factors apart from delta functions. In the non-planar case, this is no longer true, and we get up to two factors of  $\langle 1|P_2P_3|1\rangle$  left in the numerator.

## Examples

First, let us reproduce the expression (4.5.3) we obtained earlier from the direct computation using on-shell diagram,  $C$ -matrix and (4.2.40). We draw the same config-

uration again and label points  $I_1, I_2$ ,

$$(4.5.11)$$

Their  $\lambda$ -spinors are given by

$$\lambda_{I_1} = \langle 1|(5)(34) = [5|(34) \cdot \langle 15 \rangle, \quad \lambda_{I_2} = \langle 1|(26)(34) \quad (4.5.12)$$

We see that the  $\lambda_{I_1}$  spinor simplifies because there is only one point on the third line, but we keep the constant factor  $\langle 15 \rangle$  in the definition of  $\lambda_{I_1}$  – we will see that it trivially cancels against the same factors in the numerator. The argument of the fermionic delta function is given by

$$\begin{aligned} \Xi_{1,34,5} &= \langle 3|(34)(5)|1\rangle \tilde{\eta}_3 + \langle 4|(34)(5)|1\rangle \tilde{\eta}_4 + s_{34} \langle 15 \rangle \tilde{\eta}_5 \\ &= \langle 15 \rangle \langle 34 \rangle ([45] \tilde{\eta}_3 + [53] \tilde{\eta}_4 + [34] \tilde{\eta}_5). \end{aligned} \quad (4.5.13)$$

The Parke-Taylor factors evaluate to

$$PT(1, 2, I_1, 6) = \frac{1}{\langle 12 \rangle \langle 2I_1 \rangle \langle I_1 6 \rangle \langle 61 \rangle} = \frac{1}{\langle 12 \rangle \langle 16 \rangle \langle 2|34|5 \rangle \langle 6|34|5 \rangle \langle 16 \rangle \cdot \langle 15 \rangle^2} \quad (4.5.14)$$

$$PT(I_1, 3, 4, I_2) = \frac{1}{\langle I_1 3 \rangle \langle 34 \rangle \langle 4I_2 \rangle \langle I_2 I_1 \rangle} = \frac{1}{[34][45] \langle 1|26|3 \rangle \langle 1|26|5 \rangle \cdot \langle 15 \rangle^2 \langle 34 \rangle^3} \quad (4.5.15)$$

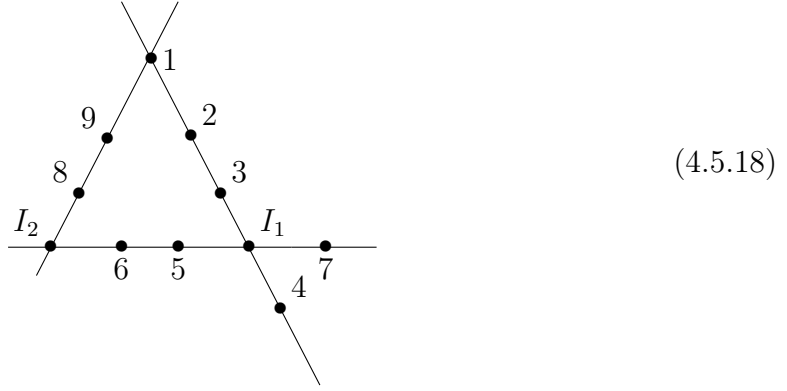
$$PT(1, 5, I_2) = \frac{1}{\langle 15 \rangle \langle 5I_2 \rangle \langle I_2 1 \rangle} = \frac{1}{s_{345} \langle 1|26|5 \rangle \langle 15 \rangle^3} \quad (4.5.16)$$

where we used the momentum conservation  $P_1 + P_2 + P_3 + p_1 = 0$  to rewrite  $\langle 1|P_1 P_3|1 \rangle = -\langle 1|P_1 P_2|1 \rangle = \langle 1|P_3 P_2|1 \rangle$  etc., and then  $\langle 1|P_1 P_3|1 \rangle = \langle 1|26|5 \rangle \langle 15 \rangle$ . Plugging all these ingredients into (4.5.9) we get

$$\mathcal{R}_{1,\{2,6\},\{34\},\{5\}} = \frac{\langle 1|26|5 \rangle \cdot \delta^4(P) \delta^8(Q) \delta^4([45] \tilde{\eta}_3 + [53] \tilde{\eta}_4 + [34] \tilde{\eta}_5)}{s_{345} \langle 12 \rangle \langle 16 \rangle [34][45] \langle 2|34|5 \rangle \langle 6|34|5 \rangle \langle 1|26|3 \rangle} \quad (4.5.17)$$

which is equal to (4.5.3).

Let us look now at a more general 9-point configuration,



The internal spinors  $I_1, I_2$ , are now

$$\lambda_{I_1} = \langle 1|(89)(567), \quad \lambda_{I_2} = \langle 1|(234)(567) \quad (4.5.19)$$

and following the same procedure we get

$$\mathcal{R} = \frac{\langle 1|(234)(89)|1\rangle^2 \cdot \delta^4(P) \delta^8(Q) \delta^4(\Xi_{1,567,89})}{\langle 12\rangle\langle 23\rangle\langle 14\rangle\langle 56\rangle\langle 89\rangle\langle 91\rangle\langle 1|(89)(567)|3\rangle\langle 1|(89)(567)|4\rangle\langle 1|(89)(67)|5\rangle\langle 1|(89)(56)|7\rangle} \\ \langle 1|(234)(57)|6\rangle\langle 1|(234)(56)|7\rangle\langle 1|(234)(567)|8\rangle \quad (4.5.20)$$

where we denoted  $\mathcal{R} \equiv \mathcal{R}_{1,\{23,4\},\{56,7\},\{89\}}$ . For a general configuration, we can plug into (4.5.9) for the Parke-Taylor factors and obtain an expression for a general  $\mathcal{R}$ ,

$$\mathcal{R}_{1,\{P_1^a, P_1^b\},\{P_2^a, P_2^b\}, P_3} = \frac{\delta^4(P) \delta^8(Q) \delta^4(\Xi_{1,P_2,P_3}) \langle 1|P_1 P_3|1\rangle^2}{(\prod \langle ab\rangle) \langle i_1 I_1\rangle\langle i_2 I_1\rangle\langle i_3 I_1\rangle\langle i_4 I_1\rangle\langle j_1 I_2\rangle\langle j_2 I_2\rangle\langle j_3 I_2\rangle} \quad (4.5.21)$$

where in the first term in the denominator we took the product of all  $\langle ab \rangle$  of the points  $a, b$  adjacent on one of the lines. There is a boundary case for which  $P_2^b$  is empty, and the new pole  $\langle I_1 I_2 \rangle$  appears from the Parke-Taylor factor.

$$\begin{aligned}
\mathcal{R}_{1, \{P_1^a, P_1^b\}, P_2^a, P_3} = & \text{Diagram} \\
= & \frac{\delta^4(P) \delta^8(Q) \delta^4(\Xi_{1, P_2, P_3}) \langle 1 | P_1 P_3 | 1 \rangle^2}{(\prod \langle ab \rangle) \langle i_1 I_1 \rangle \langle i_2 I_1 \rangle \langle i_3 I_1 \rangle \langle I_1 I_2 \rangle \langle j_1 I_2 \rangle \langle j_2 I_2 \rangle} \quad (4.5.22)
\end{aligned}$$

Because of  $\langle I_1 I_2 \rangle = \langle 1 | P_3 P_1 | 1 \rangle P_2^2$  one power in the numerator cancels and we get only a single power of  $\langle 1 | P_1 P_3 | 1 \rangle$ . If both  $P_2^b$  and  $P_1^b$  are empty, points  $i_3, i_4, j_3$  are missing and  $i_1 \rightarrow i, i_2 \rightarrow i+1, j_1 \rightarrow j, j_2 \rightarrow j+1$ , the formula simplifies to

$$\begin{aligned}
\mathcal{R}_{1, P_1^a, P_2^a, P_3} = & \text{Diagram} \\
= & \frac{\delta^4(P) \delta^8(Q) \delta^4(\Xi_{1, P_2, P_3})}{(\prod \langle ab \rangle) \langle i I_1 \rangle \langle i+1 I_1 \rangle \langle j I_2 \rangle \langle j+1 I_2 \rangle P_2^2} \quad (4.5.23)
\end{aligned}$$

which is just the usual  $\mathcal{R}$ -invariant (4.2.62).

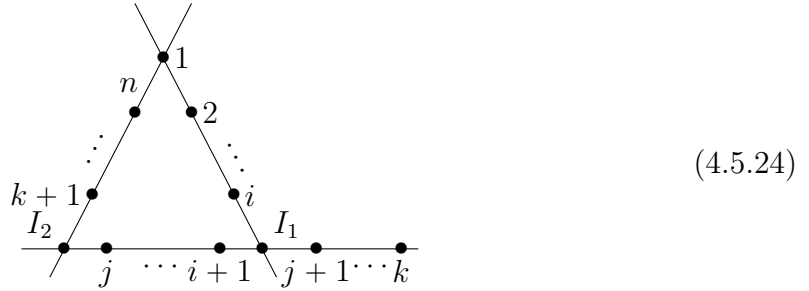
The general expression (4.5.21) has a non-trivial numerator  $\langle 1 | P_1 P_3 | 1 \rangle^2$  (the third power cancels against the  $\langle 1 P_2 \rangle$  pole), and poles from the Parke-Taylor factors. Note that 7 of these poles depend on points  $I_1, I_2$  (these are non-holomorphic after plugging

in expressions for  $\lambda_{I_1}, \lambda_{I_2}$ ). This is in contrast with  $\mathcal{R}_{1,i+1,j+1}$ , where there is no extra numerator factor and only 5 non-holomorphic poles appear in the denominator (4.5.23).

### 4.5.2 Planar expansion

There is similarity between (4.5.21) and the compact formula for MHV on-shell diagrams [102], which also has a square of certain kinematical factors in the numerator. In that case, the formula was valid for all on-shell diagrams (of dimensionality  $2n-4$ ), whereas our construction is only for BCFW cells. Nevertheless, we can explore the similarity further. As shown in [102] any MHV on-shell diagram (on-shell function) can be expressed as a linear combination of Parke-Taylor factors with various orderings, and  $\pm 1$  coefficients. We can ask the same question in the context of NMHV BCFW cells and formula (4.5.9) – can we express it as a linear combination of the original  $\mathcal{R}$ -invariants with different orderings?

Let us first look at the case where points are “misplaced” only on one of the lines while the rest are canonically ordered,



The superfunction can be built from Parke-Taylor factors as

$$\mathcal{R} = PT(1, \dots, i, I_1) PT(I_1, i+1, \dots, j, I_2, j+1, \dots, k) PT(I_2, k+1, \dots, n, 1) \langle 1|P_1 P_3|1 \rangle^3 \cdot \delta^4(\Xi) \quad (4.5.25)$$

where  $P_1 = p_2 + \dots + p_i$ ,  $P_3 = p_{k+1} + \dots + p_n$ , and  $\Xi = \Xi_{1,i+1,k+1}$ , just as in the standard  $R$ -invariant. The non-planarity of the configuration is caused by the middle Parke-Taylor factor where points  $I_1, I_2$  are not adjacent. We can use the Kleiss-Kuijff (KK) relations to rewrite this expression as a sum over Parke-Taylor factors where  $I_1$

and  $I_2$  are adjacent,

$$PT(I_1, i+1, \dots, j, I_2, j+1, \dots, k) = \sum_{\sigma} PT(I_1, \sigma, I_2) \quad (4.5.26)$$

where  $\sigma$  belongs to the shuffle product of two sets

$$\sigma \in \{i+1, \dots, j\} \sqcup \{j+1, \dots, k\}^T. \quad (4.5.27)$$

This means we sum over permutations of labels  $\{i+1, \dots, k\}$  where the relative orderings of both sets  $\{j, j-1, \dots, i+1\}$  and  $\{j+1, \dots, k\}$  (this is the transverse of the original set) are preserved. For example, in the case of  $i = 1$ ,  $j = 3$  and  $k = 5$  with  $\sigma \in \{2, 3\} \sqcup \{4, 5\}^T$ ,

The diagram shows a horizontal line with six points labeled  $I_1, 2, 3, I_2, 4, 5$  from left to right. The points  $I_1$  and  $I_2$  are red, while 2, 3, 4, 5 are black. This is equated to a sum of six terms, each representing a different shuffle of the set  $\{2, 3\}$  and the transverse set  $\{4, 5\}^T$ . The terms are:

- $I_1, 2, 3, 5, 4, I_2$
- $I_1, 2, 5, 3, 4, I_2$
- $I_1, 5, 2, 3, 4, I_2$
- $I_1, 2, 5, 4, 3, I_2$
- $I_1, 5, 2, 4, 3, I_2$
- $I_1, 5, 4, 2, 3, I_2$

(4.5.28)

Note that while the KK relation is for MHV amplitudes, it also true for the Parke-Taylor factors as the super  $\delta$ -function is the same for any ordering. We can now plug (4.5.26) into (4.5.25). Each term in the sum leads to a planar  $R$ -invariant with some given ordering. As a result, we get an expansion of  $\mathcal{R}$  as a linear combination of  $R$ -invariants,

$$\mathcal{R} = \sum_{\sigma} \mathcal{R}(1, \dots, i, \sigma, k+1, \dots, n) = \sum_{\sigma} \text{Diagram} \quad (4.5.29)$$

The diagram shows a triangle with vertices labeled 1 (top), 2 (middle right), and  $I_1$  (bottom right). The left side of the triangle has points labeled  $k+1, \dots, n$ . The right side has points labeled  $i, \dots, 2$ . The bottom side has points labeled  $I_2, \dots, \sigma, I_1$ .

Note that this is only possible because neither the Jacobian factor  $\langle 1|P_1P_3|1\rangle$  nor the fermionic delta function  $\delta^4(\Xi)$  depends on the ordering of points in  $P_2$  and they are the same for all terms in the sum (4.5.29).

As an example, let us expand the first of the 6-pt NMHV non-planar on-shell functions (4.4.29). In that case, the KK relation produces two terms,

$$\text{Diagram} = \text{Diagram} + \text{Diagram} \quad (4.5.30)$$

And we get two  $R$ -invariants for  $(123) = 0$  corresponding to orderings  $1, 2, 3, 4, 5, 6$  and  $1, 2, 3, 5, 4, 6$ . The bosonic part of the on-shell functions (the fermionic part is the same across all term as stressed before) yield (4.5.17),

$$\frac{1}{s_{123}\langle 12 \rangle \langle 23 \rangle [45] [56] \langle 1|23|4 \rangle \langle 3|45|6 \rangle} + \frac{1}{s_{123}\langle 12 \rangle \langle 23 \rangle [45] [46] \langle 1|23|5 \rangle \langle 3|45|6 \rangle} = \frac{\langle 1|23|6 \rangle}{s_{123}\langle 12 \rangle \langle 23 \rangle [46] [56] \langle 1|23|4 \rangle \langle 1|23|5 \rangle \langle 3|45|6 \rangle}. \quad (4.5.31)$$

Note that the pole  $[45]$  is spurious, ie. it is present in both  $\mathcal{R}$ -invariants but cancels in the sum. Geometrically  $[45] = 0$  corresponds to merging points  $I_1$  and  $I_2$  and indeed that is not a singularity of the non-planar configuration. The appearance of the spurious poles (which cancel in the sum) is also a feature of the Parke-Taylor expansion of the on-shell functions for MHV on-shell diagrams [102].

Finally, we can do the same for the general case where points are misplaced on two lines.

$$\text{Diagram} \quad (4.5.32)$$





## 4.6 Kinematical dlog forms

In the previous section, we see how the Grassmannian configurations directly embody superfunctions of external kinematic data, sidestepping the standard procedures of computation from constructing representative  $C$ -matrices to evaluating contour integrals. In this process, the canonical forms associated with the BCFW cells appear as auxiliary objects to be integrate over with a set of  $\delta$ -functions. On the other hand, it was shown in [216] that super-amplitudes (or super-functions for individual BCFW cells) can be viewed more fundamentally as differential forms in the on-shell kinematic space. Operationally the kinematical differential forms can be obtained as a pushforward of the canonical forms on Grassmannian cells to the kinematic space. In this section, we discuss the connection between Grassmannian configurations and the kinematical forms with logarithmic singularities in  $\mathcal{N} = 4$  sYM. In particular, we provide a method for constructing a *holomorphic dlog* representation of the kinematical forms for NMHV amplitudes, in both the planar and non-planar cases, without invoking the pushforward map.

### 4.6.1 Super-functions as kinematical differential forms

Let us first review the idea of super-functions for individual BCFW cells as differential forms in the kinematical space. This was first formulated in the momentum twistor space [58]. The relation between the dlog form  $\Omega_Z$  and the superfunction is just a simple replacement

$$\mathcal{F}(Z, \eta) = \Omega(dZ_k \rightarrow \eta_k) \tag{4.6.1}$$

where  $\eta$  are momentum twistor Grassmann variables. Summing forms on individual cells gives the tree-level amplitudes (and loop integrands) as forms with logarithmic singularities on the boundaries of the Amplituhedron space.

It was suggested in [216] how this picture extends to the spinor-helicity space and this was used in the formulation of the momentum Amplituhedron [105]. We start with a super-function for a given on-shell diagram  $\gamma$  in the non-chiral space, which is given

by a Fourier transformation of  $\mathcal{F}$  on half of the Grassmann variables  $\tilde{\eta}^I$ ,

$$\mathcal{F}_{n,k}^\gamma = \oint \omega_{n,k}^\gamma \delta^{2k}(C \cdot \tilde{\lambda}) \delta^{2(n-k)}(C^\perp \cdot \lambda) \delta^{0|2k}(C \cdot \tilde{\eta}) \delta^{0|2(n-k)}(C^\perp \cdot \eta) \quad (4.6.2)$$

In the case of BCFW cells the dimensionality of the form is  $m = 2n - 4$ . The non-chiral super function can be thought of as a differential form of degree  $(2(n - k), 2k)$  in  $(d\lambda, d\tilde{\lambda})$  space with the replacement  $\eta^{1,2} \rightarrow d\lambda^{1,2}$  and  $\tilde{\eta}^{1,2} \rightarrow d\tilde{\lambda}^{1,2}$ . The resulting  $2n$ -form vanishes identically as the super function contains  $\delta^4(P)\delta^4(Q)\delta^4(\tilde{Q})$ . Upon the replacement

$$\begin{aligned} \delta^4(Q) &\rightarrow (dq)^4 = \bigwedge_{\alpha=1}^2 \bigwedge_{\dot{\alpha}=1}^2 (dq)^{\alpha\dot{\alpha}} = \bigwedge_{\alpha=1}^2 \bigwedge_{\dot{\alpha}=1}^2 \left[ \sum_{a=1}^n \lambda_a^\alpha (d\tilde{\lambda}_a)^{\dot{\alpha}} \right], \\ \delta^4(\tilde{Q}) &\rightarrow (d\tilde{q})^4 = \bigwedge_{\alpha=1}^2 \bigwedge_{\dot{\alpha}=1}^2 (d\tilde{q})^{\alpha\dot{\alpha}} = \bigwedge_{\alpha=1}^2 \bigwedge_{\dot{\alpha}=1}^2 \left[ \sum_{a=1}^n (d\lambda_a)^\alpha \tilde{\lambda}_a^{\dot{\alpha}} \right], \end{aligned} \quad (4.6.3)$$

by virtue of momentum conservation

$$(dq)^{\alpha\dot{\alpha}} + (d\tilde{q})^{\alpha\dot{\alpha}} = 0 \quad (4.6.4)$$

the full “super momentum-conserving form” vanishes. We can factor out half of the super momentum-conserving factor explicitly by partially localizing  $C$  so that the first two rows are simply  $(\lambda_1, \dots, \tilde{\lambda}_n)$ . As a result, we get

$$\mathcal{F}^\gamma = \delta^4(P)\delta^4(Q) \times \tilde{\mathcal{F}}^\gamma(\lambda, \tilde{\lambda}, \eta, \tilde{\eta}) \quad (4.6.5)$$

Stripped of  $\delta^4(P)\delta^4(Q)$ , the remaining superfunction  $\tilde{\mathcal{F}}_\gamma$  turns into a form,

$$\Omega_{n,k}^\gamma = \int \omega_{n,k}^\gamma \prod_{\mu} \delta^2(C_\mu \cdot \tilde{\lambda}) \prod_{\mu'} \delta^2(C_{\mu'}^\perp \cdot \lambda) \bigwedge_{\mu} (C_\mu \cdot d\tilde{\lambda})^2 \bigwedge_{\mu'} (C_{\mu'}^\perp \cdot d\lambda)^2 \quad (4.6.6)$$

where  $\mu' = 3, \dots, k$ ,  $\tilde{\mu} = 1, \dots, n-k$ . The bosonic  $\delta$ -functions define a map with which allows us to pushforward the canonical form  $\omega_{n,k}^\gamma$  on the Grassmannian space,

$$\omega_{n,k}^\gamma = F(x_1, x_2, \dots, x_{2n-4}) dx_1 \dots dx_{2n-4} = \bigwedge_{i=1}^{2n-4} \frac{d\alpha_i}{\alpha_i} \quad (4.6.7)$$

to the differential form  $\Omega_{n,k}^\gamma$  on the kinematical space. Concretely, we write  $\omega_{n,k}^\gamma$  in arbitrary coordinates  $\{x_i\}$  and solve  $C(x) \cdot \tilde{\lambda} = C^\perp(x) \cdot \lambda = 0$  for  $x_i$  in terms of  $\lambda, \tilde{\lambda}$ , make the substitution in the rational function  $F(x_1, \dots, x_m)$  with the appropriate Jacobian. In a canonical parameterization, eg. edge variables  $\{\alpha_i\}$ , the canonical form  $\omega_{n,k}^\gamma$  is a trivial dlog and the resulting kinematical form is simply

$$\Omega_{n,k}^\gamma(\lambda, \tilde{\lambda}) = \bigwedge_{i=1}^{2n-4} \frac{d\alpha_i(\lambda, \tilde{\lambda})}{\alpha_i(\lambda, \tilde{\lambda})} \quad (4.6.8)$$

where the differential operator acts on  $\lambda$  and  $\tilde{\lambda}$ .

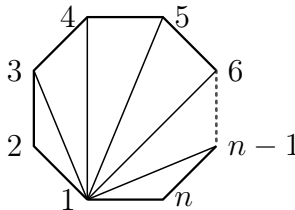
Recovering the super-function from the kinematical form  $\Omega_{n,k}^\gamma$  is straightforward. Note the full super-function corresponds to an (vanishing) invariant  $2n$  form. In order to recover the superfunction, we need to multiply the  $2n-4$  form by  $(dq)^4$

$$\mathcal{F}_{n,k}^\gamma = (dq)^4 \wedge \Omega_{n,k}^\gamma \Big|_{d\lambda \rightarrow \eta, d\tilde{\lambda} \rightarrow \tilde{\eta}}. \quad (4.6.9)$$

making the replacements  $d\lambda^{1,2} \rightarrow \eta^{1,2}$ ,  $d\tilde{\lambda}^{1,2} \rightarrow \tilde{\eta}^{1,2}$  then turns the form back to the non-chiral superfunction  $\mathcal{F}_{n,k}^\gamma$ . See [216] for more details.

The punchline: the  $2n-4$  form  $\Omega_{n,k}^\gamma$  in the kinematic space contains the same information as the super-function  $\mathcal{F}_{n,k}^\gamma$  (in a non-chiral) for a given amplitude, on-shell diagram or particular BCFW cell. They can be cast into a simple dlog form that contains all this information. The translation from the form  $\Omega_{n,k}^\gamma$  to a super-function is trivial, the construction of the kinematical form, however, involves non-trivial work. Let us look at a few examples.

**MHV** The form for the  $n$ -pt MHV amplitude can be famously obtained from a triangulation of the polygon, which results in



$$\Omega_{n,2} = \bigwedge_{i=2}^{n-1} d\log \frac{\langle 1 i \rangle}{\langle i i+1 \rangle} \wedge d\log \frac{\langle 1 i+1 \rangle}{\langle i i+1 \rangle} \quad (4.6.10)$$

and does not depend on a particular triangulation. As noted earlier,  $\Omega_{n,2}$  contains  $(d\tilde{q})^4$  which is not manifest in the dlog representation. For example, at 4-point we have

$$\Omega_{4,2} = \frac{(d\tilde{q})^4}{st} = d\log \frac{\langle 12 \rangle}{\langle 13 \rangle} \wedge d\log \frac{\langle 23 \rangle}{\langle 13 \rangle} \wedge d\log \frac{\langle 34 \rangle}{\langle 13 \rangle} \wedge d\log \frac{\langle 41 \rangle}{\langle 13 \rangle}. \quad (4.6.11)$$

**NMHV** Consider the 6-pt NMHV cell with  $(123) = 0$  discussed earlier (4.5.30). Plugging the solution of C-matrix (4.2.51) into the Grassmannian integral (4.6.6) gives

$$\Omega_{6,3} = \frac{(d\tilde{q})^4 (d\lambda_1 \langle 23 \rangle + d\lambda_2 \langle 31 \rangle + d\lambda_3 \langle 12 \rangle)^2 (d\tilde{\lambda}_4 [56] + d\tilde{\lambda}_5 [64] + d\tilde{\lambda}_6 [45])^2}{s_{123} \langle 12 \rangle \langle 23 \rangle [45] [56] \langle 1|5+6|4 \rangle \langle 3|4+5|6 \rangle}. \quad (4.6.12)$$

This is equivalent to the following dlog representation

$$\Omega_{6,3} = d\log(\alpha_1) \wedge d\log(\alpha_2) \wedge \cdots \wedge d\log(\alpha_8) \quad (4.6.13)$$

with the canonical variables given by

$$\alpha_1 = \frac{\langle 12 \rangle}{\langle 31 \rangle}, \alpha_2 = \frac{\langle 23 \rangle}{\langle 31 \rangle}, \alpha_3 = \frac{\widehat{[34]}}{\widehat{[31]}}, \alpha_4 = \frac{[46]}{\widehat{[31]}}, \alpha_5 = \frac{\widehat{[61]}}{\widehat{[31]}}, \alpha_6 = \frac{\widehat{[14]}}{\widehat{[31]}}, \alpha_7 = \frac{[54]}{[64]}, \alpha_8 = \frac{[65]}{[64]}. \quad (4.6.14)$$

where the shifted momenta defined as

$$\tilde{\lambda}_{\hat{1}} = \tilde{\lambda}_1 + \frac{\langle 23 \rangle}{\langle 13 \rangle} \tilde{\lambda}_2, \quad \tilde{\lambda}_{\hat{3}} = \tilde{\lambda}_3 + \frac{\langle 12 \rangle}{\langle 13 \rangle} \tilde{\lambda}_2. \quad (4.6.15)$$

Note the dlog form then naturally splits into two parts: an anti-holomorphic dlog form for a 5-point NMHV tree-amplitude with shifted momenta, and a holomorphic dlog form for a 3-point MHV amplitude

$$\Omega_{6,3} = \Omega_{5,3}(\hat{1}, \hat{3}, 4, 5, 6) \wedge \Omega_{3,2}(1, 2, 3). \quad (4.6.16)$$

This is reminiscent of a holomorphic ( $k$ -preserving) inverse-soft factor and indeed (4.6.15) is precisely the shift induced by adding a point 2 by to the 5-pt on-shell diagram using a holomorphic inverse-soft factor. In general, higher point NMHV forms can be built successively from repeatedly taking holomorphic ( $k$ -preserving) inverse-soft factors. In

particular, we can get the following dlog form representation of the general  $R$ -invariant  $\mathcal{R}_{1,i+1,j+1}$

$$\Omega_{1,i+1,j+1} = \Omega_{k=3}(\widehat{1}, \widehat{i}, \widehat{i+1}, \widehat{j}, \widehat{j+1}) \wedge \Omega_{k=2}(1, \dots, i) \wedge \Omega_{k=2}(i+1, \dots, j) \wedge \Omega_{k=2}(j+1, \dots, n, 1) \quad (4.6.17)$$

with the shifted  $\tilde{\lambda}$  spinors given by

$$\begin{aligned} \tilde{\lambda}_{\widehat{1}} &= \tilde{\lambda}_1 + \sum_{a=2}^{i-1} \frac{\langle i a \rangle}{\langle i 1 \rangle} \tilde{\lambda}_a + \sum_{a=j+2}^n \frac{\langle a j+1 \rangle}{\langle 1 j+1 \rangle} \tilde{\lambda}_a, \\ \tilde{\lambda}_{\widehat{i}} &= \tilde{\lambda}_i + \sum_{a=2}^{i-1} \frac{\langle 1 a \rangle}{\langle 1 i \rangle} \tilde{\lambda}_a, \quad \tilde{\lambda}_{\widehat{i+1}} = \tilde{\lambda}_{i+1} + \sum_{a=i+2}^{j-1} \frac{\langle a, j \rangle}{\langle i+1, j \rangle} \tilde{\lambda}_a \\ \tilde{\lambda}_{\widehat{j}} &= \tilde{\lambda}_j + \sum_{a=i+2}^{j-1} \frac{\langle i+1, a \rangle}{\langle i+1, j \rangle} \tilde{\lambda}_a, \quad \tilde{\lambda}_{\widehat{j+1}} = \tilde{\lambda}_{j+1} + \sum_{a=j+2}^n \frac{\langle a, 1 \rangle}{\langle j+1, 1 \rangle} \tilde{\lambda}_a. \end{aligned} \quad (4.6.18)$$

The structure of the form (4.6.17) reflects the way it is constructed. We start with the skeleton form  $\Omega(1, i, i+1, j, j+1)$  associated with five points on three lines, and by successive application of holomorphic inverse-soft factors insert extra points  $n, n-1, \dots, 2$  in reversed order to the three lines; the shifts in  $\lambda$ -spinors propagate through the neighboring points leading to (4.6.18) in the end, and the 3-point dlog forms thus added nicely join into three  $\Omega_{k=2}$  forms for the Parke-Taylor factors. For more detailed discussion on the inverse-soft construction of kinematic dlog forms see [216]. Note, however, even though the Grassmannian configuration is obvious, there is no direct geometric interpretation of (4.6.17) analogous to what we see in the last section. This is to be expected from the presence of the outstanding *anti-holomorphic* dlog factor  $\Omega_{k=3}(\widehat{1}, \widehat{i}, \widehat{i+1}, \widehat{j}, \widehat{j+1})$ .

Differential forms for higher  $k$  can also be built using the inverse-soft construction with anti-holomorphic ( $k$ -increasing) inverse-soft factors. But there is a limitation to this method. It only works for on-shell diagrams that can be built from simpler diagrams, whose form are already known, by adding points through inverse-soft factors. This is not generally the case for on-shell diagrams we encountered in the earlier discussion of BCFW cells even with adjacent shifts. Nevertheless, there is a particular

recursion scheme  $\{-2, 2, 0\}$  that yield any tree amplitude in inverse-soft constructible terms solely.

### 4.6.2 Holomorphic dlog forms

Now we turn our attention to the canonical dlog forms. The standard procedure is to use the Grassmannian formula (4.6.6) for a particular cell represented by a  $C$ -matrix. Our goal is to construct the dlog form for the general NMHV  $R$ -invariant  $\mathcal{R}_{1,i+1,j+1}$  in a different way which will also generalize to the non-planar case. Inspired by the existence of the geometrical formula (4.3.19), we propose a *holomorphic dlog form* which only depends on the holomorphic  $\lambda$ -spinors. The  $\tilde{\lambda}$ -dependency will be absorbed into the dependence on the spinors  $\lambda_{I_1}$  and  $\lambda_{I_2}$ , which we defined in (4.3.25) up to a normalization. Since (4.3.19) gives the superfunction as the product of three Parke-Taylor factors, we may naively try to take the wedge product of three MHV dlog forms on each of the lines. It is easy to see that this cannot be exactly correct as we would get dlog forms of degree  $2n - 2$  instead of  $2n - 4$ . The second problem is that the spinors  $\lambda_{I_1}$  and  $\lambda_{I_2}$  defined in (4.3.20) were not normalized.

The correct prescription for the holomorphic dlog form is the following. For a general NMHV configuration

(4.6.19)

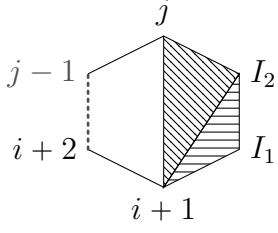
take the wedge product of three dlog forms

$$\Omega_{n,k=3} = \tilde{\Omega}_{k=2}(1, 2, \dots, i, I_1) \wedge \Omega_{k=2}(I_1, i+1, \dots, j, I_2) \wedge \tilde{\Omega}_{k=2}(I_2, j+1, \dots, n, 1). \quad (4.6.20)$$

The spinors for  $I_1$  and  $I_2$  are defined with correct normalization as follows:

$$\lambda_{I_1} = \langle 1|P_3P_2 \cdot \frac{\langle 1i \rangle}{\langle 1|P_1P_3|1 \rangle}, \quad \lambda_{I_2} = \langle 1|P_1P_2 \cdot \frac{\langle 1j+1 \rangle}{\langle 1|P_1P_3|1 \rangle} \quad (4.6.21)$$

The dlog form for the middle line is the usual MHV amplitude for points  $I_2, i+1, \dots, j, I_1$  and it is given by the triangulation of a corresponding polygon



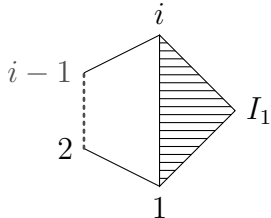
$$\begin{aligned} & \Omega_{k=2}(I_1, i+1, \dots, j, I_2) \\ &= \Omega_{k=2}(i+1, \dots, j) \wedge d\log \frac{\langle i+1 j \rangle}{\langle j I_2 \rangle} \wedge d\log \frac{\langle i+1 I_2 \rangle}{\langle j I_2 \rangle} \\ & \quad \wedge d\log \frac{\langle i+1 I_2 \rangle}{\langle I_2 I_1 \rangle} \wedge d\log \frac{\langle i+1 I_1 \rangle}{\langle I_2 I_1 \rangle} \end{aligned} \quad (4.6.22)$$

where we denoted the dlog form for the polygon  $(i+1, \dots, j)$ ,

$$\Omega_{k=2}(i+1, \dots, j) = \bigwedge_{k=i+2}^{j-1} d\log \frac{\langle i+1 k \rangle}{\langle k k+1 \rangle} \wedge d\log \frac{\langle i+1 k+1 \rangle}{\langle k k+1 \rangle} \quad (4.6.23)$$

and we added in (4.6.22) dlog forms for two triangles  $(i+1, j, I_2)$  and  $(i+1, I_2, I_1)$  which depend on extra points  $I_1, I_2$ . This all trivially follows from the triangulation.

The *reduced* dlog form  $\tilde{\Omega}_{k=2}(1, 2, \dots, i, I_1)$  also corresponds to a polygon,



$$(4.6.24)$$

We triangulate the sub-polygon with points  $(1, 2, \dots, i)$  in the standard way and write its dlog form. For the last triangle  $(1, i, I_1)$  we only associate one dlog factor rather than two,

$$\tilde{\Omega}_{k=2}(1, 2, \dots, i, I_1) = \Omega_{k=2}(1, 2, \dots, i) \wedge d\log \frac{\langle I_1 i \rangle}{\langle I_1 1 \rangle} \quad (4.6.25)$$

Interestingly the last triangle is very degenerate, therefore there is indeed only one non-trivial ratio we can construct as  $\langle 1I_1 \rangle = \langle 1i \rangle$ . In some sense it is a dlog form on

the line rather than a “half-dlog form” on a triangle. Similarly, the other reduced dlog form is

$$\tilde{\Omega}_{k=2}(I_2, j+1, \dots, n, 1) = \Omega_{k=2}(j+1, \dots, n, 1) \wedge d\log \frac{\langle I_2 j+1 \rangle}{\langle I_2 1 \rangle} \quad (4.6.26)$$

Everything combined, we can write the holomorphic dlog form for the general NMHV configuration associated with the  $R$ -invariant  $\mathcal{R}_{1,i+1,j+1}$  as

$$\begin{aligned} \Omega_{k=3} &= \Omega_{k=2}(1, \dots, i) \wedge \Omega_{k=2}(I_1, i+1, \dots, j, I_2) \wedge \Omega_{k=2}(j+1, \dots, n, 1) \\ &\wedge d\log \frac{\langle I_1 i \rangle}{\langle I_1 1 \rangle} \wedge d\log \frac{\langle I_2 j+1 \rangle}{\langle I_2 1 \rangle} \end{aligned} \quad (4.6.27)$$

which is the wedge product of three MHV amplitude dlog forms with two extra dlogs. We checked explicitly that the formula (4.6.27) is equivalent to (4.6.17) .

As an example, the 8-dimensional cell in  $G_+(3, 6)$  for  $(123) = 0$  turns into

$$\Omega_{6,3} = \Omega_{k=2}(1, 2, 3) \wedge \Omega_{k=2}(I_1, 4, 5, I_2) \wedge d\log \frac{\langle 13 \rangle}{\langle 3I_1 \rangle} \wedge d\log \frac{\langle 16 \rangle}{\langle 1I_2 \rangle} \quad (4.6.28)$$

where the  $I_1$  and  $I_2$   $\lambda$ -spinors are defined as

$$\lambda_{I_1} = (45)|6] \cdot \frac{\langle 13 \rangle}{\langle 1|23|6]}, \quad \lambda_{I_2} = \langle 1|(23)(45) \cdot \frac{\langle 16 \rangle}{\langle 1|(23)(45)|1]} \quad (4.6.29)$$

Our construction uses only holomorphic data and the dlog form is a wedge product of rational functions which only depend on the  $\lambda$ -part of  $1, 2, \dots, n$  and  $I_1, I_2$ . Obviously, the final form must also have a dependence on  $\tilde{\lambda}$ s of external momenta, which comes exclusively through the dependence on  $\lambda_{I_1}$  and  $\lambda_{I_2}$ . While the forms in [216] and the ones presented here, are completely equivalent, the holomorphicity of our representation is indicative of the geometric fact that the answer was built from the dlog forms on three lines. This underscores the notion that we can think about the Grassmannian geometry picture directly in the kinematical space. It is suggestive that the same construction can be used for higher  $k$  to build the  $N^k$ MHV dlog form from the MHV dlog forms on individual lines.



### 4.6.3 Non-planar generalization

The formula for the dlog form from the previous section directly generalizes to the non-adjacent BCFW terms and the non-planar positive geometry. Let us directly consider the general case,

(4.6.30)

The strategy is the same as before, write the dlog form for the middle line and partial dlog forms on the other two lines with two compensating terms. On the first line, the points are cyclically ordered  $(1, 2, \dots, i, I_1, i+1, \dots, j) = (i+1, \dots, j, 1, 2, \dots, i, I_1)$ . The final formula for the dlog form is

$$\begin{aligned} \Omega &= \Omega_{k=2}(i+1, \dots, j, 1, 2, \dots, i) \wedge \Omega_{k=2}(I_1, j+1, \dots, k, I_2, k+1, \dots, m) \\ &\quad \wedge \Omega_{k=2}(m+1, \dots, n) \wedge d\log \frac{\langle I_1 i \rangle}{\langle I_1 i+1 \rangle} \wedge d\log \frac{\langle I_2 m+1 \rangle}{\langle I_2 1 \rangle} \end{aligned} \quad (4.6.31)$$

where the spinors  $\lambda_{I_1}$  and  $\lambda_{I_2}$  are given by (4.6.21),

$$\lambda_{I_1} = \langle 1 | P_3 P_2 \cdot \frac{\langle 1 i \rangle}{\langle 1 | P_1 P_3 | 1 \rangle}, \quad \lambda_{I_2} = \langle 1 | P_1 P_2 \cdot \frac{\langle 1 j+1 \rangle}{\langle 1 | P_1 P_3 | 1 \rangle} \quad (4.6.32)$$

with  $P_1, P_2, P_3$  being the sums of momenta on the three lines excluding  $p_1$ . The formula for the dlog form (4.6.31) is basically identical to the planar counterpart (4.6.27), though we had to be careful about which extra dlog factor to add to the first line. Note that the argument here is  $\langle I_1 i \rangle / \langle I_1 i+1 \rangle$  from the triangle  $(i, I_1, i+1)$ . This triangle is not degenerate, so we can not use  $\langle i i+1 \rangle$  in the argument (this is indeed not a pole).

As an example, we do two 6-point non-planar configurations,

$$(4.6.33)$$

In the first case, we get

$$\Omega = \Omega_{k=2}(1, 2, 3) \wedge \Omega_{k=2}(I_1, 4, I_2, 5) \wedge d\log \frac{\langle I_1 3 \rangle}{\langle I_1 1 \rangle} \wedge d\log \frac{\langle I_2 6 \rangle}{\langle I_2 1 \rangle} \quad (4.6.34)$$

where  $I_1$  and  $I_2$  spinors are

$$\lambda_{I_1} = (45)|6] \cdot \frac{\langle 13 \rangle}{\langle 1|23|6]}, \quad \lambda_{I_2} = \langle 1|(23)(45) \cdot \frac{1}{\langle 1|23|6]}. \quad (4.6.35)$$

In the second example, the dlog form is

$$\Omega = \Omega_{k=2}(I_1, 3, 4, I_2, 5) \wedge d\log \frac{\langle I_1 2 \rangle}{\langle I_1 1 \rangle} \wedge d\log \frac{\langle I_2 6 \rangle}{\langle I_2 1 \rangle} \quad (4.6.36)$$

where

$$\lambda_{I_1} = (12)|6] \cdot \frac{1}{[26]}, \quad \lambda_{I_2} = (16)|2] \cdot \frac{1}{[26]}. \quad (4.6.37)$$

As a result, we conclude that the same formula for the holomorphic dlog form works for the planar (4.6.27) as well as the non-planar (4.6.31) cases. The planarity/convexity of the configuration does not matter; the expression only depends on the Grassmannian configuration of points on three lines in  $\mathbb{P}^2$ . The holomorphicity of the dlog form (4.6.31) and the representation of the superfunction using Parke-Taylor factors (4.5.9) shows that we can indeed think about the Grassmannian configuration of points in  $\mathbb{P}^2$  as the collection of three lines directly in the kinematical  $\lambda$ -space.

## 4.7 N<sup>2</sup>MHV and Beyond

In the previous sections, we restricted our discussion to MHV and NMHV cases. In this section, we generalize our discussion of Grassmannian geometry for BCFW cells to N<sup>2</sup>MHV, considering both adjacent and non-adjacent shifts. The same construction extends to higher  $k$  and we outline how it works for arbitrary  $k$ .

### 4.7.1 $N^2$ MHV geometries

#### Planar geometries

Let us first consider the adjacent BCFW shift  $(n1)$ . At  $N^2$ MHV, we have three types of terms in the recursion,

$$(4.7.1)$$

As before, we can express these terms as sums of on-shell diagrams. For each diagram we construct the representative  $C$ -matrix and calculate the superfunction as a Grassmannian integral. Now the  $C$ -matrix, viewed as a collection of  $n$  columns, describes a configuration of  $n$  points in  $\mathbb{P}^3$ .

The Grassmannian geometries associated with factorizations into MHV and NMHV amplitudes can be built from the MHV and NMHV configurations we found in the previous sections. In the first term in (4.7.1), we have  $A^{k=2}(I, i+1, \dots, n-1, \hat{n})$ , a MHV amplitude, represented by a line, and  $A^{k=3}(I, \hat{1}, 2, \dots, i)$ , an NMHV amplitude, given by a sum over configurations of points localized on three lines (where we sum over all  $j, k$ ),

$$(4.7.2)$$

Gluing the MHV and NMHV configurations together at points 1 and  $I$  leads to  $N^2$ MHV configurations of  $n$  points on five lines in  $\mathbb{P}^3$ . Merging the MHV line  $A^{k=2}(1, 2, \dots, i, I)$

with the collection of NMHV configurations  $A^{k=3}(I, i+1, \dots, n-1, \hat{n})$  gives the second term in (4.7.1). As a result, we get a different configuration of  $n$  points on five lines in  $\mathbb{P}^3$ ,

(4.7.3)

Moreover, it can be shown recursively that the geometries for the last term in (4.7.1) are obtained by adding more points on the  $\hat{n}, n, 1$  line of an  $N^2$ MHV configuration. This recursive construction is similar to the NMHV case. The resulting configurations complement those associated with the first two terms and in the end, the  $N^2$ MHV amplitude can be written as a sum over on-shell functions corresponding to the cells in  $G_+(4, n)$  represented by two types of configurations,

(4.7.4)

where we sum over all  $1 < j < k < i < m < n$  and  $1 < i < j < k < m < n$  labels respectively (in the ordering indicated in the figures, subject to the constraint that there are always at least two points on each line). All these  $(2n-4)$ -dimensional configurations are *convex*, which means that all  $(4 \times 4)$  ordered minors of the  $C$  matrix are positive (or zero).

### Non-planar geometries

We can now extend our discussion of Grassmannian geometries for non-adjacent BCFW shifts to  $N^2$ MHV. The non-adjacent BCFW shifts produce three types of terms in the recursion relations, differing from (4.7.1) only by having  $k, 1$  non-consecutive:

$$(4.7.5)$$

Here the last term includes the BCFW term with  $\mathcal{A}_3^{k=1}(\widehat{k}, I, k-1)$  on the left and the one with  $\mathcal{A}_3^{k=1}(\widehat{k}, k+1, I)$  on the left. Associated with the first term is a sum of configurations arising from merging NMHV and MHV configurations,

$$(4.7.6)$$

where we only denoted labels as necessary for make the gluing procedure clear. All other labels are inherited from the MHV and NMHV configurations. Note that the only difference between (4.7.2) and (4.7.6) is that some points are “misplaced” on the lines, ie. they are on both sides of the intersections points with other lines, which makes the configurations non-convex. Hence these are configurations in the general Grassmannian  $G(4, n)$ , rather than in the positive part  $G_+(4, n)$ . Similarly, for the

second term we get

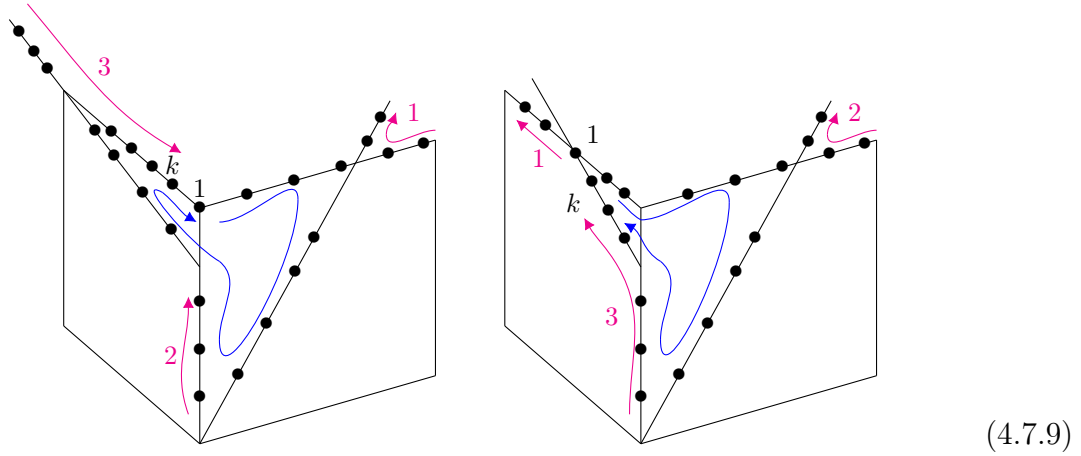
(4.7.7)

Finally, the third term, which is of the form  $((n-1)\text{-point } N^2\text{MHV}) \times (3\text{-point } \overline{\text{MHV}})$  corresponds to adding more points on the line connecting points  $k$  and  $1$ . As in the planar case, this can be shown recursively. In the end we get two types of configurations for the  $N^2\text{MHV}$  amplitude

(4.7.8)

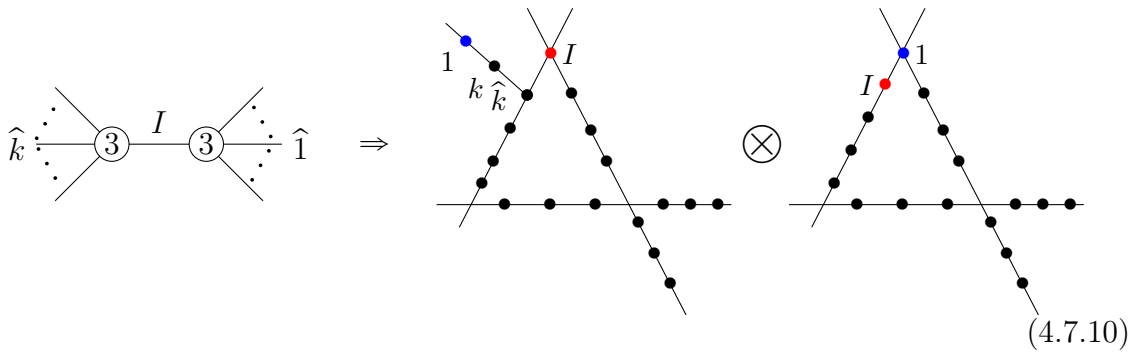
The BCFW expansion instructs us to sum over both topologies and the distribution of all labels which respect the relative ordering of  $2, \dots, k-1$  and  $k+1, \dots, n$ . It is easy

to see that the labels flows are

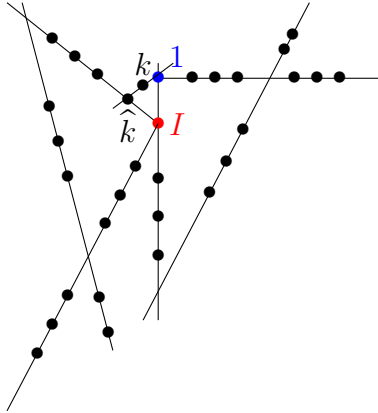


where the blue arrow represents points  $2, \dots, k-1$  and the red arrow points  $k+1, \dots, n$  (or vice versa). The red arrows go in order 1, 2, 3. The geometry configuration is projective (unlike our drawing), so the picture is actually symmetric in switching red and blue arrows (finite  $\leftrightarrow$  infinite intervals). Note that on three of the lines, the red and blue labels do not overlap, while on the remaining two lines they are mixed together, respecting the shuffle product ordering.

For higher  $k$ , we use the same procedure to glue together two geometries into a higher-dimensional configuration. For example, at  $N^3$ MHV the BCFW recursion for a  $(k1)$  shift contains a following term,



This gives rise to a configuration of  $n$  points in  $\mathbb{P}^4$ ,



$$(4.7.11)$$

This is hard to visualize, but we can see here two projective planes  $\mathbb{P}^2$ , which are glued together with an additional line ( $1\widehat{k}k$ ) that lives in an additional direction, making the space  $\mathbb{P}^4$  rather than  $\mathbb{P}^3$ . We can see that four of the lines have misplaced points, this generalizes to higher  $k$  as well. For general  $k$ , we have configurations of  $n$  points on  $2k - 3$  lines in  $\mathbb{P}^{k-1}$  where  $k-1$  lines have misplaced points.

#### 4.7.2 Holomorphic on-shell functions

From our study of MHV and NMHV amplitudes, we have seen that Grassmannian configurations, with the kinematic space interpretation, provide a fast track to the on-shell function. The geometrical formula expresses an NMHV amplitudes as a product of Parke-Taylor factors with auxiliary labels which encode special points in the Grassmannian configurations. Our goal in this subsection is to generalize this formula to  $N^2$  MHV and beyond.

#### On-shell functions from planar configurations

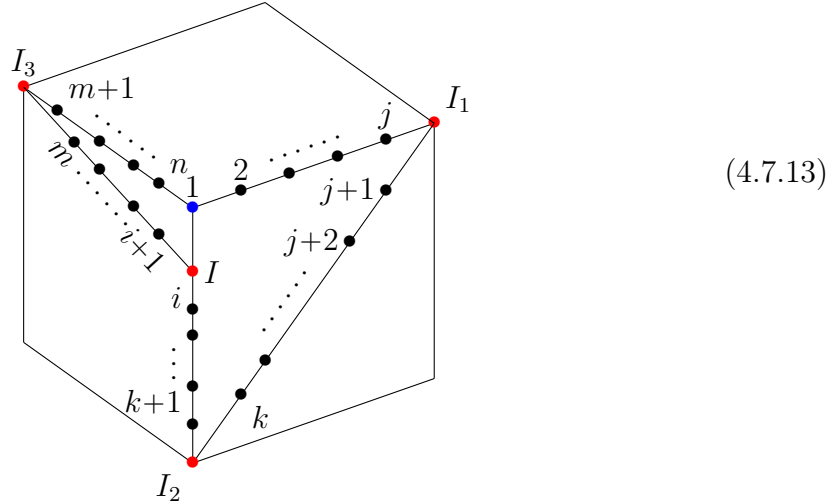
Let us begin with the planar configurations (4.7.4). Note that the five lines on which the points are localized lie in two different planes and each plane has three lines (with one line overlapping). This is precisely the structure encoded in the representation of the  $N^2$ MHV on-shell functions as a product of two  $R$ -invariants, [217],

$$\mathcal{F} = \frac{\delta^4(P)\delta^8(Q)}{\langle 12 \rangle \langle 23 \rangle \dots \langle n1 \rangle} \times R[a_1, a_2, a_3, a_4, a_5] R[b_1, b_2, b_3, b_4, b_5], \quad (4.7.12)$$



with each  $R$ -invariant being associated with one of the planes. The arguments of the  $R$ -invariants are shifted (super-)momentum twistors; the same entries can also be thought of as non-zero entries on the rows in the positive Grassmannian  $G_+(4, n)$ . This formula generalizes to higher  $k$  where each  $(2n-4)$ -dimensional configuration of  $n$  points in  $\mathbb{P}^{k-1}$  (localized on  $2k-3$  lines) gives rise to an on-shell function which can be expressed as a product of  $k$  copies of  $R$ -invariants with various shifted indices. Together they furnish a representation of the  $N^{k-2}$ MHV amplitude in terms of  $R$ -invariant products. For more details of this representation see [217].

Now back to the kinematic space of  $\{\lambda, \tilde{\lambda}, \eta\}$ . The formula (4.7.12) can be rewritten in terms of  $\lambda$ -spinors only with the introduction of some auxiliary spinors which correspond to special points in the Grassmannian configurations (4.7.4). The holomorphic expression consists of five Parke-Taylor factors. We start with the first convex configuration, and add intersection points  $I_1$ ,  $I_2$  and  $I_3$  in the figure,



To set up notation, we collectively label momenta on individual lines,

$$P_1^a = p_2 + \dots + p_j, \quad P_1^b = p_{j+1} + \dots + p_k, \quad P_1^c = p_{k+1} + \dots + p_i, \quad (4.7.14)$$

$$P_2 = p_{i+1} + \dots + p_m, \quad P_3 = p_{m+1} + \dots + p_n. \quad (4.7.15)$$

We also define  $P_1 = P_1^a + P_1^b + P_1^c$ . We need to associate momenta to the points  $I$ ,  $I_1$ ,  $I_2$  and  $I_3$ . The momentum  $p_I$  can be easily obtained directly from the BCFW term

and is analogous to the NMHV form,

$$p_I = \frac{\langle 1|P_3P_2 \times \langle 1|P_1}{\langle 1|P_1P_3|1\rangle}. \quad (4.7.16)$$

All other  $\lambda$ -spinors can be directly read off from the geometry following the same rules as we identified for  $I_1$  and  $I_2$  in the NMHV case. The first plane gives us,

$$\lambda_{I_2} = \langle 1|P_1^aP_1^b, \quad \lambda_{I_1} = \langle 1|(P_1^c + p_I)P_1^b. \quad (4.7.17)$$

substituting in  $p_I$  we get

$$\lambda_{I_1} = \langle 1|(P_1^a + P_1^b)P_1^b. \quad (4.7.18)$$

Similarly we can calculate  $\lambda_{I_3}$ , making the list of all  $\lambda$ -spinors we need

$$\lambda_I = \langle 1|P_3P_2, \quad \lambda_{I_1} = \langle 1|(P_1^a + P_1^b)P_1^b, \quad \lambda_{I_2} = \langle 1|P_1^aP_1^b, \quad \lambda_{I_3} = \langle 1|P_1P_2. \quad (4.7.19)$$

The superfunction which can be computed from (4.2.40) takes the familiar form of a product of Parke-Taylor factors,

$$\begin{aligned} \mathcal{F} &= PT(1, 2, \dots, j, I_1) \times PT(I_1, j+1, \dots, k, I_2) \times PT(I_2, k+1, \dots, i, I, 1) \\ &\quad \times PT(I, i+1, \dots, m, I_3) \times PT(I_3, m+1, \dots, n, 1) \\ &\quad \times \langle 1|P_1P_2\rangle^3 \cdot \langle 1|P_1^aP_1^b|1\rangle^3 \cdot \delta^8(\Xi). \end{aligned} \quad (4.7.20)$$

Note that we have two normalization factors coming from each of the planes  $\langle 1|P_1P_2\rangle^3$  and  $\langle 1|P_1^aP_1^b|1\rangle^3$ . Also,  $\langle 1I\rangle = \langle 1I_3\rangle = \langle 1|P_2P_3|1\rangle$  and  $\langle 1I_1\rangle = \langle 1I_2\rangle = \langle 1|P_1^aP_1^b|1\rangle$ . We have factored out and omitted momentum and super momentum-conserving delta functions  $\delta^4(P)\delta^8(Q)$  as usual. This can always be achieved by setting the first two rows of the  $C$ -matrix to  $\lambda$  with  $GL(4)$  gauge symmetry. What remains of the fermionic constraints  $\delta^{4 \times 4}(C \cdot \eta)$  evaluates to  $\delta^8(\Xi)$ , which can be written as a product of two NMHV delta functions,

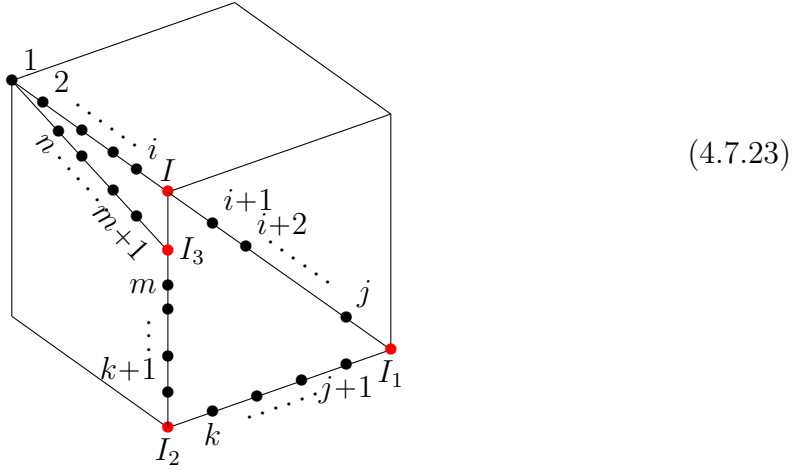
$$\delta^8(\Xi) = \delta^4(\Xi_1) \delta^4(\Xi_2). \quad (4.7.21)$$

corresponding to the third and fourth rows of the localized  $C$ -matrix. As one may expect, the expressions for  $\Xi_1$  and  $\Xi_2$  can be directly read from the Grassmannian geometry, focusing on one plane at a time,

$$\Xi_1 = \sum_{r \in P_1^b} \langle r | P_1^b P_1^a | 1 \rangle \eta_r + \sum_{s \in P_1^a} \langle 1 s | (P_1^b)^2 \eta_s, \quad \Xi_2 = \sum_{r \in P_2} \langle r | P_2 P_3 | 1 \rangle \eta_r + \sum_{s \in P_3} \langle 1 s | P_2^2 \eta_s. \quad (4.7.22)$$

Note that there are many ways to write the delta function on the support of super momentum conservation. As before, the arguments  $\Xi_1$  and  $\Xi_2$  do not depend on a particular ordering of points on the given lines.

The second configuration can be analyzed in a similar way



Denote

$$P_1 = p_2 + \dots + p_i, \quad P_2^a = p_{i+1} + \dots + p_j, \quad P_2^b = p_{j+1} + \dots + p_k, \\ P_2^c = p_{k+1} + \dots + p_m, \quad P_3 = p_{m+1} + \dots + p_n. \quad (4.7.24)$$

The momentum  $p_I$  in these conventions is

$$p_I = \frac{\langle 1 | P_3 P_2 \times \langle 1 | P_1}{\langle 1 | P_1 P_3 | 1 \rangle}, \quad (4.7.25)$$

and  $\lambda_I = \langle 1 | P_3 P_2$ . We can solve for the  $\lambda_{I_3}$  spinor from the first plane, to get  $\lambda_{I_3} = \langle 1 | P_1 P_2$ . The other two spinors can be obtained from the second plane, but now the

“center” is label  $I$  rather than 1,

$$\lambda_{I_1} = \langle I | (P_2^a + P_2^b) P_2^b, \quad \lambda_{I_2} = \langle I | P_2^a P_2^b. \quad (4.7.26)$$

The resulting superfunction is then

$$\begin{aligned} \mathcal{F} &= PT(1, 2, \dots, i, I) \times PT(I, i+1, \dots, j, I_1) \times PT(I_1, j+1, \dots, k, I_2) \\ &\times PT(I_2, k+1, \dots, m, I_3, I) \times PT(I_3, m+1, \dots, n, 1) \\ &\times \langle 1 | P_1 P_3 | 1 \rangle^3 \cdot \langle I | P_2^a P_2^b | I \rangle^3 \cdot \delta^8(\Xi). \end{aligned} \quad (4.7.27)$$

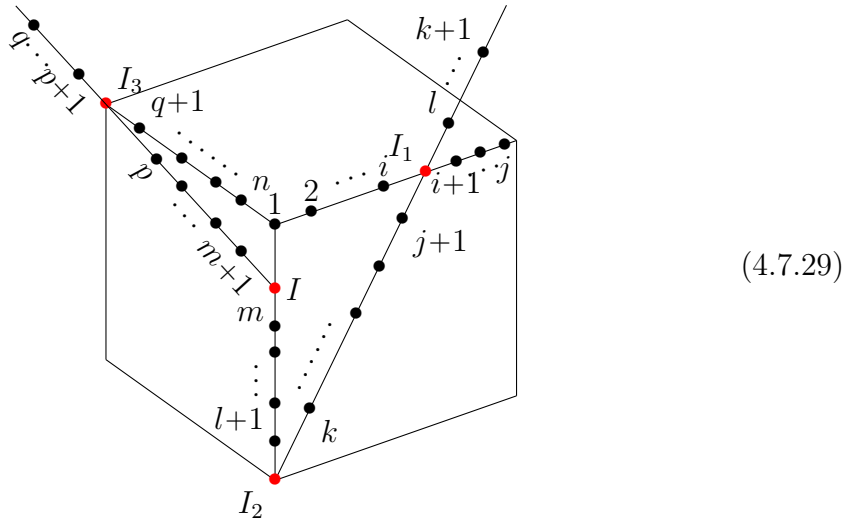
Following the same logic, we can factorize the fermionic delta function  $\delta^8(\Xi) = \delta^4(\Xi_1) \delta^4(\Xi_2)$ , where

$$\Xi_1 = \sum_{r \in P_3} \langle r | P_3 P_1 | I \rangle \eta_r + \sum_{s \in P_1} \langle I s | P_3^2 \eta_s, \quad \Xi_2 = \sum_{r \in P_2^b} \langle r | P_2^b P_2^a | I \rangle \eta_r + \sum_{s \in P_2^a} \langle I s | (P_2^b)^2 \eta_s. \quad (4.7.28)$$

Note that we used the supermomentum conservation in  $\Xi_1$  to eliminate  $\eta_{I_2}$ .

### On-shell functions from non-planar configurations

The configurations stemming from non-adjacent BCFW shifts follow an identical pattern: associate momenta for all intersection points  $I, I_1, I_2, I_3$  and take the product of Parke-Taylor factors, one for each line.



$$\begin{aligned}
\mathcal{F} &= PT(1, 2, \dots, i, I_1, i+1, \dots, j) \times PT(I_1, j+1, \dots, k, I_2, k+1, \dots, l) \\
&\times PT(I_2, l+1, \dots, m, I, 1) \times PT(I, m+1, \dots, p, I_3, p+1, \dots, q) \times PT(I_3, q+1, \dots, n, 1) \\
&\times \langle 1|P_1 P_2\rangle^3 \cdot \langle 1|P_1^a P_1^b|1\rangle^3 \cdot \delta^8(\Xi), \tag{4.7.30}
\end{aligned}$$

where the definitions of the variables  $P_1^a, P_1^b, P_1^c, P_1, P_2, P_3, I, I_1, I_2, I_3, \Xi$  are the same as in the planar configuration. Hence the normalization factors and the fermionic  $\delta$ -functions are identical. The only difference is the ordering of points in the Parke-Taylor factors.

The on-shell function (4.7.30) is a generalization of N<sup>2</sup>MHV Yangian invariants. Similar to the NMHV case, we can now decompose (4.7.30) into a linear combination of (4.7.27) with different orderings by rewriting the Parke-Taylor factors in (4.7.30). In (4.7.29), points are now misplaced on three of the lines. We use KK relations to rewrite the corresponding Parke-Taylor factors using terms which have  $(1, I_1), (I_1, I_2)$  and  $(I, I_3)$  adjacent,

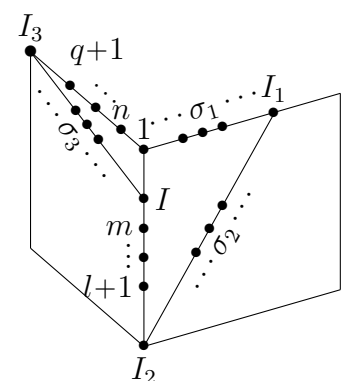
$$PT(1, 2, \dots, i, I_1, i+1, \dots, j) = \sum_{\sigma_1 \in \Sigma_1} PT(1, \sigma_1, I_1), \tag{4.7.31}$$

$$PT(I_1, j+1, \dots, k, I_2, k+1, \dots, l) = \sum_{\sigma_2 \in \Sigma_2} PT(I_1, \sigma_2, I_2), \tag{4.7.32}$$

$$PT(I, m+1, \dots, p, I_2, p+1, \dots, q) = \sum_{\sigma_3 \in \Sigma_3} PT(I, \sigma_3, I_3), \tag{4.7.33}$$

where  $\Sigma_1 = \{1, 2, \dots, i\} \sqcup \{i+1, \dots, j\}^T$ ,  $\Sigma_2 = \{j+1, \dots, k\} \sqcup \{k+1, \dots, l\}^T$  and finally  $\Sigma_3 = \{m+1, \dots, p\} \sqcup \{p+1, \dots, q\}^T$ . As before,  $\sqcup$  denotes a shuffle product and  $\{\}^T$  denotes reversal of ordering. Plugging back into (4.7.30) we get a linear combination

of Yangian-invariants,

$$\mathcal{F} = \sum_{\sigma_1, \sigma_2, \sigma_3} \mathcal{F}(1, \sigma_1, \sigma_2, l+1, \dots, m, \sigma_3, q+1, \dots, n) = \sum_{\substack{\sigma_1 \in \Sigma_1 \\ \sigma_2 \in \Sigma_2 \\ \sigma_3 \in \Sigma_3}} \mathcal{F}(1, \sigma_1, \sigma_2, l+1, \dots, m, \sigma_3, q+1, \dots, n) \quad (4.7.34)$$


**Higher  $k$**  The geometrical formula for on-shell functions extends to higher  $k$ . Regardless of planarity, an on-shell function that originates from BCFW recursion has the following structure

$$\mathcal{F} = \prod_{\text{lines}} PT(\dots) \times \prod_{\text{planes}} J \times \prod_{\text{planes}} \delta^4(\Xi). \quad (4.7.35)$$

For any non-planar  $N^k$ MHV configuration that originates from non-adjacent BCFW shifts, applying KK relations to its Parke-Taylor factors allows us to rewrite the on-shell function as a linear combination of Yangian-invariants, each of which correspond to planar configurations with various orderings.

## 4.8 Conclusion

In this chapter, we discussed non-adjacent BCFW recursion relations and the connection between individual terms and Grassmannian geometry. We found that each term corresponds to a particular cell in the Grassmannian  $G(k, n)$  which we identified using configurations of  $n$  points in  $\mathbb{P}^{k-1}$ . These Grassmannian cells are similar to the  $2n-4$  dimensional cells in the positive Grassmannian  $G_+(k, n)$  which are associated with adjacent BCFW terms, but their underlying configurations of points do not have one fixed ordering. In fact, there are two separate orderings of all points which lie between the two shifted legs 1 and  $k$ . We mostly focused on the NMHV case, extending

the analysis of MHV on-shell diagrams and geometries in [99]. We outlined a general structure beyond NMHV in Section 4.7.

We also found a new representation of the on-shell functions associated with these geometries, both planar and non-planar, as the product of Parke-Taylor factors localized on each line in Grassmannian space. We identified momenta associated with intersection points  $I_k$ , which then entered the arguments of the Parke-Taylor factors. As a result, the on-shell forms were purely holomorphic in  $\lambda$  and the only non-holomorphicity (dependence on  $\tilde{\lambda}$ ) came from the dependence on special points  $\lambda_{I_k}$ . This is a very interesting picture because it allows us to think about the Grassmannian geometry directly in the momentum space. This connection is trivial for the MHV case but it seems to have a lot of non-trivial structure for higher helicity sectors. The representation using Parke-Taylor factors allowed us to use Kleiss-Kuijf relations and rewrite any BCFW non-planar superfunction as a linear combination of planar super functions with various orderings. For a fixed ordering, the on-shell superfunction can be written as a product of  $R$ -invariants and enjoys the infinite-dimensional Yangian symmetry. Whether the Yangian structure survives in any form beyond the planar limit where the ordering is lost is an important open question, and the simple relation between the planar and non-planar on-shell functions offers a window into future investigation.

Our work opens a new direction of study of non-planar on-shell functions and geometries in  $\mathcal{N} = 4$  sYM theory. The BCFW building blocks belong to a larger family of non-planar on-shell diagrams, which appear as cuts of loop integrands to any loop order. Each non-planar on-shell diagram is associated with some Grassmannian geometry, but the concrete description is unclear. We made a first step in this direction by identifying the Grassmannian geometries associated with BCFW cells. It would be very interesting to learn what the positive geometries for all non-planar on-shell diagrams are, and find a direct way to evaluate the on-shell functions.

# Chapter 5

## Summary

In this thesis, we discussed various questions regarding the geometrization of scattering amplitudes in supersymmetric Yang-Mills theories. Within the context of  $\mathcal{N} = 4$  sYM, we explored the geometric role of local expansions of scattering amplitudes and their relations to the original and the putative dual amplituhedron. To find the amplituhedron-like geometric structures for less supersymmetric theories, a crucial first stepping stone is having a unique integrand. To this end, we showed two natural on-shell prescriptions for defining the  $\mathcal{N} = 1, 2$  one-loop amplitude integrands and several concrete constructions using a prescriptive unitarity method. Finally, there is a larger open question of extending the geometrical framework beyond the planar sector. Given the key role played by the correspondence between on-shell diagrams and positive Grassmannian as well as the on-shell diagrammatic realization of BCFW recursions in the geometric reformulation of the planar theory, we investigated the Grassmannian geometries of non-planar on-shell diagrams in the context of BCFW recursions. Below we summarize the main points of each chapter.

In chapter 2, we initiated the systematic study of *local positive spaces* arising in the context of the Amplituhedron construction for scattering amplitudes in planar maximally supersymmetric Yang-Mills theory. We showed that all local positive spaces relevant for one-loop MHV amplitudes are characterized by certain sign-flip conditions



and are associated with surprisingly simple logarithmic forms. In the maximal sign-flip case they are finite one-loop octagons. Particular combinations of sign-flip spaces can be glued into new local positive geometries. These correspond to local pentagon integrands that appear in the local expansion of the MHV one-loop amplitude. We showed that, geometrically, these pentagons do *not* triangulate the original Amplituhedron space but rather its twin “Amplituhedron-Prime.” This new geometry has the same boundary structure as the Amplituhedron (and therefore the same logarithmic form) but differs in the bulk as a geometric space. On certain two-dimensional boundaries, where the Amplituhedron geometry reduces to a polygon, we checked that both spaces map to the same dual polygon. Interestingly, we found that the pentagons internally triangulate that dual space. This gives direct evidence that the chiral pentagons are natural building blocks for a yet-to-be-discovered dual Amplituhedron.

In chapter 3, we constructed a prescriptive, bubble power-counting basis of one-loop integrands suitable for representing amplitude integrands in less-supersymmetric ( $1 \leq \mathcal{N} \leq 4$ ) Yang-Mills theory. With the exception of massless bubbles, all integrands have unambiguous, leading singularities as coefficients defined in field theory; for the massless bubbles on external legs, we found two natural choices which lead to different integrands that highlight distinct aspects of field theory. We showed explicit representations of the all-multiplicity integrands for MHV amplitudes, and the split-helicity amplitude integrand for six-particle NMHV. The basis we constructed is mostly pure and is divided into to separately UV- and IR-finite sectors of fixed transcendental weight, resulting in UV- and IR-finite ratio functions of  $n$ -particle helicity amplitudes.

In chapter 4, we studied non-adjacent BCFW recursion relations and their connection to positive geometry. For an adjacent BCFW shift, the  $n$ -point  $N^k$ MHV tree-level amplitude in  $\mathcal{N} = 4$  sYM theory is expressed as a sum over planar on-shell diagrams, corresponding to canonical “dlog” forms on the cells in the positive Grassmannian  $G_+(k, n)$ . Non-adjacent BCFW shifts naturally lead to an expansion of the amplitude in terms of a different set of objects, which do not manifest the cyclic ordering and

the hidden Yangian symmetry of the amplitude. We showed that these terms can be interpreted as dlog forms on the *non-planar positive geometries*, generalizing the cells of the positive Grassmannian  $G_+(k, n)$  to a larger class of objects which live in  $G(k, n)$ . We focused mainly on the case of NMHV amplitudes and discussed in detail the Grassmannian geometries. We also proposed an alternative way to calculate the associated on-shell functions and dlog forms using an intriguing connection between Grassmannian configurations and the geometry in the kinematical space.

# Appendix A

## Configuration of lines in momentum twistor space

There is an intimate relation between configurations of (loop) lines in momentum twistor space and certain restricted kinematic configurations of loop momenta on unitarity cuts of loop integrands or local integrals. At one loop, we can depict the off-shell configuration of lines in twistor space corresponding to a generic loop integrand (either of the amplitude or of an integral) by a set of lines corresponding to external dual momenta, together with a line  $(AB)$  in a generic configuration (parameterized via eq. (2.2.2)),

(A.0.1)

In this setup, the loop-line  $(AB)$  does not intersect any of the lines associated to external kinematic points. In the next step, one could go to codimension-one configurations by

imposing one condition, e.g.  $\langle ABii+1 \rangle = 0$ , so that the lines  $(AB)$  and  $(ii+1)$  intersect.

$$(A.0.2)$$

At the level of cuts, this corresponds to setting a single propagator  $\langle ABii+1 \rangle = 0$  to zero. This codimension-one configuration for the line  $(AB)$  can be parameterized by three degrees of freedom. The intersection implies that one of the defining points of the  $(AB)$ -loop lies on the line  $(ii+1)$ . Taking into account the projectivity of the  $Z$ 's, one possible particular parametrization is

$$Z_A = Z_i + \alpha_1 Z_{i+1}, \quad Z_B = Z_j + \alpha_2 Z_k + \alpha_3 Z_l. \quad (A.0.3)$$

In a second step, one can impose an additional constraint to end up on a codimension-two configuration of the line  $(AB)$ . Depending on the condition one imposes, there are three situations to consider

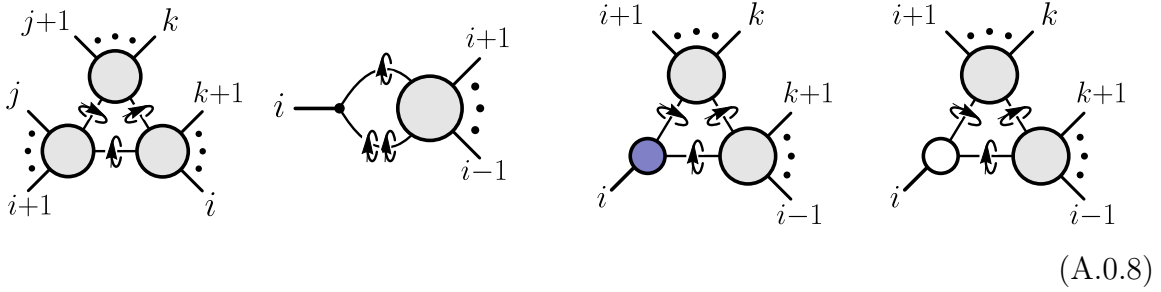
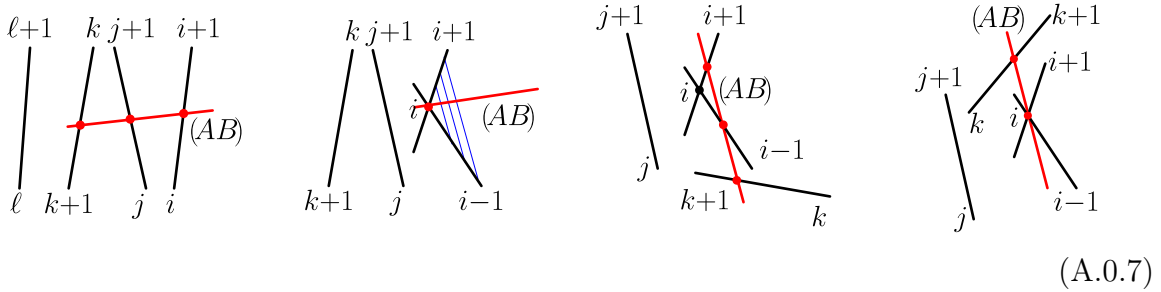
$$(A.0.4)$$

$$(A.0.5)$$

which have explicit two-dimensional parametrizations of the solution for the line  $(AB)$  given by,

$$\begin{aligned} Z_A^{(1)} &= Z_i + \gamma_1 Z_{i+1}, & Z_A^{(2)} &= Z_i + \gamma_1 Z_{i+1}, & Z_A^{(3)} &= Z_i, \\ Z_B^{(1)} &= Z_j + \gamma_2 Z_{j+1}, & Z_B^{(2)} &= Z_i + \gamma_2 Z_{i-1}, & Z_B^{(3)} &= Z_j + \gamma_1 Z_k + \gamma_2 Z_l. \end{aligned} \quad (A.0.6)$$

We can continue by imposing yet further constraints. At codimension-three, for the first time we encounter the situation associated with a *composite* residue where we localize the loop-line into a collinear configuration, depicted in the second figure below.

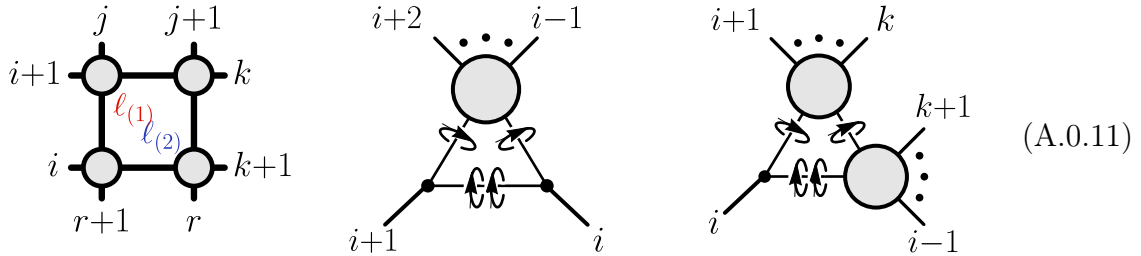
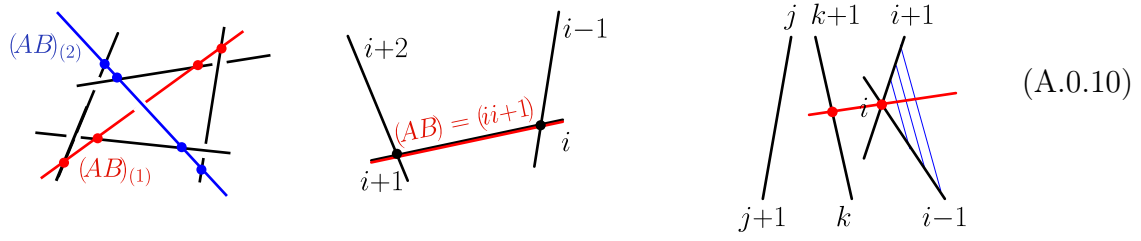


Here we have omitted two special configurations where the loop line  $(AB)$  intersects three consecutive external lines  $(i-2i-1)$ ,  $(i-1i)$  and  $(ii+1)$ . For the solutions depicted above, we can write one-parametric representations of the solution space for  $(AB)$ . The generic solution is a bit involved, so here we only give the parametrization for the simple configuration where  $(AB)$  is in the plane  $(i-1ii+1)$  and passes through the point  $Z_i$ ,

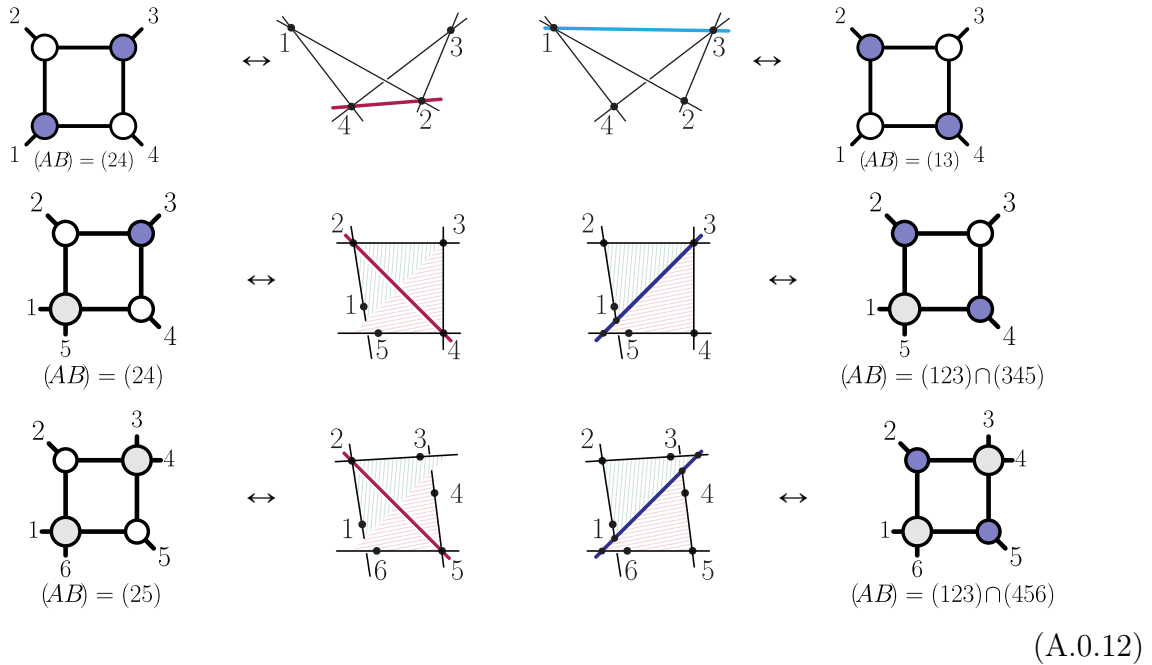
$$Z_A^{(2)} = Z_i, \quad Z_B^{(2)} = Z_{i-1} + \delta Z_{i+1}. \quad (\text{A.0.9})$$

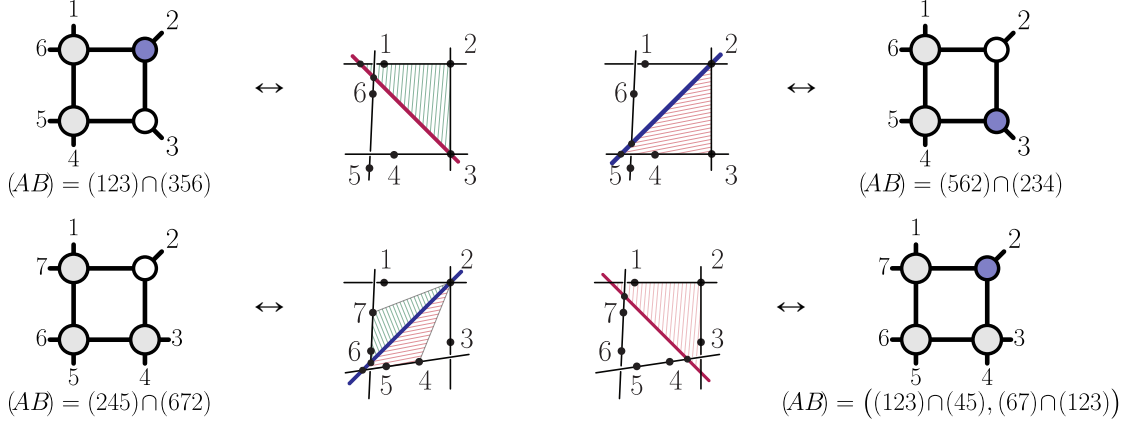
Finally, we can discuss codimension-four configurations of the line  $(AB)$  where all degrees of freedom are completely fixed. Such configurations are related to leading singularities. Again, there are various cases to consider, some of which correspond to soft composite residues that are physical, as well as spurious residues where scattering

amplitudes have no support (see the figure on the right below)



Besides the generic “four-mass” configuration depicted in the left figure above, we can have special kinematic configurations where some of the external lines intersect (corresponding to massless corners in diagrams) and the Schubert problem simplifies.





For the maximal codimension configurations, we have explicitly written the final configuration of the loop-line  $(AB)$  in terms of external twistors only. In these formulae, certain geometric quantities appear that we briefly discuss for completeness. In particular,  $(abc) \cap (def)$  denotes the intersections of two planes, spanned by twistors  $\{Z_a, Z_b, Z_c\}$  and  $\{Z_d, Z_e, Z_f\}$  respectively. In  $\mathbb{P}^3$ , the intersection of two planes is a line, which can be represented as

$$\begin{aligned}
 (abc) \cap (def) &= Z_a Z_b \langle cdef \rangle + Z_b Z_c \langle adef \rangle + Z_c Z_a \langle bdef \rangle \\
 &= \langle abcd \rangle Z_e Z_f + \langle abc f \rangle Z_d Z_e + \langle abce \rangle Z_f Z_d
 \end{aligned}
 \tag{A.0.13}$$

Additionally, there are points defined by the intersection of a line  $(ab)$  and a plane  $(cde)$ , which can be represented as

$$(ab) \cap (cde) = Z_a \langle bcde \rangle + Z_b \langle cdea \rangle = -(Z_c \langle deab \rangle + Z_d \langle eabc \rangle + Z_e \langle abcd \rangle), \tag{A.0.14}$$

which naturally reflects the antisymmetry  $(ab) \cap (cde) = -(cde) \cap (ab)$ .

## A.1 External triangulations

In this section we focus on *external triangulations*, as a first application of the systematic classification of the sign-flip spaces introduced in section 2.4. As discussed briefly in section 2.2.4, an external triangulation of a space introduces a “larger” space *outside* of the original region using spurious vertices which violate the original positivity conditions. In the context of the sign-flip spaces above, this corresponds to flipping the

signs of some brackets which defined the original space. As a warm-up, let us go back to the projective plane  $\mathbb{P}^2$ , where the analog of a line  $(AB)$  in  $\mathbb{P}^3$  is a point  $Y$  on the plane with two degrees of freedom. As heuristically described above, we can externally triangulate the quadrilateral with vertices  $z_1, z_2, z_3, z_4$  with two triangles,

$$= \begin{array}{c} 2 \\ \text{(12)} \quad \text{(23)} \\ \text{(34)} \\ \text{(12)} \cap \text{(34)} \end{array} - \begin{array}{c} \text{(41)} \\ 1 \quad 4 \\ \text{(12)} \quad \text{(34)} \\ \text{(12)} \cap \text{(34)} \end{array} \quad (\text{A.1.1})$$

Note that the codimension-one boundaries of each triangle (which are lines in  $\mathbb{P}^2$ ) are subsets of boundaries of the original quadrilateral, but there is an additional spurious vertex  $(12) \cap (34) := z_1 \langle 234 \rangle - z_2 \langle 134 \rangle$  which is used as a triangulation point that cancels between triangles.<sup>1</sup> We can also describe this triangulation in the language of the previous section as follows. The quadrilateral is defined by the following conditions:

$$\leftrightarrow \langle Y12 \rangle > 0, \langle Y23 \rangle > 0, \langle Y34 \rangle > 0, \langle Y14 \rangle > 0, \quad (\text{A.1.2})$$

where we used the same circle to visualize the constraints, but now for  $\langle Yii+1 \rangle$ . We can define the triangles in a similar way. Note that the first triangle with vertices  $\{(12) \cap (34), 2, 3\}$  in eq. (A.1.1) has an unfixed sign for  $\langle Y14 \rangle$  and therefore lacks this

<sup>1</sup>In this context, angle brackets denote contraction with a three-index Levi-Civita symbol, i.e.,  $\langle abc \rangle := \epsilon_{IJK} z_a^I z_b^J z_c^K$ .



codimension-one boundary. Pictorially this will be denoted by  $*$  for the relevant bracket in the circle-figures and can also be interpreted as marginalizing over both signs. Even though the second triangle with vertices  $\{(12) \cap (34), 1, 4\}$  has  $\langle Y_{23} \rangle > 0$  fixed, from the picture we see that this is not a boundary of the space. The two triangles are associated to the following circle diagrams:

(A.1.3)

(A.1.4)

In summary, we can re-interpret this triangulation as taking the space of the first triangle with unfixed sign of  $\langle Y_{14} \rangle$  and dividing it into two spaces: one where  $\langle Y_{14} \rangle > 0$ , which is the quadrilateral, and another where  $\langle Y_{14} \rangle < 0$  which is the second triangle.

(A.1.5)

$$\begin{array}{c} 2 \\ \circlearrowleft \\ 1 \quad 3 \\ * \\ \circlearrowright \\ 4 \end{array} = \begin{array}{c} 2 \\ \circlearrowleft \\ 1 \quad 3 \\ + \\ \circlearrowright \\ 4 \end{array} + \begin{array}{c} 2 \\ \circlearrowleft \\ 1 \quad 3 \\ - \\ \circlearrowright \\ 4 \end{array}$$

In  $\mathbb{P}^2$  the triangle is the simplest geometric space with non-vanishing form. If we remove one more boundary by marginalizing over the corresponding  $\langle Y_{ii+1} \rangle$ , we get a “wedge” defined by only two inequalities. In this case the canonical form vanishes, e.g.

$$\begin{array}{c} 2 \\ \circlearrowleft \\ 1 \quad 3 \\ * \\ \circlearrowright \\ 4 \end{array} \leftrightarrow \Omega = 0. \tag{A.1.6}$$

This vanishing can also be understood from the  $d \log$  form perspective as we need at least three brackets to form two independent projective ratios that enter the arguments of  $d \log$ 's.

### Simplest sign-flip spaces

We can almost verbatim generalize the above discussion to the configuration space of lines  $(AB)$  in  $\mathbb{P}^3$  relevant to the MHV one-loop positive geometry. In  $\mathbb{P}^3$ , the simplest space has four boundaries, and the corresponding logarithmic form is given by the box integrand. However, in this case we need to include one additional inequality which does not correspond to a boundary but is nonetheless required to define the chiral sign-flip-four space. In the simplest four-point example, we define the space

$$\begin{array}{c} 2 \\ \circlearrowleft \\ 1 \quad 3 \\ + \\ \circlearrowright \\ 4 \end{array} \leftrightarrow \omega_{1234}^{(4),-} = \frac{\langle 1234 \rangle^2}{\langle AB12 \rangle \langle AB23 \rangle \langle AB34 \rangle \langle AB14 \rangle} \equiv \begin{array}{c} 2 \quad 3 \\ \square \\ 1 \quad 4 \end{array} \tag{A.1.7}$$

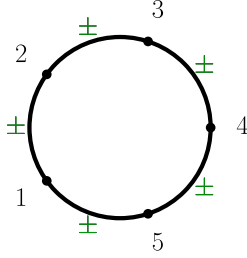
with  $\langle AB13 \rangle, \langle AB24 \rangle < 0$ . The second chiral region has  $\langle AB13 \rangle, \langle AB24 \rangle > 0$  and its form is the same up to a sign,  $\Omega_{1234}^{(4),+} = -\Omega_{1234}^{(4),-}$ . The union of these two regions is an achiral space which has vanishing form and unfixed signs for  $\langle AB13 \rangle$  and  $\langle AB24 \rangle$ ,

$$\begin{array}{c} 2 \\ \circlearrowleft \\ 1 \quad 3 \\ \circlearrowright \\ 4 \end{array} = \begin{array}{c} 2 \\ \circlearrowleft \\ 1 \quad 3 \\ \circlearrowright \\ 4 \\ \langle AB13 \rangle > 0 \\ \langle AB24 \rangle < 0 \end{array} + \begin{array}{c} 2 \\ \circlearrowleft \\ 1 \quad 3 \\ \circlearrowright \\ 4 \\ \langle AB13 \rangle < 0 \\ \langle AB24 \rangle < 0 \end{array} \quad (\text{A.1.8})$$

Directly at the level of  $d \log$  forms, four brackets  $\langle AB12 \rangle, \langle AB23 \rangle, \langle AB34 \rangle, \langle AB14 \rangle$  are insufficient to define four independent projective ratios that enter the arguments of the  $d \log$ s, and therefore the whole form must vanish. If we additionally impose  $\langle AB13 \rangle \gtrless 0$  to cut the space into chiral components, we have access to one further bracket to form four independent projective ratios, e.g.,  $\langle ABi+1 \rangle / \langle AB13 \rangle$ . The same argument applies to any other space with only four boundaries  $\langle ABi+1 \rangle$ . A less trivial example of that logic is the special sign-flip-two region we discussed in eq. (2.4.12). Even though there were many brackets with fixed signs, the space has only four boundaries – so we get a zero-form space if we drop the chiralization condition  $\langle ABi+2 \rangle \gtrless 0$ .

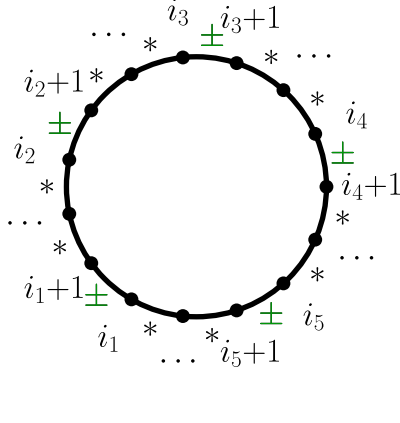
The simplest achiral space with non-vanishing form must therefore have five boundaries, and the integrand form is the general parity-odd pentagon (given by a suitable generalization of eq. (2.3.8) where none of the external legs need to be massless). In fact, because the achiral space is defined by a set of inequalities which all correspond to physical codimension-one boundaries, any of the  $2^5$  sign choices are allowed and lead to the same canonical form up to a sign. (This is distinct from the chiral components where only a subset of signs led to a consistent geometry.) For the five-point space we

get



$$\leftrightarrow \omega_5^{\text{odd}} = \frac{N_{\text{odd}}}{\langle AB12 \rangle \langle AB23 \rangle \langle AB34 \rangle \langle AB45 \rangle \langle AB15 \rangle}, \quad (\text{A.1.9})$$

where  $\pm$  indicates an arbitrary (but fixed) sign for the corresponding bracket. Exactly the same is true for higher points: if we marginalize over the signs of the  $n - 5$  brackets  $\langle ABii+1 \rangle$  for  $i \notin \{i_1, i_2, i_3, i_4, i_5\}$  and pick any of the  $2^5$  possible sign choices for the remaining  $\langle ABi_r i_r+1 \rangle$ , we find the general parity-odd pentagon



$$\leftrightarrow \omega_n^{\text{odd}} = \frac{N_{\text{odd}}}{\langle ABi_1 i_1+1 \rangle \langle ABi_2 i_2+1 \rangle \langle ABi_3 i_3+1 \rangle \times \langle ABi_4 i_4+1 \rangle \langle ABi_5 i_5+1 \rangle}, \quad (\text{A.1.10})$$

where  $\pm$  indicates that either sign choice is acceptable and  $*$  instructs us to marginalize over both sign choices.

In the rest of the section we will relate different sign-flip spaces via *external triangulations*, which allows us to write the canonical forms for more complicated spaces with many boundaries. In our discussion, we use several important facts:

1. Canonical forms of sign-flip-four spaces are chiral octagons, eq. (2.4.28), and descendants.
2. The form for a chiral space with four boundaries is a box.
3. The form for an achiral space with five boundaries is a parity-odd pentagon, eq. (A.1.10).

4. Any chiral space with three or fewer boundaries has vanishing form. Any achiral space with four or fewer boundaries has vanishing form.
5. Sign-flip-six and higher regions are empty; their form is identically zero.

### Triangulation of sign-flip-two regions

We first consider the chiral sign-flip-two space, with the additional condition  $\langle ABij \rangle > 0$ :

$$S_{ij}^{(2),+} = \begin{array}{c} \dots \\ i+1 \quad - \quad j-1 \\ \circ \quad \circ \\ \langle ABij \rangle > 0 \\ \circ \quad \circ \\ i \quad \quad j \\ + \quad \quad + \\ i-1 \quad + \quad j+1 \\ \dots \end{array} \quad (\text{A.1.11})$$

As stated in section 2.4, the codimension-one boundaries of this space correspond to the four brackets adjacent to the sign flips, as well as all other ‘negative’ brackets in the upper half of the circle, i.e.,

$$\text{boundaries: } \{\langle ABi-1i \rangle, \langle ABii+1 \rangle, \langle ABi+1i+2 \rangle, \dots, \langle ABj-1j \rangle, \langle ABjj+1 \rangle\}. \quad (\text{A.1.12})$$

(For the opposite chirality defined by  $\langle ABij \rangle < 0$ , the boundaries correspond to the four brackets adjacent to the sign flips, as well as the *positive* brackets in the lower half of the circle.) To externally triangulate this space, we use the fact that any space defined by four or fewer inequalities has a vanishing canonical form. Thus, if we marginalize over all signs in the sequence  $\{\langle ABi+1i+2 \rangle, \dots, \langle ABj-2j-1 \rangle\}$  but leave all other signs unchanged, the corresponding space has four boundaries, and is therefore trivially a two-mass-easy box form:

$$\begin{array}{c} \dots \\ i+1 \quad * \quad j-1 \\ \circ \quad \circ \\ \langle ABij \rangle > 0 \\ \circ \quad \circ \\ i \quad \quad j \\ + \quad \quad + \\ i-1 \quad + \quad j+1 \\ \dots \end{array} \leftrightarrow \begin{array}{c} i+1 \\ \diagdown \quad \diagup \\ i \quad \quad j-1 \\ \diagup \quad \diagdown \\ i-1 \quad \quad j \\ \diagdown \quad \diagup \\ j+1 \end{array} \quad (\text{A.1.13})$$

This fact can now be used in a “completeness relation” to determine the canonical form for  $S_{ij}^{(2),+}$ . If we expand eq. (A.1.13) in terms of regions with definite signs we encounter the sign-flip-two region whose form we want to determine, a collection of sign-flip-four regions, e.g.,

$$\begin{array}{c}
 \dots \\
 i+1 \quad + \quad - \quad j-1 \\
 \langle ABij \rangle > 0 \\
 i \quad - \quad + \quad j \\
 + \quad + \\
 i-1 \quad + \quad + \quad j+1 \\
 \dots
 \end{array} , \tag{A.1.14}$$

together with a number of sign-flip-six and higher regions which are empty. From this we can express the sign-flip-two region in terms of eq. (A.1.13) and sign-flip-four regions<sup>2</sup>

$$\begin{array}{c}
 k \quad - \quad - \quad \ell \\
 i+1 \quad - \quad - \quad j-1 \\
 \langle ABij \rangle > 0 \\
 i \quad - \quad + \quad j \\
 + \quad + \\
 i-1 \quad + \quad + \quad j+1 \\
 \dots
 \end{array} = \begin{array}{c}
 k \quad * \quad * \quad \ell \\
 i+1 \quad - \quad - \quad j-1 \\
 \langle ABij \rangle > 0 \\
 i \quad - \quad + \quad j \\
 + \quad + \\
 i-1 \quad + \quad + \quad j+1 \\
 \dots
 \end{array} - \sum_{\substack{k, \ell \\ \in \{i+1, \dots, j-1\}}} \begin{array}{c}
 k \quad + \quad + \quad \ell \\
 i+1 \quad - \quad - \quad j-1 \\
 \langle ABij \rangle > 0 \\
 i \quad - \quad + \quad j \\
 + \quad + \\
 i-1 \quad + \quad + \quad j+1 \\
 \dots
 \end{array} \tag{A.1.15}$$

Note that this is an external triangulation as also indicated by the minus sign between the two terms on the right-hand-side of eq. (A.1.15). Geometrically we remove sign-flip-four regions from eq. (A.1.13) leaving us with the chiral sign-flip-two region of interest. Since we already found all canonical forms associated to the regions on the right-hand-side of eq. (A.1.15), we can immediately write down the canonical form of

<sup>2</sup>In the achiral sign-flip-four space,  $\langle ABij \rangle > 0$  is automatically satisfied once we impose the ‘external’ inequalities. More details about these spaces and their fixed brackets are summarized in appendix A.2.

$$\begin{aligned}
& \Omega_{ij}^{(2),+}, \\
\Omega_{ij}^{(2),+} = & \begin{array}{c} i \\ \diagup \quad \diagdown \\ i-1 \quad j-1 \\ \diagdown \quad \diagup \\ j+1 \quad j \end{array} + \sum_{k, \ell \in \{i+1, \dots, j-1\}} \left[ \begin{array}{c} k+1 \quad \ell-1 \\ \diagup \quad \diagdown \\ k-1 \quad \ell+1 \\ \diagdown \quad \diagup \\ i-1 \quad j+1 \end{array} - \begin{array}{c} k+1 \quad \ell-1 \\ \diagup \quad \diagdown \\ k-1 \quad \ell+1 \\ \diagdown \quad \diagup \\ i-1 \quad j+1 \end{array} \right] \quad (\text{A.1.16})
\end{aligned}$$

where the sum over octagons includes all degenerations. Using this formula for the six-point example we find

$$\begin{aligned}
& \begin{array}{ccc} \begin{array}{c} 4 \quad - \quad 5 \\ \diagup \quad \diagdown \\ 3 \quad 6 \\ \diagdown \quad \diagup \\ 2 \quad + \quad 1 \end{array} & = & \begin{array}{c} 4 \quad * \quad 5 \\ \diagup \quad \diagdown \\ 3 \quad 6 \\ \diagdown \quad \diagup \\ 2 \quad + \quad 1 \end{array} & - & \begin{array}{c} 4 \quad + \quad 5 \\ \diagup \quad \diagdown \\ 3 \quad 6 \\ \diagdown \quad \diagup \\ 2 \quad + \quad 1 \end{array} \\
& \langle AB36 \rangle > 0 & \langle AB36 \rangle > 0 & \langle AB36 \rangle > 0 & & (\text{A.1.17}) \\
\Omega_{36}^{(2),+} = & \begin{array}{c} 3 \quad 4 \\ \diagup \quad \diagdown \\ 2 \quad 5 \\ \diagdown \quad \diagup \\ 1 \quad 6 \end{array} + \begin{array}{c} 4 \quad 5 \\ \diagup \quad \diagdown \\ 3 \quad 6 \\ \diagdown \quad \diagup \\ 2 \quad 1 \end{array} - \begin{array}{c} 4 \quad 5 \\ \diagup \quad \diagdown \\ 3 \quad 6 \\ \diagdown \quad \diagup \\ 2 \quad 1 \end{array}
\end{aligned}$$

As we discussed earlier in section 2.4, there are a few special cases of sign-flip-two regions. The most special case is the chiral sign-flip-two region with only a single minus sign eq. (2.4.13) which is an empty space with vanishing canonical form.

In this degenerate case, for the opposite chirality  $S_{ij}^{(2),-}$ , we can triangulate the space using exactly the same procedure, only with different boundary data: the region where all  $n - 3$  '+' signs are replaced by ' $\pm$ ' has vanishing form (as it only has three boundaries) and also the sign-flip-four regions are achiral rather than chiral. Therefore, the forms which appear on the right hand side are parity odd combinations of octagons (and descendants).

## Triangulation of sign-flip-zero region

As argued earlier in section 2.3.3, there is no external triangulation of MHV or  $\overline{\text{MHV}}$  Amplituhedra in terms of simple building blocks. However, this is not true for the achiral sign-flip-zero region eq. (2.4.7) which is defined by  $\langle ABii+1 \rangle > 0$  inequalities only. There are many ways to triangulate the  $S^{(0)}$  region externally. The simplest (though certainly not the most efficient) is to fix four plus signs and marginalize over all other signs. In light of our earlier discussions, such a region has vanishing canonical form, but when we expand  $*$  =  $+ \oplus -$  we find the sign-flip-zero region of interest



together with many sign-flip-two and four regions.

$$\begin{array}{c}
 \underbrace{\hspace{10em}}_{\text{zero-form space}} \quad \underbrace{\hspace{10em}}_{\text{achiral sf0 space}} \\
 \begin{array}{c}
 \text{Diagram 1: Circle with 12 points, alternating '+' and '*' signs} \\
 = \\
 \text{Diagram 2: Circle with 12 points, all '+' signs} \\
 \underbrace{\hspace{10em}}_{\text{achiral sf2 spaces}} \\
 + \\
 \begin{array}{c}
 \text{Diagram 3: Circle with 12 points, '+' signs, two '-' signs} \\
 + \\
 \text{Diagram 4: Circle with 12 points, '+' signs, two '-' signs} \\
 + \dots \\
 \underbrace{\hspace{10em}}_{\text{achiral sf4 spaces}} \\
 + \\
 \begin{array}{c}
 \text{Diagram 5: Circle with 12 points, '+' signs, four '-' signs} \\
 + \\
 \text{Diagram 6: Circle with 12 points, '+' signs, four '-' signs} \\
 + \dots \\
 \underbrace{\hspace{10em}}_{\text{empty sf6 and higher spaces with zero form}} \\
 + \\
 \begin{array}{c}
 \text{Diagram 7: Circle with 12 points, '+' signs, six '-' signs} \\
 + \text{ other empty regions.}
 \end{array}
 \end{array}
 \end{array}
 \end{array}
 \tag{A.1.18}$$

We already calculated the necessary canonical forms for all regions appearing in eq. (A.1.18) before in eqs. (2.4.28) and (A.1.16), which allows us to write the form for the sign-flip-zero space  $S^{(0)}$  eq. (2.4.7) more explicitly in terms of known quantities. Note that all sign-flip-two and four regions are achiral, so we must use the relevant parity-odd forms associated to those spaces by combining both chiralities in eqs. (2.4.28) and (A.1.16).

Having discussed the canonical forms of all sign-flip spaces, we now revisit to the

chiral pentagon expansion of eq. (2.2.45), together with the parity-odd one-loop amplitude given as the difference of the MHV and  $\overline{\text{MHV}}$  amplitudes. In the parity-odd case, the local expansion involves parity-odd pentagons, eq. (2.3.10), which can be associated to simple achiral spaces defined by only five inequalities (see our discussion earlier in this section) where the signs of these inequalities did not matter to get the correct parity-odd pentagon canonical form. The question is whether or not the parity-odd pentagon expansion eq. (2.3.10) can be understood geometrically as an external triangulation of some well-defined space. In other words: can we triangulate the sign-flip-zero space eq. (2.4.7) not via eq. (A.1.18), but in terms of spaces with five boundaries only? The answer is yes, and in the following we give a straightforward description of such a triangulation:

1. We start with the sign-flip-zero region  $S^{(0)}$  and triangulate it externally via the space with the sign of  $\langle AB12 \rangle$  marginalized,

$$\dots \begin{array}{c} + \\ \vdots \\ + \\ 3 \\ + \\ 2 \\ + \\ 1 \end{array} \begin{array}{c} + \\ \vdots \\ + \\ i \\ + \\ i+1 \\ \vdots \\ + \\ n \end{array} \dots = 3 \begin{array}{c} + \\ \vdots \\ + \\ 3 \\ + \\ 2 \\ * \\ 1 \end{array} \begin{array}{c} + \\ \vdots \\ + \\ i \\ + \\ i+1 \\ \vdots \\ + \\ n \end{array} \dots - 3 \begin{array}{c} + \\ \vdots \\ + \\ 3 \\ + \\ 2 \\ - \\ 1 \end{array} \begin{array}{c} + \\ \vdots \\ + \\ i \\ + \\ i+1 \\ \vdots \\ + \\ n \end{array} \dots \quad (\text{A.1.19})$$

2. For the region with  $\langle AB12 \rangle = *$  (i.e.,  $\langle AB12 \rangle \geq 0$  does not have a fixed sign), we continue by marginalizing over the sign of  $\langle AB23 \rangle$  leaving us with two spaces, one where  $\langle AB23 \rangle = *$ , and one where  $\langle AB23 \rangle < 0$ .

$$\dots \begin{array}{c} + \\ \vdots \\ + \\ 3 \\ + \\ 2 \\ + \\ 1 \end{array} \begin{array}{c} + \\ \vdots \\ + \\ i \\ + \\ i+1 \\ \vdots \\ + \\ n \end{array} \dots = 3 \begin{array}{c} + \\ \vdots \\ + \\ 3 \\ + \\ 2 \\ * \\ * \\ 1 \end{array} \begin{array}{c} + \\ \vdots \\ + \\ i \\ + \\ i+1 \\ \vdots \\ + \\ n \end{array} \dots - 3 \begin{array}{c} + \\ \vdots \\ + \\ 3 \\ + \\ 2 \\ - \\ * \\ 1 \end{array} \begin{array}{c} + \\ \vdots \\ + \\ i \\ + \\ i+1 \\ \vdots \\ + \\ n \end{array} \dots \quad (\text{A.1.20})$$

Whenever we encounter a space with a minus sign we stop, if we have \*'s only we continue. This procedure results in a collection of spaces  $S_i$  defined by

$$S_i := \{ \langle AB12 \rangle \geq 0, \dots, \langle ABi-2i-1 \rangle \geq 0, \langle ABi-1i \rangle < 0, \langle ABii+1 \rangle > 0, \dots, \langle AB1n \rangle > 0 \}, \quad i \in \{2, \dots, n-3\}, \quad (\text{A.1.21})$$

where, in the boundary case  $i = 2$ , we start with  $\langle AB12 \rangle < 0$ . Pictorially,  $S_i$  is represented by the following circle diagram

$$S_i = \text{circle diagram} \quad (\text{A.1.22})$$

This procedure stops at  $i = n - 3$  because we reach the end of the circle. Going beyond this point simply generates spaces with less than five boundaries that have vanishing form (and are therefore irrelevant for the purpose of obtaining the canonical form).

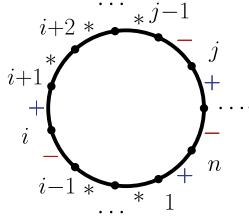
- In the third step, we continue the same procedure for each space  $S_i$  but leave  $\langle ABii+1 \rangle > 0$  untouched, marginalizing over  $\langle ABi+1i+2 \rangle$

$$\text{Diagram 1} = \text{Diagram 2} - \text{Diagram 3} \quad (\text{A.1.23})$$

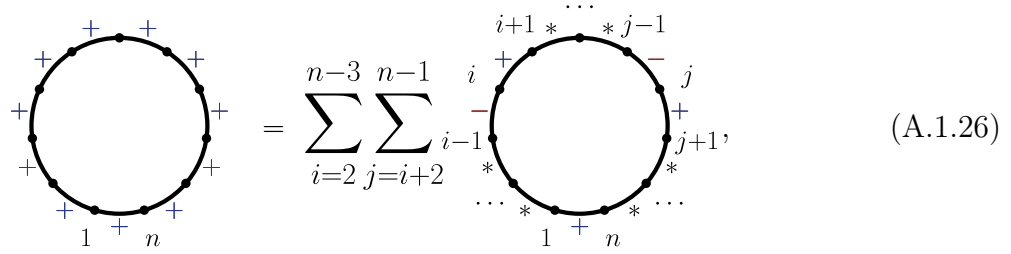
We again keep the spaces with two minus signs and marginalize further over the spaces where we have \*. As a result we generate a collection of spaces  $S_{ij}$ ,

$$S_{ij} = \text{circle diagram}, \quad i \in \{2, \dots, n-3\}, \quad j \in \{i+2, \dots, n-1\}. \quad (\text{A.1.24})$$

For each region  $S_{ij}$  the signs of  $\{\langle ABjj+1\rangle, \dots \langle AB1n\rangle\}$  are all positive. However, we can freely replace all but the  $\langle ABjj+1\rangle$  and  $\langle AB1n\rangle$  positive signs by  $+ \rightarrow *$ . This is because  $S_{ij}$  already has two non-adjacent minus signs; therefore, spaces where we introduce additional minus signs leads to empty sign-flip-six (or higher) regions, e.g.,

example of an empty region:  (A.1.25)

As a result, we triangulate the sign-flip-zero region  $S^{(0)}$  in eq. (2.4.7) in terms of spaces with five boundaries only,

 (A.1.26)

which, at the level of canonical forms, corresponds to the parity-odd pentagon expansion eq. (2.3.10). Note that on the right-hand side of eq. (A.1.26) we are suppressing spaces with zero-form which are necessary for the geometric triangulation, but unnecessary for the purposes of computing the canonical form. Geometrically, each space appearing in eq. (A.1.26) is equivalent to that of a pentagon where we forget about the signs of the last two brackets in eq. (2.3.19) (see also eq. (A.1.10)). The zero-form spaces implicit in eq. (A.1.26) demonstrates that while we were successful in interpreting the pentagon expansion eq. (2.3.10) geometrically, spaces with vanishing form had to be added in order to construct a full triangulation.

The natural question is why we can not use the same procedure to triangulate the MHV or  $\overline{\text{MHV}}$  Amplituhedra. The problem arises due to additional inequalities (such



No other signs of brackets are fixed inside  $S^{(0)}$  besides the ones indicated in eq. (A.2.1). We can cut this achiral region into two chiral components, which correspond to MHV and  $\overline{\text{MHV}}$  one-loop amplitudes by imposing the inequalities of eq. (2.2.31) and eq. (2.2.32), respectively. We denote the corresponding chiral spaces by  $S_{\text{MHV}}^{(0)}$  and  $S_{\overline{\text{MHV}}}^{(0)}$ . Concretely, the  $\overline{\text{MHV}}$  component  $S_{\overline{\text{MHV}}}^{(0)}$  can be defined by imposing additional  $n-3$  conditions eq. (2.2.32),

$$S_{\overline{\text{MHV}}}^{(0)} : \left\{ \begin{array}{l} \langle ABii+1 \rangle > 0 \quad i \in (1, \dots, n-1) \\ \langle AB1i \rangle > 0 \quad i \in (3, \dots, n-1) \end{array} \right\} \leftrightarrow \text{Diagram (A.2.2)}$$

Alternatively, imposing fixed signs for any sequence of brackets  $\{\langle AB2i \rangle > 0\}$  etc. leads to an equivalent definition of  $S_{\overline{\text{MHV}}}^{(0)}$ . While a given set of only  $n-3$  fixed signs for the additional brackets (such as  $\{\langle AB2i \rangle > 0\}$  in eq. (A.2.2)) is sufficient to define the  $\overline{\text{MHV}}$  region, in fact *all* brackets  $\langle ABij \rangle > 0$  (for  $i < j$ ) are fixed inside the  $S_{\overline{\text{MHV}}}^{(0)}$  region. Let us note that no signs of any other brackets are fixed inside  $S_{\overline{\text{MHV}}}^{(0)}$ .

The MHV chiral component is traditionally defined by a certain sign-flip constraint on the sequence  $\{\langle AB1i \rangle\}$ , see the  $k=0$  instance of eq. (2.2.12), but we can equivalently impose the  $n-3$  conditions of eq. (2.2.31),  $\{\langle AB\overline{1}i \rangle > 0\}$ ,  $i \in (3, \dots, n-1)$

$$S_{\text{MHV}}^{(0)} : \left\{ \begin{array}{l} \langle ABii+1 \rangle > 0 \quad i \in (1, \dots, n-1) \\ \langle AB\overline{1}i \rangle > 0 \quad i \in (3, \dots, n-1) \end{array} \right\} \leftrightarrow \text{Diagram (A.2.3)}$$

where we used dotted lines in the circle figure eq. (A.2.3) to denote the positivity of the respective  $\langle AB\overline{1}i \rangle$ . While this set of signs suffices to fix the MHV region, in fact all  $\langle AB\overline{1}j \rangle > 0$  (for  $i < j$ ) are positive inside  $S_{\text{MHV}}^{(0)}$ , but no other signs of brackets are fixed.

The achiral sign-flip-two space  $S_{ij}^{(2)}$  of eq. (2.4.14) is defined by a set of inequalities on  $\langle ABii+1 \rangle$  brackets only that we graphically represent as

$$S_{ij}^{(2)} \leftrightarrow \begin{array}{c} \dots \\ i+1 \quad - \quad - \quad j-1 \\ \circ \quad \circ \quad \circ \\ i \quad \quad \quad j \\ \circ \quad \circ \quad \circ \\ i-1 \quad + \quad + \quad j+1 \\ \dots \end{array} \quad (\text{A.2.4})$$

No other signs are fixed in  $S_{ij}^{(2)}$ . Compared to the sign-flip-zero space where we needed to impose  $n-3$  additional signs to chiralize the space, the achiral sign-flip-two region can be cut into two chiral components by fixing a single sign of the bracket  $\langle ABij \rangle$ . This bracket is extremely natural and involves the two positions  $i$  and  $j$  where the two sign-flips occur,

$$S_{ij}^{(2),+} : \{\text{eq. (A.2.4)}, \langle ABij \rangle > 0\} \leftrightarrow \begin{array}{c} \dots \\ i+1 \quad - \quad - \quad j-1 \\ \circ \quad \circ \quad \circ \\ i \quad \langle ABij \rangle > 0 \quad j \\ \circ \quad \circ \quad \circ \\ i-1 \quad + \quad + \quad j+1 \\ \dots \end{array}, \quad i < j,$$

$$S_{ij}^{(2),-} : \{\text{eq. (A.2.4)}, \langle ABij \rangle < 0\} \leftrightarrow \begin{array}{c} \dots \\ i+1 \quad - \quad - \quad j-1 \\ \circ \quad \circ \quad \circ \\ i \quad \langle ABij \rangle < 0 \quad j \\ \circ \quad \circ \quad \circ \\ i-1 \quad + \quad + \quad j+1 \\ \dots \end{array}, \quad i < j. \quad (\text{A.2.5})$$

In the  $S_{ij}^{(2),+}$  region we have a *fully positive index space* for certain brackets involving  $(j, j+1, \dots, i-1, i)$ . By this we mean that all signs of the following brackets are fixed to be positive:

$$S_{ij}^{(2),+} : \{\langle ABpq \rangle > 0, \langle AB\overline{pq} \rangle > 0\}, \text{ for } p < q \in \{i, i+1, \dots, j-1, j\}, \quad (\text{A.2.6})$$

where the inequalities on  $p, q$  are to be understood in the cyclic sense. In contrast, for  $S_{ij}^{(2),-}$ , arbitrary non-adjacent brackets of the “negative region” do not have fixed signs.

Similar to the discussion for  $S_{ij}^{(2),+}$ , for  $S_{ij}^{(2),-}$  we have

$$S_{ij}^{(2),-} : \{\langle ABpq \rangle < 0, \langle AB\bar{p}\bar{q} \rangle < 0\}, \quad \text{for } p < q \in \{i, i+1, \dots, j-1, j\}, \quad (\text{A.2.7})$$

in the *fully negative region* involving  $(i, i+1, \dots, j-1, j)$  the same set of brackets are fixed to be negative and the non-adjacent brackets in the “positive region” do not have a fixed sign. Note that the sign-inequalities eq. (A.2.6) and eq. (A.2.7) also apply for  $q = p+1$  where both  $\langle ABpq \rangle$  and  $\langle AB\bar{p}\bar{q} \rangle$  collapse to  $\langle ABpp+1 \rangle$  (up to a positive bracket of external twistors).

The sign-flip-four space  $S_{iklj}^{(4)}$  eq. (2.4.6) is given by four patches of positive and negative  $\langle ABaa+1 \rangle$  brackets, graphically represented as

$$S_{iklj}^{(4)} \leftrightarrow \begin{array}{c} \begin{array}{c} k+1 \quad \dots \quad \ell-1 \\ k \quad + \quad + \quad + \quad + \quad \ell \\ \dots \\ i+1 \quad - \quad - \quad - \quad - \quad j-1 \\ i \quad + \quad + \quad + \quad + \quad j \\ i-1 \quad + \quad \dots \quad + \quad j+1 \end{array} \end{array} \quad (\text{A.2.8})$$

In addition to these basic signs which define  $S_{iklj}^{(4)}$ , there are many more signs which are fixed automatically just from the  $\langle ABaa+1 \rangle$  conditions alone even *before* cutting the achiral space into its chiral sub-components. In fact, the four patches in index space are either fully positive or fully negative. This means that all signs of the following brackets are fixed

$$\begin{array}{l} \{\langle ABpq \rangle > 0, \langle AB\bar{p}\bar{q} \rangle > 0\}, \text{ for } \left[ \begin{array}{l} p < q \in \{j, j+1, \dots, i-1, i\} \\ p < q \in \{k, k+1, \dots, \ell-1, \ell\} \end{array} \right] \\ \{\langle ABpq \rangle < 0, \langle AB\bar{p}\bar{q} \rangle < 0\}, \text{ for } \left[ \begin{array}{l} p < q \in \{i, i+1, \dots, k-1, k\} \\ p < q \in \{\ell, \ell+1, \dots, j-1, j\} \end{array} \right] \end{array} \quad (\text{A.2.9})$$

Cutting  $S_{iklj}^{(4)}$  into two chiral components can be accomplished by specifying a *single sign* of one of the diagonals,  $\langle ABi\ell \rangle$ , or  $\langle ABkj \rangle$ . The first chiral component,  $S_{iklj}^{(4),+}$ ,



has both signs  $\langle ABi\ell \rangle, \langle ABkj \rangle > 0$  positive, while the second component,  $S_{iklj}^{(4),-}$  has both signs  $\langle ABi\ell \rangle, \langle ABkj \rangle < 0$  negative. But, in both cases fixing one sign implies the other. Hence we can represent the chiral components as:

$$S_{iklj}^{(4),+} \leftrightarrow \dots, S_{iklj}^{(4),-} \leftrightarrow \dots, \quad (A.2.10)$$

For each chiral component in eq. (A.2.10) the signs of many other brackets are automatically fixed. In addition to the signs eq. (A.2.9) that were already fixed in the achiral space  $S_{iklj}^{(4)}$ , we have

$$S_{iklj}^{(4),+} : \left[ \begin{array}{l} \langle ABpq \rangle > 0, \text{ for } p \in \{j, j+1, \dots, i-1, i\}, q \in (k, k+1, \dots, \ell-1, \ell) \\ \langle AB\overline{p\overline{q}} \rangle < 0, \text{ for } p \in (i, i+1, \dots, k-1, k), q \in (\ell, \ell+1, \dots, j-1, j) \end{array} \right]. \quad (A.2.11)$$

Note that these inequalities also cover the signs of the diagonals  $\langle ABi\ell \rangle > 0, \langle ABkj \rangle > 0$ , and also  $\langle ABi\overline{\ell} \rangle < 0, \langle AB\overline{k}j \rangle < 0$  so that in fact any single of these signs would be enough to specify the chiral subspace  $S_{iklj}^{(4),+}$ .

The other chiral subspace  $S_{iklj}^{(4),-}$  has a corresponding set of fixed brackets

$$S_{iklj}^{(4),-} : \left[ \begin{array}{l} \langle ABpq \rangle < 0, \text{ for } p \in \{j, j+1, \dots, i-1, i\}, q \in (k, k+1, \dots, \ell-1, \ell) \\ \langle AB\overline{p\overline{q}} \rangle > 0, \text{ for } p \in (i, i+1, \dots, k-1, k), q \in (\ell, \ell+1, \dots, j-1, j) \end{array} \right], \quad (A.2.12)$$

which also covers the boundary cases such as  $\langle ABi\ell \rangle < 0$  which is enough to define  $S_{iklj}^{(4),-}$ . Note that both set of signs for  $S_{iklj}^{(4),+}$  and  $S_{iklj}^{(4),-}$  are related by parity conjugation  $\langle ABpq \rangle \leftrightarrow \langle AB\overline{p\overline{q}} \rangle$ ; this is a consequence of the chiral nature of these spaces.

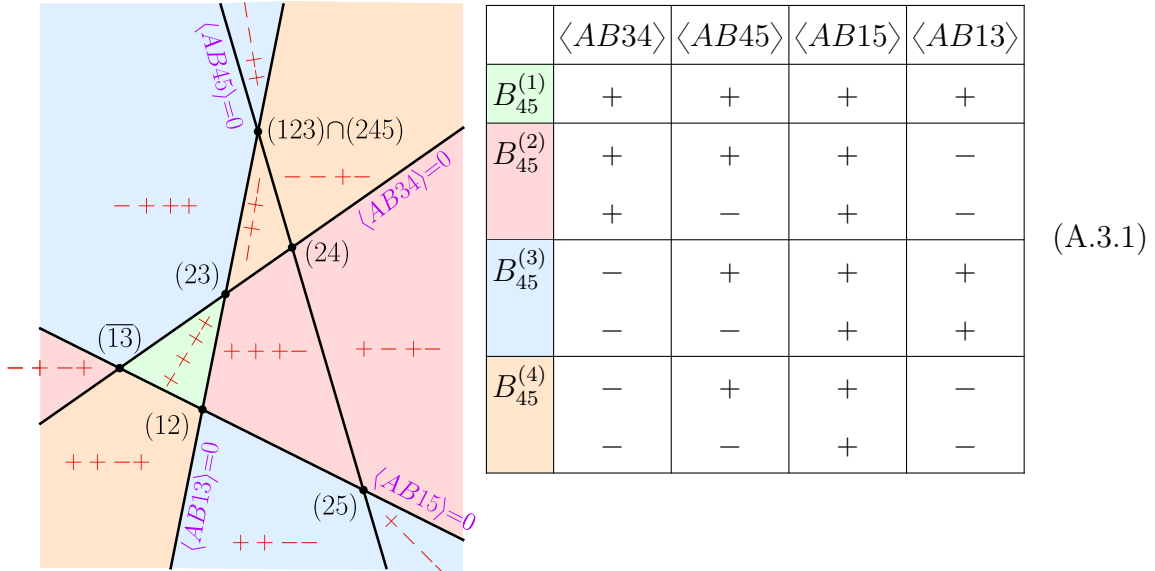
As usual, all the signs in this appendix are to be understood in the context of the usual twisted flips associated to the twisted cyclic symmetry. This means that  $\langle ABij \rangle > 0$  is valid for  $1 \leq i < j \leq n$  but we have to flip the sign if  $j$  passes  $n$  and now becomes smaller than  $i$ . Our sign-flip regions do not have an index space origin so that  $n$  can in principle be anywhere. For the explicit sign-flip regions appearing in the main text, we always fixed  $\langle AB1n \rangle > 0$ , which forced the points  $n$  and  $1$  to be in a *fully positive region*.

### A.3 Gluing local geometries from two-dimensional projections

In this appendix, we summarize in detail how demanding a consistent geometry for the collection of local integral spaces selects a unique choice for the one-mass box, two-mass-hard box and chiral pentagons. This will be done by demanding that all spurious boundaries on various codimension-two projections cancel. The result of this exercise led us to the proposed spaces in section 2.5.3.

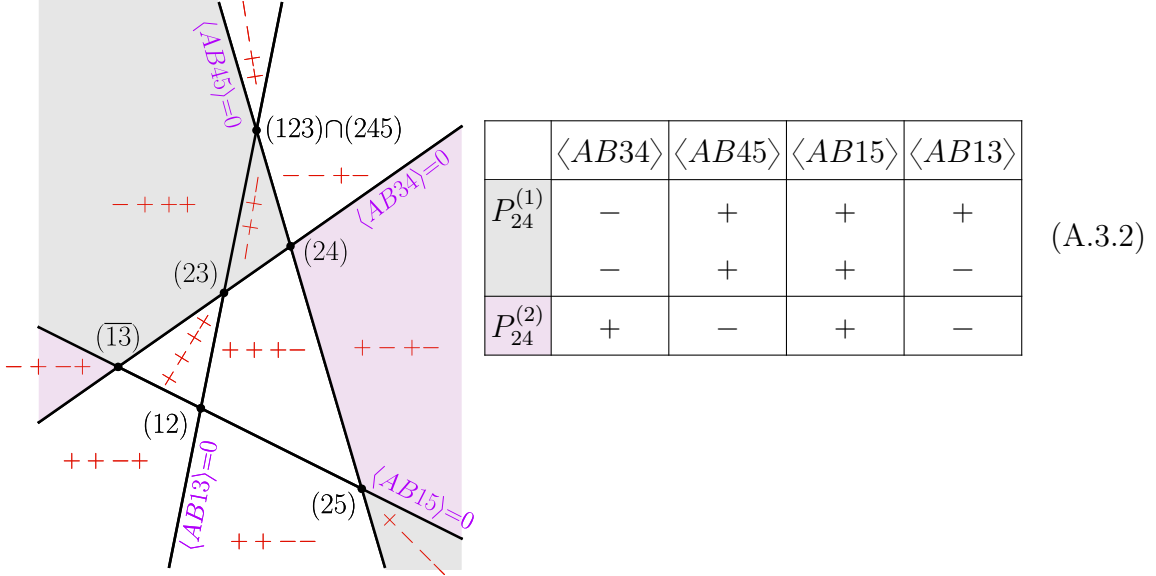
#### Five-point discussion

First, let us look at the boundary when  $(AB)$  passes through the point  $Z_2$ . On this cut surface, only the pentagon  $P_{24}$  and the box  $B_{45}$  in the expansion of the one-loop integrand in eq. (2.5.1) contribute. In eq. (2.5.11) we can identify the regions corresponding to the four options for the box  $B_{45}$  eq. (2.5.3) as well as the two different options for the pentagon eqs. (2.5.4)–(2.5.5). The  $B_{12}$  box does not contribute on this boundary. Using the labeling introduced in subsection 2.5.1, the options for the  $B_{45}$  spaces are:



Note that all four distinct regions  $B_{45}^{(i)}$  have three vertices, (12), (23) and  $(\overline{13})$ , which are the leading singularities of the box integral accessible from the codimension-two cut

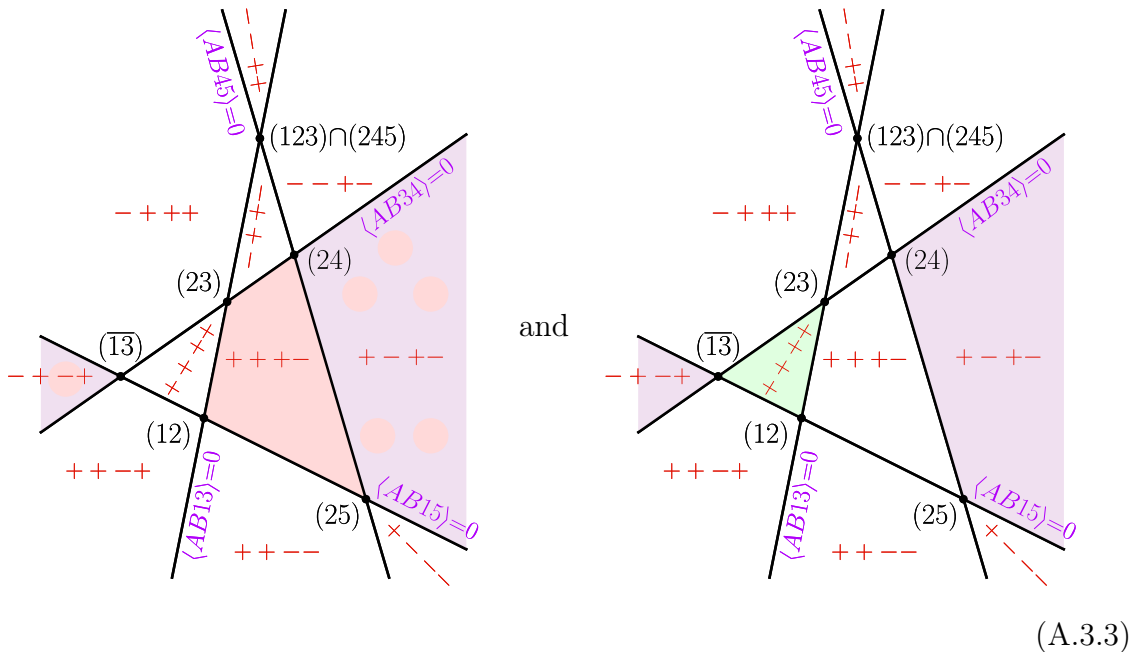
surface shown in eq. (2.5.7). The two choices for the pentagon spaces eqs. (2.5.4)–(2.5.5) correspond to the regions



In this case both pentagon spaces have three vertices, (24), (25) and  $(\overline{13})$ . As discussed throughout section 2.5.3, not all sign patterns which constitute a local integral necessarily contribute on a given cut surface; in this case, the space  $P_{24}^{(1)}$  is composed of four sign patterns, only two of which have the boundary  $(AB) = (A2)$ .

For our purposes, we require that upon combining the two pictures in eqs. (A.3.1) and (A.3.2) the spaces for  $B_{45}$  and  $P_{24}$  must be such that the spurious leading singularities  $(\overline{13})$  and  $(123) \cap (245)$  cancel geometrically (however, since  $(123) \cap (245)$  was not present in individual integrals in the first place, we do not get any constraints from this spurious leading singularity). There are multiple ways of cancelling the spurious vertex  $(\overline{13})$ . The first way of cancelling this point is by simply covering it twice with an overlapping region; an example of this is given by combining  $B_{45}^{(2)}$  and  $P_{24}^{(2)}$  as shown in the left of eq. (A.3.3). Alternatively, we can cancel the spurious point by adding an additional region on one of the “other sides” of the vertex; an example of this is given

by combining  $B_{45}^{(1)}$  and  $P_{24}^{(2)}$ , which is illustrated in the right of eq. (A.3.3).

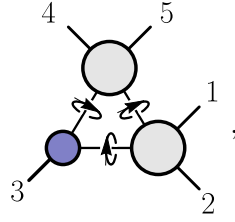


In the first example, we see that after cancelling overlapping regions we are left with exactly the same region  $\{+, +, +, -\}$  as the original MHV Amplituhedron, while in the latter we are left with a different region which has the same boundaries. In fact, it is easy to see that *any* combination of the box and pentagon spaces will cancel this spurious boundary in a rather trivial fashion. The final result of any combination is equivalent to the MHV region, up to the addition of a region with zero form. The same argument holds for any other two-dimensional projection of the form  $(AB) = (Ai)$ , so these pictures do not yield any constraints.

The parity conjugate configuration where  $(AB) \subset (123)$  depicted in eq. (2.5.12) also leads to a trivially correct space, no matter which combination of box and pentagon spaces we take. This is a consequence of the fact that only a single local integral,  $B_{45}$ , contributes on this cut. The chiral wavy-line numerator of the pentagon vanishes here.

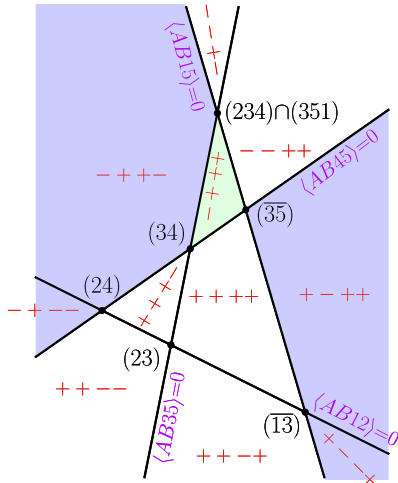
Let us now consider the configuration  $(AB) \subset (234)$ , which corresponds to the on-shell function of eq. (2.5.17), where we have the spurious boundary when  $(AB)$  cuts

the line (15),



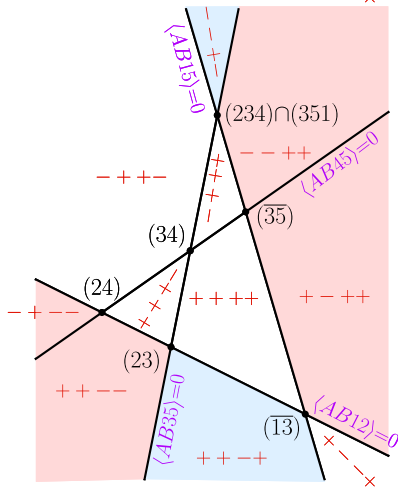
(A.3.4)

which must be absent in the final space. For the boxes  $B_{12}$ ,  $B_{45}$  and pentagon we have, respectively, the contributions



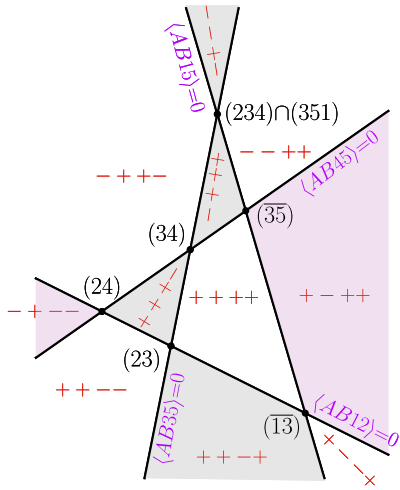
	$\langle AB_{45} \rangle$	$\langle AB_{15} \rangle$	$\langle AB_{12} \rangle$	$\langle AB_{35} \rangle$
$B_{12}^{(1,3)}$	-	+	+	+
$B_{12}^{(2,4)}$	-	+	+	-
	-	+	-	-

(A.3.5)



	$\langle AB_{45} \rangle$	$\langle AB_{15} \rangle$	$\langle AB_{12} \rangle$	$\langle AB_{35} \rangle$
$B_{45}^{(1,3)}$	+	+	-	+
$B_{45}^{(2,4)}$	+	+	-	-
	-	+	-	-

(A.3.6)

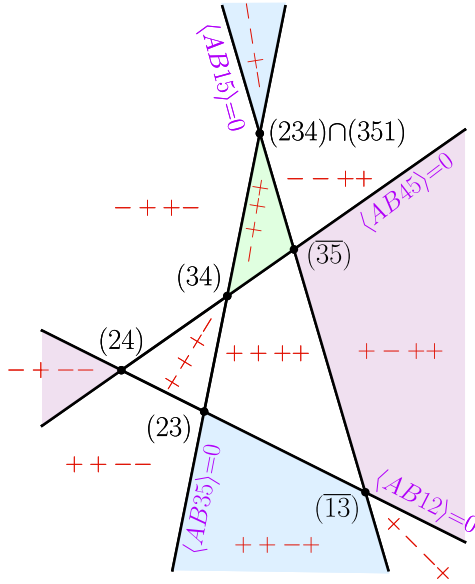


	$\langle AB45 \rangle$	$\langle AB15 \rangle$	$\langle AB12 \rangle$	$\langle AB35 \rangle$
$P_{24}^{(1)}$	+	+	-	+
	+	+	+	-
	-	+	+	+
$P_{24}^{(2)}$	-	+	-	-

(A.3.7)

In these pictures the entire line  $\langle AB15 \rangle = 0$  is spurious i.e., it is not a boundary of the Amplituhedron; therefore, it cannot be a boundary of the Amplituhedron-Prime either. Note that both regions for the boxes  $B_{12}$  and  $B_{45}$ , as well as the pentagon regions do have access to the  $\langle AB15 \rangle = 0$  boundary. As we have seen throughout chapter 2, the geometric cancellation of this spurious boundary is a stronger constraint than what is naïvely observed at the level of adding canonical forms. There are two ways to combine these spaces to get the correct form: either we honestly cancel the boundary so it disappears from the full space, or we cover the *entire* line. In the latter case the codimension-three line  $\langle AB15 \rangle = 0$  is a geometric boundary of the space, although the codimension-four points  $(234) \cap (351)$ ,  $(\overline{35})$  and  $(\overline{13})$  on this line are not. This is unacceptable for our purposes here because geometrically it does not faithfully represent the correct boundary structure. In fact, such a combination can be seen explicitly by considering the following spaces:  $B_{12}^{(1,3)}$ ,  $B_{45}^{(1,3)}$  and  $P_{24}^{(2)}$ . The union of these spaces has the same vertices  $(23), (24), (34)$  as the Amplituhedron, but also has

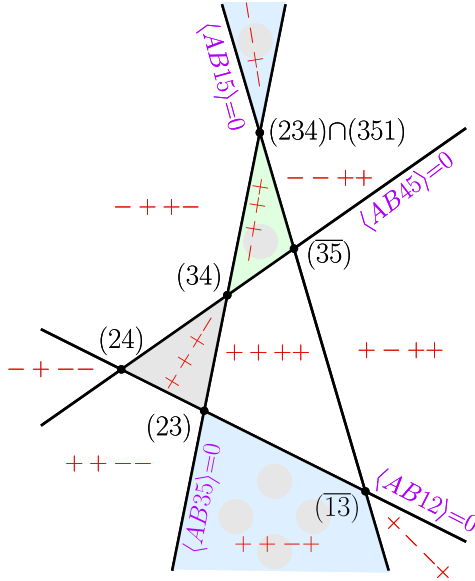
the entire line  $\langle AB15 \rangle = 0$ :



	$\langle AB45 \rangle$	$\langle AB15 \rangle$	$\langle AB12 \rangle$	$\langle AB35 \rangle$
$B_{12}^{(1,3)}$	-	+	+	+
$B_{45}^{(1,3)}$	+	+	-	+
$P_{24}^{(2)}$	-	+	-	-

(A.3.8)

If instead we use the space  $P_{24}^{(1)}$ , we cancel the spurious boundary:



	$\langle AB45 \rangle$	$\langle AB15 \rangle$	$\langle AB12 \rangle$	$\langle AB35 \rangle$
$B_{12}^{(1,3)}$	-	+	+	+
$B_{45}^{(1,3)}$	+	+	-	+
$P_{24}^{(1)}$	+	+	-	+
	+	+	+	-
	-	+	+	+

(A.3.9)

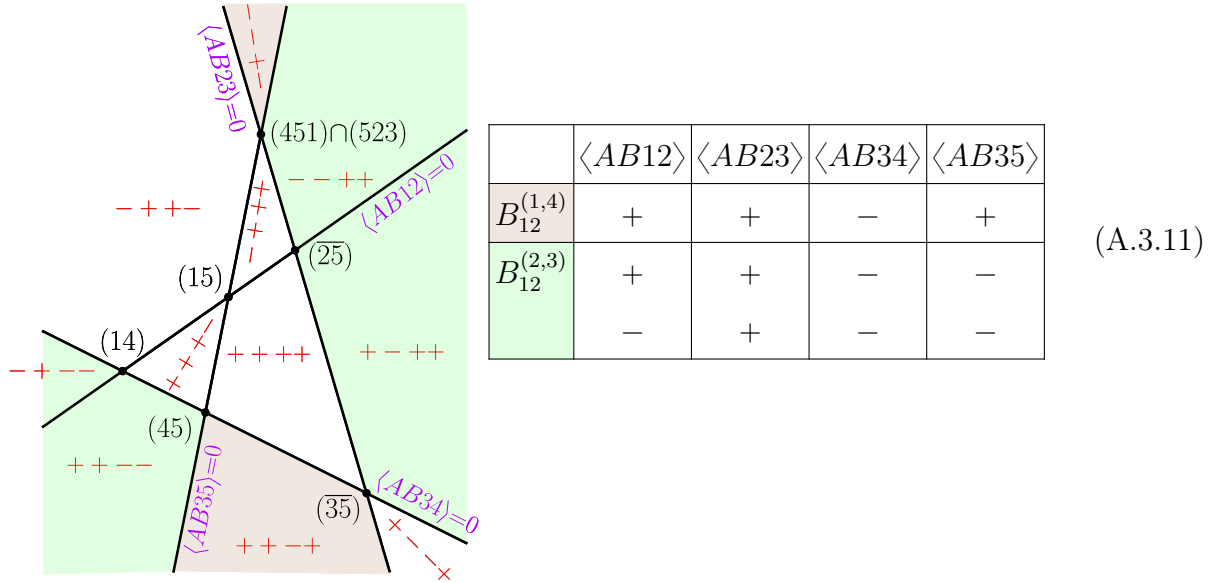
Going through the eight possible combinations of spaces in eqs. (A.3.5)–(A.3.7), we see that only the following combinations cancel the spurious line  $\langle AB15 \rangle = 0$ :

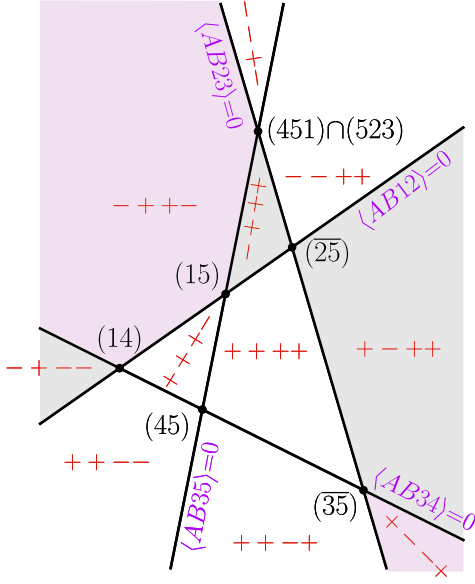
$$B_{12}^{(1,3)}, B_{45}^{(1,3)}, P_{24}^{(1)}, \quad \text{and} \quad B_{12}^{(2,4)}, B_{45}^{(2,4)}, P_{24}^{(1)}. \quad (\text{A.3.10})$$



Remarkably, we see that there is no uniform choice for the box spaces which cancels the spurious contributions of  $P_{24}^{(2)}$  on this cut!

There are three remaining configurations  $(AB) \subset (345), (451), (512)$  to check. The  $(345)$  projection is trivially matched by any space for  $B_{12}$  as no other term contributes. For the  $(451)$  projection, only the box  $B_{12}$  and the pentagon contribute. In terms of the labeling above, on this cut surface the box choices  $(1,4)$  and  $(2,3)$  become indistinguishable, respectively. The box  $B_{12}$  and pentagon correspond to the regions





	$\langle AB12 \rangle$	$\langle AB23 \rangle$	$\langle AB34 \rangle$	$\langle AB35 \rangle$
$P_{24}^{(1)}$	-	+	+	+
	+	-	+	+
$P_{24}^{(2)}$	-	+	+	-

(A.3.12)

Demanding the cancellation of the boundary  $\langle AB23 \rangle = 0$  we see that only two of the remaining four choices in eq. (A.3.10) survive,

$$B_{12}^{(2)}, B_{45}^{(2)}, P_{24}^{(1)}, \quad \text{and} \quad B_{12}^{(3)}, B_{45}^{(3)}, P_{24}^{(1)}. \quad (\text{A.3.13})$$

Following exactly the same procedure for the final configuration  $(AB) \subset (512)$  we find that both choices once again cancel the spurious boundary  $\langle AB34 \rangle = 0$ .

Thus, at five points we are forced to choose the space, eq. (2.5.4), for the pentagon, and can cancel all spurious boundaries using two different choices for the boxes. Both choices are completely satisfactory at this multiplicity. However, only one of these solutions generalizes to higher points. This can be seen directly at six points, where an additional constraint arises: our five-point choice must be compatible with (at least) one of the two spaces in eqs. (2.3.22)–(2.3.23) for the two-mass hard box.

### Six-point discussion

Let us examine the natural extensions of the five-point solutions in eq. (2.5.16) relevant for the two-dimensional projection  $(AB) \subset (234)$ , where the box and pentagon

spaces are

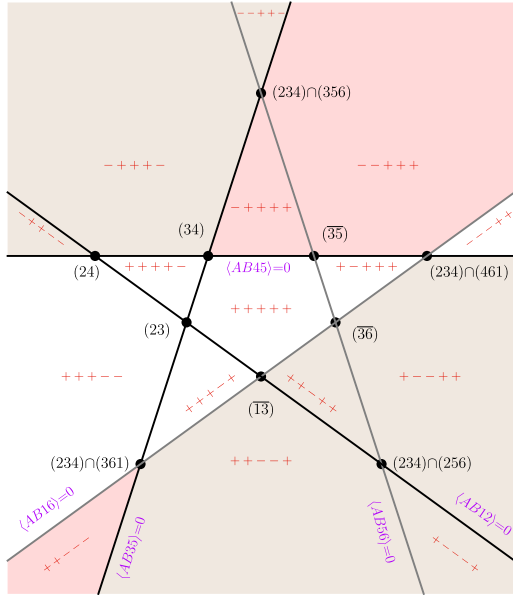
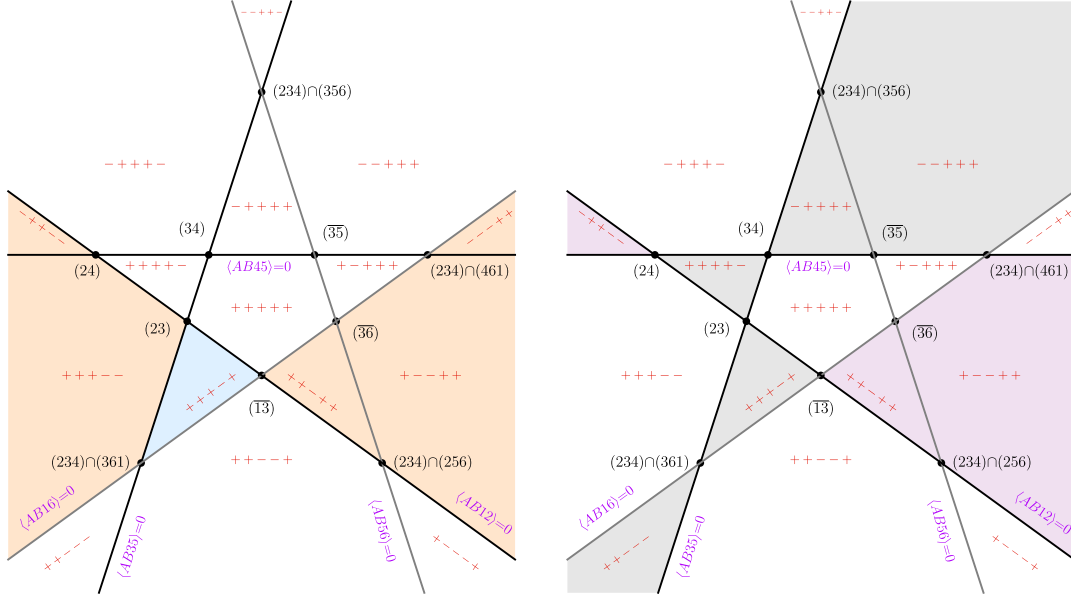
$$B_{456}^{(2)} = 2 \begin{array}{c} 3 \quad + \quad 4 \\ | \\ \langle AB13 \rangle < 0 \\ | \\ 1 \quad + \quad 6 \end{array} 5, \quad \text{and} \quad B_{456}^{(3)} = 2 \begin{array}{c} 3 \quad - \quad 4 \\ | \\ \langle AB13 \rangle > 0 \\ | \\ 1 \quad + \quad 6 \end{array} 5. \quad (\text{A.3.14})$$

$$P_{24}^{(1)} = 2 \begin{array}{c} 3 \quad - \quad 4 \\ | \\ \langle AB13 \rangle > 0 \\ | \\ 1 \quad + \quad 6 \end{array} 5+2 \begin{array}{c} 3 \quad - \quad 4 \\ / \\ \langle AB24 \rangle > 0 \\ / \\ 1 \quad + \quad 6 \end{array} 5+2 \begin{array}{c} 3 \quad + \quad 4 \\ / \\ \langle AB14 \rangle > 0 \\ / \\ 1 \quad + \quad 6 \end{array} 5+2 \begin{array}{c} 3 \quad + \quad 4 \\ / \\ \langle AB24 \rangle > 0 \\ / \\ 1 \quad + \quad 6 \end{array} 5, \quad (\text{A.3.15})$$

For the two-mass-hard box  $B_{12,56}$  we have two choices, see eqs. (2.3.22)–(2.3.23):

$$B_{12,56}^{(1)} = 2 \begin{array}{c} 3 \quad + \quad 4 \\ | \\ \langle AB(234) \cap (461) \rangle > 0 \\ | \\ 1 \quad + \quad 6 \end{array} 5, \quad \text{and} \quad B_{12,56}^{(2)} = 2 \begin{array}{c} 3 \quad + \quad 4 \\ | \\ \langle AB(234) \cap (461) \rangle < 0 \\ | \\ 1 \quad + \quad 6 \end{array} 5. \quad (\text{A.3.16})$$

Filling in the corresponding regions in eq. (2.5.20), the result for the one-mass box, pentagon and two-mass hard spaces are:

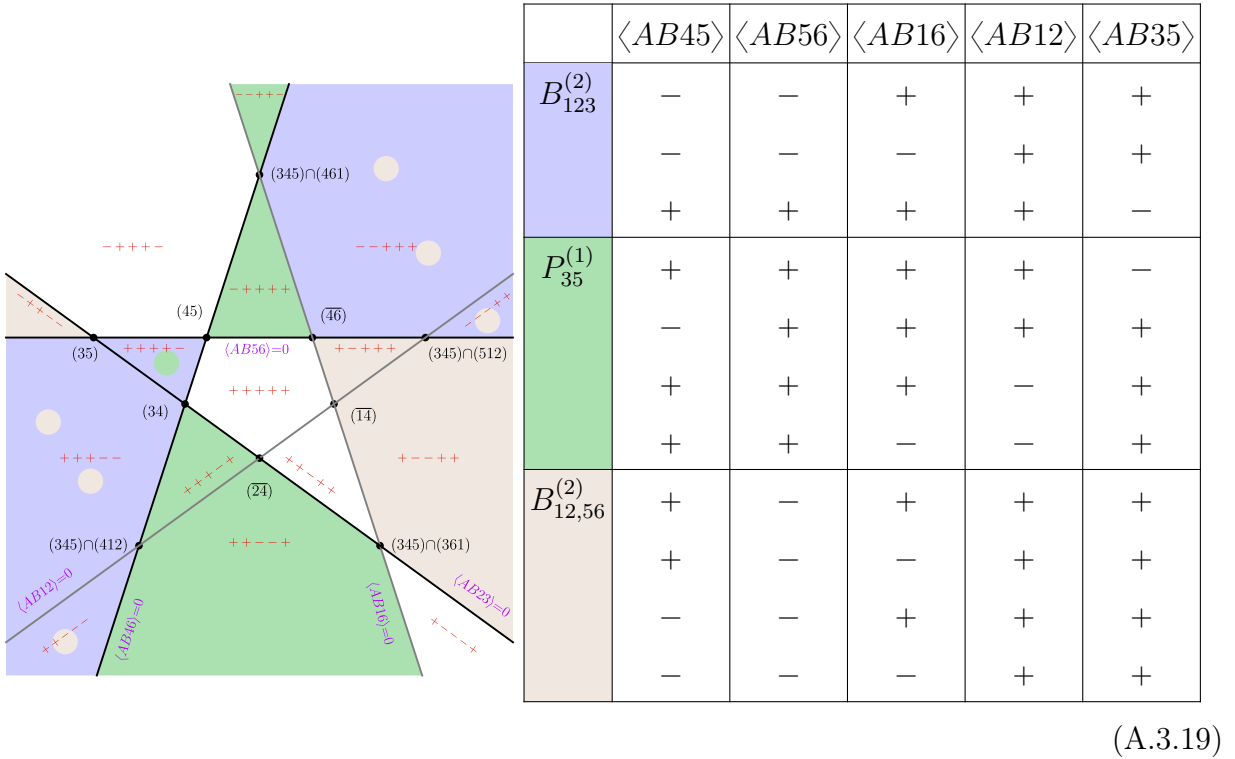


	$\langle AB45 \rangle$	$\langle AB56 \rangle$	$\langle AB16 \rangle$	$\langle AB12 \rangle$	$\langle AB35 \rangle$
$B_{456}^{(2)}$	+	+	+	-	+
	-	+	+	-	-
	-	-	+	-	-
$B_{456}^{(3)}$	+	+	+	-	+
$P_{24}^{(1)}$	+	+	+	-	+
	+	+	+	+	-
	-	+	+	+	+
	-	-	+	+	+
$P_{24}^{(2)}$	+	-	-	+	+
	+	+	-	+	+
$B_{12,56}^{(1)}$	-	+	+	+	+
	-	-	+	+	+
$B_{12,56}^{(2)}$	-	+	+	+	-
	-	-	+	+	-
	-	+	+	-	-
	-	-	+	-	-

Demanding the boundaries  $\langle AB56 \rangle = 0$  and  $\langle AB16 \rangle = 0$  cancel fixes the choice of the two-mass hard box for both solutions:

$$B_{456}^{(3)}, P_{24}^{(1)}, B_{12,56}^{(1)}, \quad \text{and} \quad B_{456}^{(2)}, P_{24}^{(1)}, B_{12,56}^{(2)}. \quad (\text{A.3.18})$$

We claim that while the first option works on all two-dimensional projections, the second option is incompatible with the cut surface where  $(AB) \subset (345)$ . Indeed, repeating the above exercise, on this boundary the one-mass box  $B_{123}$ , pentagon  $P_{35}$  and two-mass hard box contribute. Using the second option for the two-mass hard box  $B_{12,56}^{(2)}$  we find:



We see that although the boundary  $\langle AB12 \rangle = 0$  is cancelled, the entire  $\langle AB16 \rangle = 0$  boundary is present in the final space. This selects the union of  $P_{35}^{(1)}$ ,  $B_{456}^{(2)}$  and  $B_{12,56}^{(1)}$  as the *unique* (subject to the assumption that we make uniform choices for all boxes and pentagons, respectively) candidate space whose boundary structure is identical to the original Amplituhedron on this cut surface. At six points, we have verified that this

combination (together with the other local integrals which did not contribute on the (234), (345) boundaries) is free of all spurious boundaries.

# Appendix B

## Complete Bubble Power-Counting Integrand Basis $\mathfrak{B}_2^{(4)}$

Following the general strategy of prescriptive unitarity, constructing a bubble power-counting basis of integrands requires the specification of a spanning set of contours  $\{\Omega_j\}$ . Once this is done, diagonalization results in a basis such that  $\oint_{\Omega_j} \mathcal{I}_i = \delta_{i,j}$ . In this appendix, we give complete details regarding our choice of integration cycles  $\{\Omega_j\}$ , the integrands  $\{\mathcal{I}_i\}$  to which they are dual, and the integrals that result.

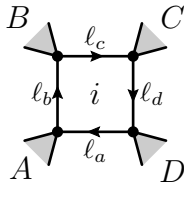
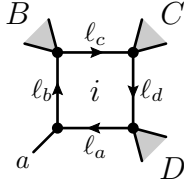
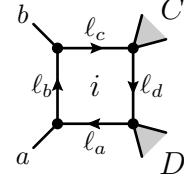
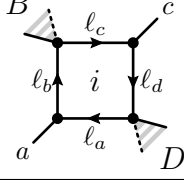
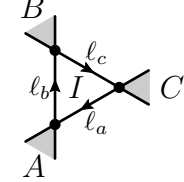
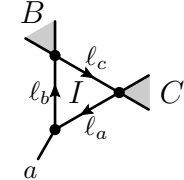
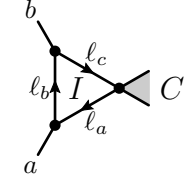
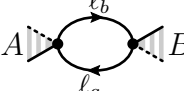
## B.1 Spanning-Set of Integration Contours Defining the Basis

$\Omega_{A,B,C,D}^i := \left\{ \begin{array}{c} \begin{array}{cc} B & CB \\ \begin{array}{c} \text{---} \end{array} \\ \begin{array}{c} \text{---} \end{array} \\ \begin{array}{c} \text{---} \end{array} \\ \begin{array}{c} \text{---} \end{array} \\ A & \ell = \ell_1^* & D \end{array} \end{array}, \begin{array}{c} \begin{array}{cc} CB & C \\ \begin{array}{c} \text{---} \end{array} \\ \begin{array}{c} \text{---} \end{array} \\ \begin{array}{c} \text{---} \end{array} \\ \begin{array}{c} \text{---} \end{array} \\ A & \ell = \ell_2^* & D \end{array} \end{array} \right\}, \Omega_{a,B,C,D}^i := \left\{ \begin{array}{c} \begin{array}{cc} B & CB \\ \begin{array}{c} \text{---} \end{array} \\ \begin{array}{c} \text{---} \end{array} \\ \begin{array}{c} \text{---} \end{array} \\ \begin{array}{c} \text{---} \end{array} \\ a & \ell = \ell_1^* & D \end{array} \end{array}, \begin{array}{c} \begin{array}{cc} CB & C \\ \begin{array}{c} \text{---} \end{array} \\ \begin{array}{c} \text{---} \end{array} \\ \begin{array}{c} \text{---} \end{array} \\ \begin{array}{c} \text{---} \end{array} \\ a & \ell = \ell_2^* & D \end{array} \end{array} \right\}$
$\Omega_{a,b,C,D}^i := \left\{ \begin{array}{c} \begin{array}{cc} b & C \\ \begin{array}{c} \text{---} \end{array} \\ \begin{array}{c} \text{---} \end{array} \\ \begin{array}{c} \text{---} \end{array} \\ \begin{array}{c} \text{---} \end{array} \\ a & \ell = \ell_1^* & D \end{array} \end{array}, \begin{array}{c} \begin{array}{cc} b & C \\ \begin{array}{c} \text{---} \end{array} \\ \begin{array}{c} \text{---} \end{array} \\ \begin{array}{c} \text{---} \end{array} \\ \begin{array}{c} \text{---} \end{array} \\ a & \ell = \ell_2^* & D \end{array} \end{array} \right\}, \Omega_{a,B,c,D}^i := \left\{ \begin{array}{c} \begin{array}{cc} B & c \\ \begin{array}{c} \text{---} \end{array} \\ \begin{array}{c} \text{---} \end{array} \\ \begin{array}{c} \text{---} \end{array} \\ \begin{array}{c} \text{---} \end{array} \\ a & \ell = \ell_1^* & D \end{array} \end{array}, \begin{array}{c} \begin{array}{cc} B & c \\ \begin{array}{c} \text{---} \end{array} \\ \begin{array}{c} \text{---} \end{array} \\ \begin{array}{c} \text{---} \end{array} \\ \begin{array}{c} \text{---} \end{array} \\ a & \ell = \ell_2^* & D \end{array} \end{array} \right\}$
$\Omega_{A,B,C}^I := \left\{ \begin{array}{c} \begin{array}{c} B \\ \begin{array}{c} \text{---} \\ \text{---} \\ \text{---} \\ \text{---} \\ A \end{array} \end{array} \end{array}, \begin{array}{c} \begin{array}{c} B \\ \begin{array}{c} \text{---} \\ \text{---} \\ \text{---} \\ \text{---} \\ A \end{array} \end{array} \end{array}, \begin{array}{c} \begin{array}{c} B \\ \begin{array}{c} \text{---} \\ \text{---} \\ \text{---} \\ \text{---} \\ A \end{array} \end{array} \end{array} \right\}$ <p style="text-align: center; margin-top: -10px;"> <math>\ell^* \rightarrow \infty</math> (odd), <math>\ell_1^* \rightarrow \infty</math> (double-pole) (odd), <math>\ell_2^* \rightarrow \infty</math> (double-pole) (even) </p>
$\Omega_{a,B,C}^I := \left\{ \begin{array}{c} \begin{array}{c} B \\ \begin{array}{c} \text{---} \\ \text{---} \\ \text{---} \\ \text{---} \\ a \end{array} \end{array} \end{array}, \begin{array}{c} \begin{array}{c} B \\ \begin{array}{c} \text{---} \\ \text{---} \\ \text{---} \\ \text{---} \\ a \end{array} \end{array} \end{array}, \begin{array}{c} \begin{array}{c} B \\ \begin{array}{c} \text{---} \\ \text{---} \\ \text{---} \\ \text{---} \\ a \end{array} \end{array} \end{array} \right\}$ <p style="text-align: center; margin-top: -10px;"> <math>\ell_1^* \rightarrow \infty</math> (double-pole), <math>\ell_2^* \rightarrow \infty</math> (double-pole) </p>
$\Omega_{a,b,C}^I := \left\{ \begin{array}{c} \begin{array}{c} b \\ \begin{array}{c} \text{---} \\ \text{---} \\ \text{---} \\ \text{---} \\ a \end{array} \end{array} \end{array}, \begin{array}{c} \begin{array}{c} b \\ \begin{array}{c} \text{---} \\ \text{---} \\ \text{---} \\ \text{---} \\ a \end{array} \end{array} \end{array}, \begin{array}{c} \begin{array}{c} b \\ \begin{array}{c} \text{---} \\ \text{---} \\ \text{---} \\ \text{---} \\ a \end{array} \end{array} \end{array} \right\}$ <p style="text-align: center; margin-top: -10px;"> <math>\ell_1^* \rightarrow \infty</math> (double-pole), <math>\ell_2^* \rightarrow \infty</math> (double-pole) </p>
$\Omega_{A,B} := \left\{ \begin{array}{c} \begin{array}{c} \text{---} \\ \text{---} \\ \text{---} \\ \text{---} \\ A \end{array} \end{array} \right\}, \Omega_{a,B} := \left\{ \begin{array}{c} \begin{array}{c} \text{---} \\ \text{---} \\ \text{---} \\ \text{---} \\ a \end{array} \end{array} \right\}$ <p style="text-align: center; margin-top: -10px;"> <math>\ell^* \rightarrow \infty</math> (single-pole <math>\Rightarrow</math> double-pole), <math>\ell^* \rightarrow \infty</math> (double-pole) </p>

**Table B.1.** A complete specification of contours to which the integrand basis  $\mathfrak{B}_2^{(4)}$  is dual.



## B.2 Explicit Numerators for Basis Integrands in $\mathfrak{B}_2^{(4)}$

	$\mathfrak{n}_{A,B,C,D}^{i=1} := \llbracket p_A, \ell_b, \ell_c, p_C \rrbracket - \frac{1}{2} s_{AB} s_{BC} (1-u-v-\Delta)$ $+ \frac{1}{2} \left[ \llbracket p_B, p_C \rrbracket \ell_a^2 - \llbracket p_{AB}, p_C \rrbracket \ell_b^2 - \llbracket p_{BC}, p_A \rrbracket \ell_c^2 + \llbracket p_B, p_A \rrbracket \ell_d^2 \right]$
	$\mathfrak{n}_{A,B,C,D}^{i=2} := \llbracket \ell_b, \ell_c, p_C, p_A \rrbracket - \frac{1}{2} s_{AB} s_{BC} (1-u-v-\Delta)$ $+ \frac{1}{2} \left( \llbracket p_B, p_C \rrbracket \ell_a^2 - \llbracket p_{AB}, p_C \rrbracket \ell_b^2 - \llbracket p_{BC}, p_A \rrbracket \ell_c^2 + \llbracket p_B, p_A \rrbracket \ell_d^2 \right)$
where $\Delta := \sqrt{(1-u-v)^2 - 4uv}$ , $u := s_{AS} / (s_{AB} s_{BC})$ , $v := s_{BS} / (s_{AB} s_{BC})$	
	$\mathfrak{n}_{a,B,C,D}^{i=1} := \llbracket p_a, \ell_b, \ell_c, p_C \rrbracket + \frac{1}{2} \left( \llbracket p_B, p_C \rrbracket \ell_a^2 - \llbracket p_{a,B}, p_C \rrbracket \ell_b^2 \right)$
	$\mathfrak{n}_{a,B,C,D}^{i=2} := \llbracket \ell_b, \ell_c, p_C, p_a \rrbracket + \frac{1}{2} \left( \llbracket p_B, p_C \rrbracket \ell_a^2 - \llbracket p_{a,B}, p_C \rrbracket \ell_b^2 \right)$
	$\mathfrak{n}_{a,b,C,D}^{i=1} := \llbracket p_a, \ell_b, \ell_c, p_C \rrbracket - \frac{1}{2} \llbracket p_{a,b}, p_C \rrbracket \ell_b^2$
	$\mathfrak{n}_{a,b,C,D}^{i=2} := \llbracket \ell_b, \ell_c, p_C, p_a \rrbracket + \frac{1}{2} \llbracket p_{a,b}, p_C \rrbracket \ell_b^2$
	$\mathfrak{n}_{a,B,c,D}^{i=1} := \llbracket p_a, \ell_b, \ell_c, p_C \rrbracket$
	$\mathfrak{n}_{a,B,c,D}^{i=2} := \llbracket \ell_b, \ell_c, p_C, p_a \rrbracket$
	$\mathfrak{n}_{A,B,C}^{I=1} := -\frac{1}{2} s_C \sqrt{(1-u-v)^2 - 4uv}, \quad \text{where } u := s_A / s_C, v := s_B / s_C$
	$\mathfrak{n}_{A,B,C}^{I=2} := \frac{1}{2} \left( \llbracket p_A, \ell_a, p_C, p_X \rrbracket - \llbracket p_X, p_A, \ell_a, p_C \rrbracket \right) / \llbracket p_B, p_X \rrbracket$
	$\mathfrak{n}_{A,B,C}^{I=3} := \frac{1}{2} \left( \llbracket p_A, \ell_a, p_C, p_X \rrbracket + \llbracket p_X, p_A, \ell_a, p_C \rrbracket + s_A \llbracket p_C, p_X \rrbracket \right. \\ \left. - \ell_a^2 \llbracket p_A - p_C, p_X \rrbracket - \ell_b^2 \llbracket p_C, p_X \rrbracket - \ell_c^2 \llbracket p_A, p_X \rrbracket \right) / \llbracket p_A, p_X \rrbracket$
	$\mathfrak{n}_{a,B,C}^{I=1} := s_B - s_C$
	$\mathfrak{n}_{a,B,C}^{I=2} := - \left( \llbracket \ell_a, \ell_b, p_B, p_X \rrbracket + \llbracket \ell_b, \ell_a, p_C, p_X \rrbracket \right) / \llbracket p_a, p_X \rrbracket$
	$\mathfrak{n}_{a,B,C}^{I=3} := - \left( \llbracket p_X, \ell_a, \ell_b, p_B \rrbracket + \llbracket p_X, \ell_b, \ell_a, p_C \rrbracket \right) / \llbracket p_a, p_X \rrbracket$
	$\mathfrak{n}_{a,b,C}^{I=1} := -s_C$
	$\mathfrak{n}_{a,b,C}^{I=2} := -\frac{1}{2} \left( \llbracket \ell_a, \ell_a + \ell_b, p_b, p_X \rrbracket + \llbracket \ell_b, \ell_a, p_C, p_X \rrbracket \right) / \llbracket p_A - p_B, p_X \rrbracket$
	$\mathfrak{n}_{a,b,C}^{I=3} := -\frac{1}{2} \left( \llbracket p_X, \ell_a, \ell_a + \ell_b, p_b \rrbracket + \llbracket p_X, \ell_b, \ell_a, p_C \rrbracket \right) / \llbracket p_A - p_B, p_X \rrbracket$
	$\mathfrak{n}_{A,B} := \mathfrak{n}_{a,B} := 1/2$

**Table B.2.** Numerators for all box, triangle, and bubble integrands in  $\mathfrak{B}_2^{(4)}$ .

### B.3 Integrals of Basis Integrands in Dimensional Regularization

	$\int \mathcal{I}_{A,B,C,D}^{i=1,2} = \text{Li}_2(1-\bar{u}) + \text{Li}_2(1-\bar{v}) - \text{Li}_2(1) - \log(1-\bar{u}) \log(1-\bar{v})$ $+ \frac{1}{2} \log(u) \log(v)$ $\bar{u} := \frac{1}{2}(1+u-v-\Delta), \bar{v} := \frac{1}{2}(1-u+v-\Delta), \Delta := \sqrt{(1-u-v)^2 - 4uv}$ <p>with <math>u := s_A s_C / (s_A B s_B C)</math> and <math>v := s_B s_D / (s_A B s_B C)</math></p>
	$\int \mathcal{I}_{a,B,C,D}^{I=1,2} = \text{Li}_2\left(1 - \frac{s_B s_D}{s_A B s_B C}\right) - \text{Li}_2\left(1 - \frac{s_B}{s_A B}\right) - \text{Li}_2\left(1 - \frac{s_D}{s_B C}\right)$ $+ \frac{1}{2} \left[ \log\left(\frac{s_B}{s_A B}\right) \log\left(\frac{s_C}{s_B C}\right) + \log\left(\frac{s_C}{s_A B}\right) \log\left(\frac{s_D}{s_B C}\right) \right]$
	$\int \mathcal{I}_{a,b,C,D}^{I=1,2} = -\text{Li}_2\left(1 - \frac{s_C}{s_b C}\right) - \text{Li}_2\left(1 - \frac{s_D}{s_b C}\right)$ $- \frac{1}{2} \left[ \log\left(\frac{s_D}{s_b C}\right) \log\left(\frac{s_{ab}}{s_b C}\right) - \frac{1}{2} \log\left(\frac{s_D}{s_{ab}}\right) \log\left(\frac{s_D}{s_b C}\right) \right]$
	$\int \mathcal{I}_{a,B,C,D}^{I=1,2} = \text{Li}_2\left(1 - \frac{s_B s_D}{s_A B s_B C}\right) - \text{Li}_2\left(1 - \frac{s_B}{s_B C}\right) - \text{Li}_2\left(1 - \frac{s_B}{s_A B}\right)$ $- \text{Li}_2\left(1 - \frac{s_D}{s_B C}\right) - \text{Li}_2\left(1 - \frac{s_D}{s_A B}\right) - \frac{1}{2} \log\left(\frac{s_A B}{s_B C}\right)^2$
	$\int \mathcal{I}_{A,B,C}^{I=1} = \text{Li}_2(1-\bar{u}) + \text{Li}_2(1-\bar{v}) - \text{Li}_2(1) - \log(1-\bar{u}) \log(1-\bar{v}) + \frac{1}{2} \log(u) \log(v)$ $\bar{u} := \frac{1}{2}(1+u-v-\Delta), \bar{v} := \frac{1}{2}(1-u+v-\Delta), \Delta := \sqrt{(1-u-v)^2 - 4uv}$ <p>with <math>u := s_A / s_C</math> and <math>v := s_B / s_C</math></p>
	$\int \mathcal{I}_{A,B,C}^{I=2} = \mathcal{O}(\epsilon), \quad \int \mathcal{I}_{A,B,C}^{I=3} = -\frac{1}{\epsilon} + \frac{1}{2} \log\left(\frac{s_A s_B}{\mu^4}\right) - 2 + \mathcal{O}(\epsilon)$
	$\int \mathcal{I}_{a,B,C}^{I=1} = \frac{1}{\epsilon} \log\left(\frac{s_C}{s_B}\right) - \frac{1}{2} [\log(s_C)^2 - \log(s_B)^2] - \log(\mu^2) \log\left(\frac{s_B}{s_C}\right) + \mathcal{O}(\epsilon)$
	$\int \mathcal{I}_{a,B,C}^{I=2,3} = \frac{1}{\epsilon} - \frac{1}{2} \log\left(\frac{s_B s_C}{\mu^2}\right) + 2 + \log\left(\frac{s_B}{s_C}\right) \frac{1}{2 \llbracket p_A, p_X \rrbracket} \left[ \llbracket p_B - p_C, p_X \rrbracket - 4 \llbracket p_B, p_A, p_C, p_X \rrbracket / (s_B - s_C) \right] + \mathcal{O}(\epsilon)$
	$\int \mathcal{I}_{a,b,C}^{I=1} = -\frac{1}{\epsilon^2} + \frac{1}{\epsilon} \log\left(\frac{s_C}{\mu^2}\right) - \frac{1}{2} \log\left(\frac{s_C}{\mu^2}\right)^2 + \mathcal{O}(\epsilon)$
	$\int \mathcal{I}_{a,b,C}^{I=2,3} = \frac{1}{2} \left( \frac{1}{\epsilon} - \log\left(\frac{s_C}{\mu^2}\right) + 2 \right) + \mathcal{O}(\epsilon)$
	$\int \mathcal{I}_{A,B} = \frac{1}{2} \left( \frac{1}{\epsilon} - \log\left(\frac{s_A}{\mu^2}\right) + 2 \right) + \mathcal{O}(\epsilon)$
	$\int \mathcal{I}_{a,B} = \mathcal{O}(\epsilon)$

**Table B.3.** Integration results for all box, triangle, and bubble integrands in  $\mathfrak{B}_2^{(4)}$ .

## REFERENCES

- [1] S. J. Parke and T. R. Taylor, *An Amplitude for  $n$  Gluon Scattering*, *Phys. Rev. Lett.* **56** (1986) 2459.
- [2] Z. Bern, L. J. Dixon, D. C. Dunbar and D. A. Kosower, *One loop  $n$  point gauge theory amplitudes, unitarity and collinear limits*, *Nucl. Phys. B* **425** (1994) 217 [[hep-ph/9403226](#)].
- [3] Z. Bern, L. J. Dixon, D. C. Dunbar and D. A. Kosower, *Fusing gauge theory tree amplitudes into loop amplitudes*, *Nucl. Phys. B* **435** (1995) 59 [[hep-ph/9409265](#)].
- [4] R. Britto, F. Cachazo and B. Feng, *New recursion relations for tree amplitudes of gluons*, *Nucl. Phys. B* **715** (2005) 499 [[hep-th/0412308](#)].
- [5] R. Britto, F. Cachazo, B. Feng and E. Witten, *Direct proof of tree-level recursion relation in Yang-Mills theory*, *Phys. Rev. Lett.* **94** (2005) 181602 [[hep-th/0501052](#)].
- [6] Z. Bern, J. J. M. Carrasco and H. Johansson, *New Relations for Gauge-Theory Amplitudes*, *Phys. Rev. D* **78** (2008) 085011 [[0805.3993](#)].
- [7] Z. Bern, J. J. M. Carrasco and H. Johansson, *Perturbative Quantum Gravity as a Double Copy of Gauge Theory*, *Phys. Rev. Lett.* **105** (2010) 061602 [[1004.0476](#)].
- [8] Z. Bern, J. J. Carrasco, M. Chiodaroli, H. Johansson and R. Roiban, *The Duality Between Color and Kinematics and its Applications*, [1909.01358](#).
- [9] E. Witten, *Perturbative gauge theory as a string theory in twistor space*, *Commun.Math.Phys.* **252** (2004) 189 [[hep-th/0312171](#)].
- [10] F. Cachazo, S. He and E. Y. Yuan, *Scattering Equations and Kawai-Lewellen-Tye Orthogonality*, *Phys. Rev.* **D90** (2014) 065001 [[1306.6575](#)].
- [11] F. Cachazo, S. He and E. Y. Yuan, *Scattering of Massless Particles in Arbitrary Dimensions*, *Phys. Rev. Lett.* **113** (2014) 171601 [[1307.2199](#)].
- [12] F. Cachazo, S. He and E. Y. Yuan, *Scattering in Three Dimensions from Rational Maps*, *JHEP* **1310** (2013) 141 [[1306.2962](#)].

- [13] F. Cachazo, S. He and E. Y. Yuan, *Scattering of Massless Particles: Scalars, Gluons and Gravitons*, *JHEP* **1407** (2014) 033 [[1309.0885](#)].
- [14] L. J. Dixon, J. M. Drummond and J. M. Henn, *Analytic result for the two-loop six-point NMHV amplitude in  $N=4$  super Yang-Mills theory*, *JHEP* **01** (2012) 024 [[1111.1704](#)].
- [15] S. Caron-Huot, L. J. Dixon, F. Dulat, M. von Hippel, A. J. McLeod and G. Papathanasiou, *Six-Gluon amplitudes in planar  $\mathcal{N} = 4$  super-Yang-Mills theory at six and seven loops*, *JHEP* **08** (2019) 016 [[1903.10890](#)].
- [16] S. Caron-Huot, L. J. Dixon, F. Dulat, M. Von Hippel, A. J. McLeod and G. Papathanasiou, *The Cosmic Galois Group and Extended Steinmann Relations for Planar  $\mathcal{N} = 4$  SYM Amplitudes*, *JHEP* **09** (2019) 061 [[1906.07116](#)].
- [17] B. Basso, L. J. Dixon and G. Papathanasiou, *Origin of the Six-Gluon Amplitude in Planar  $N = 4$  Supersymmetric Yang-Mills Theory*, *Phys. Rev. Lett.* **124** (2020) 161603 [[2001.05460](#)].
- [18] L. J. Dixon, O. Gürdogan, A. J. McLeod and M. Wilhelm, *Bootstrapping a Stress-Tensor Form Factor through Eight Loops*, [2204.11901](#).
- [19] L. J. Dixon, O. Gürdogan, A. J. McLeod and M. Wilhelm, *Folding Amplitudes into Form Factors: An Antipodal Duality*, *Phys. Rev. Lett.* **128** (2022) 111602 [[2112.06243](#)].
- [20] L. Brink, J. H. Schwarz and J. Scherk, *Supersymmetric Yang-Mills Theories*, *Nucl. Phys. B* **121** (1977) 77.
- [21] F. Gliozzi, J. Scherk and D. I. Olive, *Supersymmetry, Supergravity Theories and the Dual Spinor Model*, *Nucl. Phys. B* **122** (1977) 253.
- [22] H. Elvang and Y.-t. Huang, *Scattering Amplitudes*, [1308.1697](#).
- [23] J. M. Henn and J. C. Plefka, *Scattering Amplitudes in Gauge Theories*, vol. 883. Springer, Berlin, 2014, [10.1007/978-3-642-54022-6](#).

- [24] C. Cheung, *TASI Lectures on Scattering Amplitudes*, pp. 571–623. 2018. [1708.03872](#).  
[10.1142/9789813233348\\_0008](#).
- [25] J. M. Drummond, J. Henn, V. A. Smirnov and E. Sokatchev, *Magic identities for conformal four-point integrals*, *JHEP* **01** (2007) 064 [[hep-th/0607160](#)].
- [26] L. F. Alday and J. M. Maldacena, *Gluon scattering amplitudes at strong coupling*, *JHEP* **06** (2007) 064 [[0705.0303](#)].
- [27] J. M. Drummond, J. Henn, G. P. Korchemsky and E. Sokatchev, *Dual superconformal symmetry of scattering amplitudes in  $N=4$  super-Yang-Mills theory*, *Nucl. Phys. B* **828** (2010) 317 [[0807.1095](#)].
- [28] J. M. Drummond, J. M. Henn and J. Plefka, *Yangian symmetry of scattering amplitudes in  $N=4$  super Yang-Mills theory*, *JHEP* **05** (2009) 046 [[0902.2987](#)].
- [29] A. B. Goncharov, M. Spradlin, C. Vergu and A. Volovich, *Classical Polylogarithms for Amplitudes and Wilson Loops*, *Phys. Rev. Lett.* **105** (2010) 151605 [[1006.5703](#)].
- [30] J. Golden, A. B. Goncharov, M. Spradlin, C. Vergu and A. Volovich, *Motivic Amplitudes and Cluster Coordinates*, *JHEP* **01** (2014) 091 [[1305.1617](#)].
- [31] J. M. Drummond, G. Papathanasiou and M. Spradlin, *A Symbol of Uniqueness: The Cluster Bootstrap for the 3-Loop MHV Heptagon*, *JHEP* **03** (2015) 072 [[1412.3763](#)].
- [32] J. Drummond, J. Foster and O. Gürdogan, *Cluster Adjacency Properties of Scattering Amplitudes in  $N = 4$  Supersymmetric Yang-Mills Theory*, *Phys. Rev. Lett.* **120** (2018) 161601 [[1710.10953](#)].
- [33] J. Drummond, J. Foster, O. Gürdoğan and C. Kalousios, *Tropical Grassmannians, cluster algebras and scattering amplitudes*, *JHEP* **04** (2020) 146 [[1907.01053](#)].
- [34] J. Mago, A. Schreiber, M. Spradlin and A. Volovich, *Symbol alphabets from plabic graphs*, *JHEP* **10** (2020) 128 [[2007.00646](#)].
- [35] L. Ren, M. Spradlin and A. Volovich, *Symbol alphabets from tensor diagrams*, *JHEP* **12** (2021) 079 [[2106.01405](#)].

- [36] J. Drummond, G. Korchemsky and E. Sokatchev, *Conformal properties of four-gluon planar amplitudes and Wilson loops*, *Nucl.Phys.* **B795** (2008) 385 [[0707.0243](#)].
- [37] A. Brandhuber, P. Heslop and G. Travaglini, *MHV amplitudes in  $N=4$  super Yang-Mills and Wilson loops*, *Nucl. Phys.* **B794** (2008) 231 [[0707.1153](#)].
- [38] J. M. Drummond, J. Henn, G. P. Korchemsky and E. Sokatchev, *Conformal Ward Identities for Wilson Loops and a Test of the Duality with Gluon Amplitudes*, *Nucl. Phys.* **B826** (2010) 337 [[0712.1223](#)].
- [39] L. Mason and D. Skinner, *The Complete Planar S-matrix of  $N=4$  SYM as a Wilson Loop in Twistor Space*, *JHEP* **1012** (2010) 018 [[1009.2225](#)].
- [40] S. Caron-Huot, *Notes on the scattering amplitude / Wilson loop duality*, *JHEP* **07** (2011) 058 [[1010.1167](#)].
- [41] N. Arkani-Hamed, J. L. Bourjaily, F. Cachazo, S. Caron-Huot and J. Trnka, *The All-Loop Integrand For Scattering Amplitudes in Planar  $N=4$  SYM*, *JHEP* **01** (2011) 041 [[1008.2958](#)].
- [42] N. Arkani-Hamed, F. Cachazo, C. Cheung and J. Kaplan, *A Duality For The S Matrix*, *JHEP* **03** (2010) 020 [[0907.5418](#)].
- [43] N. Arkani-Hamed, F. Cachazo and C. Cheung, *The Grassmannian Origin Of Dual Superconformal Invariance*, *JHEP* **03** (2010) 036 [[0909.0483](#)].
- [44] L. J. Mason and D. Skinner, *Dual Superconformal Invariance, Momentum Twistors and Grassmannians*, *JHEP* **11** (2009) 045 [[0909.0250](#)].
- [45] N. Arkani-Hamed, J. Bourjaily, F. Cachazo and J. Trnka, *Unification of Residues and Grassmannian Dualities*, *JHEP* **01** (2011) 049 [[0912.4912](#)].
- [46] N. Arkani-Hamed, J. Bourjaily, F. Cachazo and J. Trnka, *Local Spacetime Physics from the Grassmannian*, *JHEP* **01** (2011) 108 [[0912.3249](#)].
- [47] N. Arkani-Hamed, J. L. Bourjaily, F. Cachazo, A. B. Goncharov, A. Postnikov and J. Trnka, *Grassmannian Geometry of Scattering Amplitudes*. Cambridge University Press, 4, 2016, [10.1017/CBO9781316091548](#), [[1212.5605](#)].

- [48] A. Hodges, *Eliminating spurious poles from gauge-theoretic amplitudes*, *JHEP* **05** (2013) 135 [[0905.1473](#)].
- [49] A. Hodges, *The Box Integrals in Momentum-Twistor Geometry*, *JHEP* **08** (2013) 051 [[1004.3323](#)].
- [50] N. Arkani-Hamed, J. L. Bourjaily, F. Cachazo, A. Hodges and J. Trnka, *A Note on Polytopes for Scattering Amplitudes*, *JHEP* **04** (2012) 081 [[1012.6030](#)].
- [51] N. Arkani-Hamed, J. L. Bourjaily, F. Cachazo and J. Trnka, *Local Integrals for Planar Scattering Amplitudes*, *JHEP* **06** (2012) 125 [[1012.6032](#)].
- [52] J. M. Drummond and J. M. Henn, *Simple loop integrals and amplitudes in  $N=4$  SYM*, *JHEP* **05** (2011) 105 [[1008.2965](#)].
- [53] J. L. Bourjaily, S. Caron-Huot and J. Trnka, *Dual-Conformal Regularization of Infrared Loop Divergences and the Chiral Box Expansion*, *JHEP* **01** (2015) 001 [[1303.4734](#)].
- [54] N. Arkani-Hamed, A. Hodges and J. Trnka, *Positive Amplitudes In The Amplituhedron*, *JHEP* **08** (2015) 030 [[1412.8478](#)].
- [55] J. L. Bourjaily and J. Trnka, *Local Integrand Representations of All Two-Loop Amplitudes in Planar SYM*, *JHEP* **08** (2015) 119 [[1505.05886](#)].
- [56] N. Arkani-Hamed and J. Trnka, *The Amplituhedron*, *JHEP* **10** (2014) 030 [[1312.2007](#)].
- [57] N. Arkani-Hamed and J. Trnka, *Into the Amplituhedron*, *JHEP* **12** (2014) 182 [[1312.7878](#)].
- [58] N. Arkani-Hamed, H. Thomas and J. Trnka, *Unwinding the Amplituhedron in Binary*, *JHEP* **01** (2018) 016 [[1704.05069](#)].
- [59] E. Herrmann and J. Trnka, *The SAGEX Review on Scattering Amplitudes, Chapter 7: Positive Geometry of Scattering Amplitudes*, [2203.13018](#).
- [60] N. Arkani-Hamed, Y. Bai and T. Lam, *Positive Geometries and Canonical Forms*, *JHEP* **11** (2017) 039 [[1703.04541](#)].
- [61] C. Even-Zohar, T. Lakrec and R. J. Tessler, *The Amplituhedron BCFW Triangulation*, [2112.02703](#).

- [62] A. Yellespur Srikant, *Emergent unitarity from the amplituhedron*, *JHEP* **01** (2020) 069 [[1906.10700](#)].
- [63] R. Kojima, *Triangulation of 2-loop MHV Amplituhedron from Sign Flips*, *JHEP* **04** (2019) 085 [[1812.01822](#)].
- [64] R. Kojima and C. Langer, *Sign Flip Triangulations of the Amplituhedron*, *JHEP* **05** (2020) 121 [[2001.06473](#)].
- [65] R. Kojima and J. Rao, *Triangulation-free Trivialization of 2-loop MHV Amplituhedron*, *JHEP* **10** (2020) 140 [[2007.15650](#)].
- [66] Y. An, Y. Li, Z. Li and J. Rao, *All-loop Mondrian Diagrammatics and 4-particle Amplituhedron*, *JHEP* **06** (2018) 023 [[1712.09994](#)].
- [67] N. Arkani-Hamed, C. Langer, A. Yellespur Srikant and J. Trnka, *Deep Into the Amplituhedron: Amplitude Singularities at All Loops and Legs*, *Phys. Rev. Lett.* **122** (2019) 051601 [[1810.08208](#)].
- [68] J. Rao, *4-particle amplituhedronics for 3-5 loops*, *Nucl. Phys. B* **943** (2019) 114625 [[1806.01765](#)].
- [69] C. Langer and A. Yellespur Srikant, *All-loop cuts from the Amplituhedron*, *JHEP* **04** (2019) 105 [[1902.05951](#)].
- [70] T. Lam, *Amplituhedron cells and Stanley symmetric functions*, *Commun. Math. Phys.* **343** (2016) 1025 [[1408.5531](#)].
- [71] S. Franco, D. Galloni, A. Mariotti and J. Trnka, *Anatomy of the Amplituhedron*, *JHEP* **03** (2015) 128 [[1408.3410](#)].
- [72] S. N. Karp and L. K. Williams, *The  $m=1$  amplituhedron and cyclic hyperplane arrangements*, *Int. Math. Res. Not.* **5** (2019) 1401 [[1608.08288](#)].
- [73] S. N. Karp, L. K. Williams and Y. X. Zhang, *Decompositions of amplituhedra*, [1708.09525](#).
- [74] T. Lukowski, *On the Boundaries of the  $m=2$  Amplituhedron*, [1908.00386](#).



- [75] T. Lukowski and R. Moerman, *Boundaries of the Amplituhedron with amplituhedronBoundaries*, [2002.07146](#).
- [76] T. Lukowski, M. Parisi and L. K. Williams, *The positive tropical Grassmannian, the hypersimplex, and the  $m=2$  amplituhedron*, [2002.06164](#).
- [77] M. Parisi, M. Sherman-Bennett and L. Williams, *The  $m=2$  amplituhedron and the hypersimplex: signs, clusters, triangulations, Eulerian numbers*, [2104.08254](#).
- [78] L. K. Williams, *The positive Grassmannian, the amplituhedron, and cluster algebras*, in *International Congress of Mathematicians*, 10, 2021, [2110.10856](#).
- [79] R. Moerman and L. K. Williams, *Grass trees and forests: Enumeration of Grassmannian trees and forests, with applications to the momentum amplituhedron*, [2112.02061](#).
- [80] I. Prlina, M. Spradlin, J. Stankowicz and S. Stanojevic, *Boundaries of Amplituhedra and NMHV Symbol Alphabets at Two Loops*, *JHEP* **04** (2018) 049 [[1712.08049](#)].
- [81] I. Prlina, M. Spradlin, J. Stankowicz, S. Stanojevic and A. Volovich, *All-Helicity Symbol Alphabets from Unwound Amplituhedra*, *JHEP* **05** (2018) 159 [[1711.11507](#)].
- [82] T. Dennen, I. Prlina, M. Spradlin, S. Stanojevic and A. Volovich, *Landau Singularities from the Amplituhedron*, *JHEP* **06** (2017) 152 [[1612.02708](#)].
- [83] L. J. Dixon, M. von Hippel, A. J. McLeod and J. Trnka, *Multi-loop positivity of the planar  $\mathcal{N} = 4$  SYM six-point amplitude*, *JHEP* **02** (2017) 112 [[1611.08325](#)].
- [84] Y. Bai and S. He, *The Amplituhedron from Momentum Twistor Diagrams*, *JHEP* **02** (2015) 065 [[1408.2459](#)].
- [85] Y. Bai, S. He and T. Lam, *The Amplituhedron and the One-loop Grassmannian Measure*, *JHEP* **01** (2016) 112 [[1510.03553](#)].
- [86] L. Ferro, T. Lukowski, A. Orta and M. Parisi, *Towards the Amplituhedron Volume*, *JHEP* **03** (2016) 014 [[1512.04954](#)].
- [87] L. Ferro, T. Łukowski, A. Orta and M. Parisi, *Yangian symmetry for the tree amplituhedron*, *J. Phys. A* **50** (2017) 294005 [[1612.04378](#)].

- [88] L. Ferro, T. Lukowski, A. Orta and M. Parisi, *Tree-level scattering amplitudes from the amplituhedron*, *J. Phys. Conf. Ser.* **841** (2017) 012037 [[1612.06276](#)].
- [89] L. Ferro, T. Lukowski and M. Parisi, *Amplituhedron meets Jeffrey–Kirwan residue*, *J. Phys. A* **52** (2019) 045201 [[1805.01301](#)].
- [90] L. Ferro, T. Lukowski and R. Moerman, *From momentum amplituhedron boundaries to amplitude singularities and back*, *JHEP* **07** (2020) 201 [[2003.13704](#)].
- [91] G. Salvatori and S. L. Cacciatori, *Hyperbolic Geometry and Amplituhedra in 1+2 dimensions*, *JHEP* **08** (2018) 167 [[1803.05809](#)].
- [92] P. Benincasa, *On-shell diagrammatics and the perturbative structure of planar gauge theories*, [1510.03642](#).
- [93] P. Benincasa and D. Gordo, *On-shell diagrams and the geometry of planar  $\mathcal{N} < 4$  SYM theories*, *JHEP* **11** (2017) 192 [[1609.01923](#)].
- [94] E. Herrmann and J. Trnka, *Gravity On-shell Diagrams*, *JHEP* **11** (2016) 136 [[1604.03479](#)].
- [95] P. Heslop and A. E. Lipstein, *On-shell diagrams for  $\mathcal{N} = 8$  supergravity amplitudes*, *JHEP* **06** (2016) 069 [[1604.03046](#)].
- [96] R. Frassek, D. Meidinger, D. Nandan and M. Wilhelm, *On-shell diagrams, Grassmannians and integrability for form factors*, *JHEP* **01** (2016) 182 [[1506.08192](#)].
- [97] J. Kim and S. Lee, *Positroid Stratification of Orthogonal Grassmannian and ABJM Amplitudes*, *JHEP* **09** (2014) 085 [[1402.1119](#)].
- [98] Y.-t. Huang, C. Wen and D. Xie, *The Positive orthogonal Grassmannian and loop amplitudes of ABJM*, *J. Phys. A* **47** (2014) 474008 [[1402.1479](#)].
- [99] N. Arkani-Hamed, J. L. Bourjaily, F. Cachazo and J. Trnka, *Singularity Structure of Maximally Supersymmetric Scattering Amplitudes*, *Phys. Rev. Lett.* **113** (2014) 261603 [[1410.0354](#)].
- [100] Z. Bern, E. Herrmann, S. Litsey, J. Stankowicz and J. Trnka, *Logarithmic Singularities and Maximally Supersymmetric Amplitudes*, *JHEP* **06** (2015) 202 [[1412.8584](#)].

- [101] Z. Bern, E. Herrmann, S. Litsey, J. Stankowicz and J. Trnka, *Evidence for a Nonplanar Amplituhedron*, *JHEP* **06** (2016) 098 [[1512.08591](#)].
- [102] N. Arkani-Hamed, J. L. Bourjaily, F. Cachazo, A. Postnikov and J. Trnka, *On-Shell Structures of MHV Amplitudes Beyond the Planar Limit*, *JHEP* **06** (2015) 179 [[1412.8475](#)].
- [103] S. Franco, D. Galloni, B. Penante and C. Wen, *Non-Planar On-Shell Diagrams*, *JHEP* **06** (2015) 199 [[1502.02034](#)].
- [104] J. L. Bourjaily, S. Franco, D. Galloni and C. Wen, *Stratifying On-Shell Cluster Varieties: the Geometry of Non-Planar On-Shell Diagrams*, *JHEP* **10** (2016) 003 [[1607.01781](#)].
- [105] D. Damgaard, L. Ferro, T. Lukowski and M. Parisi, *The Momentum Amplituhedron*, *JHEP* **08** (2019) 042 [[1905.04216](#)].
- [106] P. Tourkine, *On integrands and loop momentum in string and field theory*, [1901.02432](#).
- [107] R. Ben-Israel, A. G. Tumanov and A. Sever, *Scattering amplitudes — Wilson loops duality for the first non-planar correction*, *JHEP* **08** (2018) 122 [[1802.09395](#)].
- [108] N. Arkani-Hamed, Y. Bai, S. He and G. Yan, *Scattering Forms and the Positive Geometry of Kinematics, Color and the Worldsheet*, *JHEP* **05** (2018) 096 [[1711.09102](#)].
- [109] N. Arkani-Hamed, S. He, T. Lam and H. Thomas, *Binary Geometries, Generalized Particles and Strings, and Cluster Algebras*, [1912.11764](#).
- [110] N. Arkani-Hamed, S. He and T. Lam, *Stringy canonical forms*, *JHEP* **02** (2021) 069 [[1912.08707](#)].
- [111] L. Ferro and T. Lukowski, *Amplituhedra, and beyond*, *J. Phys. A* **54** (2021) 033001 [[2007.04342](#)].
- [112] P. Banerjee, A. Laddha and P. Raman, *Stokes polytopes: the positive geometry for  $\varphi^4$  interactions*, *JHEP* **08** (2019) 067 [[1811.05904](#)].
- [113] A. Herderschee, S. He, F. Teng and Y. Zhang, *On Positive Geometry and Scattering Forms for Matter Particles*, [1912.08307](#).
- [114] A. Herderschee and F. Teng, *Open associahedra and scattering forms*, [2008.06418](#).

- [115] M. Jagadale and A. Laddha, *On the Positive Geometry of Quartic Interactions III : One Loop Integrands from Polytopes*, [2007.12145](#).
- [116] P. Aneesh, P. Banerjee, M. Jagadale, R. Rajan, A. Laddha and S. Mahato, *On positive geometries of quartic interactions: Stokes polytopes, lower forms on associahedra and world-sheet forms*, *JHEP* **04** (2020) 149 [[1911.06008](#)].
- [117] B. Eden, P. Heslop and L. Mason, *The Correlahedron*, *JHEP* **09** (2017) 156 [[1701.00453](#)].
- [118] N. Arkani-Hamed, Y.-T. Huang and S.-H. Shao, *On the Positive Geometry of Conformal Field Theory*, *JHEP* **06** (2019) 124 [[1812.07739](#)].
- [119] N. Arkani-Hamed, T.-C. Huang and Y.-T. Huang, *The EFT-Hedron*, *JHEP* **05** (2021) 259 [[2012.15849](#)].
- [120] N. Arkani-Hamed, P. Benincasa and A. Postnikov, *Cosmological Polytopes and the Wavefunction of the Universe*, [1709.02813](#).
- [121] N. Arkani-Hamed and P. Benincasa, *On the Emergence of Lorentz Invariance and Unitarity from the Scattering Facet of Cosmological Polytopes*, [1811.01125](#).
- [122] P. Benincasa and M. Parisi, *Positive Geometries and Differential Forms with Non-Logarithmic Singularities I*, [2005.03612](#).
- [123] N. Arkani-Hamed, J. L. Bourjaily, F. Cachazo and J. Trnka, *Local Integrals for Planar Scattering Amplitudes*, *JHEP* **06** (2012) 125 [[1012.6032](#)].
- [124] R. Penrose, *Twistor algebra*, *J. Math. Phys.* **8** (1967) 345.
- [125] N. Arkani-Hamed, J. L. Bourjaily, F. Cachazo, S. Caron-Huot and J. Trnka, *The All-Loop Integrand For Scattering Amplitudes in Planar  $N=4$  SYM*, *JHEP* **01** (2011) 041 [[1008.2958](#)].
- [126] F. Cachazo, *Sharpening The Leading Singularity*, [0803.1988](#).
- [127] E. Herrmann and J. Parra-Martinez, *Logarithmic forms and differential equations for Feynman integrals*, *JHEP* **02** (2020) 099 [[1909.04777](#)].
- [128] E. Herrmann, C. Langer, J. Trnka and M. Zheng, *Positive Geometries for One-Loop Chiral Octagons*, [2007.12191](#).

- [129] R. Britto, F. Cachazo and B. Feng, *Generalized unitarity and one-loop amplitudes in  $N=4$  super-Yang-Mills*, *Nucl. Phys. B* **725** (2005) 275 [[hep-th/0412103](#)].
- [130] Z. Bern, N. E. J. Bjerrum-Bohr and D. C. Dunbar, *Inherited twistor-space structure of gravity loop amplitudes*, *JHEP* **05** (2005) 056 [[hep-th/0501137](#)].
- [131] N. E. J. Bjerrum-Bohr, D. C. Dunbar, H. Ita, W. B. Perkins and K. Risager, *The No-Triangle Hypothesis for  $\mathcal{N}=8$  Supergravity*, *JHEP* **12** (2006) 072 [[hep-th/0610043](#)].
- [132] Z. Bern, J. J. Carrasco, D. Forde, H. Ita and H. Johansson, *Unexpected Cancellations in Gravity Theories*, *Phys. Rev.* **D77** (2008) 025010 [[0707.1035](#)].
- [133] N. E. J. Bjerrum-Bohr and P. Vanhove, *Absence of Triangles in Maximal Supergravity Amplitudes*, *JHEP* **10** (2008) 006 [[0805.3682](#)].
- [134] J. L. Bourjaily, E. Herrmann, C. Langer and J. Trnka, *Building bases of loop integrands*, *JHEP* **11** (2020) 116 [[2007.13905](#)].
- [135] G. Passarino and M. Veltman, *One Loop Corrections for  $e^+ e^-$  Annihilation Into  $\mu^+ \mu^-$  in the Weinberg Model*, *Nucl. Phys.* **B160** (1979) 151.
- [136] G. Ossola, C. G. Papadopoulos and R. Pittau, *Reducing Full One-Loop Amplitudes to Scalar Integrals at the Integrand Level*, *Nucl. Phys.* **B763** (2007) 147 [[hep-ph/0609007](#)].
- [137] P. Mastrolia, G. Ossola, T. Reiter and F. Tramontano, *Scattering Amplitudes from Unitarity-Based Reduction Algorithm at the Integrand-Level*, *JHEP* **08** (2010) 080 [[1006.0710](#)].
- [138] J. L. Bourjaily, E. Herrmann and J. Trnka, *Prescriptive Unitarity*, *JHEP* **06** (2017) 059 [[1704.05460](#)].
- [139] H. Elvang, Y.-t. Huang and C. Peng, *On-shell superamplitudes in  $N<4$  SYM*, *JHEP* **09** (2011) 031 [[1102.4843](#)].
- [140] T. Hahn, *Generating and calculating one loop Feynman diagrams with FeynArts, FormCalc, and LoopTools*, in *6th International Workshop on New Computing Techniques in Physics Research: Software Engineering, Artificial Intelligence Neural Nets, Genetic Algorithms, Symbolic Algebra, Automatic Calculation*, 4, 1999, [hep-ph/9905354](#).

- [141] G. Ossola, C. G. Papadopoulos and R. Pittau, *CutTools: A Program Implementing the OPP Reduction Method to Compute One-Loop Amplitudes*, *JHEP* **0803** (2008) 042 [[0711.3596](#)].
- [142] C. F. Berger et al., *An Automated Implementation of On-Shell Methods for One-Loop Amplitudes*, *Phys. Rev.* **D78** (2008) 036003 [[0803.4180](#)].
- [143] S. Abreu, J. Dormans, F. Febres Cordero, H. Ita, M. Kraus, B. Page et al., *Caravel: A C++ framework for the computation of multi-loop amplitudes with numerical unitarity*, *Comput. Phys. Commun.* **267** (2021) 108069 [[2009.11957](#)].
- [144] S. J. Bidder, N. E. J. Bjerrum-Bohr, D. C. Dunbar and W. B. Perkins, *One-Loop Gluon A scattering Amplitudes in Theories with  $\mathcal{N} < 4$  Supersymmetries*, *Phys. Lett. B* **612** (2005) 75 [[hep-th/0502028](#)].
- [145] R. Britto, E. Buchbinder, F. Cachazo and B. Feng, *One-loop amplitudes of gluons in SQCD*, *Phys. Rev. D* **72** (2005) 065012 [[hep-ph/0503132](#)].
- [146] D. C. Dunbar, W. B. Perkins and E. Warrick, *The Unitarity Method using a Canonical Basis Approach*, *JHEP* **06** (2009) 056 [[0903.1751](#)].
- [147] A. Ochirov, *All one-loop NMHV gluon amplitudes in  $\mathcal{N} = 1$  SYM*, *JHEP* **12** (2013) 080 [[1311.1491](#)].
- [148] E. W. Nigel Glover and C. Williams, *One-Loop Gluonic Amplitudes from Single Unitarity Cuts*, *JHEP* **12** (2008) 067 [[0810.2964](#)].
- [149] R. Britto, *Loop Amplitudes in Gauge Theories: Modern Analytic Approaches*, *J. Phys. A* **44** (2011) 454006 [[1012.4493](#)].
- [150] R. Runkel, Z. Ször, J. P. Vesga and S. Weinzierl, *Integrands of loop amplitudes within loop-tree duality*, *Phys. Rev. D* **101** (2020) 116014 [[1906.02218](#)].
- [151] H. Johansson and A. Ochirov, *Pure Gravities via Color-Kinematics Duality for Fundamental Matter*, *JHEP* **11** (2015) 046 [[1407.4772](#)].
- [152] J. Nohle, *Color-Kinematics Duality in One-Loop Four-Gluon Amplitudes with Matter*, *Phys. Rev.* **D90** (2014) 025020 [[1309.7416](#)].

- [153] J. L. Bourjaily, E. Herrmann, C. Langer, K. Patatoukos, J. Trnka and M. Zheng, *Integrands of less-supersymmetric Yang-Mills at one loop*, *JHEP* **03** (2022) 126 [[2112.06901](#)].
- [154] J. Broedel, C. Duhr, F. Dulat, B. Penante and L. Tancredi, *Elliptic Feynman Integrals and Pure Functions*, *JHEP* **01** (2019) 023 [[1809.10698](#)].
- [155] J. M. Henn, *Multiloop integrals in dimensional regularization made simple*, *Phys. Rev. Lett.* **110** (2013) 251601 [[1304.1806](#)].
- [156] D. Forde, *Direct extraction of one-loop integral coefficients*, *Phys. Rev. D* **75** (2007) 125019 [[0704.1835](#)].
- [157] R. Britto and B. Feng, *Integral coefficients for one-loop amplitudes*, *JHEP* **02** (2008) 095 [[0711.4284](#)].
- [158] J. L. Bourjaily, C. Langer and K. Patatoukos, *Locally-Finite Quantities in sYM*, *JHEP* **04** (2021) 298 [[2102.02821](#)].
- [159] N. Arkani-Hamed and E. Y. Yuan, *One-Loop Integrals from Spherical Projections of Planes and Quadrics*, [1712.09991](#).
- [160] J. L. Bourjaily, E. Gardi, A. J. McLeod and C. Vergu, *All-Mass n-gon Integrals in n Dimensions*, *JHEP* **08** (2020) 029 [[1912.11067](#)].
- [161] J. L. Bourjaily, E. Herrmann, C. Langer, A. J. McLeod and J. Trnka, *Prescriptive Unitarity for Non-Planar Six-Particle Amplitudes at Two Loops*, *JHEP* **12** (2019) 073 [[1909.09131](#)].
- [162] J. L. Bourjaily, E. Herrmann, C. Langer, A. J. McLeod and J. Trnka, *All-Multiplicity Nonplanar Amplitude Integrands in Maximally Supersymmetric Yang-Mills Theory at Two Loops*, *Phys. Rev. Lett.* **124** (2020) 111603 [[1911.09106](#)].
- [163] S. Caron-Huot and K. J. Larsen, *Uniqueness of Two-Loop Master Contours*, *JHEP* **1210** (2012) 026 [[1205.0801](#)].
- [164] G. Kälin, G. Mogull and A. Ochirov, *Two-loop  $\mathcal{N} = 2$  SQCD amplitudes with external matter from iterated cuts*, *JHEP* **07** (2019) 120 [[1811.09604](#)].
- [165] S. Badger, G. Mogull and T. Peraro, *Local integrands for two-loop all-plus Yang-Mills amplitudes*, *JHEP* **08** (2016) 063 [[1606.02244](#)].

- [166] Z. Bern and A. G. Morgan, *Massive loop amplitudes from unitarity*, *Nucl. Phys. B* **467** (1996) 479 [[hep-ph/9511336](#)].
- [167] N. Arkani-Hamed, F. Cachazo and J. Kaplan, *What is the Simplest Quantum Field Theory?*, *JHEP* **09** (2010) 016 [[0808.1446](#)].
- [168] M. Berg, I. Buchberger and O. Schlotterer, *String-motivated one-loop amplitudes in gauge theories with half-maximal supersymmetry*, *JHEP* **07** (2017) 138 [[1611.03459](#)].
- [169] Z. Bern, L. J. Dixon and D. A. Kosower, *Two-loop  $g \rightarrow gg$  splitting amplitudes in QCD*, *JHEP* **08** (2004) 012 [[hep-ph/0404293](#)].
- [170] R. Britto and E. Mirabella, *Single Cut Integration*, *JHEP* **01** (2011) 135 [[1011.2344](#)].
- [171] B. Feng, T. Li and X. Li, *Analytic Tadpole Coefficients of One-Loop Integrals*, [2107.03744](#).
- [172] R. Baumeister, D. Mediger, J. Pečovnik and S. Weinzierl, *Vanishing of Certain Cuts or Residues of Loop Integrals with Higher Powers of the Propagators*, *Phys. Rev. D* **99** (2019) 096023 [[1903.02286](#)].
- [173] G. F. Sterman, *An Introduction to Quantum Field Theory*. Cambridge University Press, 8, 1993.
- [174] T. Kinoshita, *Mass Singularities of Feynman Amplitudes*, *J. Math. Phys.* **3** (1962) 650.
- [175] T. D. Lee and M. Nauenberg, *Degenerate Systems and Mass Singularities*, *Phys. Rev.* **133** (1964) B1549.
- [176] C. L. Basham, L. S. Brown, S. D. Ellis and S. T. Love, *Energy Correlations in electron-Positron Annihilation: Testing QCD*, *Phys. Rev. Lett.* **41** (1978) 1585.
- [177] C. L. Basham, L. S. Brown, S. D. Ellis and S. T. Love, *Energy Correlations in Electron-Positron Annihilation in Quantum Chromodynamics: Asymptotically Free Perturbation Theory*, *Phys. Rev. D* **19** (1979) 2018.
- [178] A. Strominger, *Asymptotic Symmetries of Yang-Mills Theory*, *JHEP* **1407** (2014) 151 [[1308.0589](#)].
- [179] A. Strominger, *Lectures on the Infrared Structure of Gravity and Gauge Theory*, [1703.05448](#).



- [180] W. T. Giele, E. W. N. Glover and D. A. Kosower, *Higher order corrections to jet cross-sections in hadron colliders*, *Nucl. Phys.* **B403** (1993) 633 [[hep-ph/9302225](#)].
- [181] S. Frixione, Z. Kunszt and A. Signer, *Three-Jet Cross-Sections to Next-to-Leading Order*, *Nucl. Phys. B* **467** (1996) 399 [[hep-ph/9512328](#)].
- [182] S. Catani and M. H. Seymour, *A General algorithm for calculating jet cross-sections in NLO QCD*, *Nucl. Phys.* **B485** (1997) 291 [[hep-ph/9605323](#)].
- [183] A. Gehrmann-De Ridder, T. Gehrmann and E. W. N. Glover, *Antenna Subtraction at NNLO*, *JHEP* **09** (2005) 056 [[hep-ph/0505111](#)].
- [184] G. Somogyi, Z. Trocsanyi and V. Del Duca, *A Subtraction Scheme for Computing QCD Jet Cross Sections at NNLO: Regularization of Doubly-Real Emissions*, *JHEP* **01** (2007) 070 [[hep-ph/0609042](#)].
- [185] S. Catani, *The Singular behavior of QCD amplitudes at two loop order*, *Phys. Lett.* **B427** (1998) 161 [[hep-ph/9802439](#)].
- [186] N. Kidonakis, G. Oderda and G. F. Sterman, *Evolution of color exchange in QCD hard scattering*, *Nucl. Phys.* **B531** (1998) 365 [[hep-ph/9803241](#)].
- [187] S. M. Aybat, L. J. Dixon and G. F. Sterman, *The Two-loop soft anomalous dimension matrix and resummation at next-to-next-to leading pole*, *Phys. Rev.* **D74** (2006) 074004 [[hep-ph/0607309](#)].
- [188] L. J. Dixon, L. Magnea and G. F. Sterman, *Universal structure of subleading infrared poles in gauge theory amplitudes*, *JHEP* **08** (2008) 022 [[0805.3515](#)].
- [189] E. Gardi and L. Magnea, *Factorization constraints for soft anomalous dimensions in QCD scattering amplitudes*, *JHEP* **03** (2009) 079 [[0901.1091](#)].
- [190] T. Becher and M. Neubert, *Infrared singularities of scattering amplitudes in perturbative QCD*, *Phys. Rev. Lett.* **102** (2009) 162001 [[0901.0722](#)].
- [191] O. Almelid, C. Duhr and E. Gardi, *Three-loop corrections to the soft anomalous dimension in multileg scattering*, *Phys. Rev. Lett.* **117** (2016) 172002 [[1507.00047](#)].
- [192] G. F. Sterman, *Partons, factorization and resummation*, *TASI 95*, in *QCD and beyond*.

*Proceedings, Theoretical Advanced Study Institute in Elementary Particle Physics, TASI-95, Boulder, USA, June 4-30, 1995*, pp. 327–408, 1995, [hep-ph/9606312](#).

- [193] Z. Bern, M. Czakon, L. J. Dixon, D. A. Kosower and V. A. Smirnov, *The Four-Loop Planar Amplitude and Cusp Anomalous Dimension in Maximally Supersymmetric Yang-Mills Theory*, *Phys.Rev.* **D75** (2007) 085010 [[hep-th/0610248](#)].
- [194] Z. Bern, J. Carrasco, H. Johansson and D. Kosower, *Maximally Supersymmetric Planar Yang-Mills Amplitudes at Five Loops*, *Phys. Rev.* **D76** (2007) 125020 [[0705.1864](#)].
- [195] L. J. Dixon, J. M. Drummond and J. M. Henn, *Bootstrapping the three-loop hexagon*, *JHEP* **1111** (2011) 023 [[1108.4461](#)].
- [196] L. J. Dixon and Y.-T. Liu, *Lifting Heptagon Symbols to Functions*, *JHEP* **10** (2020) 031 [[2007.12966](#)].
- [197] Z. Bern, M. Enciso, H. Ita and M. Zeng, *Dual Conformal Symmetry, Integration-by-Parts Reduction, Differential Equations and the Nonplanar Sector*, *Phys. Rev. D* **96** (2017) 096017 [[1709.06055](#)].
- [198] Z. Bern, M. Enciso, C.-H. Shen and M. Zeng, *Dual Conformal Structure Beyond the Planar Limit*, *Phys. Rev. Lett.* **121** (2018) 121603 [[1806.06509](#)].
- [199] J. L. Bourjaily, E. Herrmann and J. Trnka, *Maximally supersymmetric amplitudes at infinite loop momentum*, *Phys. Rev. D* **99** (2019) 066006 [[1812.11185](#)].
- [200] D. Chicherin, J. M. Henn and E. Sokatchev, *Implications of nonplanar dual conformal symmetry*, *JHEP* **09** (2018) 012 [[1807.06321](#)].
- [201] Z. Bern, L. J. Dixon, M. Perelstein and J. S. Rozowsky, *Multileg one loop gravity amplitudes from gauge theory*, *Nucl. Phys. B* **546** (1999) 423 [[hep-th/9811140](#)].
- [202] H. Elvang and D. Z. Freedman, *Note on graviton MHV amplitudes*, *JHEP* **05** (2008) 096 [[0710.1270](#)].
- [203] J. M. Drummond, M. Spradlin, A. Volovich and C. Wen, *Tree-Level Amplitudes in  $N=8$  Supergravity*, *Phys. Rev. D* **79** (2009) 105018 [[0901.2363](#)].

- [204] L. J. Mason and D. Skinner, *Gravity, Twistors and the MHV Formalism*, *Commun. Math. Phys.* **294** (2010) 827 [[0808.3907](#)].
- [205] D. Nguyen, M. Spradlin, A. Volovich and C. Wen, *The Tree Formula for MHV Graviton Amplitudes*, *JHEP* **07** (2010) 045 [[0907.2276](#)].
- [206] A. Hodges, *New expressions for gravitational scattering amplitudes*, *JHEP* **07** (2013) 075 [[1108.2227](#)].
- [207] A. Hodges, *A simple formula for gravitational MHV amplitudes*, [1204.1930](#).
- [208] J. Trnka, *Towards the Gravituhedron: New Expressions for NMHV Gravity Amplitudes*, *JHEP* **04** (2021) 253 [[2012.15780](#)].
- [209] Z. Bern, S. Davies, T. Dennen and Y.-t. Huang, *Ultraviolet Cancellations in Half-Maximal Supergravity as a Consequence of the Double-Copy Structure*, *Phys. Rev. D* **86** (2012) 105014 [[1209.2472](#)].
- [210] Z. Bern, S. Davies and T. Dennen, *Enhanced ultraviolet cancellations in  $\mathcal{N} = 5$  supergravity at four loops*, *Phys. Rev. D* **90** (2014) 105011 [[1409.3089](#)].
- [211] Z. Bern, M. Enciso, J. Parra-Martinez and M. Zeng, *Manifesting enhanced cancellations in supergravity: integrands versus integrals*, *JHEP* **05** (2017) 137 [[1703.08927](#)].
- [212] E. Herrmann and J. Trnka, *UV cancellations in gravity loop integrands*, *JHEP* **02** (2019) 084 [[1808.10446](#)].
- [213] A. Edison, E. Herrmann, J. Parra-Martinez and J. Trnka, *Gravity loop integrands from the ultraviolet*, *SciPost Phys.* **10** (2021) 016 [[1909.02003](#)].
- [214] N. Arkani-Hamed, J. L. Bourjaily, F. Cachazo, A. B. Goncharov, A. Postnikov and J. Trnka, *Grassmannian Geometry of Scattering Amplitudes*. Cambridge University Press, 4, 2016, [10.1017/CBO9781316091548](#), [[1212.5605](#)].
- [215] R. Kleiss and H. Kuijf, *Multi - Gluon Cross-sections and Five Jet Production at Hadron Colliders*, *Nucl. Phys. B* **312** (1989) 616.
- [216] S. He and C. Zhang, *Notes on Scattering Amplitudes as Differential Forms*, *JHEP* **10** (2018) 054 [[1807.11051](#)].

[217] J. M. Drummond and J. M. Henn, *All tree-level amplitudes in  $N=4$  SYM*, *JHEP* **04** (2009) 018 [[0808.2475](#)].